York Schröder

Cumulative Habilitation

presented to the
Faculty of Physics
University of Bielefeld
Germany

24 April 2006

"A complete three-loop calculation of the free energy therefore has the special significance that it is the best anyone will ever do with perturbation theory."

from: P. Arnold and C. Zhai, Phys. Rev. D **50** (1994) 7603

In the past couple of years, we have progressed to the four-loop level. In the following, the major breakthroughs and challenges will be presented, under the subjective light of my own contributions to the field.

Y. Schröder

Contents

Chapter 1

Abstract

In this cumulative Habilitation thesis, I have collected and discussed the publications that came out of my research during the last five years.

Evolving around the main theme of weak-coupling expansions in Quantum Chromodynamics (QCD) at finite temperature, one of the key achievements of this research line is the successful implementation of four-loop perturbative computations.

This level of precision allows to make progress with the long-standing problem of incorporating long-distance contributions into the thermal QCD pressure, an observable that is phenomenologically relevant in heavy ion physics, cosmology as well as astrophysics.

Furthermore, as an interesting example of technology transfer, the same higher-order perturbative techniques could be applied to observables relevant for (zero-temperature) collider physics, for example to the electroweak rho parameter, and to threshold effects of heavy quarks in the strong coupling constant.

Chapter 2

List of publications presented in this thesis

[YS1] *Resumming Long-Distance Contributions to the QCD Pressure*
with K. Kajantie, M. Laine, K. Rummukainen,
Phys. Rev. Lett. **86** (2001) 10.

[YS2] *Simple way to generate high order vacuum graphs*
with K. Kajantie, M. Laine,
Phys. Rev. **D 65** (2002) 045008.

[YS3] *Automatic reduction of four-loop bubbles*
Nucl. Phys. Proc. Suppl. **116** (2003) 402.

[YS4] *Pressure of hot QCD up to $g^6 \ln(1/g)$*
with K. Kajantie, M. Laine, K. Rummukainen
Phys. Rev. **D 67** (2003) 1050008.

[YS5] *Four–loop vacuum energy density of the $SU(N_c)$ + adjoint Higgs theory*
with K. Kajantie, M. Laine, K. Rummukainen,
JHEP **0304** (2003) 036.

[YS6] *Tackling the infrared problem of thermal QCD*
Nucl. Phys. Proc. Suppl. **129** (2004) 572.

[YS7] *High-precision evaluation of four-loop vacuum bubbles in three dimensions*
with A. Vuorinen,
arXiv:hep-ph/0311323.

[YS8] *3-d lattice Yang-Mills free energy to four loops*
with F. Di Renzo, A. Mantovi, V. Miccio,
JHEP **0405** (2004) 006.

[YS9] *Plaquette expectation value and gluon condensate in three dimensions*
with A. Hietanen, K. Kajantie, M. Laine, K. Rummukainen,
JHEP **0501** (2005) 013.

[YS10] *Two-loop static QCD potential for general colour state*
with B. A. Kniehl, A. A. Penin, V. A. Smirnov and M. Steinhauser,
Phys. Lett. **B 607** (2005) 96.

[YS11] *Two-loop QCD gauge coupling at high temperatures*
with M. Laine,
JHEP **0503** (2005) 067.

[YS12] *High-precision epsilon expansions of single-mass-scale four-loop vacuum bubbles*
with A. Vuorinen,
JHEP **0506** (2005) 051.

[YS13] *Four-loop singlet contribution to the electroweak rho parameter*
with M. Steinhauser,
Phys. Lett. **B 622** (2005) 124.

[YS14] *Four-loop plaquette in 3d with a mass regulator*
with C. Torrero, F. Di Renzo, V. Miccio, M. Laine,
PoS LAT2005:189,2005.

[YS15] *Four-Loop decoupling relations for the strong coupling*
with M. Steinhauser,
JHEP **0601** (2006) 051.

[YS16] *Quark mass thresholds in QCD thermodynamics*
with M. Laine,
Phys. Rev. **D** (2006), in print (May 2006 issue).

Chapter 3

Introduction

- **QCD**

Quantum Chromodynamics (QCD) has been established more than 30 years ago, as the theory that describes the strong interaction which binds quarks and gluons into hadrons, such as protons and pions. Besides its overwhelming phenomenological success, QCD is one of the most outstanding achievements of theoretical particle physics. Its property of asymptotic freedom singles it out to be the only quantum field theory that is believed to be mathematically well-defined.

However, QCD is extremely difficult to solve analytically. While its Lagrangian is formulated in terms of quark and gluon fields, the hadronic world around us corresponds to complicated bound states of these fundamental degrees of freedom. Indeed, even after more than 30 years of intense efforts, the only hope for reliably deriving fundamental properties of nature (such as the proton mass) from first principles are large-scale numerical lattice Monte Carlo simulations. These numerical studies of the theory utilize the most powerful computer systems available, and in fact even drive developments in computing technology.

QCD has deep consequences in other contexts (than hadrons) as well: Its properties determine the expansion of the early universe, corresponding to times between 10^{-10}s to 1s after the big bang, which is of clear phenomenological significance for relic densities of various forms of dark matter appearing in cosmology [1]. Interestingly, in current and future heavy ion collision experiments (RHIC, Brookhaven National Lab; LHC, CERN, starting 2007) matter with properties similar to those in the early universe can be created and studied in the laboratory, hinting towards a nearly ideal hydrodynamic expansion [2]. In another context, QCD determines the properties of (extremely) dense matter, such as that in the cores of neutron stars. Compact star phenomenology is of central interest in astrophysics, driven by

many new observations.

The properties of a hot, expanding system (be it in heavy ion collisions or in cosmology) are determined by the equation of state (EoS). In its conceptually simplest form, the EoS gives the pressure p of the system as a function of the temperature T and the baryon chemical potential μ. Other quantities such as energy density or baryon density can be derived from the pressure via basic thermodynamic relations, rendering it one of the most fundamental objects of finite temperature field theory.

- **Pressure perturbatively**

Given this motivation, there have been impressive efforts on the determination of the hot QCD pressure over the past 25 years or so. Due to asymptotic freedom, at high enough temperatures the coupling is guaranteed to be small. Hence, perturbation theory should become applicable, and the pressure should be expressible as an expansion in the renormalized gauge coupling g. In the extreme limit $g \to 0$, one obtains the familiar Stefan-Boltzmann (SB) result, describing the pressure of a gas of non-interacting particles. At phenomenologically relevant temperatures, corrections to this limit become important.

The first of these corrections, being of orders $\mathcal{O}(g^2)$ and $\mathcal{O}(g^3)$, have been computed already in 1978-79 [3, 4]. Showing very slow convergence, it was clear however that a deeper expansion was needed. The next contribution, of $\mathcal{O}(g^4 \ln g)$, has been computed in 1983 [5]. Completing the full $\mathcal{O}(g^4)$ result presented an outstanding challenge, however, that was only met by a 3-loop calculation in 1994 [6]. It turned out that the next term in the series, $\mathcal{O}(g^5)$, was much more accessible [7]. The order $\mathcal{O}(g^6)$ then represents another qualitative increase in difficulty. As pointed out by Linde already in 1980 [8], at this order one meets genuine infrared divergences, making this order inaccessible to a purely perturbative expansion.

Nevertheless, the availability of several orders in the expansion allows to experiment with different resummations [9], in order to improve convergence properties. Another avenue is to abandon the strict weak-coupling expansion, and try to find improved resummation schemes, in the hope to achieve better convergence. There has been quite some impressive work along these lines during the last few years (for a review, see [10]).

- **Pressure on the lattice**

Lattice Monte Carlo methods, on the other hand, have proven to work for determining the hot QCD pressure, at least when the effects of quarks are neglected [11, 12], which formally represents the limit of QCD with infinitely heavy quarks. Unfortunately, this approach works only up to rather low temperatures ($T \lesssim 1 \text{GeV}$, which is still small for cosmological applications). Including the effects of light quarks into this numerical approach represents a formidable task,

due to the difficulties of computing fermionic determinants, and due to the even harder sign problem if one allows for non-zero chemical potential. First results in the same temperature range are available, but they still contain uncontrolled systematic errors [13].

While the lattice approach to full QCD is plagued with the problems just mentioned, it is worth noting that there are already definite qualitative results: It has become clear that there is no sharp phase transition between the quark-gluon plasma phase at high temperatures and our low-temperature hadronic world (for a recent review, see [14]). By adiabatically changing the parameters (T, μ and quark masses m), one can smoothly change from one "phase" to the other. Therefore, to learn about the different regions of the phase diagram, and to understand under which circumstances QCD looks more hadronic than deconfined, it is not anymore sufficient to concentrate on a small section around some "transition", but rather to try to sample the system's behavior in as large a parameter range as possible.

- **Combined method**

One of the options to confront the difficult situation is to combine perturbative and numerical methods. A key observation is that QCD at high temperatures is a multiscale system, exhibiting three parametrically distinct momentum scales: the purely perturbative "hard" scale $p \sim 2\pi T$, as well as the two "soft scales", $p \sim gT, g^2T$, which are generated dynamically and are related to collective plasma phenomena. Given this scale hierarchy, perturbation theory can be used to construct effective field theories for the low-energy soft modes, a process that is called dimensional reduction [15, 16, 17] since the effective theories turn out to be three-dimensional.

In practice, integrating out the hard modes $p \sim \pi T$, (which in QCD amounts to all quarks, as well as all gluonic degrees of freedom except for the so-called zero Matsubara modes), one arrives at a three-dimensional (3d) effective theory containing the dynamical scales $p \sim gT, g^2T$. This effective theory, being a 3d gauge theory coupled to an adjoint Higgs field, is called "Electrostatic QCD" (EQCD). In principle one can go even further and integrate out the soft modes $p \sim gT$ from EQCD, getting a 3d pure Yang-Mills theory, containing the dynamical scale $p \sim g^2T$. This effective theory, dubbed "Magnetostatic QCD" (MQCD), is purely non-perturbative [8] and hence has to be treated numerically, e.g. by lattice Monte Carlo simulations.

Note that, since all effects of fermions have already been mapped out in the first reduction step, numerical treatment is required only for a 3d purely bosonic theory within this setup, a task that is evidently much more realistic than performing a full 4d QCD simulation. Hence, one could hope to be able to apply the combined method in a wide temperature range, while treating fully dynamical quarks with their physical properties (masses and chemical potentials).

- **Status**

Motivated by the prospects of the combined method just described, we have tackled a number of different open tasks that are needed to incorporate the longest-distance (MQCD) contributions into the QCD pressure.

Notably, the logarithmically enhanced four-loop contributions from all scales are now available **[YS4]**, corresponding to $\mathcal{O}(g^6 \ln g)$ in the weak-coupling expansion of the pressure. This result has in the meantime been generalized to include small chemical potentials [18].

Furthermore, a number of milestones on the way to the main goal, accounting for the full order $\mathcal{O}(g^6)$, have already been reached, leaving a single well-defined perturbative computation to be done, which does not pose any conceptual problems, but is technically demanding.

Apart from purely theoretical interest, reaching the full order $\mathcal{O}(g^6)$ would greatly improve the accuracy of the result for the pressure **[YS4]**. The main reason is that then, for the first time, all physical length scales have contributed. In chapter 4, the present status of the QCD pressure will be described in great detail.

- **Methods**

To include the logarithmically enhanced $\mathcal{O}(g^6 \ln g)$ contributions into the pressure **[YS4]**, we had to deal with evaluating four-loop vacuum graphs in perturbation theory. Hence, a large amount of work had to be invested into implementing methods that could cope with the corresponding level of complexity. To this end, we used the computer algebra program FORM [19], which enabled us to deal with very large intermediate expressions. To start off, a method for efficiently generating the Feynman graphs needed was implemented **[YS2]**. Faced with millions of integrals to evaluate, we then constructed an automatized routine which, based on the general method of integration by parts (IBP) [20] combined with lexicographic ordering [21], reduced the huge number of different integrals to a few "master" integrals **[YS3]**. In EQCD, these master integrals were then computed manually **[YS5]**, while for MQCD (where proper care had to be taken to screen infrared divergences), the relevant integrals have been obtained manually first **[YS6]**, and later been confirmed in a fully automated fashion **[YS7]** utilizing the method of numerically solving recurrence relations [21] for the required class of integrals.

To drive the precision towards inclusion of the full order $\mathcal{O}(g^6)$, the techniques that are needed span an even wider field. First of all, to determine the non-perturbative contribution of MQCD, numerical simulations had to be performed **[YS9]**. To reach the continuum limit, all ultraviolet divergences of the relevant operator had to be known, a task that in a 3d theory can be performed exactly by computing a finite number of terms. This required a

four-loop computation in lattice regularization **[YS8]**, a daunting task that could however be mastered by using a radically different expansion method, Numerical Stochastic Perturbation Theory (NSPT) [22]. Furthermore, to match between the lattice and continuum regularization schemes, a comparable lattice-regularized computation should be performed with properly screened gauge field propagators. While the final result is not yet available, we have shown that NSPT has the potential to deal with this challenge as well **[YS14]**.

Furthermore, a number of purely perturbative (continuum-) matching parameters for the effective theory setup are needed to a certain precision, requiring on the technical side the systematic classification, reduction and evaluation of one- and two-loop sum-integrals without **[YS11]** and with **[YS16]** masses and chemical potentials. Note that, at least for the massless case, many sum-integrals have been evaluated up to the three-loop level already [6, 18]. The final matching parameter to be computed requires the evaluation of four-loop sum-integrals. It is unfortunately not yet clear which approach would be optimal for tackling this challenge, be it an algorithmic reduction via IBP, a numerical treatment, or a combination of both, or whether even a completely independent idea would be needed.

- **Technology transfer**

Apart from driving the knowledge of thermodynamic quantities to a new level, there are other viable directions to put the acquired perturbative techniques to work. Generalizing the methods of generating, reducing and integrating Feynman diagrams to allow for different actions and observables, we were able to compute the two-loop static potential of QCD, checking existing results in the singlet sector, while obtaining new results in the octet sector **[YS10]**, which naturally appears in computations of heavy quarkonium spectra and decay rates.

Another main avenue for "technology transfer" is the determination of corrections to observables studied in collider physics. A first example is the R–ratio (defined as $\sigma(e^+e^- \to \mathrm{hadrons})/\sigma(e^+e^- \to \mu^+\mu^-)$), which is connected to the imaginary part of the photon self-energy $\Pi(q^2)$. A practical strategy to calculate its higher-order corrections is to compute different limits, to then reconstruct the full answer using analyticity arguments and threshold behavior [23]. The most difficult part of this program, the small–momentum expansion of $\Pi(q^2)$ up to α_s^3, requires the treatment of 4-loop vacuum integrals.

The next example are QCD corrections to the ρ–parameter, which is proportional to the difference of the Z– and W–self-energies at zero momentum [24]. This fundamental parameter is sensitive to e.g. m_{top}^2 through loop corrections, and hence requires an accurate theoretical determination, in order to be a significant discriminator for 'new physics'.

As a third example, note that threshold effects of heavy quarks in the running of the strong coupling constant α_s, conveniently parameterized by so-called decoupling parameters,

are related to vacuum polarization functions at zero external momentum [25]. Being a most fundamental parameter in the Standard model, it is clear that a precise knowledge of α_s and its scale dependence is needed, hence requiring high-order calculations.

In **[YS12]**, **[YS13]** and **[YS15]** we have demonstrated the use of our methods in these fields.

Chapter 4

Status of the QCD pressure: Details

The QCD pressure, being the central pillar of my research during the last few years, and hence constituting the main driving force behind all technical development sketched above, certainly deserves to be discussed in more detail. In this chapter, I will therefore present all necessary details in a unified notation, while linking them to the papers presented here as well as to the literature.

As already explained in the Introduction, thermal (equilibrium) QCD possesses three distinct physical scales, two of them generated dynamically. The contributions to the pressure (and to any other thermodynamic observable) from each of these scales can be obtained from carefully constructing and matching a series of effective theories ([26],**[YS4]**).

The theories under consideration are (hard) QCD, Electrostatic QCD (EQCD) and Magnetostatic QCD (MQCD), governing physics on length scales $1/T$, $1/gT$ and $1/g^2T$, respectively. While the first two are amenable to perturbative calculations, MQCD is purely non-perturbative and has to be treated on the lattice. Viewing the gauge coupling $g(T)$ as parametrically small (which is certainly justified at asymptotically high temperatures), these three scales are well separated, and can hence be dealt with individually via the effective theory setup. Schematically, for the pressure one can write $p_{\mathrm{QCD}} = p_E + p_M + p_G$, where each contribution depends on the matching scales. This scale-dependence will cancel in the sum, rendering p_{QCD} a well-defined physical observable.

Below, we specify the contributions to the $\overline{\mathrm{MS}}$ pressure $p_{\mathrm{QCD}} = p_G + p_M + p_E$ [26] from each physical scale individually, for the case of gauge group $\mathrm{SU}(N_\mathrm{c})$ and N_f quark flavors. We will work at zero quark masses $m_{q_i} = 0$ and vanishing chemical potentials $\mu_f = 0$, and display all dependence on the $\overline{\mathrm{MS}}$ scale $\bar{\mu}^2 = 4\pi e^{-\gamma_0}\mu^2$ by $L \equiv \ln\frac{\bar{\mu}}{4\pi T}$. Effects due to finite quark masses ([4, 27],**[YS16]**) and chemical potentials [28, 18], as well as generalizations to

the Standard Model [29] are available in the literature, but will not be discussed here.

4.1 Contributions from the ultra-soft scale g^2T, i.e. from MQCD

Ultra-soft physics is not accessible by perturbative methods, due to the unscreened transverse gluonic sector, which would lead to severe infrared problems [8]. This sector is governed by a three-dimensional pure gauge theory. Its only parameter is the dimensionful 3d gauge coupling g_M^2, which we write as $\hat{g}_M^2 \equiv \frac{N_c g_M^2}{16\pi^2 T}$. The screening length gets generated non-perturbatively, making a numerical lattice Monte-Carlo treatment necessary. The detailed setup for how to incorporate the ultra-soft contribution into the physical pressure by a carefully defined mixture of perturbative and non-perturbative coefficients is explained in detail in **[YS16]**. The result is

$$
\begin{aligned}
\frac{p_G(T)}{\mu^{-2\epsilon}} \;=\; & d_A 16\pi^2 T^4 \hat{g}_M^6 \left[8\alpha_G \left(\frac{1}{8\epsilon} + L + \ln\frac{N_c^2}{4\pi\hat{g}_M^2} + 1 \right) + \frac{1}{3} \right. \\
& + \left. [\textbf{pert}] - [\textbf{nspt}] + [\textbf{non-pert}] + \mathcal{O}(\epsilon) \right],
\end{aligned}
\tag{4.1}
$$

where $d_A = N_c^2 - 1$, and $\alpha_G = \frac{43}{96} - \frac{157}{6144}\pi^2$ (**[YS4]**,**[YS6]**) is a perturbative 4-loop coefficient. The three coefficients enclosed in square brackets originate from measuring the 3d YM pressure on the lattice and matching the result to the $\overline{\text{MS}}$ scheme. To be more precise, they are the following.

• The first number stems from a non-perturbative lattice Monte-Carlo measurement of the 3d plaquette in pure SU(N_c) theory **[YS9]**,

$$
\begin{aligned}
[\textbf{non-pert}] \;=\; & \frac{(4\pi)^4}{8 d_A N_c^6} \lim_{\beta\to\infty} \left\{ \beta^4 \left\langle 1 - \frac{1}{N_c}\text{Tr}\, P \right\rangle_a - \left[c_1\beta^3 + c_2\beta^2 + c_3\beta + c_4 \ln\beta \right] \right\} \\
\;=\; & 10.7(4) \quad \text{at } N_c = 3 \,,
\end{aligned}
\tag{4.2}
$$

where $\beta = \frac{2N_c}{g_M^2 a}$ denotes the dimensionless lattice coupling, and $c_{1..4}$ are divergences of the 3d lattice-regularized plaquette which can be computed in lattice perturbation theory. They read

$$
c_1 \;=\; \frac{d_A}{3} \,,
\tag{4.3}
$$

$$
c_2 \;=\; \frac{d_A}{(4\pi)^2} \left(-\frac{8\pi^2}{9} + 5.25449 N_c^2 \right) \,,
\tag{4.4}
$$

$$
c_3 \;=\; d_A \left([0.04978944(1)] + [-0.04289464(7)] N_c^2 + [0.0147397(3)] N_c^4 \right)
\tag{4.5}
$$

$$= \quad 6.8612(2) \quad \text{at } N_c = 3 \ ,$$

$$c_4 \quad = \quad \frac{d_A N_c^6}{(4\pi)^4} 64 \alpha_G \ . \tag{4.6}$$

The number in c_2 is a sum of typical 2-loop (infinite–volume) lattice integrals ([30],[YS9]),

$$-\frac{2}{3}\left(\frac{\Sigma^2}{4} - \pi\Sigma - \frac{\pi^2}{2} + 4\kappa_1 + \frac{2}{3}\kappa_5\right) \quad \approx \quad 5.25449 \ , \tag{4.7}$$

with (K is the complete elliptic integral of first kind) ([31, 32],[YS9])

$$\Sigma \quad = \quad \frac{1}{\pi^2} \int_0^\pi \mathrm{d}^3 x \frac{1}{\sum_i \sin^2 x_i} \tag{4.8}$$

$$= \quad \frac{8}{\pi}\left(18 + 12\sqrt{2} - 10\sqrt{3} - 7\sqrt{6}\right) K^2\left((2-\sqrt{3})^2(\sqrt{3}-\sqrt{2})^2\right) \approx 3.1759114 \ , \tag{4.9}$$

$$\kappa_1 \quad = \quad \frac{1}{4\pi^4} \int_{-\pi/2}^{\pi/2} \mathrm{d}^3 x \mathrm{d}^3 y \frac{\sum_i \sin^2 x_i \sin^2(x_i + y_i)}{\sum_i \sin^2 x_i \sum_i \sin^2(x_i + y_i) \sum_i \sin^2 y_i} \approx 0.958382(1) \ , \tag{4.10}$$

$$\kappa_5 \quad = \quad \frac{1}{\pi^4} \int_{-\pi/2}^{\pi/2} \mathrm{d}^3 x \mathrm{d}^3 y \frac{\sum_i \sin^2 x_i \sin^2(x_i + y_i)\sin^2(y_i)}{\sum_i \sin^2 x_i \sum_i \sin^2(x_i + y_i) \sum_i \sin^2 y_i} \approx 1.013041(1) \ . \tag{4.11}$$

The coefficient c_3 has been estimated by numerical stochastic perturbation theory (NSPT) for $N_c = 3$ [YS8] and, with higher numerical accuracy and full N_c dependence, computed from 3-loop diagrams in lattice perturbation theory [33]. In principle, it would be nice to know the full N_c-dependence of Eq. (4.2).

• The second number stems from an estimation of (the sum of all) 4-loop vacuum diagrams in lattice perturbation theory by NSPT [22], with the IR divergence regulated by massive gluon- and ghost-propagators (mass term $\frac{m^2}{2}A^2$ and $m^2\bar{c}c$ in the action) [YS14]. NSPT works on a finite lattice of volume $(aL)^3$, so the infinite–volume limit has to be taken first to ensure that the IR is regulated by the mass term only. A very preliminary result is [34]

$$[\textbf{nspt}] \quad = \quad \frac{(4\pi)^4}{8 d_A N_c^6} \lim_{am \to 0} \lim_{L \to \infty} \left\{ \left\langle 1 - \frac{1}{N_c}\mathrm{Tr}\, P \right\rangle_{am}\bigg|_{\beta^{-4} \text{ term}} - c_4 \ln\frac{1}{am} \right\} \tag{4.12}$$

$$= \quad \frac{(4\pi)^4}{8 d_A N_c^6}\left[c'_{40} + c'_{41}N_c^2 + c'_{42}N_c^4 + c'_{43}N_c^6\right]$$

$$\approx \quad \frac{4\pi^4}{729} 30 \quad \text{in Feynman gauge at } N_c = 3 \ .$$

To match the precision obtained for [**non-pert**], this number should be estimated with at least 2% accuracy. It would be nice to know all four coefficients, in Feynman gauge, either by a direct diagrammatic evaluation, or by doing NSPT for (at least) four different values of N_c.

• The third number stems from a matching 4-loop computation in the $(3-2\epsilon)$d continuum theory, regulated in the IR by gluon- and ghost-masses, with gauge parameter ξ. Gauge

dependence, introduced by the IR regulator, is guaranteed to cancel against that in [**nspt**]. The result reads

$$\sum[\text{4loop YM vac diags}] \;=\; g^6 d_A N_c^3 \left(\frac{1}{m}J\right)^4 \left\{\frac{\alpha_G}{\epsilon} + [\textbf{pert}] + \mathcal{O}(\epsilon)\right\} \qquad (4.13)$$

where J is the 1-loop massive tadpole integral $\int_p 1/(p^2+m^2)$. We choose Feynman gauge $\xi = 1$ which here leads to modified propagators $1/p^2 \to 1/(p^2+m^2)$, and obtain [35]

$$[\textbf{pert}] = -3.73134481146281478501 \quad \text{in Feynman gauge} \qquad (4.14)$$

where the number can be expressed in terms of 18 fully massive 4-loop scalar master integrals (**[YS3]**,**[YS7]**). For general ξ, we would have to calculate vacuum diagrams with two mass scales (m^2 and ξm^2), which presently is beyond our computational capabilities.

The matching condition for the 3d gauge coupling reads ([36, 37],**[YS11]**)

$$\hat{g}_M^2 \equiv \frac{N_c g_M^2}{16\pi^2 T} = \hat{g}_E^2 \left[1 - \frac{1}{12}\frac{\hat{g}_E^2}{\hat{m}_E} - \frac{17}{288}\frac{\hat{g}_E^4}{\hat{m}_E^2} - \frac{2-\hat{n}}{24}\frac{\hat{g}_E^2\hat{\lambda}_E^{(1)}}{\hat{m}_E^2} - \frac{3\hat{n}-1}{24}\frac{\hat{g}_E^2\hat{\lambda}_E^{(2)}}{\hat{m}_E^2}\right] + \mathcal{O}(\frac{\hat{g}_E^8}{\hat{m}_E^3}) \quad (4.15)$$

where $\hat{n} \equiv \frac{N_c^2-1}{N_c^2}$. For the g^6 pressure, only the leading coefficient is relevant.

4.2   Contributions from the soft scale gT, i.e. from EQCD

Soft-scale physics is governed by a three-dimensional gauge theory, coupled to an adjoint Higgs field. This adjoint Higgs theory possesses a small number of dimensionful coupling constants, which are related to the parameters of full QCD (being g^2 and T) by the equations given below. The contribution of this sector to the pressure is given by

$$\begin{aligned}
\frac{p_M(T)}{\mu^{-2\epsilon}} \;=\;& d_A 16\pi^2 T^4 \left\{\hat{m}_E^3 \left[\frac{1}{3} + \mathcal{O}(\epsilon)\right]\right.\\
+\;& \hat{g}_E^2\hat{m}_E^2 \left[-\frac{1}{4\epsilon} + \left(-L + \frac{1}{2}\ln\hat{m}_E^2 + \ln 2 - \frac{3}{4}\right) + \mathcal{O}(\epsilon)\right]\\
+\;& \hat{g}_E^4\hat{m}_E \left[\left(-\frac{89}{24} - \frac{\pi^2}{6} + \frac{11}{6}\ln 2\right) + \mathcal{O}(\epsilon)\right]\\
+\;& \hat{g}_E^6 \left[\alpha_M \left(\frac{1}{\epsilon} + 8L - 4\ln\hat{m}_E^2 - 8\ln 2\right) + \beta_M + \mathcal{O}(\epsilon)\right]\\
+\;& \hat{\lambda}_E^{(1)}\hat{m}_E^2 \left[\frac{\hat{n}-2}{4} + \mathcal{O}(\epsilon)\right] + \hat{\lambda}_E^{(2)}\hat{m}_E^2 \left[\frac{1-3\hat{n}}{4} + \mathcal{O}(\epsilon)\right]\\
+\;& \left.\mathcal{O}(\hat{g}_E^8\hat{m}_E^{-1}, \hat{\lambda}_E^2\hat{m}_E)\right\},
\end{aligned} \qquad (4.16)$$

with the 4-loop coefficients $\alpha_M = \frac{43}{32} - \frac{491}{6144}\pi^2$, $\beta_M = -\frac{311}{256} - \frac{43}{32}\ln 2 - \frac{19}{6}\ln^2 2 + \frac{77}{9216}\pi^2 - \frac{491}{1536}\pi^2\ln 2 + \frac{1793}{512}\zeta(3) + \gamma_{10} = -1.391512$ **[YS5]**, where γ_{10} is the leading coefficient of a finite 3d scalar 4-loop integral that is known numerically only **[YS5]**,

$$\gamma_{10} = (4\pi)^4 \int_{-\infty}^{\infty} \frac{\mathrm{d}^3 x_1}{(2\pi)^3}\frac{\mathrm{d}^3 x_2}{(2\pi)^3}\frac{\mathrm{d}^3 x_3}{(2\pi)^3}\frac{\mathrm{d}^3 x_4}{(2\pi)^3}\frac{1}{(x_1-x_3)^2}\frac{1}{(x_2-x_3)^2} \times$$

$$\times \frac{1}{x_1^2+1}\frac{1}{x_2^2+1}\frac{1}{(x_1-x_4)^2+1}\frac{1}{(x_2-x_4)^2+1}\frac{1}{(x_3-x_4)^2+1} \qquad (4.17)$$

$$= 0.171007009753(1) , \qquad (4.18)$$

and the matching parameters are [31, 26]

$$\hat{m}_E^2 \equiv \left(\frac{m_E}{4\pi T}\right)^2 = \hat{g}^2\left[\tilde{\alpha}_{E4} + (2\tilde{\alpha}_{E4}L + \tilde{\alpha}_{E5})\epsilon + \mathcal{O}(\epsilon^2)\right]$$

$$+ \hat{g}^4\left[\left(2\hat{\beta}_0\tilde{\alpha}_{E4}L + \tilde{\alpha}_{E6}\right) + (6\hat{\beta}_0\tilde{\alpha}_{E4}L^2 + \tilde{\beta}_{E2}^{(L)}L + \tilde{\beta}_{E2})\epsilon + \mathcal{O}(\epsilon^2)\right]$$

$$+ \mathcal{O}(\hat{g}^6) , \qquad (4.19)$$

$$\hat{g}_E^2 \equiv \frac{N_c g_E^2}{16\pi^2 T} = \hat{g}^2 + \hat{g}^4\left[\left(2\hat{\beta}_0 L + \tilde{\alpha}_{E7}\right) + (2\hat{\beta}_0 L^2 + 2\tilde{\alpha}_{E7}L + \tilde{\beta}_{E3})\epsilon + \mathcal{O}(\epsilon^2)\right]$$

$$+ \hat{g}^6\left[4\hat{\beta}_0^2 L^2 + 2\left(\hat{\beta}_1 + 2\hat{\beta}_0\tilde{\alpha}_{E7}\right)L + \tilde{\gamma}_{E1} + \mathcal{O}(\epsilon)\right] + \mathcal{O}(\hat{g}^8) , \qquad (4.20)$$

$$\hat{\lambda}_E^{(1)} \equiv \frac{N_c^2 \lambda_E^{(1)}}{16\pi^2 T} = \hat{g}^4\left[4 + \mathcal{O}(\epsilon)\right] + \mathcal{O}(\hat{g}^6) , \qquad (4.21)$$

$$\hat{\lambda}_E^{(2)} \equiv \frac{N_c \lambda_E^{(2)}}{16\pi^2 T} = \hat{g}^4\left[\frac{4}{3}(1-z) + \mathcal{O}(\epsilon)\right] + \mathcal{O}(\hat{g}^6) , \qquad (4.22)$$

where we have used the beta-function coefficients $\hat{\beta}_0 = \frac{11-2z}{3}$, $\hat{\beta}_1 = \frac{34}{3} - \frac{10}{3}z - z\hat{n}$ and, for brevity, set $z \equiv N_f/N_c$. Writing $Z_n \equiv \zeta'(-n)/\zeta(-n)$, the coefficients read [26, 16, 38]

$$\tilde{\alpha}_{E4} = \frac{2+z}{6} , \qquad (4.23)$$

$$\tilde{\alpha}_{E5} = 2\tilde{\alpha}_{E4}Z_1 + \frac{z}{6}(1 - 2\ln 2) , \qquad (4.24)$$

$$\tilde{\alpha}_{E6} = \frac{1}{3}\tilde{\alpha}_{E4}(6\hat{\beta}_0\gamma_0 + 5 + 2z - 8z\ln 2) - \frac{z}{2}\hat{n} , \qquad (4.25)$$

$$\tilde{\alpha}_{E7} = 2\hat{\beta}_0\gamma_0 + \frac{1}{3} - \frac{8}{3}z\ln 2 , \qquad (4.26)$$

as well as ([39],**[YS11]**)

$$\tilde{\beta}_{E2}^{(L)} = 4\hat{\beta}_0\tilde{\alpha}_{E4}(2\gamma_0 + Z_1) + \frac{1}{9}(20 + 29z + 2z^2) - 2z(\hat{n} + 3\ln 2) - \frac{4}{3}z^2\ln 2 , \qquad (4.27)$$

$$\tilde{\beta}_{E2} = \frac{1}{4}\hat{\beta}_0\tilde{\alpha}_{E4}\left(+\pi^2 - 16\gamma_1\right) + \frac{2}{3}\tilde{\alpha}_{E4}Z_1(6\hat{\beta}_0\gamma_0 + 5 + 2z - 8z\ln 2)$$

$$+ \frac{2}{9}\gamma_0(5 + 10z - (19 + 2z)z\ln 2) + \frac{2}{9} + \frac{z}{18}(7 + 6\ln 2 - 16\ln^2 2)$$

$$+ \quad \frac{z^2}{9}\left(1 - 2\ln 2 + 4\ln^2 2\right) - \frac{z}{6}\,\hat{n}(3 + 6\gamma_0 + 6Z_1 + 10\ln 2)\,, \tag{4.28}$$

$$\tilde{\beta}_{\mathrm{E3}} = \left(\frac{\pi^2}{4} - 4\gamma_1\right)\hat{\beta}_0 + \frac{2}{3}\gamma_0 - \frac{8}{3}\ln 2(\ln 2 + 2\gamma_0)z\,, \tag{4.29}$$

$$\tilde{\gamma}_{\mathrm{E1}} = 2\hat{\beta}_1\gamma_0 + \tilde{\alpha}_{\mathrm{E7}}^2 + \frac{341}{18} - \frac{10}{9}\zeta(3)$$
$$- \quad \frac{z}{9}(43 + 24\ln 2 + 5\zeta(3)) - \frac{z}{12}\hat{n}(23 + 80\ln 2 - 14\zeta(3))\,, \tag{4.30}$$

where the γ_n are expansion coefficients of the Zeta function $\zeta(1-\epsilon) = -\frac{1}{\epsilon} + \sum_{n=0}^{\infty} \frac{\epsilon^n}{n!}\gamma_n$ (note that $\gamma_0 \equiv \gamma_E = 0.577216$). For the g^6 pressure, the $\hat{g}^6$ terms of Eq. (4.20) are irrelevant.

4.3 Contributions from the hard scale $2\pi T$, i.e. from hard QCD

Hard-scale physics can be treated perturbatively, in a simple g^2-expansion, without the need for resummations, thermal masses, or hard thermal loops. This is due to all IR effects being properly incorporated into EQCD and MQCD, and is one of the main conceptual advantages of using the effective theory setup. The contribution to the pressure from hard momentum scales reads

$$\frac{p_E(T)}{\mu^{-2\epsilon}} = d_A 16\pi^2 T^4 \frac{1}{16}\frac{1}{45}\left\{\tilde{\alpha}_{\mathrm{E1}} + \hat{g}^2\left[\tilde{\alpha}_{\mathrm{E2}} + \mathcal{O}(\epsilon)\right]\right.$$
$$+ \quad \hat{g}^4\left[\tilde{\alpha}_{\mathrm{E4}}\frac{180}{\epsilon} + (180\cdot 6\tilde{\alpha}_{\mathrm{E4}} + 2\hat{\beta}_0\tilde{\alpha}_{\mathrm{E2}})L + \tilde{\alpha}_{\mathrm{E3}} + \mathcal{O}(\epsilon)\right]$$
$$+ \quad \left.\hat{g}^6\left[\frac{\tilde{\beta}_{\mathrm{E1}}^{(\mathrm{div})}}{\epsilon} + \tilde{\beta}_{\mathrm{E1}}^{(L^2)}L^2 + \tilde{\beta}_{\mathrm{E1}}^{(L)}L + \tilde{\beta}_{\mathrm{E1}} + \mathcal{O}(\epsilon)\right] + \mathcal{O}(\hat{g}^8)\right\}\,, \tag{4.31}$$

with ideal-gas coefficient $\tilde{\alpha}_{\mathrm{E1}} = 1 + \frac{7}{4}\frac{z}{\hat{n}}$, $\tilde{\alpha}_{\mathrm{E2}} = -\frac{5}{4}(4 + 5z)$ [3], and [6]

$$\tilde{\alpha}_{\mathrm{E3}} = 180(\tilde{\alpha}_{\mathrm{E4}})^2\gamma_0 + 5\left[\left(\frac{116}{5} + \frac{220}{3}Z_1 - \frac{38}{3}Z_3\right)\right.$$
$$+ \quad \frac{z}{2}\left(\frac{1121}{60} - \frac{157}{5}\ln 2 + \frac{146}{3}Z_1 - \frac{1}{3}Z_3\right)$$
$$+ \quad \left.\frac{z^2}{4}\left(\frac{1}{3} - \frac{88}{5}\ln 2 + \frac{16}{3}Z_1 - \frac{8}{3}Z_3\right) + \frac{z}{4}\hat{n}\left(\frac{105}{4} - 24\ln 2\right)\right]\,, \tag{4.32}$$

and unknown coefficients β_{E1}, which can be determined e.g. by a 4-loop computation of vacuum diagrams in thermal QCD. Since p_{QCD} is physical, the divergent and scale-dependent parts of β_{E1} are related to the other coefficients introduced in the above, serving as a valuable

check on this open computation. Specifically, from 2-loop running of the 4d gauge coupling

$$\hat{g}^2 \equiv \frac{N_{\rm c} g^2(\bar{\mu})}{16\pi^2} \;\; = \;\; \hat{g}^2(\bar{\mu}_0) + \hat{g}^4(\bar{\mu}_0)(-2\hat{\beta}_0 \ell) + \hat{g}^6(\bar{\mu}_0)(4\hat{\beta}_0^2 \ell^2 - 2\hat{\beta}_1 \ell) \;, \qquad (4.33)$$

where $\ell \equiv \ln\frac{\bar{\mu}}{\bar{\mu}_0} = L - \ln\frac{\bar{\mu}_0}{4\pi T}$, one can already fix

$$\tilde{\beta}_{\rm E1}^{({\rm div})} \;\; = \;\; 180\left[4\hat{\beta}_0\tilde{\alpha}_{\rm E4}L + \tilde{\alpha}_{\rm E6} + \tilde{\alpha}_{\rm E4}\tilde{\alpha}_{\rm E7} - 4(\alpha_G + \alpha_M)\right], \qquad (4.34)$$

$$\tilde{\beta}_{\rm E1}^{(L^2)} \;\; = \;\; 180\left[28\hat{\beta}_0\tilde{\alpha}_{\rm E4}\right] + 4\hat{\beta}_0^2\tilde{\alpha}_{\rm E2} \;, \qquad (4.35)$$

$$\tilde{\beta}_{\rm E1}^{(L)} \;\; = \;\; 180\left[4\tilde{\alpha}_{\rm E6} + 8\tilde{\alpha}_{\rm E4}\tilde{\alpha}_{\rm E7} - 2\hat{\beta}_0\tilde{\alpha}_{\rm E5} - 32(\alpha_G + \alpha_M) + \tilde{\beta}_{\rm E2}^{(L)}\right]$$
$$+ \;\; 2\hat{\beta}_1\tilde{\alpha}_{\rm E2} + 4\hat{\beta}_0\tilde{\alpha}_{\rm E3} \;. \qquad (4.36)$$

The remaining g^6-coefficient, $\tilde{\beta}_{\rm E1}$ however, entails a four-loop computation of all connected vacuum diagrams involving quarks, gluons and ghosts, a computation that has so far not been tackled due to the formidable task of solving many genuine 4-loop sum-integrals. From diagrammatic arguments, it is clearly a polynomial in $z = N_{\rm f}/N_{\rm c}$,

$$\tilde{\beta}_{\rm E1} = \#_0 + z\#_1 + z^2\#_2 + z^3\#_3 \;, \qquad (4.37)$$

and we will in the following indicate how two of its coefficients (the first and last) can be crudely estimated numerically already.

4.4 Putting everything together

Expanding in ϵ, all poles cancel, as they should. In practice we make use of Eqs. (4.15),(4.19) and (4.20) to re-expand all terms with a factor $1/\epsilon$ or L in Eqs. (4.1) and (4.16) in terms of $\hat{g}^2$. After cancellation of the poles (and taking into account terms like $\frac{1}{\epsilon}\cdot\epsilon$), we can now take the limit $\epsilon \to 0$ in Eqs. (4.19), (4.20), whence

$$\hat{m}_E^2 \;\; = \;\; \hat{g}^2\tilde{\alpha}_{\rm E4} + \hat{g}^4\left[2\hat{\beta}_0\tilde{\alpha}_{\rm E4}L + \tilde{\alpha}_{\rm E6}\right] + \mathcal{O}(\hat{g}^6) \;, \qquad (4.38)$$

$$\hat{g}_E^2 \;\; = \;\; \hat{g}^2 + \hat{g}^4\left[2\hat{\beta}_0 L + \tilde{\alpha}_{\rm E7}\right] + \hat{g}^6\left[4\hat{\beta}_0^2 L^2 + 2\left(\hat{\beta}_1 + 2\hat{\beta}_0\tilde{\alpha}_{\rm E7}\right)L + \tilde{\gamma}_{\rm E1}\right] + \mathcal{O}(\hat{g}^8) \;. \,(4.39)$$

Collecting explicit logarithms L, they precisely cancel the scale dependence of $\hat{g}^2$ up to the order of the computation, and can hence be absorbed by writing

$$\tilde{g}^2 \;\; = \;\; \hat{g}^2 + \hat{g}^4 2\hat{\beta}_0 L + \hat{g}^6(4\hat{\beta}_0^2 L^2 + 2\hat{\beta}_1 L) + \mathcal{O}(\hat{g}^8) \;. \qquad (4.40)$$
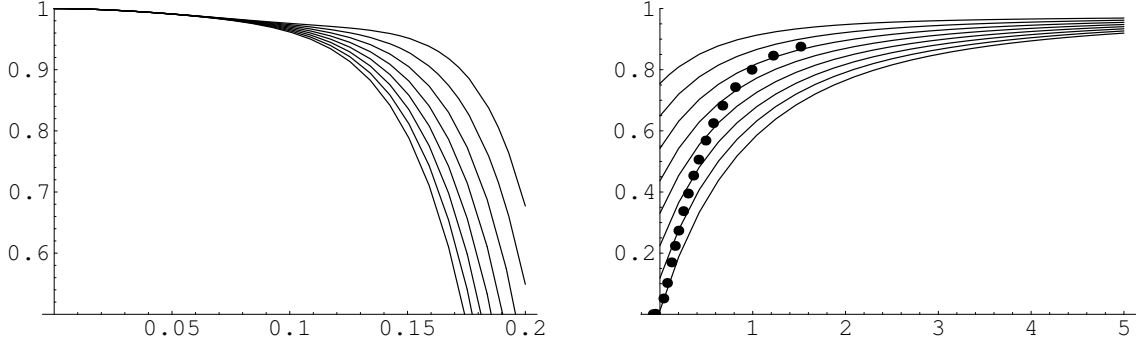
Figure 4.1: *Left panel:* The normalized QCD pressure $p_{\mathrm{QCD}}/p_{\mathrm{SB}}$ at $N_{\mathrm{f}} = 0$ plotted versus the effective coupling $\tilde{g}$ from Eq. (4.40). The $\tilde{g}^6$ coefficient depends on an unknown parameter Δ as defined in Eq. (4.45), and the different curves correspond to choosing $\Delta = -2000$ (lowest curve) to $\Delta = +12000$, in steps of 2000. *Left panel:* The same, plotted versus $\ln \frac{T}{T_c}$. The black dots correspond to lattice data from [11].

Note that this coupling is explicitly scale independent to the order we are working, $\partial_{\ln \bar{\mu}^2} \tilde{g}^2 = \mathcal{O}(\tilde{g}^8)$. We now have the full pressure as a sum of its ultra-soft, soft and hard parts as

$$p_{\mathrm{QCD}} = d_A \pi^2 T^4 \left\{ 16 \hat{p}_{\mathrm{us}} + 16 \hat{p}_{\mathrm{s}} + \frac{1}{45} \hat{p}_{\mathrm{h}} \right\} , \tag{4.41}$$

$$\hat{p}_{\mathrm{us}} = \hat{g}_M^6 \left[8 \alpha_G \left(\ln \frac{N_c^2}{4 \pi \hat{g}_M^2} + 1 \right) + \frac{1}{3} + [\textbf{pert}] - [\textbf{nspt}] + [\textbf{non-pert}] \right] , \tag{4.42}$$

$$\hat{p}_{\mathrm{s}} = \hat{m}_E^3 \frac{1}{3} + \hat{g}_E^2 \hat{m}_E^2 \left[\ln(2 \hat{m}_E) - \frac{3}{4} \right] + \hat{g}_E^4 \hat{m}_E \left[-\frac{89}{24} - \frac{\pi^2}{6} + \frac{11}{6} \ln 2 \right]$$

$$+ \hat{g}_E^6 \left[\beta_M - 8 \alpha_M \ln(2 \hat{m}_E) \right] + \hat{\lambda}_E^{(1)} \hat{m}_E^2 \frac{\hat{n} - 2}{4} + \hat{\lambda}_E^{(2)} \hat{m}_E^2 \frac{1 - 3\hat{n}}{4} , \tag{4.43}$$

$$\hat{p}_{\mathrm{h}} = \tilde{\alpha}_{\mathrm{E1}} + \tilde{g}^2 \tilde{\alpha}_{\mathrm{E2}} + \tilde{g}^4 \left[\tilde{\alpha}_{\mathrm{E3}} - 180 \tilde{\alpha}_{\mathrm{E5}} \right]$$

$$+ \tilde{g}^6 \left[\tilde{\beta}_{\mathrm{E1}} - 180 \left(\tilde{\beta}_{\mathrm{E2}} + \tilde{\alpha}_{\mathrm{E4}} \tilde{\beta}_{\mathrm{E3}} + \tilde{\alpha}_{\mathrm{E5}} \tilde{\alpha}_{\mathrm{E7}} \right) \right] . \tag{4.44}$$

The g^6 coefficient of p_{QCD} hence depends on a constant

$$\Delta \equiv \tilde{\beta}_{\mathrm{E1}} \pm 720 \delta_{\mathrm{NP}} \pm 384.826 \delta_{\mathrm{NSPT}} , \tag{4.45}$$

where we recall that $\tilde{\beta}_{\mathrm{E1}}$ stands for the result of the open 4-loop computation, and the δ parameterize the error-bars of the numerical constants from Eqs. (4.3,4.13) as $[10.7 \pm \delta_{\mathrm{NP}}]$ and $[30 \pm \delta_{\mathrm{NSPT}}]$, respectively. Assuming that the NSPT computation will finally have an error-bar of about 2%, which is comparable in precision to the lattice error-bar $\delta_{\mathrm{NP}} = 0.4$, $\Delta = \tilde{\beta}_{\mathrm{E1}} \pm 600$. In the following, we will for simplicity set $\delta_{\mathrm{NP}} = \delta_{\mathrm{NSPT}} = 0$, remembering the induced error-bar on $\tilde{\beta}_{\mathrm{E1}}$. Using the same coupling as in p_{h}, the above matching conditions

now read

$$\hat{m}_E^2 = \tilde{g}^2 \tilde{\alpha}_{E4} + \tilde{g}^4 \tilde{\alpha}_{E6} + \mathcal{O}(\tilde{g}^6), \tag{4.46}$$

$$\hat{g}_E^2 = \tilde{g}^2 + \tilde{g}^4 \tilde{\alpha}_{E7} + \tilde{g}^6 \tilde{\gamma}_{E1} + \mathcal{O}(\tilde{g}^8), \tag{4.47}$$

$$\hat{\lambda}_E^{(1)} = \tilde{g}^4 4 + \mathcal{O}(\tilde{g}^6), \tag{4.48}$$

$$\hat{\lambda}_E^{(2)} = \tilde{g}^4 \frac{4}{3}(1-z) + \mathcal{O}(\tilde{g}^6). \tag{4.49}$$

We would now like to plot the result for p_{QCD}. Identifying the non-interacting (ideal-gas; Stefan-Boltzmann) limit as $p_{\mathrm{SB}} = d_A T^4 \frac{\pi^2}{45} \tilde{\alpha}_{E1}$, we could display the normalized pressure $p_{\mathrm{QCD}}/p_{\mathrm{SB}}$ as a function of the coupling $\tilde{g}$, for fixed N_{f}. This is done in the left panel of Fig. 4.1, at $N_{\mathrm{f}} = 0$ and for various Δ. Our goal, however, should be to try to make contact to existing lattice determinations of the full pressure, where typically $p_{\mathrm{QCD}}/p_{\mathrm{SB}}$ is given as a function of T/T_c. Continuum-extrapolated lattice data exist for $N_{\mathrm{f}} = 0$ only, so in the following we will restrict to this special case. Aiming for this rather phenomenological comparison, we evidently need to make some choices, specified below.

We use the running 4d coupling from the exact solution of the 2-loop RGE equation,

$$\hat{g}^2(\bar{\mu}) = \frac{-\hat{\beta}_0/\hat{\beta}_1}{1 + W_{-1}\left(-\frac{\hat{\beta}_0^2}{\hat{\beta}_1} \exp\left[-1 - 2\frac{\hat{\beta}_0^2}{\hat{\beta}_1}\left(L + \ln\frac{4\pi T}{\Lambda_{\overline{\mathrm{MS}}}}\right)\right]\right)}. \tag{4.50}$$

Here, $W_{-1}(z)$ is one of the two real branches of the Lambert W function (see e.g. [40] and the left panel of Fig. 4.2; $W(z)$ is the function that satisfies $W \exp(W) = z$). Note that the above solution entails two choices: The branch of the W-function and the integration constant were chosen in accord with asymptotic freedom (note that the argument of W $\to 0^-$ for $\bar{\mu} \to \infty$) and the 'usual' definition of $\Lambda_{\overline{\mathrm{MS}}}$ (being the absence of a $1/\ln^2 \bar{\mu}$ term in the asymptotic expansion of $\hat{g}(\bar{\mu})$ at large $\bar{\mu}$). Indeed, at large $\hat{L} = \ln\frac{\bar{\mu}}{\Lambda_{\overline{\mathrm{MS}}}}$ the expansion $W_{-1}(-\epsilon) = \ln\epsilon - \ln\ln\frac{1}{\epsilon} + \mathcal{O}(1/\ln\epsilon)$ reproduces $\hat{g}^2(\bar{\mu}) = 1/(2\hat{\beta}_0\hat{L} + \frac{\hat{\beta}_1}{\hat{\beta}_0}\ln(2\hat{L}) + \mathcal{O}(\hat{L}^{-1})) = \frac{1}{2\hat{\beta}_0\hat{L}} - \frac{\hat{\beta}_1\ln(2\hat{L})}{4\hat{\beta}_0^3\hat{L}^2} + \mathcal{O}(\hat{L}^{-3})$, in accord with e.g. Ref. [41].

Although in principle all dependence on the renormalization scale $\bar{\mu}$, entering through L, is of higher order, in practice we need to fix it once we need numerical values for the coupling $\tilde{g}$. Following **[YS11]**, we choose the scale $\bar{\mu}$ by the principle of minimal sensitivity applied to the 1-loop result for $\hat{g}_E^2$, and then estimate the scale-dependence by a variation of a factor of $\delta_\mu = [0.8..2.0]$ around this $\bar{\mu}_{\mathrm{opt}}$, obtaining $L = -\frac{\tilde{\alpha}_{E7}}{2\hat{\beta}_0} + \ln\frac{\bar{\mu}}{\bar{\mu}_{\mathrm{opt}}}$. The slightly asymmetric choice of δ_μ here reflects the fact that the 1-loop $\hat{g}_E^2$ falls off more steeply on one side of the plateau than on the other.

To compare with continuum-extrapolated lattice data [11], we use $\frac{T_c}{\Lambda_{\overline{\mathrm{MS}}}} = 1.22\,\delta_{T_c}$ where $\delta_{T_c} = [0.9..1.1]$ encompasses the central values and error bars of estimates of this quantity
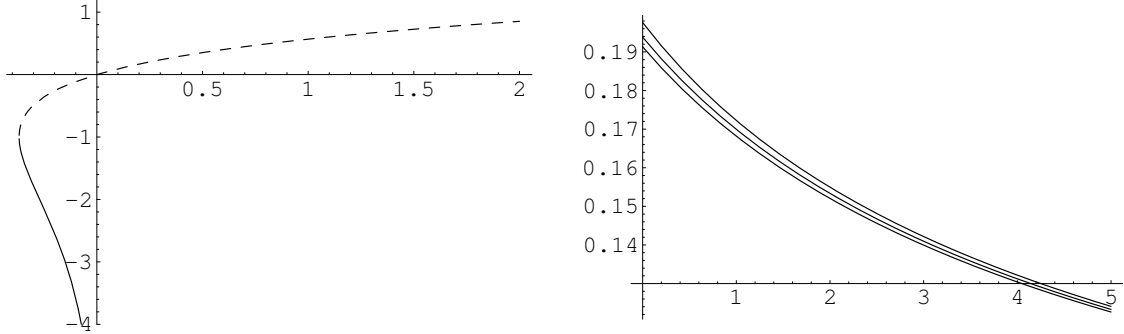
Figure 4.2: *Left panel:* The two real branches of $W(z)$ versus z. The upper (dashed) branch is $W_0(z)$, the lower (solid) branch is $W_{-1}(z)$. *Right panel:* The effective coupling $\tilde{g}$ from Eq. (4.40) plotted versus $\ln \frac{T}{T_c}$, using the choices explained in Sec. 4.4. The upper/lower curve corresponds to the uncertainty in scale choice stemming from fixing $\bar{\mu}$ and determining $T_c/\Lambda_{\overline{\text{MS}}}$ with $(\delta_\mu, \delta_{T_c}) = (2.0, 0.9)/(0.8, 1.1)$, the bigger effect coming from the latter parameter.

from different lattice collaborations (for a summary of the different methods and results, see **[YS11]**). This would translate into a horizontal error bar for the lattice data when plotted against $T/\Lambda_{\overline{\text{MS}}}$.

In the right panel of Fig. 4.2, we have plotted the effective coupling $\tilde{g}$ as defined in Eq. (4.40), converted to a function of $\ln \frac{T}{T_c}$. Note that its value is smaller than 0.2 even at T_c.

The normalized pressure $p_{\text{QCD}}/p_{\text{SB}}$, converted to a function of $\ln \frac{T}{T_c}$ along the lines above, is displayed in the right panel of Fig. 4.1. For comparison, the continuum-extrapolated lattice data of Ref. [11] has been included as black dots. The figure suggests a value for the $N_{\text{f}} = 0$ coefficient of the unknown constant $\tilde{\beta}_{\text{E}1}$, $\#_0 \approx 8500 \pm 600$, bearing in mind the error bar defined in Eq. (4.45).

4.5 Outlook

We have currently no idea what the 4-loop hard-scale coefficient $\tilde{\beta}_{\text{E}1}$ is, even though it can be computed diagrammatically. As already mentioned above, it should be a polynomial in $z = N_{\text{f}}/N_{\text{c}}$, $\tilde{\beta}_{\text{E}1} = \#_0 + z\#_1 + z^2\#_2 + z^3\#_3$, where only a single (ring) diagram contributes to $\#_3$, suggesting it as the first test-case for 4-loop sum-integral technology.

It seems possible to give an estimate of the highest-N_{f} contribution to $\tilde{\beta}_{\text{E}1}$ from the large-N_{f} solution for the pressure, since terms of order $g^6 N_{\text{f}}^3$ originate from the hard-

scale pressure p_{E} only. In [42] this was attempted by fitting the numerically known exact large-N_{f} pressure with a polynomial in g. This results in $\#_3 = \frac{45}{8\pi^2}[+20(2)] - \frac{20}{9}\ln 2\left(1 + 12\gamma_0 - \frac{364}{5}\ln 2 + 16Z_1 - 8Z_3\right) \approx [+36(1)]$, where the terms proportional to $\ln 2$ originate from translating the choice of renormalization scale $\bar{\mu} = \pi T$ of [42] to our definition of $\tilde{\beta}_{\mathrm{E}1}$, where powers of $L = \ln\frac{\bar{\mu}}{4\pi T}$ were subtracted out.

Furthermore, fitting the full g^6 pressure at $N_{\mathrm{f}} = 0$ and $N_{\mathrm{c}} = 3$ to lattice data around $4T_c$ [11] suggests a value $\#_0 \approx 8500 \pm 600$, if one takes the conjecture for granted that all higher-order corrections sum up to a subdominant contribution. There is no guarantee whatsoever that this conjecture holds, making a perturbative computation of the $\#_i$ unavoidable. We take the above check against the lattice data as indication that the effective theory setup has a chance to analytically describe the transition from temperatures as low as a few times T_c to infinite temperatures, in terms of computable corrections to the ideal-gas limit.

Chapter 5

Presentation of the papers
with identification of own contributions

- **[YS1] Resumming Long-Distance Contributions to the QCD Pressure**

In this paper, we propose a method for summing the slowly convergent perturbative series for the QCD pressure by employing numerical lattice Monte Carlo techniques within EQCD. The idea is to perform a lattice measurement of the adjoint Higgs condensates $\langle \mathrm{Tr}\, A_0^2 \rangle$ and $\langle (\mathrm{Tr}\, A_0^2)^2 \rangle$ along a line in the EQCD parameter space that corresponds to keeping 4d physics fixed. This has to be supplemented with two perturbative computations of those condensates, in lattice and continuum regularization schemes, respectively, allowing then for taking the continuum limit, and for subtracting out the scheme difference. Note that the condensates are nothing but different derivatives of the EQCD pressure, making it possible to integrate back to the pressure.

While this "derivative method" is employed in 4d simulations of the full pressure as well, there is an important conceptual difference: while in 4d, the integration constant is fixed to be zero at some small temperature, hence introducing an ambiguity (which is numerically small however), we can fix the 3d integration constant perturbatively at very high temperature, in principle to arbitrary precision. In practice, there remains sensitivity to unknown higher-order coefficients in that integration constant of course, which can (and do) become relevant when they are evolved to lower temperatures.

Having the status of a proof of principle, this paper offers a number of possible extensions, such as including higher-order perturbative corrections, and/or other condensates, which will hopefully be attacked in the near future.

My main contribution to the project was on the perturbative and the conceptual sector,

while I was not involved in the lattice simulation part.

- **[YS2] Simple way to generate high order vacuum graphs**

The enumeration of Feynman diagrams contributing to a specific loop order together with a derivation of the accompanying symmetry factors seems to be the 'trivial' part of any perturbative calculation. At higher orders, it is our experience however that an efficient algorithmic setup of this initial step proves necessary. This does not only assure completeness of the required set of diagrams, but it also has the potential of streamlining the subsequent integration step considerably by grouping together sets of related diagrams, thereby avoiding an unnecessary repetition of subdiagram computations.

The main idea is to utilize the very efficient notion of skeleton (2-particle-irreducible, 2PI) diagrams to achieve the above-mentioned grouping (into so-called *skeleton* and *ring* diagrams). For simplicity, let us explain the main point using a generic bosonic $\phi^3 + \phi^4$ theory here. The skeleton expansion for the free energy as a functional of the full propagator D reads

$$-F[D] = -\frac{1}{2}\left(\operatorname{Tr}\ln D^{-1} + \operatorname{Tr}\Pi[D]D\right) + \Phi[D] \ .$$

Here $\Phi[D]$ collects all 2PI vacuum diagrams. The full propagators D are related to their corresponding self-energies by $D^{-1} = \Delta^{-1} - \Pi$ where Δ are the free propagators. The partition function has an extremal property, such that the variation of F with respect to the full propagator vanishes, giving a relation between skeletons and self-energies, $\partial_D \Phi[D] = \frac{1}{2}\Pi[D]$. Pictorially, this corresponds to obtaining a self-energy by "cutting a propagator" in all possible ways in the set of vacuum skeletons. Hence, knowing the skeletons alone provides full information.

In this paper, we have succeeded in giving a closed formula from which all skeletons can be generated. This is most useful for an algorithmic implementation, and even systematizes the generation of combinatorical ("symmetry") factors in an efficient way.

I was involved in all levels of this project.

- **[YS3] Automatic reduction of four-loop bubbles**

In this paper, I report on an implementation of an algorithm that reduces two generic classes of (up to) four-loop vacuum Feynman integrals to a small number of so-called master integrals. To be more explicit, these classes are single-mass-scale scalar momentum integrals, whose integrands consist of products of either fully massive scalar progagators $1/(p^2 + m^2)$, or of a mixture of massive and massless propagators.

While the general method, relying on integration by parts and lexicographic ordering, is much more flexible, these specific examples have been chosen since they are precisely the

structures that arise in the two effective theories EQCD and MQCD. For both classes, I have identified the relevant master integrals, opening the way to tackle this important set of integrals in realistic higher-loop calculations.

I am the only author of this paper.

- **[YS4] Pressure of hot QCD up to $g^6 \ln(1/g)$**

In this paper, we report on the successful calculation of the highest coefficient for the QCD pressure that can be computed in perturbation theory alone. It corresponds to the logarithmically enhanced four-loop contributions. This computation combines a number of different highly technical steps (such as higher-order vacuum diagram generation, automatized algebra, reduction to master integrals, and actual analytic evaluation of the latter) for the first time, in a physically relevant setup. Most of the details are given in the other papers discussed here.

Phenomenologically, the result gives very encouraging hints that the effective theory setup does indeed have a chance to correctly describe the pressure in a huge temperature interval, once the full order $\mathcal{O}(g^6)$ is known.

I assumed a key role in most calculations needed for the realization of this project.

- **[YS5] Four–loop vacuum energy density of the SU(N_c) + adjoint Higgs theory**

Here, we give details about a well-defined subset of the calculation needed in the previous paper. We provide explicit expressions for the vacuum energy density of EQCD, and not only enumerate the EQCD parameters that will be needed for the full $\mathcal{O}(g^6)$ of the QCD pressure, but also give most of them in an analytic form.

Furthermore, we discuss the evaluation of master integrals in an expansion around $d = 3 - 2\epsilon$ dimensions in quite some detail, providing formulae which are useful for a more generic set of massive integrals than the specific ones we encountered in this concrete calculation.

I assumed a key role in most calculations needed for the realization of this project.

- **[YS6] Tackling the infrared problem of thermal QCD**

Here, I give details about a well-defined subset of the calculation needed in **[YS4]**. I discuss the steps that have been performed in order to get the MQCD contribution the the four-loop logarithmically enhanced terms in the QCD pressure.

While the generic techniques that were employed are in complete analogy to the those decribed above, I would like to highlight one very interesting point that occurred in the computation: While the final result for the overall divergence of the sum of all diagrams

seemed to contain finite parts of fully massive four-loop master integrals that are not yet known, checking the cancellation of the gauge parameter (in principle a 9th order polynomial) revealed one linear relation between those unknowns. This linear relation then in fact absorbed all unknowns from the final result.

I am the only author of this paper.

- **[YS7] High-precision evaluation of four-loop vacuum bubbles in three dimensions**

In this work, we employ an interesting and very generic method to numerically compute ϵ expansions of master integrals to – in principle – arbitrary depth and precision. We test this algorithm on the set of fully massive scalar vacuum integrals in 3d, which corresponds to the integrals needed for (the properly infrared-regularized version of) MQCD, and obtain many new coefficients.

The technique starts from deriving recurrence relations for suitably generalized master integrals, introducing one extra dimensionless parameter. To derive these recurrence relations, we use techniques analogous to those that were employed for the reduction step in earlier calculations. After formally solving a hierarchy of recurrence relations in terms of factorial series and computing a sufficient number of initial (or boundary) values, the infinite series representing each master integral can be truncated, and the remaining finite (but large) number of terms can then be summed up numerically.

I was responsible for all but the last (numerical) part of this project.

- **[YS8] 3-d lattice Yang-Mills free energy to four loops**

Lattice perturbation theory can be useful to evaluate renormalization constants, and to match between lattice and continuum schemes, in order to permit incorporating lattice measurements into the (continuum) QCD pressure. Due to superrenormalizability, a 3d theory can actually be renormalized exactly, to all orders, by only computing a finite number of potentially divergent diagrams. To complete the renormalization program for the plaquette in 3d pure gauge theory, the four leading terms of its expansion around the continuum limit $(\beta = 2N_c/(ag^2) \to \infty)$ are actually needed,

$$\langle 1 - \Pi_P \rangle = \frac{c_1}{\beta} + \frac{c_2}{\beta^2} + \frac{c_3}{\beta^3} + \frac{c_4}{\beta^4} + \dots .$$

Doing a diagrammatic expansion in lattice regularization to this order seems to be a formidable problem.

Using the method of Numerical Stochastic Perturbation Theory (NSPT), however, allows to obtain numerical estimates for these coefficients, which might be sufficiently precise for

practical use. In this paper, we determine all four coefficients by this method, with an error that increases with the loop order, and reaches about 1.5% for c_4.

I played a rather minor role in this project, delivering perturbative (continuum) coefficients, and being more involved on the conceptual level. All numerical work originates from my collaborators.

- **[YS9] Plaquette expectation value and gluon condensate in three dimensions**

To obtain the non-perturbative contribution to the QCD pressure, we perform lattice measurements in MQCD. The observable we consider here is the elementary plaquette expectation value. As already mentioned above, the theory being super-renormalisable, one can match the lattice regularization scheme exactly to the continuum $(\overline{\text{MS}})$ scheme. This requires a perturbative 4-loop computation on the lattice which, unfortunately, has not been completed yet. Knowing all the divergences, we could however already perform a stable continuum limit, getting a result that awaits the perturbative coefficient.

I played a minor role only in this project, since I was not involved in the large-scale numerical simulations that formed the core of it.

- **[YS10] Two-loop static QCD potential for general colour state**

This paper summarizes a non-trivial 4d calculation, which could interestingly be performed by a generalization of the techniques that were discussed above in the framework of dimensionally reduces effective theories.

As a result, while checking an older result for the static singlet potential, we were able to obtain a new coefficient for the octet case at the two-loop level.

I assumed a key role in most calculations needed for the realization of this project.

- **[YS11] Two-loop QCD gauge coupling at high temperatures**

We determine new coefficients for two of the matching coefficients that occur in the dimensional reduction step from QCD to EQCD, via a systematic expansion in the gauge coupling. Some of the obtained coefficients contribute to the $\mathcal{O}(g^6)$ part of the pressure, and hence represent further building blocks on the road to this level of precision.

Knowing the relation between QCD and EQCD gauge couplings to this precision actually allows to assess the performance of the effective theory setup by comparing predictions for the spatial string tension to 4d lattice measurements of the same quantity. We find good agreement, down to surprisingly low temperatures.

I was involved in all parts of this project.

- **[YS12] High-precision epsilon expansions of single-mass-scale four-loop vacuum bubbles**

Following the same strategy employed already in the 3d paper **[YS7]**, we now obtain numerical results for expansions of master integrals in four dimensions. We treat a larger class of integrals here, to set the stage for actual four-loop computations in the framework of Standard Model precision tests. As a service to the community, we furthermore collect all results that are known analytically, making them available in computer-readable form as well.

As an amusing twist, we even used the integer-relation finding algorithm PSLQ combined with educated guesses about the number content of certain integrals, to uncover analytical values from our high-precision numerics. Most of these new analytical values have now been proven to be correct by completely orthogonal methods.

I was responsible for all but the numerical part of this project.

- **[YS13] Four-loop singlet contribution to the electroweak rho parameter**

The electroweak ρ parameter measures the relative strengths of the charged and neutral currents. Being a parameter vital for precision tests of the Standard Model, we have determined a (gauge-invariant) subset of four-loop contributions. The choice of our class of diagrams is motivated by the relatively large contribution of the corresponding set at the 3-loop level.

Again, we were able to use all the computational technology outlined above even in this 4d setting. As a result, we find a satisfyingly small correction to the ρ parameter, signalling good convergence of the perturbative series.

I assumed a key role in most calculations needed for the realization of this project, except for the diagram generation step.

- **[YS14] Four-loop plaquette in 3d with a mass regulator**

This paper documents a generalization of the above Ref. **[YS8]**. Aiming at fully incorporating MQCD into the QCD pressure, note that there is a small twist: In the absence of sufficient infrared screening of the 3d gluonic fields, for technical reasons a mass term had to be introduced into the continuum calculation, cf. **[YS6]**. Hence, to cancel the induced effect, the perturbative matching computation on the lattice side has to be performed with exactly the same regulator.

Hence, we demonstrate that NSPT is capable of dealing with a massive regulator. While we analyze data up to the three-loop level only, it becomes clear that, given a sufficient amount of computing time, the four-loop result that is needed to match the continuum scheme in MQCD can be obtained with this method.

Again, my role in this project was delivering perturbative (continuum) coefficients, and being involved on the conceptual level.

- **[YS15] Four-Loop decoupling relations for the strong coupling**

The strong coupling constant α_s is a most fundamental parameter in the Standard Model. Its precise value as well as scale dependence are vitally important for many theoretical predictions. To incorporate effects of heavy quarks into its running, it is convenient to define matching (or decoupling) parameters, which arise from comparing an effective $(N_f - 1)$-quark theory with the original one. As usual, this matching can be performed accurately in perturbation theory.

Like above, we could make use of our reduction and integration techniques, enabling us to write down an analytic value for the four-loop correction to the decoupling constant for α_s.

I assumed a key role in most calculations needed for the realization of this project, except for the diagram generation step.

- **[YS16] Quark mass thresholds in QCD thermodynamics**

We derive two-loop expressions for some of the coefficients entering the QCD pressure in the effective theory setup, including quark masses m_i and chemical potentials μ_i. Our results can be given in terms of a minimal set of basic integrals, which in certain limits like $T \rightarrow 0$ or $m_i \rightarrow 0$ reduce to analytically known terms.

These general expressions then allow us to give phenomenological results for thermodynamic quantities for QCD and the Standard Model, accounting correctly for physical quark mass effects.

I was involved in most calculations needed for the realization of this project.

Bibliography

[1] K. N. Abazajian and G. M. Fuller, Phys. Rev. D **66** (2002) 023526;
M. Hindmarsh and O. Philipsen, Phys. Rev. D **71** (2005) 087302.

[2] U. W. Heinz, AIP Conf. Proc. **739** (2005) 163 [nucl-th/0407067].

[3] E. V. Shuryak, Sov. Phys. JETP **47** (1978) 212;
S. A. Chin, Phys. Lett. B **78** (1978) 552.

[4] J. I. Kapusta, Nucl. Phys. B **148** (1979) 461.

[5] T. Toimela, Phys. Lett. B **124** (1983) 407.

[6] P. Arnold and C. X. Zhai, Phys. Rev. D **50** (1994) 7603; *ibid.* **51** (1995) 1906.

[7] C. X. Zhai and B. M. Kastening, Phys. Rev. D **52** (1995) 7232.

[8] A. D. Linde, Phys. Lett. B **96** (1980) 289;
D. J. Gross, R. D. Pisarski and L. G. Yaffe, Rev. Mod. Phys. **53** (1981) 43.

[9] J. P. Blaizot, E. Iancu and A. Rebhan, Phys. Rev. D **68** (2003) 025011;
G. Cvetič and R. Kögerler, Phys. Rev. D **70** (2004) 114016;
M. Inui, A. Niegawa and H. Ozaki, Prog. Theor. Phys. **115** (2006) 411.

[10] U. Kraemmer and A. Rebhan, Rept. Prog. Phys. **67** (2004) 351.

[11] G. Boyd, J. Engels, F. Karsch, E. Laermann, C. Legeland, M. Lütgemeier and B. Petersson, Nucl. Phys. B **469** (1996) 419.

[12] B. Beinlich, F. Karsch, E. Laermann and A. Peikert, Eur. Phys. J. C **6** (1999) 133;
M. Okamoto *et al.* [CP-PACS Collaboration], Phys. Rev. D **60** (1999) 094510;
Y. Namekawa *et al.* [CP-PACS Collaboration], Phys. Rev. D **64** (2001) 074507;
R. V. Gavai, S. Gupta and S. Mukherjee, Phys. Rev. D **71** (2005) 074013.

[13] F. Karsch, E. Laermann and A. Peikert, Phys. Lett. B **478** (2000) 447;
     A. Ali Khan *et al.* [CP-PACS collaboration], Phys. Rev. D **64** (2001) 074510;
     C. Bernard *et al.*, PoS **LAT2005** (2005) 156;
     Y. Aoki, Z. Fodor, S. D. Katz and K. K. Szabo, JHEP **01** (2006) 089;
     S. Ejiri, F. Karsch, E. Laermann and C. Schmidt, Phys. Rev. D **73** (2006) 054506.

[14] E. Laermann and O. Philipsen, Ann. Rev. Nucl. Part. Sci. **53** (2003) 163.

[15] P. H. Ginsparg, Nucl. Phys. B **170** (1980) 388;
     T. Appelquist and R. D. Pisarski, Phys. Rev. D **23** (1981) 2305.

[16] K. Kajantie, M. Laine, K. Rummukainen and M. E. Shaposhnikov, Nucl. Phys. B **458** (1996) 90.

[17] E. Braaten and A. Nieto, Phys. Rev. D **51** (1995) 6990.

[18] A. Vuorinen, Phys. Rev. D **67** (2003) 074032; *ibid.* **68** (2003) 054017.

[19] J. A. M. Vermaseren, math-ph/0010025.

[20] K. G. Chetyrkin and F. V. Tkachov, Nucl. Phys. B **192** (1981) 159;
     F. V. Tkachov, Phys. Lett. B **100** (1981) 65.

[21] S. Laporta, Int. J. Mod. Phys. A **15** (2000) 5087.

[22] F. Di Renzo and L. Scorzato, JHEP **0410** (2004) 073.

[23] M. Steinhauser, Phys. Rept. **364** (2002) 247.

[24] M. J. G. Veltman, Nucl. Phys. B **123** (1977) 89.

[25] K. G. Chetyrkin, B. A. Kniehl and M. Steinhauser, Nucl. Phys. B **510** (1998) 61.

[26] E. Braaten and A. Nieto, Phys. Rev. Lett. **76** (1996) 1417; Phys. Rev. D **53** (1996) 3421.

[27] E. S. Fraga and P. Romatschke, Phys. Rev. D **71** (2005) 105014.

[28] C. P. Korthals Altes, R. D. Pisarski and A. Sinkovics, Phys. Rev. D **61** (2000) 056007;
     J. P. Blaizot, E. Iancu and A. Rebhan, Phys. Lett. B **523**, 143 (2001);
     A. Hart, M. Laine and O. Philipsen, Nucl. Phys. B **586** (2000) 443;
     A. Ipp, K. Kajantie, A. Rebhan and A. Vuorinen, hep-ph/0604060.

[29] A. Gynther and M. Vepsäläinen, JHEP **01** (2006) 060; *ibid.* **03** (2006) 011.

[30] U. M. Heller and F. Karsch, Nucl. Phys. B **251** (1985) 254.

[31] K. Farakos, K. Kajantie, K. Rummukainen and M. E. Shaposhnikov, Nucl. Phys. B **442** (1995) 317.

[32] M. Laine and A. Rajantie, Nucl. Phys. B **513** (1998) 471.

[33] H. Panagopoulos, A. Skouroupathis and A. Tsapalis, Phys. Rev. D **73** (2006) 054511.

[34] C. Torrero, PhD thesis 2006, Parma University, Italy (unpublished).

[35] Y. Schröder, unpublished.

[36] K. Farakos, K. Kajantie, K. Rummukainen and M. E. Shaposhnikov, Nucl. Phys. B **425** (1994) 67.

[37] P. Giovannangeli, Phys. Lett. B **585** (2004) 144; Nucl. Phys. B **738** (2006) 23.

[38] S. z. Huang and M. Lissia, Nucl. Phys. B **438** (1995) 54; *ibid.* **480** (1996) 623.

[39] Y. Schröder, hep-ph/0410130.

[40] R. M. Corless, G. H. Gonnet, D. E. G. Hare, D. J. Jeffrey, and D. E. Knuth, *On the Lambert W Function*, Advances in Computational Mathematics, volume 5, 1996, pp. 329–359.

[41] S. Eidelman *et al.* [Particle Data Group], Phys. Lett. B **592** (2004) 1.

[42] A. Ipp and A. Rebhan, JHEP **0306** (2003) 032.

Chapter 7

Full list of own publications

Refereed Journal Articles

[R14] *Quark mass thresholds in QCD thermodynamics*
with M. Laine,
Phys. Rev. **D** (2006), in print (May 2006 issue).

[R13] *Four-Loop decoupling relations for the strong coupling*
with M. Steinhauser,
JHEP **0601** (2006) 051.

[R12] *Four-loop singlet contribution to the electroweak rho parameter*
with M. Steinhauser,
Phys. Lett. **B 622** (2005) 124.

[R11] *High-precision epsilon expansions of single-mass-scale four-loop vacuum bubbles*
with A. Vuorinen,
JHEP **0506** (2005) 051.

[R10] *Two-loop QCD gauge coupling at high temperatures*
with M. Laine,
JHEP **0503** (2005) 067.

[R9] *Two-loop static QCD potential for general colour state*
with B. A. Kniehl, A. A. Penin, V. A. Smirnov and M. Steinhauser,
Phys. Lett. **B 607** (2005) 96.

[R8] *Plaquette expectation value and gluon condensate in three dimensions*
     with A. Hietanen, K. Kajantie, M. Laine, K. Rummukainen,
     JHEP **0501** (2005) 013.

[R7] *3-d lattice Yang-Mills free energy to four loops*
     with F. Di Renzo, A. Mantovi, V. Miccio,
     JHEP **0405** (2004) 006.

[R6] *Four–loop vacuum energy density of the $SU(N_c)$ + adjoint Higgs theory*
     with K. Kajantie, M. Laine, K. Rummukainen,
     JHEP **0304** (2003) 036.

[R5] *Pressure of hot QCD up to $g^6 \ln(1/g)$*
     with K. Kajantie, M. Laine, K. Rummukainen
     Phys. Rev. **D 67** (2003) 1050008.

[R4] *Simple way to generate high order vacuum graphs*
     with K. Kajantie, M. Laine,
     Phys. Rev. **D 65** (2002) 045008.

[R3] *Resumming Long-Distance Contributions to the QCD Pressure*
     with K. Kajantie, M. Laine, K. Rummukainen,
     Phys. Rev. Lett. **86** (2001) 10.

[R2] *The static potential in QCD to two loops*
     Phys. Lett. **B 447** (1999) 321.

[R1] *Thermal variational principle and gauge fields*
     with H. Schulz,
     Phys. Rev. **D 54** (1996) 7677.

Proceedings and Preprints

[P17] *Weak-coupling expansion of the hot QCD pressure*
      Johns Hopkins workshop 05, PoS JHW2005:029,2006.

[P16] *Four-loop plaquette in 3d with a mass regulator*
      with C. Torrero, F. Di Renzo, V. Miccio, M. Laine,
      Lattice 05, PoS LAT2005:189,2005.

[P15] *Non-perturbative plaquette in 3d pure SU(3)*
with A. Hietanen, K. Kajantie, M. Laine, K. Rummukainen,
Lattice 05, PoS LAT2005:174,2005.

[P14] *Spatial string tension revisited*
with M. Laine,
Lattice 05, PoS LAT2005:180,2005.

[P13] *Evading the infrared problem of thermal QCD*
in: K. Eskola, K. Kainulainen, K. Kajantie, K. Rummukainen (eds.), Strong and Elec-
troweak Matter 04 (World Scientific, 2004).

[P12] *3-d lattice SU(3) free energy to four loops*
with F. Di Renzo, A. Mantovi, V. Miccio, C. Torrero,
Lattice 04, Nucl. Phys. Proc. Suppl. **140** (2005) 586.

[P11] *High-precision evaluation of four-loop vacuum bubbles in three dimensions*
with A. Vuorinen,
arXiv:hep-ph/0311323.

[P10] *Tackling the infrared problem of thermal QCD*
Lattice 03, Nucl. Phys. Proc. Suppl. **129** (2004) 572.

[P9] *Four–loop stochastic perturbation theory in 3d SU(3)*
with F. Di Renzo, A. Mantovi, V. Miccio,
Lattice 03, Nucl. Phys. Proc. Suppl. **129** (2004) 590.

[P8] *The pressure of Hot QCD*
in: H. M. Fried, B. Müller and Y. Gabellini, proceedings of the seventh QCD workshop,
Villefranche, 2003.

[P7] *Automatic reduction of four-loop bubbles*
RADCOR 02, Nucl. Phys. Proc. Suppl. **116** (2003) 402.

[P6] *Four–loop logarithms in 3-D Gauge+Higgs theory*
with K. Kajantie, M. Laine, K. Rummukainen,
Lattice 02, Nucl. Phys. Proc. Suppl. **119** (2003) 577.

[P5] *Long–distance contributions to the QCD pressure*
Statistical QCD, Nucl. Phys. **A 702** (2002) 123.

[P4] *Measuring infrared contributions to the QCD pressure*
with K. Kajantie, M. Laine, K. Rummukainen,
Lattice 01, Nucl. Phys. Proc. Suppl. **106** (2002) 525.

[P3] *The Free Energy of Hot QCD*
Quark Matter 01, Nucl. Phys. **A 698** (2002) 448.

[P2] *The Two-Loop Static Potential*
QCD 99, Nucl. Phys. Proc. Suppl. **86** (2000) 525.

[P1] *The static potential in QCD$_3$ at one loop*
in: F. Csikor and Z. Fodor (eds.), Strong and Electroweak Matter 97,
(World Scientific, 1998).

Theses

[T2] *The static potential in QCD*
Doctoral thesis, DESY-Thesis-1999-021, June 1999.
`http://www-library.desy.de/cgi-bin/showprep.pl?desy-thesis99-021`

[T1] *Gluon–Plasma und thermisches Variationsverfahren*
(*Gluon–Plasma and the thermal variational principle*)
Diploma thesis (in German), Hannover U., May 1995.

Acknowledgments

Chapter 8

Curriculum vitae

Personal data

Name:	York Schröder
Date of birth:	July 5, 1968
Place of birth:	Celle (Germany)
Nationality:	German
Marital status:	Single
Present employer:	Faculty of Theoretical Physics, University of Bielefeld, Germany
Position:	Scientific Assistant (C1)
Previous employer:	Center for Theoretical Physics, MIT, Cambridge, U.S.A.
Previous position:	Senior Postdoctoral Associate, September 2001 – August 2004

Degrees

- **Deutsches Elektronen Synchrotron (DESY), Hamburg, Germany**
  Ph.D., Magna Cum Laude, DESY Theory Group, June 1999.
  Thesis: "The Static Potential in QCD".
  Advisor: Prof. Dr. W. Buchmüller.

- **University of Hannover, Germany**
  Diplom (Masters) in Physics, Department of Physics, June 1995.
  Thesis: "Gluon Plasma and Thermal Variational Principle".
  Advisor: Prof. Dr. H. Schulz.

- **University of Hannover, Germany**
  Vordiplom (Bachelor) in Physics, July 1991.

- **GTG Barsinghausen, Germany**
  Abitur (high school degree), June 1987.

Education

- **Postdoctoral research**
  2001–2004, senior post-doc at MIT/CTP (U.S.A.).
  1999–2001, EU TMR post-doc at Helsinki U. (Finland).
  1999, short-term post-doc at DESY (Germany).

- **Ph.D. studies**
  1995–1999, at Hamburg U./DESY (Germany).

- **University studies: Physics**
  1989–1995, at Hannover U. (Germany),
  Purdue U. (U.S.A.),
  ETH Zürich (Switzerland).

- **Civil service**
  1987–1989, education and work as a paramedic with 'Johanniter Unfallhilfe'.

- **Primary school and High school**
  1974–1987, in Gross Munzel, Kirchdorf and Barsinghausen (Germany).

Honors and Awards

- Fulbright fellow, Sep 1993 – Aug 1994.

- Fellowship of the German Academic Exchange Service (DAAD),
  Sep 1993 – Aug 1994.

8.1   Scientific expert tasks

- Representative for the Department of Physics, Bielefeld, at a major recruiting fair aimed at high-school seniors ("Einstieg Abi 2006") in Cologne, Germany

- Public talks for selected high-school students, Center for interdisciplinary studies (ZiF), Bielefeld, and Vlotho, Germany

- Public talks honoring the Einstein year 2005, in Bielefeld and in Rheda-Wiedenbrück, Germany

- Co-Organizer of the Hot QCD workshop at the ECT* Trento (with M. Laine), September 2005

- Co-Organizer of the MIT/CTP Nuclear Theory Seminar (with I. Stewart), 2003/2004

- meeting with the LNS Dean's Advisory Committee, November 2003

- Research presentations during the visits of the Department of Energy (D.O.E.) at MIT, May 2003 and July 2004

- Co-Organizer of the EU TMR meeting '*Phase transitions in hot matter*'
  in Helsinki (with K. Kajantie), April 2001

- Referee for Phys. Rev. D

8.2   External Funding ("Drittmittel")

- Sachbeihilfe (external funding) for research project
  "Precision Physics with Hot Quantum Chromo Dynamics",
  starting 2006 (together with M. Laine, Bielefeld U.).
  Granted by the DFG (German Research Foundation),
  including a 2-year BAT IIa post-doc position.

- Computing time on the ECT* Teraflop cluster Ben
  for the project "NSPT for 3d gauge theories",
  for 2005 and 2006 (30000 and 60000 CPU hours, respectively).
  Granted by the board of the ECT, Trento, Italy.

8.3 Teaching experience

- Introductory seminar on physics (Proseminar)
  Bielefeld University, spring semester 2006.
  See also `http://www.physik.uni-bielefeld.de/~yorks/`
  Level: Mandatory course (2h/week) for undergraduate students in their 4th semester.
  Content: In this seminar, each student is required to give an oral presentation about a topic connected to the grander theme "Milestones in modern physics". Topics cover a broad range of (mostly Nobel-price worthy) 20th century physics. My role is to set the stage by introducing all topics to be covered, and to guide students to give successful talks, which includes learning skills like efficient literature research, organizing comprehensible and entertaining presentations, and initiating scientific discussions.

- Lecture on Finite Temperature Field Theory
  Bielefeld University, fall semester 2005.
  See also `http://www.physik.uni-bielefeld.de/~yorks/`
  Level: Specialized lecture (2h/week) for graduate students and PhD students.
  Content: In this lecture, I introduced the subject of field theory at finite temperature. Building upon concepts from Quantum Mechanics and Statistical Mechanics, topics included path integrals, Greens functions, perturbative expansions, renormalization, infrared resummations, collective excitations, hard thermal loops. While the main vehicle to introduce various concepts was scalar field theory, full QCD was also covered in detail.

- Seminar on Elementary Particle Physics
  Bielefeld University, spring semester 2005.
  See also `http://www.physik.uni-bielefeld.de/~yorks/`
  Level: Optional course (2h/week) for graduate students.
  Content: In this seminar, each student was required to give an oral presentation about a modern problem in Elementary Particle Physics. My role was to give a 6-hour introduction into the Standard Model, key experimental efforts, and current research frontiers, and to motivate a number of topics that would form the backbones of the students' presentations. Furthermore, my role was to guide each student towards identifying key strategies to prepare for research talks on current topics, and to sharpen their presentation and scientific discussion skills.

- Elementary Particle Physics (exercise session)
  Bielefeld University, fall semester 2004.
  Level: Optional course (4h/week lecture + 2h/week exercise) for graduate students.

Content: For a theory-course covering topics from Relativistic Quantum Mechanics to the Standard Model, I led the weekly exercise session.

- Taming Feynman diagrams
  MIT, fall 2002.
  Level: Mini-course (4h total) for graduate and PhD students.
  Content: In this mini-course, I gave a pedagogical introduction into higher order perturbative calculations, introducing state-of-the-art algorithmic techniques for generation, reduction and computation of Feynman integrals.

- Lecture on Finite Temperature Field Theory
  Helsinki University, spring semester 2000.
  See also Physics Department library for lecture notes.
  Level: Specialized course (2h/week) for graduate students and PhD students.
  Content: See above (lecture at Bielefeld University, fall semester 2005).

- Theoretical Physics I: Mechanics (exercise session)
  Hannover University, fall semester 1994.
  Level: Core course (4h/week lecture + 2h/week exercise) for undergraduate students.
  Content: For a course on theoretical mechanics that covered the content of Landau and Lifshitz volume 1, I led the weekly exercise sessions, which included blackboard presentations as well as grading of homework problems.

- Course on Modern Physics (undergraduate, laboratory)
  Purdue University, fall/spring semesters 1992/93.
  Level: Mandatory laboratory course (3h/week) for undergraduate students.
  Content: This lab course covered key experiments of modern physics, including photoelectric effect, determination of the electron's e/m, X-ray diffraction and holograms. In each weekly session, my role was to give a 20 minute blackboard presentation of the theoretical background, to quiz the students on their prepared material, and then to guide each group in setting up and running the lab experiments. Furthermore, I was responsible for grading the lab writeups.

Chapter 9

Reprints of publications [YS1] – [YS16]

[YS1]

Resumming Long-Distance Contributions to the QCD Pressure

Resumming Long-Distance Contributions to the QCD Pressure

K. Kajantie,[1] M. Laine,[2,1] K. Rummukainen,[3,4] and Y. Schröder[1]

[1]*Department of Physics, P.O. Box 9, FIN-00014 University of Helsinki, Finland*
[2]*Theory Division, CERN, CH-1211 Geneva 23, Switzerland*
[3]*NORDITA, Blegdamsvej 17, DK-2100 Copenhagen Ø, Denmark*
[4]*Helsinki Institute of Physics, P.O. Box 9, FIN-00014 University of Helsinki, Finland*
(Received 13 July 2000)

The strict coupling constant expansion for the free energy of hot QCD plasma shows bad convergence at all reasonable temperatures, and does not agree well with its 4D lattice determination. This has recently led to various refined resummations, whereby the agreement with the lattice result should improve, at the cost of a loss of a formal agreement with the coupling constant expansion and particularly with its large infrared sensitive "long-distance" contributions. We show here how to resum the dominant long-distance effects by using a 3D effective field theory, and determine their magnitude by simple lattice Monte Carlo simulations.

Introduction.— At temperatures above 200 MeV, the properties of matter described by the laws of QCD are expected to change. The system should look more like a collection of free quarks and gluons than a collection of their bound states, such as mesons. It is a challenge to find observables which would clearly manifest this change, and hopefully also be directly or indirectly measurable in heavy ion collision experiments.

From the theoretical point of view, one of the simplest observables witnessing the change is the free energy of the plasma, or its pressure [1]. Indeed, according to the Stefan-Boltzmann law, the value of the free energy counts the number of light elementary excitations in the plasma, be they quarks and gluons, or mesons.

The reality is somewhat more complicated. Interactions change the Stefan-Boltzmann law, so that pressure is no longer proportional to the number of degrees of freedom. And in fact, interactions are strong. An explicit computation of the free energy to order $\mathcal{O}(g^5T^4)$ [2–4] shows that there are large corrections, with alternating signs, such that convergence is poor at any reasonable temperature. Of course, at least without light dynamical fermions, the full pressure can still be obtained with 4D finite temperature lattice simulations [1]. However, in order to really understand the properties of the QCD plasma phase, one should also have some analytical understanding of the origin of this result.

A way of at least understanding why the convergence is poor is the observation that, when $\alpha_s = g^2/(4\pi) \ll 1$, the system undergoes dimensional reduction [4–9], and its static long wavelength "soft" or "light" degrees of freedom can be described by a three-dimensional (3D) effective field theory,

$$\mathcal{L}_{3D} = \tfrac{1}{2}\mathrm{Tr}F_{ij}^2 + \mathrm{Tr}[D_i,A_0]^2 + m_D^2\,\mathrm{Tr}A_0^2 + \lambda_A(\mathrm{Tr}A_0^2)^2,$$

where $m_D^2 \sim g^2T^2$, $\lambda_A \sim g^4T$ are parameters computed perturbatively up to optimized next-to-leading-order level

(see below). This effective theory is confining, and therefore nonperturbative [10,11]. In [4], $\mathcal{L}_{3D}$ was used to reproduce the perturbative free energy up to order $\mathcal{O}(g^5T^4)$ [2,3], and the bad convergence was shown to be due precisely to these degrees of freedom.

Our objective here is to study the free energy of QCD by including the dominant, badly convergent contributions from $\mathcal{L}_{3D}$ nonperturbatively, to all orders, by using lattice Monte Carlo simulations. In this way, we can find out how important the combined effect of the badly convergent series really is in the free energy.

It is important to keep in mind that infrared sensitive effects can be different in various quantities. For instance, the free energy is dominated by ultraviolet degrees of freedom, and the long-distance effects we study here may turn out to be subdominant. Thus it would be wrong to conclude that any approach which manages to reproduce the numerical data for the free energy in a satisfactory way would also reproduce other quantities. A good testing ground for this is the longest static correlation lengths in the QCD plasma: they are fully nonperturbative, but it is already known that the results of 4D simulations [12] are reproduced precisely by the infrared degrees of freedom that we employ in $\mathcal{L}_{3D}$ [6,9,13].

The relation of our approach to the other recent approaches for the determination of the free energy of QCD [14–16] can be described as follows. At present, these approaches do not reproduce the known $\mathcal{O}(g^5T^4)$ result in the limit of a weak coupling, nor do they account for any genuine nonperturbative contributions. Thus large infrared effects are suppressed without an *a priori* justification; the justification comes *a posteriori* through the reasonable agreement with numerical data. Our results here attempt to provide a theoretical understanding of why the long-distance contributions need not be important in the QCD pressure.

Method.— The pressure or the free energy density of QCD is a quantity which formally gets contributions

from both short-distance physics $[l \lesssim (\pi T)^{-1}]$ and long-distance physics $[l \gtrsim (gT)^{-1}]$. The separation of the free energy into these two different types of contributions was discussed in detail in [4]. Interactions between the short- and long-distance modes account for the parameters of the effective long-distance theory $\mathcal{L}_{3D}$, and in addition there is an additive part coming directly from the short-distance modes, as we will presently specify.

To describe the effects of the short-distance modes in detail, we find it useful to introduce the dimensionless parameters $y = m_D^2/g_3^4$, $x = \lambda_A/g_3^2$, where g_3^2 is the gauge coupling within the effective theory. In terms of the physical parameters $T, \Lambda_{\overline{MS}}$ of QCD, next-to-leading-order "fastest apparent convergence" optimized perturbation theory tells that [9] (for a number of flavors, $N_f = 0$, and colors, $N_c = 3$),

$$\frac{g_3^2}{T} = \frac{8\pi^2}{11\ln(6.742\,T/\Lambda_{\overline{MS}})}, \tag{1}$$

$$x = \frac{3}{11\ln(5.371\,T/\Lambda_{\overline{MS}})}, \qquad y = \frac{3}{8\pi^2 x} + \frac{9}{16\pi^2}. \tag{2}$$

The result of [4], Eq. (36), can now be expressed as follows. Using the $\overline{MS}$ scheme with the scale parameter $\overline{\mu}_{3D}$, let us compute the dimensionless quantity

$$\mathcal{F}_{\overline{MS}}(x, y) = -\frac{1}{V g_3^6} \ln\left[\int \mathcal{D}A \exp\left(-\int d^3x\, \mathcal{L}_{3D}\right)\right], \tag{3}$$

where V is the volume. The pressure can then be expressed as (we have here again put $N_f = 0$, $N_c = 3$)

$$p(T) = p_0(T) \times \left[1 - \frac{5}{2}x - \frac{45}{8\pi^2}\left(\frac{g_3^2}{T}\right)^3 \times \left(\mathcal{F}_{\overline{MS}}(x, y) - 24\frac{y}{(4\pi)^2}\ln\frac{\overline{\mu}_{3D}}{T}\right)\right], \tag{4}$$

where $p_0(T) = (\pi^2 T^4/45)(N_c^2 - 1 + (7/4)N_c N_f)$ is the noninteracting Stefan-Boltzmann result. The $\overline{\mu}_{3D}$ dependence here is canceled by that in $\mathcal{F}_{\overline{MS}}(x, y)$.

A few comments on Eq. (4) are in order. First, the term proportional to y could also be written as $\sim \mathcal{O}(x^2)$, and at the present level of accuracy there is no unique way of making a distinction. We have chosen the present form because the relatively large logarithmic term is then dealt with in connection with $\mathcal{F}_{\overline{MS}}$, whereby cancellations occur. Second, strictly speaking, $\ln(\overline{\mu}_{3D}/T)$ should be replaced with $\ln(\overline{\mu}_{3D}/T) + \delta$, but $\delta = \gamma_E - \ln 2 - 41/2160 - (17/72)\ln 2\pi - (37/36)[\ln\zeta]'(2) + (19/72)[\ln\zeta]'(4) \approx 1.35 \times 10^{-4}$ can be ignored for all practical purposes. Finally, with the expressions available at present, the relation in Eq. (4) has an error starting at order $\mathcal{O}(g^6)$, corresponding to $\mathcal{O}[1/(4\pi)^4]$ within the parentheses. This correction is, however, from short-distance physics alone, and we shall ignore it here.

By using Eqs. (1), (2), and (4), the perturbative short-distance contribution to the pressure has been accounted for to a satisfactory level, and we are left with evaluating the long-distance part, $\mathcal{F}_{\overline{MS}}(x, y)$. The perturbative expression for $\mathcal{F}_{\overline{MS}}(x, y)$ is known up to the 3-loop level, corresponding to $\mathcal{O}(g^5 T^4)$ accuracy in $p(T)$. Adding terms involving the scalar self-interaction x to the result of [4], we can write

$$\frac{\mathcal{F}_{\overline{MS}}(x, y)}{d_A} = \frac{y^{3/2}}{4\pi}\left[-\frac{1}{3}\right] + \frac{y}{(4\pi)^2}\left[C_A\left(\frac{3}{4} - \frac{1}{2}\ln 4y + \ln\frac{\overline{\mu}_{3D}}{g_3^2}\right) + \frac{d_A + 2}{4}x\right]$$
$$+ \frac{y^{1/2}}{(4\pi)^3}\left[C_A^2\left(\frac{89}{24} - \frac{11}{6}\ln 2 + \frac{\pi^2}{6}\right) - C_A\frac{d_A + 2}{2}\left(\frac{1}{2} - \ln 4y\right)x + \frac{d_A + 2}{2}\left(\frac{10 - d_A}{4} - \ln 16y\right)x^2\right]$$
$$+ \frac{\Delta\mathcal{F}_{\overline{MS}}(x, y)}{d_A}, \tag{5}$$

where $d_A = N_c^2 - 1$, $C_A = N_c$, and $\Delta\mathcal{F}_{\overline{MS}}(x, y)$ accounts for the higher-order corrections. In terms of the 4D coupling constant, all contributions involving x in Eq. (5) are of order $\mathcal{O}(g^6)$ or higher, while the terms $\sim y^{3/2}$, $y\ln y$, $y^{1/2}$ are of orders g^3, $g^4\ln(1/g)$, g^5, respectively.

As is well known [2–4], the convergence of the perturbative expansion in Eq. (5) is quite poor when values of x, y corresponding to any reasonable physical temperature $T/\Lambda_{\overline{MS}}$ are chosen. For future reference, we illustrate this in Fig. 1. We have used Eqs. (1), (2), and (4) together with terms up to order $y^{1/2}$ in Eq. (5).

The idea of our approach of improving the determination of $\mathcal{F}_{\overline{MS}}(x, y)$ is the following. We write

$$\Delta\mathcal{F}_{\overline{MS}}(x, y) = \Delta\mathcal{F}_{\overline{MS}}(x_0, y_0) + \int_{y_0}^{y} dy\left(\frac{\partial\Delta\mathcal{F}_{\overline{MS}}}{\partial y} + \frac{dx}{dy}\frac{\partial\Delta\mathcal{F}_{\overline{MS}}}{\partial x}\right), \tag{6}$$

where $y = y(x)$ is defined in Eq. (2). The partial derivatives are now given by adjoint Higgs field condensates:

$$\frac{\partial\Delta\mathcal{F}_{\overline{MS}}}{\partial y} = \left\langle\frac{\mathrm{Tr}A_0^2}{g_3^2}\right\rangle_{\overline{MS}} - \left\langle\frac{\mathrm{Tr}A_0^2}{g_3^2}\right\rangle_{\overline{MS},\mathrm{pert}}, \tag{7}$$

where $\langle\mathrm{Tr}A_0^2/g_3^2\rangle_{\overline{MS},\mathrm{pert}}$ is the perturbative result up to $\mathcal{O}(y^{-1/2})$, obtained by taking a derivative of Eq. (5) with respect to y. In the case of $\partial\Delta\mathcal{F}_{\overline{MS}}/\partial x$, a similar relation is obtained but with the condensate $\langle(\mathrm{Tr}A_0^2)^2\rangle$.

On the other hand, with a computation in lattice perturbation theory, a condensate measured in lattice Monte Carlo simulations can be related to the condensates $\langle\mathrm{Tr}A_0^2\rangle_{\overline{MS}}$, $\langle(\mathrm{Tr}A_0^2)^2\rangle_{\overline{MS}}$. Because of the super-renormalizable nature of $\mathcal{L}_{3D}$, such analytical relations can be computed exactly near the continuum limit [17,18].
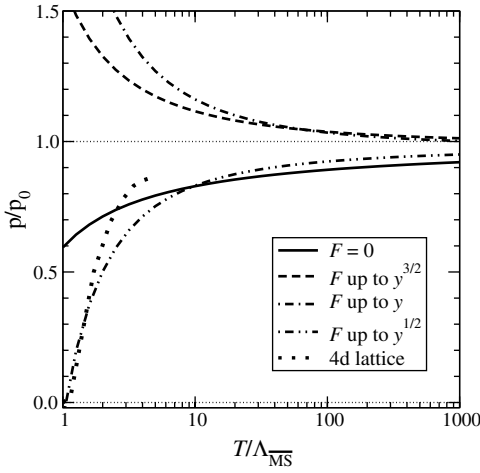
FIG. 1. The pressure in Eq. (4), with the long-distance part from Eq. (5) included in various loop orders. The 4D lattice results are from the first reference in [1]. It should be noted that they have a normalization ambiguity at low temperatures $T \lesssim T_c$ allowing for a small shift of the curve.

Thus, we need to evaluate the condensates on the lattice, transform the result to the $\overline{\text{MS}}$ scheme, and perform finally the integration in Eq. (6) numerically. When added to $\Delta \mathcal{F}_{\overline{\text{MS}}}(x_0, y_0)$, we obtain a nonperturbative result, which we can plug into Eq. (4).

What remains is to determine the integration constant $\Delta \mathcal{F}_{\overline{\text{MS}}}(x_0, y_0)$. The idea is that, despite the bad convergence shown in Fig. 1, at high enough temperatures the form of $\Delta \mathcal{F}_{\overline{\text{MS}}}(x_0, y_0)$ is known. Indeed, inspecting the general structure of Eq. (5), we know that

$$\Delta \mathcal{F}_{\overline{\text{MS}}}(x_0, y_0) = \frac{e_0}{(4\pi)^4} d_A C_A^3 \left[1 + \mathcal{O}\left(\frac{x_0}{C_A}, \frac{C_A}{4\pi y_0^{1/2}} \right) \right].$$

(8)

Here e_0, containing an unknown logarithmic dependence on y_0, represents the famous nonperturbative $\mathcal{O}(g^6 T^4)$ term [10]. Suppose now that we choose $T \equiv T_0 \sim 10^{11} \Lambda_{\overline{\text{MS}}}$, corresponding to $x_0 = 1.0 \times 10^{-2}$, $y_0 = 3.86$. Then the higher-order terms in Eq. (8) are expected to be subdominant, since $C_A/(4\pi y_0^{1/2}) \sim 0.1$ and $x_0/C_A \sim 0.01$, and we only need to know e_0.

The main error sources of this nonperturbative and unambiguous setup are as follows.

(a) Even though, in principle, an independent nonperturbative determination of e_0 is possible, for instance, by measuring the condensate $\langle \text{Tr} F_{ij}^2 \rangle$ along the lines in [19], doing this systematically requires a 4-loop computation in lattice perturbation theory, and this is beyond our scope here. Therefore we will treat e_0 as a free integration constant whose magnitude will be fixed below.

(b) Because of the smallness of x/C_A, we will also ignore here the term arising from $\partial \Delta \mathcal{F}_{\overline{\text{MS}}}/\partial x$ in Eq. (6).

(c) The numerical procedure introduces small statistical errors, as well as systematic errors, from the extrapolations to the infinite volume and continuum limits.

(d) Finally, we should of course remember that the effective theory $\mathcal{L}_{3D}$ loses its accuracy when higher-order

operators, not included, become important. In fact, for $N_f = 0$ the QCD phase transition is related to the so-called $Z(3)$ symmetry [11,20], and this symmetry is not fully reproduced by $\mathcal{L}_{3D}$ [9,21] without all of the higher-order operators. There are many indications, however, that the effective theory should be rather accurate down to low temperatures, $T \sim 2T_c$ [6,9,13]. Below that, some other effective description may apply (see, e.g., [22]).

Numerical results.—After this background, we show in Fig. 2 the difference in Eq. (7), measured with lattice simulations. This result is then used in Eq. (6) to obtain $\Delta \mathcal{F}_{\overline{\text{MS}}}(x, y)$. When added to Eqs. (4) and (5), we obtain Fig. 3. As discussed above, the boundary value at (almost) infinite temperature, determined by e_0, is for the moment a free parameter.

We observe that at low temperatures the outcome depends strongly on the value of e_0. The correct value would appear to be $e_0 \approx 10.0 \pm 2.0$. Even then, the present results lose their accuracy at $T \sim 5T_c$, but seem to work well above this. Exploiting the full power of the dimensionally reduced theory down to its limit $T \sim 2T_c$ would also necessitate the inclusion of $\langle (\text{Tr} A_0^2)^2 \rangle$.

Discussion.—In 4D lattice simulations, there is a (numerically small) ambiguity in the determination of the pressure, because only pressure differences can be measured, and thus an integration constant has to be specified at low temperatures in a nonperturbative regime. Here we fix the integration constant by starting from the opposite direction, from very high temperatures. This allows us to determine all quantities in terms of $T/\Lambda_{\overline{\text{MS}}}$ and the number of fermion flavors, without ambiguities. We can also address a huge range of temperatures, unlike 4D simulations which can only go up to $T \sim$ a few $\times T_c$.

The result of our procedure is summarized by Eqs. (4)–(7) and Fig. 3. We draw two important conclusions. The first is that the outcome depends strongly on the nonperturbative contribution of order $\mathcal{O}(g^6 T^4)$ [10],
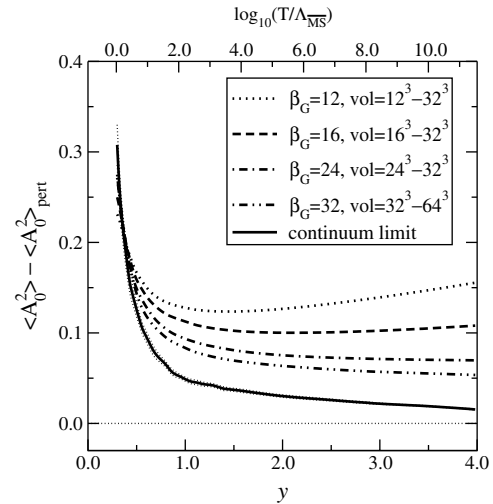

FIG. 2. The difference in Eq. (7). Here $\beta_G = 6/(g_3^2 a)$, where a is the lattice spacing, and the continuum limit corresponds to the extrapolation $\beta_G \to \infty$.

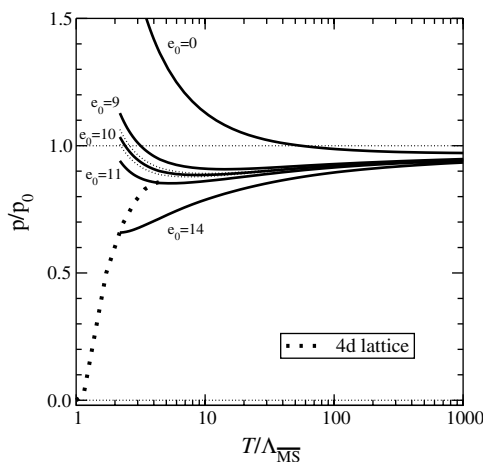FIG. 3. The pressure after the inclusion of $\Delta \mathcal{F}_{\overline{\mathrm{MS}}}(x, y)$ from Eq. (6). Statistical errors are shown only for $e_0 = 10$.

as can be observed from the e_0 dependence in Fig. 3. The value of e_0 could, in principle, be determined by a well-defined procedure, although in practice it is a project of considerable technical complication. But our present study provides an estimate for what the result should be. The order of magnitude $\mathcal{O}(10)$ seems reasonable, since it is known from other contexts such as the Debye mass [13] that nonperturbative constants tend to be large.

The second is that, when the large nonperturbative $\mathcal{O}(g^6 T^4)$ term is summed together with the set of all higher-order terms determined via $\langle \mathrm{Tr} A_0^2 \rangle$, then these long-distance contributions almost cancel at $T \gtrsim 30 \Lambda_{\overline{\mathrm{MS}}}$. Indeed, the sum, the curve with $e_0 \sim 10$ in Fig. 3, does not differ much from the term $\mathcal{O}(y^{1/2})$ in Fig. 1. For smaller temperatures, $5\Lambda_{\overline{\mathrm{MS}}} \lesssim T \lesssim 30\Lambda_{\overline{\mathrm{MS}}}$, on the other hand, only our numerical results are trustworthy.

Finally, we also find that, although the dependence on the effective scalar self-coupling x is of high perturbative order, in practice it is expected to play a role as one approaches T_c. Its contribution can be obtained from the condensate $\langle (\mathrm{Tr} A_0^2)^2 \rangle$. To relate this to the $\overline{\mathrm{MS}}$ scheme requires again a perturbative 4-loop computation.

Let us end with a philosophical note. When one wants to understand 4D simulation results, one could argue that one should aim at almost fully analytical resummations [14–16]. However, we suspect that these are unavoidably specific for the particular observable considered: they may work for the entropy or pressure because the result is short-distance dominated, but would fail, for instance, for Debye screening where long-distance effects are dominant. It seems to us that it may ultimately be more useful to obtain a unified understanding of the relevant degrees of freedom in the system, even if some observables have to be evaluated numerically.

[1] G. Boyd *et al.,* Nucl. Phys. **B469**, 419 (1996); A. Papa, Nucl. Phys. **B478**, 335 (1996); B. Beinlich, F. Karsch, E. Laermann, and A. Peikert, Eur. Phys. J. C **6**, 133 (1999); CP-PACS Collaboration, M. Okamoto *et al.,* Phys. Rev. D **60**, 094510 (1999).

[2] P. Arnold and C. Zhai, Phys. Rev. D **50**, 7603 (1994); *ibid.* **51**, 1906 (1995).

[3] C. Zhai and B. Kastening, Phys. Rev. D **52**, 7232 (1995).

[4] E. Braaten and A. Nieto, Phys. Rev. D **53**, 3421 (1996).

[5] P. Ginsparg, Nucl. Phys. **B170**, 388 (1980); T. Appelquist and R. D. Pisarski, Phys. Rev. D **23**, 2305 (1981).

[6] S. Nadkarni, Phys. Rev. Lett. **60**, 491 (1988); T. Reisz, Z. Phys. C **53**, 169 (1992); L. Kärkkäinen *et al.,* Phys. Lett. B **282**, 121 (1992); Nucl. Phys. **B418**, 3 (1994); Nucl. Phys. **B395**, 733 (1993).

[7] S. Huang and M. Lissia, Nucl. Phys. **B438**, 54 (1995); *ibid.* **B480**, 623 (1996).

[8] K. Kajantie *et al.,* Nucl. Phys. **B458**, 90 (1996); Phys. Lett. B **423**, 137 (1998).

[9] K. Kajantie *et al.,* Nucl. Phys. **B503**, 357 (1997).

[10] A. D. Linde, Phys. Lett. B **96**, 289 (1980).

[11] D. J. Gross, R. D. Pisarski, and L. G. Yaffe, Rev. Mod. Phys. **53**, 43 (1981).

[12] S. Datta and S. Gupta, Nucl. Phys. **B534**, 392 (1998); Phys. Lett. B **471**, 382 (2000).

[13] M. Laine and O. Philipsen, Nucl. Phys. **B523**, 267 (1998); Phys. Lett. B **459**, 259 (1999); A. Hart and O. Philipsen, Nucl. Phys. **B572**, 243 (2000); A. Hart, M. Laine, and O. Philipsen, Nucl. Phys. **B586**, 443 (2000).

[14] J. O. Andersen, E. Braaten, and M. Strickland, Phys. Rev. Lett. **83**, 2139 (1999); Phys. Rev. D **61**, 014017 (2000); Phys. Rev. D **61**, 074016 (2000).

[15] J. P. Blaizot, E. Iancu, and A. Rebhan, Phys. Rev. Lett. **83**, 2906 (1999); Phys. Lett. B **470**, 181 (1999); hep-ph/0005003.

[16] A. Peshier, hep-ph/9910451.

[17] K. Farakos *et al.,* Nucl. Phys. **B442**, 317 (1995); M. Laine and A. Rajantie, Nucl. Phys. **B513**, 471 (1998).

[18] G. D. Moore, Nucl. Phys. **B493**, 439 (1997); *ibid.* **B523**, 569 (1998).

[19] F. Karsch, M. Lütgemeier, A. Patkós, and J. Rank, Phys. Lett. B **390**, 275 (1997).

[20] C. P. Korthals Altes, Nucl. Phys. **B420**, 637 (1994).

[21] K. Kajantie, M. Laine, A. Rajantie, K. Rummukainen, and M. Tsypin, J. High Energy Phys. **9811**, 011 (1998).

[22] R. D. Pisarski, hep-ph/0006205.

[YS2]

Simple way to generate high order vacuum graphs

Simple way to generate high order vacuum graphs

K. Kajantie*

Department of Physics, P.O. Box 64, FIN-00014 University of Helsinki, Finland

M. Laine[†]

Theory Division, CERN, CH-1211 Geneva 23, Switzerland

Y. Schröder[‡]

Department of Physics, P.O. Box 64, FIN-00014 University of Helsinki, Finland

We describe an efficient practical procedure for enumerating and regrouping vacuum Feynman graphs of a given order in perturbation theory. The method is based on a combination of Schwinger-Dyson equations and the two-particle-irreducible ("skeleton") expansion. The regrouping leads to skeletons containing only free propagators, together with "ring diagrams" containing all the self-energy insertions. As a consequence, relatively few diagrams need to be drawn and integrations carried out at any single stage of the computation and, in low dimensions, overlapping ultraviolet and infrared subdivergences can be cleanly isolated. As an illustration we enumerate the graphs contributing to the four-loop free energy in QCD, explicitly in a continuum and more compactly in a lattice regularization.

PACS number(s): 11.15.Bt, 11.10.Wx, 12.38.Bx

I. INTRODUCTION

There are many physics contexts where multiloop Feynman diagram computations are carried out. In QED one goes up to the four-loop level (for reviews see, e.g., [1]) because experiments are so precise. In particle physics phenomenology, particularly QCD, one goes up to the four-loop level (see, e.g., [2]) because the coupling constant is not small. In studying critical phenomena in the simplest O(N) condensed matter systems, one goes up to the five-loop level (see, e.g., [3]) because the effective expansion parameter is not small.

Studies of QCD at a finite temperature T are faced with a similar challenge. Indeed, the coupling constant expansion converges even worse than at zero temperature requiring at least $T \gg 10^3 \Lambda_{QCD}$ to make any sense at all [4,5]. So far, though, only the resummed three-loop level has been reached for the simplest physical observable, the free energy [6], because a broken Lorentz symmetry makes the analysis much more complicated than in the cases mentioned above. In fact, even in principle only one more order is (partly) computable, and then the expansion breaks down completely [7]. Multiloop computations are not useless, though: the infrared problems can be isolated to a simple three-dimensional (3D) effective field theory [8] and studied nonperturbatively there [9], but to convert the results to physical units from lattice regularization still necessitates a number of fixed-order perturbative computations [10,11,12].

As the loop order increases, so does the computational effort. The sheer enumeration of various diagrams and their symmetry factors becomes nontrivial. The group-theoretic and Lorentz structures of single graphs are involved. Finally,

the scalar integrals remaining are hard to evaluate analytically. It is therefore clear that, ideally, one would like to automatize the whole procedure (for a review of the current status see, e.g., [13]).

In this paper we concentrate on the first step of any multiloop computation, the enumeration of various Feynman diagrams. This step should be the easiest to automatize, since all one needs is a straightforward evaluation of Wick contractions. Indeed, various packages, such as FEYNARTS [14] and QGRAF [15], are available for determining n-point functions in a given particle physics model.

For vacuum graphs in condensed matter systems a similar approach is possible. For the quartic O(N) scalar model the combinatorics is not yet too hard, but variants thereof already require some work. Consequently, graphical algorithms have been developed at four-loop order and beyond for a number of simple models [16].

In many cases, though, a straightforward generation of the full set of diagrams of a given loop order may not be the ideal way to go. In realistic theories there are very many graphs, and all integrals would have to be evaluated on the same footing. This is almost impossible, particularly if many different masses appear.

Here we wish to present what would seem to us to be a maximally manageable setup. All vacuum graphs are generated, but they are cleanly separated into two groups: one, of two-particle-irreducible (2PI) "skeletons" with free propagators, and the other, of "ring diagrams" with various self-energy insertions (see also [17]). The self-energies, in turn, are directly obtained from lower order skeletons. We find that this setup economizes the generation of the various graphs quite significantly. We also point out that in low dimensions, relevant for statistical physics applications, the integrations remaining are qualitatively different in the two sets.

As an illustration of the setup, we enumerate the diagrams

---

*Email address: keijo.kajantie@helsinki.fi

[†]Email address: mikko.laine@cern.ch

[‡]Email address: york.schroder@helsinki.fi

contributing to the four-loop free energy of finite temperature QCD (as well as QED and the symmetric phases of the electroweak theory and scalar electrodynamics). We hope, though, that the setup may be applicable to some other cases as well. That is why we wish to separate it from the evaluation of the integrals arising in the finite T context [18], specific for that physical situation.

Our plan is the following. We summarize our basic notation in Sec. II, reorganize the standard skeleton expansion in Sec. III, review the Schwinger-Dyson equations for n-point and vacuum graphs in Sec. IV, and combine them with the modified skeleton expansion to obtain a generating formula for skeleton diagrams in Sec. V. The corresponding results are given for a lattice regularization of a generic model in Sec. VI. As an illustration, we show the loop expansion for the free energy of QCD and related models in Sec. VII. We discuss some basic properties of our setup and conclude in Sec. VIII.

II. NOTATION

Let us start by introducing a concise notation. While the method is valid for any theory, we explicitly give all equations for a generic $\varphi^3 + \varphi^4$ model. Later on we discuss more specific examples within this class, in particular QCD, as well as some extensions of this class. The generic class also includes the electroweak sector of the standard model, both in its symmetric and its spontaneously broken phase.

The partition function is defined as

$$Z[J] = \int \mathcal{D}\varphi \, e^{S[\varphi] + J\varphi}, \tag{1}$$

where $S[\varphi]$ is the action,

$$S[\varphi] = -\frac{1}{2} \varphi_i \Delta_{ij}^{-1} \varphi_j + \frac{1}{3!} \gamma_{ijk} \varphi_i \varphi_j \varphi_k + \frac{1}{4!} \gamma_{ijkl} \varphi_i \varphi_j \varphi_k \varphi_l, \tag{2}$$

and summations over various indices, numbering (real scalar) fields and their internal and spacetime structures, are implied. Two comments are in order. First, we will for the moment not display fermions explicitly. As far as vacuum graphs are concerned, they do not introduce any complications apart from the usual overall minus sign for each closed

loop and can thus be introduced only at the end [19]. Second, one should notice that the sign conventions in Eqs. (1), (2) are such that in the case of Euclidean actions, γ_{ijkl} is typically negative.

For a theory with a broken symmetry, the inverse free propagator Δ^{-1} and the couplings $\gamma_{ijk...}$ are functions of the order parameter, but otherwise there are no essential complications. We return to this point in Sec. IV A.

The partition function $Z[J]$ in Eq. (1) is the generating functional for full Green's functions, $\Gamma_n^{\text{full}} = \delta_J^n Z[J]|_{J=0}$. As usual, we define

$$W[J] = \ln Z[J], \tag{3}$$

the generating functional of connected Green's functions, $\Gamma_n^{\text{conn}} = \delta_J^n W[J]|_{J=0}$. Finally, one can define the effective action via

$$S_{\text{eff}}[\phi] = W[J] - \phi J, \qquad \phi = \delta_J W[J], \tag{4}$$

which generates 1PI Green's functions, $\Gamma_n^{\text{1PI}} = \delta_\phi^n S_{\text{eff}}[\phi]|_{\phi=0}$. Note, in particular, that $\delta_\phi S_{\text{eff}}[\phi] = -J$. The vacuum, or free energy F (made dimensionless by a division with the temperature T), can be obtained from any of the generating functionals as

$$F = -\ln Z[0] = -W[0] = -S_{\text{eff}}[0]. \tag{5}$$

From the basic relations $\phi = \delta_J W[J]$, $\delta_\phi S_{\text{eff}}[\phi] = -J$, it follows that

$$\delta_J^2 W[J] \delta_\phi^2 S_{\text{eff}}[\phi] = -1. \tag{6}$$

Defining, as usual, the "proper" self-energy by

$$\delta_\phi^2 S_{\text{eff}}[\phi] \equiv -\Delta^{-1} + \Pi, \tag{7}$$

we see from Eq. (6) that $\delta_J^2 W[J]$ is the full propagator:

$$\delta_J^2 W[J] \equiv D[\phi] = \frac{1}{\Delta^{-1} - \Pi} \equiv \Delta + \Delta\Pi\Delta + \Delta\Pi\Delta\Pi\Delta + \cdots. \tag{8}$$

We shall use here the following notation for free and full propagators, the proper self-energy, as well as general 1PI vertices:

$$\Delta \quad = \quad \text{————} \qquad \text{(free propagator)}, \tag{9}$$

$$D \quad = \quad \text{████} \quad = \quad \text{————} \; + \; \text{—}\bigcirc\!\!\pi\!\!\bigcirc\text{—} \; + \; \text{—}\bigcirc\!\!\pi\!\!\bigcirc\text{—}\bigcirc\!\!\pi\!\!\bigcirc\text{—} \; + \ldots \text{(full propagator)}, \tag{10}$$

$$\Pi \quad = \quad \text{--}\bigcirc\!\!\pi\!\!\bigcirc\text{--} \qquad \text{(proper self-energy, with legs ``amputated'')}, \tag{11}$$

$$\Delta^{-1} \quad = \quad \text{--}\blacktriangleleft\text{--} \qquad \text{(inverse free propagator, with legs amputated)}, \tag{12}$$

$$\delta_\phi^n S_{\text{eff}} \quad = \quad \bigcirc\!\!\!\!\!< \qquad \text{(general amputated 1PI vertex)}. \tag{13}$$

III. SKELETON EXPANSION WITH FREE PROPAGATORS

We next review the skeleton expansion for the free energy F [20,21] and modify it such that full propagators can be replaced with free propagators [17]. By a skeleton we mean a 2PI vacuum diagram: one that remains connected even if any two lines are cut. The skeleton expansion has been used as the starting point also in [17].

It can be shown [20,21] that the loop expansion for Eq. (5) can be written as

$$F[D] = \sum_i c_i (\text{Tr}\ln D_i^{-1} + \text{Tr}\Pi_i[D]D_i) - \Phi[D], \quad (14)$$

where $i = \{\text{bosons, fermions}\}$, $c_{\text{boson}} = 1/2$, and $c_{\text{fermion}} = -1$. Here $\Phi[D]$ collects all 2PI vacuum diagrams. The full propagators D_i are related to their corresponding self-energies by $D^{-1} = \Delta^{-1} - \Pi$ [cf. Eq. (8)], where Δ are the free propagators. Both F, Π, and Φ can be regarded as functionals of the full propagators. The partition function has an extremal property, such that the variation of F with respect to any of the full propagators vanishes [20,21,22], giving a relation between skeletons and self-energies:

$$\delta_{D_i}\Phi[D] = c_i\Pi[D]. \quad (15)$$

Here we have introduced the implicit notation that whenever a term is multiplied by c_i, the Π's and D's following it are assumed to carry the same subscript. Pictorially, Eq. (15) corresponds to getting a self-energy by "cutting a propagator" in all possible ways in the set of vacuum skeletons. Hence knowing the skeletons alone provides full information.

In Eqs. (14), (15), it is the full propagators D which appear in the skeleton graphs and self-energies. We would instead like to obtain skeletons with free propagators. As a first step in this direction, we expand D in terms of the self-energy insertions $\Pi[D]$, $D = \Delta\sum_{n\geq 0}(\Pi\Delta)^n$, to get

$$F = \sum_i c_i\text{Tr}\left[\ln\Delta^{-1} + \sum_{n\geq 2}\left(1 - \frac{1}{n}\right)(\Pi\Delta)^n\right]$$
$$- \Phi\left[\Delta\sum_{n\geq 0}(\Pi\Delta)^n\right]. \quad (16)$$

We then have to evaluate $\Pi[D]$.

To go forward more explicitly, we restrict ourselves to the five-loop level here. Let the subscript n denote the loop order, and write $\Pi = \Sigma_{n\geq 1}\Pi_n$. It turns out that we need at most Π_3. In a straightforward way, we obtain

$$\Pi_1 = \Pi_1[\Delta] \equiv \Pi_1^{\text{irr}}[\Delta], \quad (17)$$

$$\Pi_2 = \Pi_2^{\text{irr}}[\Delta] + (\Pi_1^{\text{irr}}[\Delta + \Delta\Pi_1^{\text{irr}}\Delta])_2$$
$$\equiv \Pi_2^{\text{irr}}[\Delta] + \Pi_2^{\text{red}(1)}[\Delta], \quad (18)$$

$$\Pi_3 = \Pi_3^{\text{irr}}[\Delta] + (\Pi_2^{\text{irr}}[\Delta + \Delta\Pi_1^{\text{irr}}\Delta])_3$$
$$+ (\Pi_1^{\text{irr}}[\Delta + \Delta\Pi\Delta + \Delta\Pi_1^{\text{irr}}\Delta\Pi_1^{\text{irr}}\Delta])_3$$
$$\equiv \Pi_3^{\text{irr}}[\Delta] + \Pi_3^{\text{red}(1)}[\Delta] + \Pi_3^{\text{red}(2)}[\Delta], \quad (19)$$

where Π_n^{irr} are n-loop 1PI graphs, while $\Pi_n^{\text{red}(m)}$ are obtained by cutting m lines in a lower order $\Pi_n^{\text{irr}}[\Delta]$ and dressing them appropriately:

$$\Pi_2^{\text{red}(1)}[\Delta] = (\Delta\Pi_1^{\text{irr}}\Delta)_j\delta_{\Delta_j}\Pi_1^{\text{irr}}[\Delta], \quad (20)$$

$$\Pi_3^{\text{red}(1)}[\Delta] = (\Delta\Pi_1^{\text{irr}}\Delta)_j\delta_{\Delta_j}\Pi_2^{\text{irr}}[\Delta]$$
$$+ (\Delta\Pi_2\Delta + \Delta\Pi_1^{\text{irr}}\Delta\Pi_1^{\text{irr}}\Delta)_j\delta_{\Delta_j}\Pi_1^{\text{irr}}[\Delta], \quad (21)$$

$$\Pi_3^{\text{red}(2)}[\Delta] = \frac{1}{2}(\Delta\Pi_1^{\text{irr}}\Delta)_j(\Delta\Pi_1^{\text{irr}}\Delta)_k\delta_{\Delta_j}\delta_{\Delta_k}\Pi_1^{\text{irr}}[\Delta]. \quad (22)$$

For the explicit diagrammatic characteristics of $\Pi_2^{\text{red}(1)}$, see Sec. V B.

It is easy now to unfold the loop expansion also for $\Phi[D] = \Sigma_{n\geq 2}\Phi_n$, the last term in Eq. (16). Up to the five-loop level, we can write

$$(\Phi_2[D])_{n\leq 5} = (\Phi_2[\Delta + \Delta(\Pi_1 + \Pi_2 + \Pi_3)\Delta$$
$$+ \Delta(\Pi_1 + \Pi_2)\Delta(\Pi_1 + \Pi_2)\Delta$$
$$+ \Delta\Pi_1\Delta\Pi_1\Delta\Pi_1\Delta])_{n\leq 5}, \quad (23)$$

$$(\Phi_3[D])_{n\leq 5} = (\Phi_3[\Delta + \Delta(\Pi_1 + \Pi_2)\Delta$$
$$+ \Delta\Pi_1\Delta\Pi_1\Delta])_{n\leq 5}, \quad (24)$$

$$(\Phi_4[D])_{n\leq 5} = (\Phi_4[\Delta + \Delta\Pi_1\Delta])_{n\leq 5}, \quad (25)$$

$$(\Phi_5[D])_{n\leq 5} = \Phi_5[\Delta], \quad (26)$$

where the arguments are to be Taylor expanded, with first derivatives obeying [cf. the diagrammatic identity Eq. (15), evaluated with free propagators]

$$\delta_{\Delta_i}\Phi_n[\Delta] = c_i\Pi_{n-1}^{\text{irr}}[\Delta], \quad (27)$$

and higher ones bringing back reducible self-energies, defined in Eqs. (20)–(22).

Inserting these expansions into Eq. (16), we finally get, up to the five-loop level,

$$-F = -\sum_i c_i \text{Tr} \ln \Delta^{-1} + \Phi_2[\Delta] + \Phi_3[\Delta] + \sum_i c_i \text{Tr}\left[\frac{1}{2}(\Delta\Pi_1)^2\right] + \Phi_4[\Delta] + \sum_i c_i \text{Tr}\left[\frac{1}{3}(\Delta\Pi_1)^3\right.$$

$$\left. + \Delta\Pi_1 \Delta\left(\Pi_2^{\text{red}} + \frac{1}{2}\Pi_2^{\text{red}(1)}\right)\right] + \Phi_5[\Delta] + \sum_i c_i \text{Tr}\left[\frac{1}{4}(\Delta\Pi_1)^4 + (\Delta\Pi_1)^2\Delta\left(\Pi_2^{\text{irr}} + \frac{1}{2}\Pi_2^{\text{red}(1)}\right)\right.$$

$$\left. + \frac{1}{2}\Delta\Pi_2^{\text{irr}}\Delta(\Pi_2^{\text{irr}} + \Pi_2^{\text{red}(1)}) + \Delta\Pi_1\Delta\left(\Pi_3^{\text{irr}} + \frac{1}{2}\Pi_3^{\text{red}(1)} + \frac{1}{3}\Pi_3^{\text{red}(2)}\right)\right] \tag{28}$$

or, written diagrammatically (and denoting by F_0 the noninteracting result),

$$-F \;=\; -F_0 + \Phi_2[\Delta]$$

$$\tag{29}$$

Here a circle with n inside denotes Π_n^{irr}, a square $\Pi_n^{\text{red}(1)}$, and a double square $\Pi_n^{\text{red}(2)}$. We will term the skeletons with free propagators, $\Phi_n[\Delta]$, *irreducible*. Note that the numerical factors in front of various types of ring diagrams do not appear to trivially follow from any simple symmetry argument (particularly in the case of reducible self-energy insertions), but are best worked out explicitly via the Taylor expansions we have described.

Equation (29) is the starting point of our setup. It expresses the free energy in an economic way in terms of the irreducible skeletons $\Phi_n[\Delta]$: either as direct contributions or as self-energy insertions obtained from the same skeletons via Eqs. (27) and (20)–(22). We note that at the n-loop level, one needs $\Phi_n[\Delta]$, but only $\Pi_{n-2}[\Delta]$, obtained from $\Phi_{n-1}[\Delta]$.

IV. SCHWINGER-DYSON EQUATIONS WITH FULL PROPAGATORS

Next, we need to generate the skeletons $\Phi_n[\Delta]$, needed in Sec. III. To do that, we first review briefly the general setup of Schwinger-Dyson (SD) equations, converted to our notation. The SD equations will then play a central role in our main result, Eq. (49), which is an explicit formula allowing for a systematic generation of all skeletons $\Phi_n[\Delta]$—in principle to any order. In this section, we follow closely the very enjoyable presentation by Cvitanović [19].

A. General n-point functions

The basic SD equation for the generating functional $Z[J]$ of full Green's functions derives from the trivial fact that the integral of a total derivative vanishes:

$$0 = \int \mathcal{D}\varphi\, \delta_\varphi e^{S[\varphi]+J\varphi} = (S'[\delta_J]+J)Z[J]. \tag{30}$$

For the generating functional of the connected Green's functions, Eq. (3), one gets

$$0 = S'[W'[J]+\delta_J]+J. \tag{31}$$

Finally, for the effective action, Eq. (4), we use from Sec. II that $W'[J]=\phi$, $\delta_J=(\delta\phi/\delta J)\delta_\phi = W''[J]\delta_\phi = D[\phi]\delta_\phi$, and $J=-S'_{\text{eff}}[\phi]$ to obtain

$$S'_{\text{eff}}[\phi] = S'[\phi+D[\phi]\delta_\phi]. \tag{32}$$

Putting $\phi\to 0$ on the right-hand side, this gives the SD equation for the one-point function, while taking derivatives with respect to ϕ on both sides of Eq. (32) and putting $\phi\to 0$ only afterwards generates SD equations for higher-point Green's functions,

$$\Gamma_n^{\text{1PI}} = \delta_\phi^{n-1} S'[\phi+D[\phi]\delta_\phi]\big|_{\phi=0}. \tag{33}$$

Here $D[\phi]$ is in Eq. (8), and we note that

$$\delta_\phi D[\phi] = D[\phi](\delta_\phi^3 S_{\text{eff}}[\phi])D[\phi]. \tag{34}$$

A note may be in order here concerning theories with spontaneously broken symmetries. In that case, ϕ corresponds to the fluctuating field around some reference value v, typically $v\equiv\langle\varphi\rangle$. The quantity we should ultimately be computing is the free energy density as a function of v: i.e., the effective potential $V(v)=F/(\text{volume})$. Then everything goes as before: we still put $\phi\to 0$ in the equa-

tions above after differentiation, while the condensate v appears as a parameter in the free propagators as well as in the cubic and quartic couplings in Eq. (2) [the term $J\varphi$ linear in φ in Eq. (1) need not be changed [23]]. The graphs also remain the same: only 1PI graphs, generated by the loop expansion in Eq. (29), are to be included [23]. Tadpole-type graphs often associated with broken symmetries would only be generated if we want to reexpand the value of $V(v)$ at the broken minimum in a strict loop expansion: writing $V = \Sigma_{n \geq 0} V_n$, $v = \Sigma_{n \geq 0} v_n$, such that $V_0'(v_0) = 0$, implies

$$V(v)|_{V'(v)=0} = V_0(v_0) + V_1(v_0) + \left[V_2 - \frac{1}{2} \frac{(V_1')^2}{V_0''} \right]_{v=v_0}$$

$$+ \left[V_3 - \frac{V_1' V_2'}{V_0''} + \frac{1}{2} \frac{(V_1')^2 V_1''}{(V_0'')^2} - \frac{1}{6} \frac{(V_1')^3 V_0'''}{(V_0'')^3} \right]_{v=v_0}$$

$$+ \left[V_4 - \frac{1}{2} \frac{(V_2')^2 + 2 V_1' V_3'}{V_0''} + \frac{1}{2} \frac{2 V_1' V_2' V_1'' + (V_1')^2 V_2''}{(V_0'')^2} \right.$$

$$\left. - \frac{1}{6} \frac{3(V_1')^2 (V_1'')^2 + 3(V_1')^2 V_2' V_0''' + (V_1')^3 V_1'''}{(V_0'')^3} \right.$$

$$+ \frac{1}{24} \frac{12(V_1')^3 V_1'' V_0''' + (V_1')^4 V_0''''}{(V_0'')^4} - \frac{1}{8} \frac{(V_1')^4 (V_0''')^2}{(V_0'')^5} \right]_{v=v_0} + \cdots, \tag{35}$$

where the latter terms inside the square brackets correspond to various tadpole graphs, with obvious notation: $1/V_0''$ is the free propagator of the Higgs particle with a vanishing momentum, $V_1'(V_1'')$ is a one-loop diagram with one leg (two legs), V_0''' is a three-vertex, etc.

Let us now illustrate the structure of Eq. (33) for the generic model in Eq. (2). Starting from Eq. (2), writing down indices, and employing Eq. (34), we obtain, for the right-hand side of Eq. (32),

$$\delta_{\phi_i} S = -\Delta_{ij}^{-1} \phi_j + \frac{1}{2} \gamma_{ijk} (\phi_j \phi_k + D_{jk}) + \frac{1}{6} \gamma_{ijkl} (\phi_j \phi_k \phi_l$$

$$+ D_{jk} \phi_l + D_{kl} \phi_j + D_{lj} \phi_k$$

$$+ D_{jm} D_{kn} D_{lo} \delta_{\phi_m} \delta_{\phi_n} \delta_{\phi_o} S_{\text{eff}}[\phi]). \tag{36}$$

We now take further derivatives according to Eq. (33). Putting $\phi = 0$ after each differentiation, we thus obtain the standard equations [written in the notation of Eqs. (9)–(13)]

$$\tag{37}$$

$$\tag{38}$$

$$\tag{39}$$

$$\tag{40}$$

$$+ \{\text{2-loop terms}\}, \tag{41}$$

where "cyclic $(n_1, n_2, \ldots)$" denotes cyclic permutations of the legs numbered. We have not written down the two-loop terms in Eq. (41), since they are not needed in our explicit four-loop demonstration below. Likewise, all higher-point 1PI functions Γ_n^{1PI}, $n \geq 5$, start with one-loop graphs in the model of Eq. (2) and will again not contribute at this order; they will for Φ_5, as well as in the model of

Sec. VI.

Let us stress that in a local theory the manipulations needed in Eq. (33) can essentially be made using regular derivatives and can thus easily be implemented algebraically. Introducing furthermore $\hbar$ as a loop counting parameter [24] allows for an iterative solution of the corresponding SD equations.

B. Vacuum diagrams

The SD formalism above provides equations relating n-point Green's functions. To incorporate vacuum diagrams, one can use another simple trick: scaling. Noting that, e.g., $Z[J]$ is a functional of all interaction parameters present in the action, $Z[J, \gamma_{ij}, \gamma_{ijk}, \ldots]$, one can derive hosts of relations by varying any of these parameters.

A most useful example is to rescale the entire action as $S[\varphi] \to (1/\hbar) S[\varphi]$ and then vary $\hbar$:

$$-\hbar \partial_\hbar \ln Z[J] = \left\langle \frac{1}{\hbar} S[\varphi] \right\rangle = \frac{1}{Z[J]} \frac{1}{\hbar} S[\delta_J] Z[J]. \quad (42)$$

Rewriting this in the "connected" language (recall $W = \ln Z$),

$$-\hbar \partial_\hbar W[J] = \frac{1}{\hbar} S[W'[J] + \delta_J], \quad (43)$$

allows one to finally go over to 1PI functions ($\partial_\hbar W = \partial_\hbar S_{\text{eff}} + S'_{\text{eff}} \partial_\hbar \phi + J \partial_\hbar \phi = \partial_\hbar S_{\text{eff}}$, $W' = \phi$, and $\delta_J = W'' \delta_\phi = D[\phi] \delta_\phi$):

$$-\hbar \partial_\hbar S_{\text{eff}}[\phi] = \left\langle \frac{1}{\hbar} S[\varphi] \right\rangle = \frac{1}{\hbar} S[\phi + D[\phi] \delta_\phi]. \quad (44)$$

The free energy $F = -S_{\text{eff}}[0]$ can now be obtained by setting $\phi = 0$ and integrating over $\hbar$.

Noting again that after a rescaling of the integration variables an expansion in $\hbar$ is equivalent to the loop expansion [24], one can integrate the left-hand side of Eq. (44) by $\int_\hbar (1/\hbar)[\cdots]$, but on the right-hand side one integrates over the loop number. Writing

$$-S_{\text{eff}}[0] = F = F_0 + F_{\text{int}} = F_0 + \sum_{n \geq 2} F_n^{\text{int}}, \quad (45)$$

where n counts the number of loops, it follows that

$$F_n^{\text{int}} = \frac{1}{n-1} \{ S[\phi + D[\phi] \delta_\phi] |_{\phi=0} \}_n, \quad n \geq 2. \quad (46)$$

Illustrating Eq. (46) for our generic theory in Eq. (2), we get

$$F_n^{\text{int}} = \frac{1}{n-1} \left\{ -\frac{1}{2} \bigcirc + \frac{1}{6} \ominus + \frac{1}{8} \bigcirc\bigcirc + \frac{1}{8} \bigoplus + \frac{1}{24} \bigcirc\!\!\!\bigcirc \right\}_n, \quad (47)$$

where we again use the notation of Eqs. (9)–(13).

In principle the whole loop expansion can now be generated from Eq. (47), using Eqs. (38)–(41). The n-loop vacuum diagrams are expressed in terms of 1PI n-point functions, which in turn are governed by a set of SD equations. Looking closer at it, though, it is somewhat of a mess: one has to expand full propagators in terms of free ones and the Π's, use SD equations to iterate loops for Π's, which brings back full propagators, etc. Fortunately, none of this is necessary for Eq. (29), as we now explain.

V. GENERATING THE IRREDUCIBLE SKELETONS $\Phi[\Delta]$

The key observation for combining Schwinger-Dyson equations and the skeleton notation in a useful way is that we need to extract from Eq. (47) only a specific part $\Phi[\Delta]$: we already know, by Eq. (29), what all the rest combines into. But then full propagators can be replaced by free propagators in all but the first term in Eq. (47). Indeed, any self-energy insertion within one of the other graphs leads to a two-particle-reducible (2PR) diagram. For the same reason, the 1PI vertices in Eq. (47) can be iterated by using the SD equations of the form in Eqs. (40), (41), but with free propagators. More precisely, it goes as follows.

To generate the *irreducible* skeletons $\Phi[\Delta]$ from Eq. (47), it is sufficient to expand the first term as

$$\bigcirc = \bigcirc + \bigotimes + \{2PR\}$$

$$= \text{Tr}\, 1 + \frac{1}{2} \ominus + \frac{1}{2} \bigcirc\bigcirc + \frac{1}{2} \bigoplus + \frac{1}{6} \bigcirc\!\!\!\bigcirc + \{2PR\}, \quad (48)$$

where in the second step Eq. (38) was used. Taking into account the minus sign in the relation of F and $\Phi[\Delta]$ [cf. Eq. (29)] and writing again the loop expansion as $\Phi = \Sigma_{n \geq 2} \Phi_n$, one finally obtains a closed exact equation

$$\Phi_n[\Delta] = \frac{1}{n-1} \left\{ \frac{1}{12} \ominus + \frac{1}{8} \bigcirc\bigcirc + \frac{1}{8} \bigoplus + \frac{1}{24} \bigcirc\!\!\!\bigcirc \right\}_n, \quad n \geq 2. \quad (49)$$

Equation (49) is our main result. It generates all skeletons of all orders in the theory of Eq. (2), once Eqs. (40), (41) are used (with free propagators). The skeletons, in turn, generate self-energies via Eq. (27) and the analogues of Eqs. (20)–(22). Inserted finally into Eq. (29), we obtain the free energy F.

A. Vacuum skeletons up to the five-loop level

The procedure of working out Eq. (49) is simple and mechanical and can, at least up to the four-loop level, even be carried out by hand, as we shall demonstrate. The only complication arising is the identification of equivalent topologies: the same graph can be written in very many different ways. In order to deal with this situation, it appears easiest to assign an algebraic notation for the different topologies, rather than a mere graphical one. For example, one can count the numbers of three-point and four-point vertices appearing in the graph, and within those equivalence classes, one can use a matrix notation for how the vertices are connected. The significant entries of the matrix can be ordered to a single number, and by doing the same for all possible orderings of the vertices, a unique representative (say, the smallest of such numbers) can be assigned to each topology. For an explicit implementation of this kind of a procedure, see the second paper in [16].

Let us now explicitly work out the diagram classes in Eq. (49) up to the four-loop level. For the first one, inserting Eq. (40) gives either a two-loop graph, or three-loop graphs to be iterated further on, or directly four-loop graphs:

$$\left.\ominus\right|_4 = \ominus + \left[\oplus + \tfrac{1}{2}\oslash + \oslash \right]_4 + \oplus + \oslash + \oplus + \tfrac{1}{2}\ominus . \tag{50}$$

Here the further iterations give

$$\left.\oplus\right|_4 = \oplus + 2\,\left.\oplus\right|_4 = \oplus + 2\,\boxminus + 3\,\oslash , \tag{51}$$

$$\tfrac{1}{2}\left.\oslash\right|_4 = \tfrac{1}{2}\oslash + \boxminus + \tfrac{1}{2}\oslash + 2\,\oplus + \oslash + \tfrac{1}{2}\oplus + \tfrac{1}{4}\oslash , \tag{52}$$

$$\left.\oslash\right|_4 = \oslash + \oslash + \tfrac{1}{2}\oslash + \ominus . \tag{53}$$

We have dropped five-point functions each time they appear, since in the model of Eq. (2), they start with a one-loop term, so that diagrams containing them generate higher loop orders.

The second class in Eq. (49) only contributes to $\Phi_2[\Delta]$ and is trivial. For the third class in Eq. (49),

$$\left.\oslash\right|_4 = \oslash + 2\,\left.\oslash\right|_4 = \oslash + 2\,\oslash + \oslash + 2\,\ominus . \tag{54}$$

For the fourth class, we only need the one-loop terms in Eq. (41),

$$\left.\bigcirc\bigcirc\right|_4 = \bigcirc\bigcirc + 3\,\oplus + 6\,\oplus + \tfrac{3}{2}\triangle . \tag{55}$$

Collecting finally these different contributions together with coefficients according to Eq. (49), we get

$$\Phi_2 = \tfrac{1}{12}\ominus + \tfrac{1}{8}\bigcirc\bigcirc , \tag{56}$$

$$\Phi_3 = \tfrac{1}{24}\oplus + \tfrac{1}{8}\oslash + \tfrac{1}{48}\bigcirc\bigcirc , \tag{57}$$

$$\Phi_4 = \tfrac{1}{72}\oslash + \tfrac{1}{12}\boxminus + \tfrac{1}{8}\oplus + \tfrac{1}{4}\oslash + \tfrac{1}{8}\oplus + \tfrac{1}{8}\ominus + \tfrac{1}{16}\oslash + \tfrac{1}{48}\triangle . \tag{58}$$

Proceeding to higher loop orders, an automatized treatment proves essential, for the reasons outlined above. Implementing our generic formulas as well as an ordering algorithm separating topologies in FORM [25], we obtain in a straightforward way

the complete set of five-loop skeletons,

$$\Phi_5 = \tfrac{1}{4}\left(\vcenter{\hbox{\includegraphics{}}}\right) + \tfrac{1}{48}(\ldots) + \tfrac{1}{16}(\ldots) + \tfrac{1}{12}(\ldots) + \tfrac{1}{4}(\ldots) + \tfrac{1}{2}(\ldots) + \tfrac{1}{2}(\ldots)$$

$$+ \tfrac{1}{8}(\ldots) + \tfrac{1}{4}(\ldots) + \tfrac{1}{4}(\ldots) + \tfrac{1}{8}(\ldots) + \tfrac{1}{8}(\ldots) + \tfrac{1}{4}(\ldots) + \tfrac{1}{4}(\ldots)$$

$$+ \tfrac{1}{8}(\ldots) + \tfrac{1}{2}(\ldots) + \tfrac{1}{8}(\ldots) + \tfrac{1}{4}(\ldots) + \tfrac{1}{16}(\ldots) + \tfrac{1}{8}(\ldots) + \tfrac{1}{4}(\ldots)$$

$$+ \tfrac{1}{2}(\ldots) + \tfrac{1}{16}(\ldots) + \tfrac{1}{12}(\ldots) + \tfrac{1}{16}(\ldots) + \tfrac{1}{32}(\ldots) + \tfrac{1}{16}(\ldots) + \tfrac{1}{8}(\ldots)$$

$$+ \tfrac{1}{4}(\ldots) + \tfrac{1}{8}(\ldots) + \tfrac{1}{4}(\ldots) + \tfrac{1}{8}(\ldots) + \tfrac{1}{12}(\ldots) + \tfrac{1}{128}(\ldots) + \tfrac{1}{32}(\ldots) \ . \tag{59}$$

Note once more that these skeletons are all that is needed for generating the loop expansion for the full free energy, as discussed above.

B. Self-energies up to the two-loop level

Now that we have $\Phi_n[\Delta]$ in Eqs. (56)–(59), irreducible as well as reducible self-energies can easily be obtained with Eqs. (27), (20)–(22), etc. For bosonic particles, for instance ($c_i = \tfrac{1}{2}$), we get

$$\Pi_1^{\text{irr}} = -\!\!-\!\!\bigcirc\!\!1\!\!\bigcirc\!\!-\!\!- = \tfrac{1}{2} \cdot \bigcirc \cdot + \tfrac{1}{2} \, \bigcirc \ , \tag{60}$$

$$\Pi_2^{\text{irr}} = -\!\!-\!\!\bigcirc\!\!2\!\!\bigcirc\!\!-\!\!- = \tfrac{1}{2} \cdot \bigcirc \cdot + \tfrac{1}{2} \cdot \bigcirc \cdot + \tfrac{1}{2} \cdot \bigcirc \cdot + \tfrac{1}{4} \cdot \bigcirc\!\!\bigcirc \cdot + \tfrac{1}{6} \cdot \bigcirc \cdot \ , \tag{61}$$

$$\Pi_2^{\text{red}(1)} = -\!\!-\!\!\boxed{2}\!\!-\!\!- = 1 \cdot \bigcirc \cdot + \tfrac{1}{2} \, \bigcirc \ , \tag{62}$$

etc. Note that the outcome of the derivative in Eq. (27) must be symmetric in all (bosonic) indices. The three and four-loop self-energies could be derived from Φ_4 and Φ_5, respectively, but we choose not to give them here, since they are not needed for the set of four-loop vacuum diagrams that we will display explicitly in Sec. VII.

With Eqs. (60)–(62), the ring diagrams in Eq. (29) are readily written down.

VI. GENERIC MODEL ON THE LATTICE

So far we have considered the generic model in Eq. (2). However, in a lattice regularization of gauge theories, higher vertices appear as well, without spoiling renormalizability. At the generic level, it is straightforward to add such couplings to the theory in Eq. (2). We can include, e.g., terms up to $\sim (1/8!) \gamma_{ijklmnop} \varphi_i \varphi_j \varphi_k \varphi_l \varphi_m \varphi_n \varphi_o \varphi_p$, as would arise in lattice perturbation theory for SU(N) gauge theories, if one keeps terms contributing to four-loop vacuum graphs. Such computations would be needed when one converts results of three-dimensional numerical Monte Carlo studies from lattice to continuum regularization [10].

In this case, everything goes as before, except for the appearance of extra vertices in the SD equations, as well as in Eq. (49). We shall here simply spell out the final results, without rewriting explicitly the modified SD equations. We obtain the following additional skeletons:

$$\Phi_3 \Big|_{\text{lat}} = \tfrac{1}{12} \, \bigcirc\!\!\bigcirc + \tfrac{1}{48} \, \bigcirc \ , \tag{63}$$

$$\Phi_4 \Big|_{\text{lat}} = \tfrac{1}{8} (\ldots) + \tfrac{1}{12} (\ldots) + \tfrac{1}{240} (\ldots) + \tfrac{1}{12} (\ldots) + \tfrac{1}{8} (\ldots) + \tfrac{1}{16} (\ldots)$$

$$+ \tfrac{1}{48} \, \bigcirc\!\!\bigcirc + \tfrac{1}{72} \, \bigcirc\!\!\bigcirc + \tfrac{1}{48} \, \bigcirc\!\!\bigcirc\!\!\bigcirc + \tfrac{1}{48} \, \bigcirc + \tfrac{1}{384} \, \bigcirc \ , \tag{64}$$

as well as the additional irreducible self-energy

$$\Pi_2^{\text{irr}}\Big|_{\text{lat}} = \;-\!\!\!\text{—}\!\bigcirc\!\!\!\!2\!\!\!\!\bigcirc\!\text{—}\!\!\!-\Big|_{\text{lat}} \;= \;+\frac{1}{4}\cdot\bigcirc\!\!\!\!\cdot\;+\frac{1}{4}\cdot\bigcirc\!\!\!\!\cdot\;+\frac{1}{6}\;\bigcirc\!\!\!\!\bigcirc\;+\frac{1}{8}\cdots\!\!\text{—}\!\!\bigcirc\!\!\bigcirc\!\!\text{—}\!\!\cdots\;,$$

(65)

where we again assumed $c_i = \frac{1}{2}$.

VII. APPLICATIONS: QCD, QED, SQED, ELECTROWEAK THEORY

As an application of the generic formulas derived above, we consider in this section SU(N) gauge theory with fermions and a scalar field. This class includes QCD and QED (where graphs containing scalar propagators and, in the latter case, gauge field self-interactions are to be dropped out), as well as the electroweak theory and scalar electrodynamics (SQED). For brevity, we display here only the vertices appearing in the symmetric phases of the latter theories. We mostly use the language of QCD, referring to the gauge fields as gluons, etc.

The Lagrangian is specified by giving Feynman rules for the free propagators and free vertices,

$$\text{—}\!\!\!\text{—}\!\!\!\text{—}\;,\;\cdots\!\!\blacktriangleright\!\!\cdots\;,\;\text{———}\;,\;\text{⋏}\;,\;\text{⋏}\;,\;\text{⋏}\;,\;\text{⋈}\;,\;\text{⋈}\;,\;\text{✕}\;,$$

(66)

where gluons (scalars) are denoted by wavy (straight) lines. Both quarks and ghosts are denoted here by dotted lines; the Feynman rules for them are different, but the symmetry factors agree—the only exception being diagrams with more than one closed fermion loop, in which case both ghosts and quarks can appear in the same diagram simultaneously, reducing the symmetry by an obvious factor.

We do not here write down counterterms explicitly. Coupling constant counterterms can be viewed as a part of the cubic and quartic couplings, while wave function and mass counterterms can be treated as a part of the *irreducible* self-energies Π_n^{irr}, making their appearance only in ring diagrams according to Eq. (29).

Let us first note that once we write down the summation over the field content explicitly in Eq. (2), the "natural" symmetry factors in front of the vertices change. For instance, writing the four-point vertex in the case of two sets of fields, $\{\varphi_i\} \to \{A_i\} + \{B_\alpha\}$, and using the symmetry of γ_{ijkl}, one gets

$$\frac{1}{4!}\gamma_{ijkl}\varphi_i\varphi_j\varphi_k\varphi_l = \frac{1}{4!}\gamma_{ijkl}A_iA_jA_kA_l + \frac{1}{3!}\gamma_{ijk\alpha}A_iA_jA_kB_\alpha$$

$$+\frac{1}{(2!)^2}\gamma_{ij\alpha\beta}A_iA_jB_\alpha B_\beta + \cdots. \quad (67)$$

Similarly, writing the three-point vertex for three different fields, $\{\varphi_i\} \to \{A_i\} + \{B_\alpha\} + \{C_M\}$, one finds

$$\frac{1}{3!}\gamma_{ijk}\varphi_i\varphi_j\varphi_k = \frac{1}{3!}\gamma_{ijk}A_iA_jA_k + \frac{1}{2!}\gamma_{ij\alpha}A_iA_jB_\alpha$$

$$+\gamma_{i\alpha M}A_iB_\alpha C_M + \cdots. \quad (68)$$

With these conventions, each tree-level vertex in the graphical notation corresponds just to γ_{ijkl}, $\gamma_{ijk\alpha}$, etc., without any symmetry factors there: all of them are shown explicitly.

The only thing remaining is to write the summation over particle species explicitly also in the propagators of Eqs. (56)–(58),

$$\text{———} \equiv \text{~~~~} + \cdots\!\!\blacktriangleright\!\!\cdots + \cdots\!\!\blacktriangleleft\!\!\cdots + \text{———}\;.$$

(69)

Only the vertices allowed by the Feynman rules are kept after this substitution. This generates all the graphs, with the correct symmetry factors.

A. Vacuum skeletons up to the four-loop level

The procedure outlined above can easily be carried out explicitly, and up to the four-loop level even by hand. The main complication is again the identification of various equivalent topologies, and for this a suitable algebraic notation may be more useful than a graphical one. As a result, for the field content in Eq. (66), we finally obtain

$$\Phi_2 \;=\; \tfrac{1}{8}\;\bigcirc\!\!\bigcirc\; +\;\tfrac{1}{12}\; \cdots\; -\;\tfrac{1}{2}\; \cdots\; +\;\tfrac{1}{4}\; \bigcirc\!\!\bigcirc\; +\;\tfrac{1}{4}\; \cdots\; +\;\tfrac{1}{8}\; \bigcirc\!\!\bigcirc\;, \tag{70}$$

$$\Phi_3 \;=\; \tfrac{1}{24}\; \cdots\; -\;\tfrac{1}{3}\; \cdots\; -\;\tfrac{1}{4}\; \cdots\; +\;\tfrac{1}{8}\; \cdots\; +\;\tfrac{1}{48}\; \cdots\; +\;\tfrac{1}{6}\; \cdots\; +\;\tfrac{1}{8}\; \cdots$$

$$+\;\tfrac{1}{2}\; \cdots\; +\;\tfrac{1}{4}\; \cdots\; +\;\tfrac{1}{8}\; \cdots\; +\;\tfrac{1}{8}\; \cdots\; +\;\tfrac{1}{48}\; \cdots\;, \tag{71}$$

$$\Phi_4 \;=\; \tfrac{1}{72}\; \cdots\; -\;\tfrac{1}{4}\; \cdots\; -\;\tfrac{1}{6}\; \cdots\; +\;\tfrac{1}{12}\; \cdots\; -\;\tfrac{1}{2}\; \cdots\; -\;\tfrac{1}{2}\; \cdots$$

$$-\;1\; \cdots\; -\;\tfrac{1}{3}\; \cdots\; +\;\tfrac{1}{6}\; \cdots\; +\;\tfrac{1}{6}\; \cdots\; +\;\tfrac{1}{8}\; \cdots\; -\;\tfrac{1}{4}\; \cdots$$

$$+\;\tfrac{1}{4}\; \cdots\; -\;\tfrac{1}{2}\; \cdots\; +\;\tfrac{1}{8}\; \cdots\; +\;\tfrac{1}{8}\; \cdots\; +\;\tfrac{1}{16}\; \cdots\; +\;\tfrac{1}{48}\; \cdots$$

$$+\;\tfrac{1}{8}\; \cdots\; +\;\tfrac{1}{12}\; \cdots\; -\;\tfrac{1}{3}\; \cdots\; +\;\tfrac{1}{4}\; \cdots\; +\;\tfrac{1}{4}\; \cdots\; +\;\tfrac{1}{2}\; \cdots$$

$$+\;\tfrac{1}{6}\; \cdots\; +\;\tfrac{1}{12}\; \cdots\; +\;\tfrac{1}{2}\; \cdots\; +\;\tfrac{1}{2}\; \cdots\; +\;\tfrac{1}{2}\; \cdots\; +\;\tfrac{1}{8}\; \cdots\; +\;\tfrac{1}{4}\; \cdots$$

$$+\;\tfrac{1}{4}\; \cdots\; -\;\tfrac{1}{2}\; \cdots\; +\;\tfrac{1}{4}\; \cdots\; +\;\tfrac{1}{4}\; \cdots\; +\;\tfrac{1}{4}\; \cdots\; +\;1\; \cdots\; +\;1\; \cdots$$

$$+\;\tfrac{1}{4}\; \cdots\; +\;\tfrac{1}{8}\; \cdots\; +\;\tfrac{1}{2}\; \cdots\; +\;\tfrac{1}{2}\; \cdots\; +\;\tfrac{1}{8}\; \cdots\; +\;\tfrac{1}{4}\; \cdots$$

$$+\;\tfrac{1}{8}\; \cdots\; +\;\tfrac{1}{2}\; \cdots\; +\;\tfrac{1}{2}\; \cdots\; +\;\tfrac{1}{8}\; \cdots\; +\;\tfrac{1}{16}\; \cdots\; +\;\tfrac{1}{2}\; \cdots\; +\;\tfrac{1}{16}\; \cdots$$

$$+\;\tfrac{1}{16}\; \cdots\; +\;\tfrac{1}{6}\; \cdots\; +\;\tfrac{1}{4}\; \cdots\; +\;\tfrac{1}{4}\; \cdots\; +\;\tfrac{1}{4}\; \cdots\; +\;\tfrac{1}{4}\; \cdots\; +\;\tfrac{1}{2}\; \cdots$$

$$+\;\tfrac{1}{8}\; \cdots\; +\;\tfrac{1}{16}\; \cdots\; +\;\tfrac{1}{8}\; \cdots\; +\;\tfrac{1}{16}\; \cdots\; +\;\tfrac{1}{48}\; \cdots\;. \tag{72}$$

B. Self-energies up to the two-loop level

Using Eqs. (27), (20), the skeletons above immediately produce the self-energies of the model in Eq. (66). We obtain

$$\cdots\;①\;\cdots\;=\;\tfrac{1}{2}\; \cdots\; -\;1\; \cdots\; +\;\tfrac{1}{2}\; \cdots\; +\;\tfrac{1}{2}\; \cdots\; +\;\tfrac{1}{2}\; \cdots\;, \tag{73}$$

$$\cdots\;①\;\cdots\;=\;1\; \cdots\;, \tag{74}$$

$$\cdots\;①\;\cdots\;=\;1\; \cdots\; +\;\tfrac{1}{2}\; \cdots\; +\;\tfrac{1}{2}\; \cdots\;, \tag{75}$$

$$\cdots\;②\;\cdots\;=\;\tfrac{1}{2}\; \cdots\; -\;1\; \cdots\; -\;1\; \cdots\; -\;1\; \cdots\; +\;\tfrac{1}{2}\; \cdots\; +\;\tfrac{1}{2}\; \cdots$$

$$+\;\tfrac{1}{4}\; \cdots\; +\;\tfrac{1}{6}\; \cdots\; +\;\tfrac{1}{2}\; \cdots\; +\;\tfrac{1}{2}\; \cdots\; +\;\tfrac{1}{2}\; \cdots$$

$$+\;1\; \cdots\; +\;1\; \cdots\; +\;\tfrac{1}{2}\; \cdots\; +\;\tfrac{1}{2}\; \cdots$$

$$+\;\tfrac{1}{4}\; \cdots\; +\;\tfrac{1}{4}\; \cdots\; +\;\tfrac{1}{2}\; \cdots\; +\;\tfrac{1}{4}\; \cdots\;, \tag{76}$$

$$\blacktriangleright\!\!-\!\!\circlednumber{2}\!\!-\!\!\blacktriangleright \quad = \quad 1 \;\; \cdots\!\!\bigcirc\!\!\cdots \;\; + 1 \;\; \cdots\!\!\bigcirc\!\!\cdots \quad , \tag{77}$$

$$-\!\!\circlednumber{2}\!\!- \quad = \quad 1 \;\; -\!\!\bigcirc\!\!- \;\; + 1 \;\; -\!\!\bigcirc\!\!- \;\; + \tfrac{1}{2} \;\; -\!\!\bigcirc\!\!- \;\; + \tfrac{1}{2} \;\; -\!\!\bigcirc\!\!- \;\; + 1 \;\; -\!\!\bigcirc\!\!- \;\; + 1 \;\; -\!\!\bigcirc\!\!-$$

$$+ 1 \;\; -\!\!\bigcirc\!\!\bigcirc\!\!- \;\; + \tfrac{1}{2} \;\; -\!\!\bigcirc\!\!- \;\; + \tfrac{1}{2} \;\; -\!\!\bigcirc\!\!- \;\; + \tfrac{1}{2} \;\; -\!\!\bigcirc\!\!- \;\; + \tfrac{1}{6} \;\; -\!\!\bigcirc\!\!- \quad , \tag{78}$$

$$\sim\!\!\boxed{2}\!\!\sim \quad = \quad 1 \;\; \sim\!\!\bigcirc\!\!\sim \;\; - 1 \;\; \sim\!\!\bigcirc\!\!\sim \;\; - 1 \;\; \sim\!\!\bigcirc\!\!\sim \;\; + \tfrac{1}{2} \;\; \sim\!\!\bigcirc\!\!\sim \;\; + 1 \;\; \sim\!\!\bigcirc\!\!\sim \;\; + \tfrac{1}{2} \;\; \sim\!\!\bigcirc\!\!\sim \quad , \tag{79}$$

$$\blacktriangleright\!\!-\!\!\boxed{2}\!\!-\!\!\blacktriangleright \quad = \quad 1 \;\; \cdots\!\!\bigcirc\!\!\cdots \;\; + 1 \;\; \cdots\!\!\bigcirc\!\!\cdots \quad , \tag{80}$$

$$-\!\!\boxed{2}\!\!- \quad = \quad 1 \;\; -\!\!\bigcirc\!\!- \;\; + 1 \;\; -\!\!\bigcirc\!\!- \;\; + \tfrac{1}{2} \;\; -\!\!\bigcirc\!\!- \;\; + \tfrac{1}{2} \;\; -\!\!\bigcirc\!\!- \quad . \tag{81}$$

C. Ring diagrams up to the four-loop level

To be exhaustive up to the four-loop level, let us finally give the set of ring diagrams for the model of Eq. (66). While there are no ring diagrams up to the two-loop level, from Eq. (29) we get

$$\left(-F_{(\text{rings})}\right)_3 \quad = \quad \tfrac{1}{4} \;\; \bigcirc\!\!\bigcirc \;\; - \tfrac{1}{2} \;\; \bigcirc\!\!\bigcirc \;\; + \tfrac{1}{4} \;\; \bigcirc\!\!\bigcirc \quad , \tag{82}$$

$$\left(-F_{(\text{rings})}\right)_4 \quad = \quad \tfrac{1}{6} \;\; \bigcirc\!\!\bigcirc \;\; + \tfrac{1}{2} \;\; \bigcirc\!\!\bigcirc \;\; + \tfrac{1}{4} \;\; \bigcirc\!\!\boxed{2} \;\; - \tfrac{1}{3} \;\; \bigcirc\!\!\bigcirc \;\; - 1 \;\; \bigcirc\!\!\bigcirc \;\; - \tfrac{1}{2} \;\; \bigcirc\!\!\boxed{2}$$

$$+ \tfrac{1}{6} \;\; \bigcirc\!\!\bigcirc \;\; + \tfrac{1}{2} \;\; \bigcirc\!\!\bigcirc \;\; + \tfrac{1}{4} \;\; \bigcirc\!\!\boxed{2} \quad . \tag{83}$$

Note the extremely economic structure of the skeleton expansion of Eq. (29): the few ring diagrams above summarize 22 (276) three-loop (four-loop) diagrams.

VIII. DISCUSSION

In this paper we have described a simple practical procedure for systematically generating all vacuum diagrams of a given loop order in a generic field theory.

We have shown that the sum of vacuum diagrams can be written in the form of a modified skeleton expansion, Eq. (29). It contains two-particle-irreducible "skeletons" with free propagators, as well as various self-energy insertions inside "ring diagrams." The self-energies are, in turn, determined by the skeletons. Thus, all one really needs is the skeletons.

The two-particle-irreducible skeletons of a given order are, then, generated by Eq. (49). It contains a number of full three-point and four-point vertices, which can in turn be expanded using specific "irreducible" Schwinger-Dyson equations [Eqs. (40), (41), etc.], where full propagators have been replaced with free propagators. In this way, all vacuum graphs are generated simultaneously, with the correct symmetry factors. Finally, the precise particle content of the

theory one is interested in can be specified as discussed in Sec. VII. Our method is also directly applicable to theories with spontaneous symmetry breaking, as only free propagators and vertices are modified; tadpole graphs are generated by Eq. (35).

This iterative procedure is very straightforward and can be automatized, but up to the four-loop level the computations are easily carried out even by hand, as we have demonstrated. Thus, we believe that our setup economizes the generation of the set of high-order vacuum diagrams, compared with techniques where all types of graphs have to be dealt with on the same footing, without a separation into skeletons with free propagators and ring diagrams.

Up to this point, we have not discussed at all the integrations remaining to be carried out after the diagrams have been generated. Let us end by pointing out that our setup is beneficial as far as their structure is considered, as well, in dimensions lower than 4 [17].

The point is that low-dimensional field theories of the type in Eq. (2) are superrenormalizable. In fact, for $d = 2,3$, only the two-point function suffers from ultraviolet divergences, as can be seen by simple power counting. Therefore the skeleton graphs, which by definition do not have any genuine two-point functions inside them, do not contain any

ultraviolet divergences in subdiagrams. The ring diagrams, on the other hand, do have ultraviolet divergences in subdiagrams. Note, in particular, that since Π_n^{irr}, $\Pi_n^{\text{red}(m)}$ come with different symmetry factors in Eq. (29), the counterterms in Π_n^{irr}, which make the whole Π_n finite, do not in general immediately cancel all the ultraviolet subdivergences of the ring diagrams.

Consequently, various ring diagram classes can contribute to the overall divergences of the vacuum graphs with potentially infrared sensitive coefficients, coming from the other parts of the final integration, while skeleton diagrams cannot. Fortunately, the ring diagram integrations are simpler than those in the skeleton graphs, and this problem can thus be dealt with in a tractable setting [18].

[1] V. W. Hughes and T. Kinoshita, Rev. Mod. Phys. **71**, S133 (1999); A. Czarnecki and W. J. Marciano, Nucl. Phys. B (Proc. Suppl.) **76**, 245 (1999).

[2] T. van Ritbergen, J. A. Vermaseren, and S. A. Larin, Phys. Lett. B **400**, 379 (1997); K. G. Chetyrkin, *ibid.* **404**, 161 (1997); J. A. Vermaseren, S. A. Larin, and T. van Ritbergen, *ibid.* **405**, 327 (1997).

[3] K. G. Chetyrkin, A. L. Kataev, and F. V. Tkachov, Phys. Lett. **99B**, 147 (1981); **101B**, 457(E) (1981); K. G. Chetyrkin, S. G. Gorishnii, S. A. Larin, and F. V. Tkachov, *ibid.* **132B**, 351 (1983); H. Kleinert, J. Neu, V. Schulte-Frohlinde, K. G. Chetyrkin, and S. A. Larin, Phys. Lett. B **272**, 39 (1991); **319**, 545(E) (1991); B. Kastening, Phys. Rev. D **57**, 3567 (1998); S. A. Larin, M. Monnigmann, M. Strosser, and V. Dohm, Phys. Rev. B **58**, 3394 (1998).

[4] E. Braaten and A. Nieto, Phys. Rev. Lett. **76**, 1417 (1996).

[5] K. Kajantie, M. Laine, K. Rummukainen, and M. Shaposhnikov, Nucl. Phys. **B503**, 357 (1997).

[6] P. Arnold and C. Zhai, Phys. Rev. D **50**, 7603 (1994); **51**, 1906 (1995); C. Zhai and B. Kastening, *ibid.* **52**, 7232 (1995); E. Braaten and A. Nieto, *ibid.* **53**, 3421 (1996).

[7] A. D. Linde, Phys. Lett. **96B**, 289 (1980).

[8] P. Ginsparg, Nucl. Phys. **B170**, 388 (1980); T. Appelquist and R. D. Pisarski, Phys. Rev. D **23**, 2305 (1981).

[9] K. Kajantie, M. Laine, K. Rummukainen, and Y. Schröder, Phys. Rev. Lett. **86**, 10 (2001).

[10] K. Farakos, K. Kajantie, K. Rummukainen, and M. Shaposhnikov, Nucl. Phys. **B442**, 317 (1995).

[11] M. Laine, Nucl. Phys. **B451**, 484 (1995); M. Laine and A. Rajantie, *ibid.* **B513**, 471 (1998).

[12] G. D. Moore, Nucl. Phys. **B493**, 439 (1997); **B523**, 569 (1998).

[13] R. Harlander and M. Steinhauser, Prog. Part. Nucl. Phys. **43**, 167 (1999).

[14] J. Küblbeck, M. Böhm, and A. Denner, Comput. Phys. Commun. **60**, 165 (1990); T. Hahn, *ibid.* **140**, 418 (2001); http://www.feynarts.de/

[15] P. Nogueira, J. Comput. Phys. **105**, 279 (1993); ftp://gtae2.ist.utl.pt/pub/qgraf/

[16] M. Bachmann, H. Kleinert, and A. Pelster, Phys. Rev. D **61**, 085017 (2000); H. Kleinert, A. Pelster, B. Kastening, and M. Bachmann, Phys. Rev. E **62**, 1537 (2000); B. Kastening, *ibid.* **61**, 3501 (2000); H. Kleinert, A. Pelster, and B. Van den Bossche, hep-th/0107017; A. Pelster, H. Kleinert, and M. Bachmann, hep-th/0109014.

[17] M. Achhammer, Ph.D. thesis, University of Regensburg, 2000.

[18] K. Kajantie, M. Laine, K. Rummukainen, and Y. Schröder (in preparation).

[19] P. Cvitanović, *Field Theory*, Nordita Lecture Notes (Nordita, Copenhagen, 1983); http://www.nbi.dk/˜predrag/field_the see also P. Cvitanović, B. Lautrup, and R. B. Pearson, Phys. Rev. D **18**, 1939 (1978).

[20] J. M. Luttinger and J. C. Ward, Phys. Rev. **118**, 1417 (1960); G. Baym, *ibid.* **127**, 1391 (1962); C. De Dominicis and P. C. Martin, J. Math. Phys. **5**, 31 (1964).

[21] J. M. Cornwall, R. Jackiw, and E. Tomboulis, Phys. Rev. D **10**, 2428 (1974).

[22] J. Reinbach and H. Schulz, Phys. Lett. B **404**, 291 (1997).

[23] R. Jackiw, Phys. Rev. D **9**, 1686 (1974); R. Fukuda and E. Kyriakopoulos, Nucl. Phys. **B85**, 354 (1975).

[24] S. Coleman and E. Weinberg, Phys. Rev. D **7**, 1888 (1973).

[25] J. A. M. Vermaseren, math-ph/0010025; http: //www.nikhef.nl/˜form/

[YS3]

Automatic reduction of four-loop bubbles

Automatic reduction of four-loop bubbles

Y. Schröder [a]

[a]Center for Theoretical Physics, MIT, Cambridge, MA 02139, USA

We give technical details about the computational strategy employed in a recently completed investigation of the four-loop QCD free energy. In particular, the reduction step from generic vacuum bubbles to master integrals is described from a practical viewpoint, for fully massive as well as QED-type integrals.

1. Introduction

Vacuum integrals, i.e. integrals without external momenta (often also called tadpoles or bubbles), constitute an important class of multi-loop Feynman integrals. While the perturbative expansion of quantities like the free energy can be directly expressed in terms of vacuum integrals, they also serve as essential building blocks for many other computations, being the coefficient functions in asymptotic expansions of diagrams with external legs, and encoding the ultraviolet behavior of multi-scale integrals.

A typical perturbative calculation proceeds in four conceptually independent steps. First, all relevant diagrams including their combinatoric factors are generated. For an algorithm that does this for vacuum integrals, see [1]. Second, the Feynman rules of the theory under consideration are inserted, and the color and Lorentz algebra is performed. Since in general individual loop integrals are divergent, a regularization scheme has to be adopted, the most practical one at present being dimensional regularization (DR). Third, linear relations between the regularized integrals are exploited, to systematically reduce all integrals occurring in the computation to a small set of so-called master integrals. In the framework of DR, the most important class of relations can be derived from integration-by-parts (IBP) identities [2]. Fourth, the master integrals have to be evaluated, either, in some fortunate cases, fully analytically, or as an expansion in terms of the regularization parameter, in which case – and only here – the number of dimensions d has to be specified. For results on the 4-loop level, see [3] ($d = 4 - 2\epsilon$)

and [4] ($d = 3 - 2\epsilon$).

At higher loop orders, it is inevitable to automate the above setup to a large degree. There exist many approaches to implement automated perturbative calculations, and this is not the place to give a comprehensive review (see e.g. [5]). Instead, it is the third of the above steps that we wish to elaborate on in this contribution.

A computer algebra system that is particularly well suited to cope with the demands of higher order perturbative calculations is FORM [6]. While by no means mandatory to use, we have adopted it to implement our algorithms, and hence we will indicate in a few places which specific FORM commands turned out to be extremely helpful.

2. Notation and general considerations

Consider the generic vacuum topologies of Fig. 1. In this intuitive graphical notation, every line represents a propagator $(p_i^2 + m_i^2)^{-a_i}$, with integer power $a_i > 0$, where the index i labels the different lines with momenta p_i, which in turn can be expressed as a linear combination of the ℓ loop momenta k_j. The vertices do not have any structure, except for assuring momentum conservation. Each diagram can carry a nontrivial numerator structure, which in the general case consists of powers of scalar products of the loop momenta. At ℓ loops, there are $\ell(\ell + 1)/2$ different combinations $k_i \cdot k_j$.

Let us distinguish three different representations of our integrals, which naturally appear at various levels of the reduction process: *generic integrals*, their *standard representations*, and the *master integrals*. The goal of step three is then to
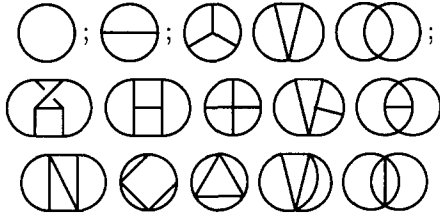
Figure 1. *The 1+1+3+10 generic vacuum topologies up to four loops. The 0+1+2+6 factorized topologies are not shown here.*

formulate the algorithms which transform generic to standard to master integrals:

$$\int_{k_1\ldots\ell}^{(d)} \frac{\prod_{1\le i\le j\le\ell}(k_i\cdot k_j)^{b_{ij}}}{\prod_i(p_i^2+m_i^2)^{a_i}}$$

$$\overset{\text{Filter}}{\longrightarrow} \int_{k_1\ldots\ell}^{(d)} \frac{\prod(k_i\cdot k_j)^{b_{ij}}_{\text{irred.}}}{\prod_i(p_i^2+m_i^2)^{a_i}} \equiv (\{a_i\},\{b_{ij},m_i\})$$

$$\overset{\text{Tables}}{=} \sum_j c_j(d)\,\text{Master}_j^{(d)}(\{m_i\}) \tag{1}$$

Above, the label 'Filter' symbolizes a collection of low-level routines, whose main action is to complete squares in the numerator and cancel against propagators such that only irreducible numerators remain. At this point, it is possible to represent an ℓ-loop vacuum integral by a list of $\ell(\ell+1)$ non-negative numbers $(\{a_i\},\{b_{ij},m_i\})$, the first half of them collecting the powers of propagators a_i, while the second half contains either the power of an irreducible numerator (if the corresponding a_i is zero) or the mass of the line. Furthermore, at this step equivalent topologies are re-labeled in a unique way by shifting the loop momenta, i.e. assigning a characteristic pattern of zeroes among the a_i to each topology of Fig. 1.

In the remainder, we will specialize on two different general classes of vacuum diagrams. First, we will consider all lines to have the same mass, $m_i = m$. This class of integrals is useful when computing infrared-safe quantities like renormalization coefficients, in which case the infrared sector of individual diagrams can be regulated by introducing masses into massless propagators. Second, we will allow for all m_i to be either zero or m, with the restriction that the number of massive lines at each vertex be even. This includes theo-

ries like QED and gauge+Higgs models, whence we call this class 'QED-like'.

The label 'Tables' in Eq. (1) symbolizes a lookup in a database, which contains the necessary relations in a tabulated form. These tables are the main ingredient of the reduction step, and their organization and generation, which systematically exploits IBP identities, will be described in more detail below.

The intermediate step of applying the 'Filter' algorithms not only serves the purpose of allowing for a fairly compact representation of the integral, but can also be used to keep the number of entries in the database, the memory requirements, and the CPU time needed for their derivation, in manageable bounds. To this end, we found it advantageous to add further routines to the 'Filter' package:

- Early detection of zeroes: massless (sub-) tadpoles are zero in DR, as are integrals whose integrand does not depend on one of the loop momenta.

- Symmetrization of the integrand: use the full symmetry group of the corresponding topology to order the list, and hence enable early cancellations in big expressions.

- Decouple scalar products involving the loop momentum of a factorized one-loop tadpole: $\int_k \frac{k_{\mu_1}\ldots k_{\mu_n}}{(k^2+m^2)^a}$ vanishes for odd n and is proportional to a totally symmetric combination of metric tensors $g_{\{\mu_1\mu_2}\cdots g_{\mu_{n-1}\mu_n\}}$. The FORM function dd_ is perfectly suited for this symmetrization. This eliminates the need to derive relations for 8 (out of 9, the 9th being the two-loop × two-loop case) of the factorized topologies, since after decoupling the numerator, factorization into scalar vacuum integrals of the type of Eq. (1) is complete.

- Reduce powers of factorized one-loop tadpoles to one:

$$\int \frac{d^d k}{(k^2+m^2)^{a+1}} = -\frac{d-2a}{2am^2}\int \frac{d^d k}{(k^2+m^2)^a}$$

- Employ the 'triangle relation' [2]: for integrals involving massless lines, this helps

to reduce the number of different topologies that have to be treated in the database considerably.

Another potentially useful routine, which we have however not implemented, would be to use T-operators [7] in order to trade *all* numerator structure for higher dimensions of the integral measure, hence also immediately decoupling the factorized (two-loop × two-loop)-topology.

One more practical note: To not miss cancellations, it is important to have a unique representation for coefficients. Partial fractioning of terms like $\frac{d}{d-a}$ and $\frac{1}{d-a_1}\frac{1}{d-a_2}$ helps here, ensuring the coefficients $c_i(d)$ to be a sum of powers of simple poles $\frac{1}{d-a}$ and powers of d.

In principle however, all these further relations are redundant since they would be automatically covered by the IBP identities. As mentioned above, their sole purpose is to optimize the derivation of relations among the integrals, to be discussed next.

3. Reduction

Integration by parts relies on the fact that an integral over a total derivative of any of the loop momenta vanishes in dimensional regularization. For the case of vacuum integrals, which we are interested in here, the IBP identities read

$$0 = \int \frac{d^d k_{1...\ell}}{(2\pi)^{\ell d}}\, \partial_{p_\mu} q_\mu \left(\{a_i\}, \{b_{ij}, m_i\}\right)\,, \qquad (2)$$

where $p, q \in \{k_1, \ldots, k_\ell\}$ cover all ℓ^2 different ℓ-loop identities, and we have made use of the standard representation introduced above.

There are two possible general strategies implementing the IBP identities to find relations useful for reducing the integrals from their standard representation to master integrals.

The first strategy is to derive general relations, valid for symbolic list-entries. These general symbolic relations can then be applied repeatedly to any integral of the specified class, no matter how large the powers are, to achieve the reduction. In practice however, it turns out that it is quite an art to shuffle IBP identities for integrals with symbolic indices such as to obtain useful reduc-
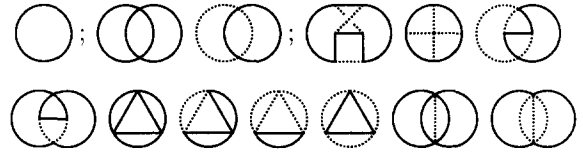
Figure 2. *The 1+0+2+10 master integrals of QED type, up to four loops. Full lines carry a mass m, dotted lines are massless. All numerators are 1, all powers of propagators are 1. Note that there is no two-loop representative needed.*

tion relations. In absence of a generic algorithmic formulation, it involves extensive handwork, and typically there are many special cases to be considered when pre-factors vanish at special parameter values. At lower loop orders, there are complete solutions, see e.g. [9] for two-loop two-point functions with general masses, or [10] for three-loop vacuum integrals with one mass.

The second strategy, nowadays constituting the mainstream of higher-loop computations, is a more brute-force approach, which however has the huge advantage of being perfectly suited to be completely automated. The main idea is to write down IBP identities for specific values of the indices. Introducing a lexicographic ordering among the integrals [8], it is then possible to solve every single one of the IBP identities for the 'most difficult' integral occurring. By starting from simple topologies (low number of lines), one systematically generates relations which express 'difficult' integrals in terms of 'simpler' (in the sense of the ordering) ones. Solving an adequate set of fixed-index IBP relations, it is possible to express every integral of interest in terms of a few simple ones, ultimately the master integrals.

The reason why the second strategy is sufficient for most computations is that in practice, one does not meet the most general integrals, but only a subset, typically characterized by an upper cutoff on the sum of indices. Indeed, dealing with a concrete model like QCD, knowledge of the vertex and propagator structure allows to constrain the set of possible indices ($\{a_i\}, \{b_{ij}, m_i\}$), hence rendering the search-space to be covered with IBP identities finite.

Building up the relations proceeds as follows:

- Pick a list of indices ($\{a_i\}, \{b_{ij}, m_i\}$) that is 'simple', typically meaning a low number of loops, a low number of different lines, a low number of extra powers on the propagators, a low number of powers on the irreducible numerators. In FORM, these lists are most naturally represented by sparse tables.
- Generate the first of the IBP identities.
- Call 'Filter' to transform the resulting sum of integrals to the standard representation.
- Label the 'most difficult' integral, according to the lexicographic ordering. A global operation like that became possible with the introduction of '$-variables' in FORM v3.
- Invert its coefficient and multiply it into the equation. We do so only if we can factorize the coefficient into terms which are linear in d, to preserve the generic structure of coefficients. While (at present) there is no factorization algorithm in FORM, we implemented one by 'guessing' zeroes, utilizing the fact that since the coefficients are generated by IBP, most of them have factors $(nd \pm a)$ where n is not bigger than the number of loops, and a is an integer of moderate size. To check that no relations are missed when factorization fails, it is useful to keep track of those cases and check in the end.
- Bring the most difficult integral (having coefficient 1) to the left-hand-side, taking the generated equation as a definition. In FORM, this is done by the `fill` statement.
- Take the next IBP identity, repeat the above steps. Increase list-indices. Repeat...
- Write the relations found to disk in intervals. Large intervals ensure a high degree of re-substitution (of relations for integrals that are found later but that appeared on the right-hand-sides earlier), but are risky when the program execution crashes.

Solving the IBP relations one by one like described above seems to be simpler than solving large systems of linear equations at once. In the end, it might be advantageous to re-substitute relations, which is possible by re-loading sets of relations into memory and re-writing them to disk.

Figure 3. *The 0+0+0+3 fully massive master integrals, in addition to those 1+1+3+10 of Fig. 1, taken at powers and numerators 1. A dot on a line means it carries an extra power.*

In the end, one has to check whether the set of generated identities is sufficiently large to achieve a reduction of all integrals occurring in the physics problem at hand. While a first educated guess on the maximum powers needed can be obtained by scanning the terms to be calculated after application of the 'Filter' package, it might be necessary to enlarge the set of relations in further runs. To this end, the `tablebase` statement of FORM, implemented in version 3.1, allows for a good control over large amounts of data in the form of tables and table elements.

The resulting master integrals are depicted in Fig. 2 for the 'QED-like' case, and in Figs. 3,1 for the fully massive case.

4. Master integrals

Once the reduction algorithm 'stops', are we guaranteed to arrive at the desired *minimal* set of master integrals? If we had followed the path of deriving generic reduction relations, valid for symbolic indices, the answer would be yes. For the implementation in terms of specific indices, one can however not be absolutely sure not to miss a relation which would only be detected when increasing the upper cutoff on indices of the integrand. For most practical purposes it might already be sufficient to work with an incomplete, but small, basis.

In the case of gauge theories, it is also amusing to watch the gauge-parameter dependence as an indicator of how 'close' one is to the minimal set, since in a full reduction gauge-parameter dependent terms cancel at an algebraic level, in d dimensions, before evaluating the master integrals.

The basis of master integrals is of course not unique, but depends on the actual choice of the lexicographic ordering. While we label an integral with unit numerator as 'simpler' than one with in-

Figure 4. *Relations for a basis conversion from the set of massive masters found in [3] to our notation.*

creased powers on the lines, one could as well have put priority on always reducing powers of propagators to one. The latter choice was adopted in a recent paper [3], where the three master integrals of Fig. 3 are replaced by ones of equivalent topology, but with irreducible numerators. Consequently, there must be linear relations between the two choices of basis, valid analytically in d dimensions. From our tables, we simply read them off, see Fig. 4.

5. Discussion

We did not comment on the problem of so-called spurious poles here. Spurious poles are singular pre-factors, which can occur in the reduction relations. They are difficult to avoid in general, if one is not willing to specify the dimension yet in the reduction process. However, in our four-loop computation of the QCD free energy, we treated them after the reduction was performed successfully, by changing basis with the help of the tables.

In principle, the package at hand can be used for other calculations requiring a four-loop reduction of massive vacuum bubbles. One such application would be the re-evaluation of the QCD beta function.

REFERENCES

1. K. Kajantie, M. Laine and Y. Schröder, Phys. Rev. D **65**, 045008 (2002).
2. K. G. Chetyrkin and F. V. Tkachov, Nucl. Phys. B **192**, 159 (1981); F. V. Tkachov, Phys. Lett. B **100**, 65 (1981).
3. S. Laporta, arXiv:hep-ph/0210336.
4. A. Vuorinen, Master's Thesis, Helsinki University, 2001.
5. R. Harlander and M. Steinhauser, Prog. Part. Nucl. Phys. **43**, 167 (1999).
6. J.A.M. Vermaseren, arXiv:math-ph/0010025; http://www.nikhef.nl/~form/.
7. O. V. Tarasov, Phys. Rev. D **54**, 6479 (1996).
8. S. Laporta, Int. J. Mod. Phys. A **15**, 5087 (2000).
9. O. V. Tarasov, Nucl. Phys. B **502**, 455 (1997).
10. D.J. Broadhurst, Z. Phys. C 54 (1992) 599; L. V. Avdeev, Comput. Phys. Commun. **98**, 15 (1996); P. A. Baikov and M. Steinhauser, Comput. Phys. Commun. **115**, 161 (1998).

[YS4]

Pressure of hot QCD up to $g^6 \ln(1/g)$

Pressure of hot QCD up to $g^6\ln(1/g)$

K. Kajantie,[1] M. Laine,[2] K. Rummukainen,[1] and Y. Schröder[3]

[1]*Department of Physics, P.O. Box 64, FIN-00014 University of Helsinki, Finland*
[2]*Theory Division, CERN, CH-1211 Geneva 23, Switzerland*
[3]*Center for Theoretical Physics, MIT, Cambridge, Massachusetts 02139*

The free energy density, or pressure, of QCD has at high temperatures an expansion in the coupling constant g, known so far up to order g^5. We compute here the last contribution which can be determined perturbatively, $g^6\ln(1/g)$, by summing together results for the 4-loop vacuum energy densities of two different three-dimensional effective field theories. We also demonstrate that the inclusion of the new perturbative $g^6\ln(1/g)$ terms, once they are summed together with the so far unknown perturbative and nonperturbative g^6 terms, could potentially extend the applicability of the coupling constant series down to surprisingly low temperatures.

I. INTRODUCTION

Because of asymptotic freedom, the properties of QCD might be expected to be perturbatively computable in various "extreme" limits, such as high virtuality, high baryon density, or high temperature. We concentrate here on the last of these circumstances, that is, temperatures T larger than a few hundred MeV.

The physics observable we consider is the pressure, or minus the free energy density, of the QCD plasma. Potential phenomenological applications include the expansion rate of the early Universe after it has settled into the standard model vacuum, as well as the properties of the apparently ideal hydrodynamic expansion observed in on-going heavy ion collision experiments, just shortly after impact.

In these environments, it turns out that the naive expectation concerning the validity of perturbation theory is too optimistic. Indeed, even assuming an arbitrarily weak coupling constant g, perturbation theory can only be worked out to a finite order in it, before the serious infrared problems of finite temperature field theory deny further analytic progress [1,2]. For the pressure, the problem is met at the 4-loop order, or $\mathcal{O}(g^6)$.

This leads to the interesting situation that there is a definite limit to how far perturbation theory needs to be pushed. So far, there are known loop contributions at orders $\mathcal{O}(g^2)$ [3], $\mathcal{O}(g^3)$ [4], $\mathcal{O}(g^4\ln(1/g))$ [5], $\mathcal{O}(g^4)$ [6], and $\mathcal{O}(g^5)$ [7]. There is also an all-orders numerical result available for a theory with an asymptotically large number of fermion flavors [8]. The purpose of the present paper is to collect together results from two accompanying papers [9,10], allowing us to determine analytically the last remaining perturbative contribution, $\mathcal{O}(g^6\ln(1/g))$, for the physical QCD.

It must be understood that even if computed up to such a high order, the perturbative expansion could well converge only very slowly, requiring perhaps something like $T \gg$ TeV, to make any sense at all [7,11,12]. With one further coefficient available, we can to some extent now reinspect this issue. To do so we actually also need to assume something about the unknown $\mathcal{O}(g^6)$ term, since the numerical factor inside the logarithm in $\mathcal{O}(g^6\ln(1/g))$ remains otherwise undetermined. Therefore, our conclusions on this point remain on a conjectural level, but turn out to show nevertheless a somewhat interesting pattern, which is why we would like to include them in this presentation.

Finally, it should be stressed that even if the perturbative expansion as such were to remain numerically useless at realistic temperatures, these multiloop computations are still worthwhile: the infrared problems of finite temperature QCD can be isolated to a three-dimensional (3D) effective field theory [13] and studied nonperturbatively there with simple lattice simulations [14]. However, to convert the results from 3D lattice regularization to 3D continuum regularization, and from the 3D continuum theory to the original four-dimensional (4D) physical theory, still necessitates a number of perturbative "matching" computations. Both of these steps are very closely related to what we do here, although we discuss explicitly only the latter one.

II. THE BASIC SETTING

We start by reviewing briefly how it is believed that the properties of QCD at a finite temperature T can be reduced to a number of perturbatively computable matching coefficients, as well as some remaining contributions from a series of effective field theories [13]. Our presentation follows mostly that in [11], but there are a few significant differences.

The underlying theory is finite temperature QCD with the gauge group SU(N_c), and N_f flavors of massless quarks. In dimensional regularization the bare Euclidean Lagrangian reads, before gauge fixing,

$$S_{\text{QCD}} = \int_0^{\beta\hbar} d\tau \int d^d x \, \mathcal{L}_{\text{QCD}}, \tag{2.1}$$

$$\mathcal{L}_{\text{QCD}} = \frac{1}{4} F^a_{\mu\nu} F^a_{\mu\nu} + \bar{\psi}\gamma_\mu D_\mu \psi, \tag{2.2}$$

where $\beta = T^{-1}$, $d = 3 - 2\epsilon$, $\mu, \nu = 0, \ldots, d$, $F^a_{\mu\nu} = \partial_\mu A^a_\nu - \partial_\nu A^a_\mu + g f^{abc} A^b_\mu A^c_\nu$, $D_\mu = \partial_\mu - ig A_\mu$, $A_\mu = A^a_\mu T^a$, $\gamma^\dagger_\mu = \gamma_\mu$, $\{\gamma_\mu, \gamma_\nu\} = 2\delta_{\mu\nu}$, and ψ carries Dirac, color, and flavor indices.

Denoting the generators of the adjoint representation by $(F^a)_{bc} = -if^{abc}$, we define the usual group theory factors:

$$C_A \delta_{ab} = [F^c F^c]_{ab}, \quad C_F \delta_{ij} = [T^a T^a]_{ij}, \quad (2.3)$$

$$T_A \delta^{ab} = \text{Tr}\, F^a F^b, \quad T_F \delta^{ab} = \text{Tr}\, T^a T^b, \quad (2.4)$$

$$d_A = \delta^{aa} = N_c^2 - 1, \quad d_F = \delta_{ii} = T_F d_A / C_F. \quad (2.5)$$

Obviously $T_A = C_A$. For the standard normalization, with N_f quark flavors, $C_A = N_c$, $C_F = (N_c^2 - 1)/(2N_c)$, $T_A = N_c$, $T_F = N_f/2$, $d_A = N_c^2 - 1$, $d_F = N_c N_f$.

We use dimensional regularization throughout this paper. The spatial part of each momentum integration measure is written as

$$\int_p \equiv \int \frac{d^d p}{(2\pi)^d} = \mu^{-2\epsilon} \left[\bar{\mu}^{2\epsilon} \left(\frac{e^\gamma}{4\pi} \right)^\epsilon \int \frac{d^d p}{(2\pi)^d} \right], \quad (2.6)$$

where $\mu = \bar{\mu}(e^\gamma/4\pi)^{1/2}$, and the expression in square brackets has integer dimensionality. From now on we always assume implicitly that the factor $\mu^{-2\epsilon}$ is attached to some relevant coupling constant, so that the 4D g^2 is dimensionless, while the dimensionalities of $g_E^2, \lambda_E^{(1)}, \lambda_E^{(2)}$ and g_M^2, to be introduced presently, are GeV.

The basic quantity of interest to us here is minus the free energy density $f_{\text{QCD}}(T)$, or the pressure $p_{\text{QCD}}(T)$, defined by

$$p_{\text{QCD}}(T) \equiv \lim_{V \to \infty} \frac{T}{V} \ln \int \mathcal{D}A^a_\mu \, \mathcal{D}\psi \, \mathcal{D}\bar{\psi} \exp\left(-\frac{1}{\hbar} S_{\text{QCD}} \right), \quad (2.7)$$

where V denotes the d-dimensional volume. Boundary conditions over the compact time-like direction are periodic for bosons and anti-periodic for fermions. Moreover, we assume $p_{\text{QCD}}(T)$ renormalized such that it vanishes at $T = 0$. To simplify the notation, we do not show the infinite volume limit explicitly in the following.

At high temperatures and a small coupling, there are parametrically three different mass scales in the problem, $\sim 2\pi T, gT, g^2 T$ [13]. All the effects of the hard mass scale $\sim 2\pi T$ can be accounted for by a method called dimensional reduction [13,15]. Specifically,

$$p_{\text{QCD}}(T) \equiv p_E(T) + \frac{T}{V} \ln \int \mathcal{D}A^a_k \mathcal{D}A^a_0 \exp(-S_E), \quad (2.8)$$

$$S_E = \int d^d x \, \mathcal{L}_E, \quad (2.9)$$

$$\mathcal{L}_E = \frac{1}{2} \text{Tr}\, F_{kl}^2 + \text{Tr}\,[D_k, A_0]^2 + m_E^2 \text{Tr}\, A_0^2 + \lambda_E^{(1)} (\text{Tr}\, A_0^2)^2 + \lambda_E^{(2)} \text{Tr}\, A_0^4 + \ldots. \quad (2.10)$$

Here $k = 1, \ldots, d$, $F_{kl} = (i/g_E)[D_k, D_l]$, $D_k = \partial_k - ig_E A_k$, and we have used the shorthand notation $A_k = A^a_k \bar{T}^a, A_0 = A^a_0 \bar{T}^a$, where $\bar{T}^a$ are Hermitean generators of SU(N_c) normalized such that $\text{Tr}\, \bar{T}^a \bar{T}^b = \delta^{ab}/2$. Note that the quartic couplings $\lambda_E^{(1)}, \lambda_E^{(2)}$ are linearly independent only for $N_c \geq 4$.

The relation in Eq. (2.8) contains five different matching coefficients, $p_E, m_E^2, g_E^2, \lambda_E^{(1)}, \lambda_E^{(2)}$. We are interested in the expression for $p_{\text{QCD}}(T)$ up to order $\mathcal{O}(g^6 T^4)$. They will then have to be determined to some sufficient depths, as we will specify later on. Let us here note that the leading order magnitudes are $p_E \sim T^4$, $m_E^2 \sim g^2 T^2$, $g_E^2 \sim g^2 T$, $\lambda_E^{(1)} \sim g^4 T$, $\lambda_E^{(2)} \sim g^4 T$.

Apart from the operators shown explicitly in Eq. (2.10), there are of course also higher order ones in $\mathcal{L}_E$. The lowest such operators have been classified in [16]. Their general structure is that one must add at least two powers of D_k or gA_0 to the basic structures in Eq. (2.10). Since higher order operators are generated through interactions with the scales that have been integrated out, $\sim 2\pi T$, they must also contain an explicit factor of at least g^2. For dimensional reasons, the schematic structure is thus

$$\delta \mathcal{L}_E \sim g^2 \frac{D_k D_l}{(2\pi T)^2} \mathcal{L}_E. \quad (2.11)$$

To estimate the largest possible contributions such operators could give, let us assume the most conservative possibility that the only dynamical scale in the effective theory is $\sim gT$. By dimensional analysis, we then obtain a contribution

$$\frac{\delta p_{\text{QCD}}(T)}{T} \sim \delta \mathcal{L}_E \sim g^2 \frac{(gT)^2}{(2\pi T)^2} (gT)^3 \sim g^7 T^3. \quad (2.12)$$

Therefore, all higher dimensional operators can be omitted from the action in Eq. (2.10), if we are only interested in computing $p_{\text{QCD}}(T)$ up to order $\mathcal{O}(g^6 T^4)$.

The theory in Eq. (2.10) contains still two dynamical scales, $gT, g^2 T$. All the effects of the "color-electric" scale, gT, can be accounted for by integrating out A_0 [13]. Specifically,

$$\frac{T}{V} \ln \int \mathcal{D}A^a_k \mathcal{D}A^a_0 \exp(-S_E) \equiv p_M(T)$$
$$+ \frac{T}{V} \ln \int \mathcal{D}A^a_k \exp(-S_M), \quad (2.13)$$

$$S_M = \int d^d x \, \mathcal{L}_M, \quad (2.14)$$

$$\mathcal{L}_M = \frac{1}{2} \text{Tr}\, F_{kl}^2 + \ldots, \quad (2.15)$$

where $F_{kl} = (i/g_M)[D_k, D_l]$, $D_k = \partial_k - ig_M A_k$, and $A_k = A^a_k \bar{T}^a$.

The relation in Eq. (2.13) contains two matching coefficients, p_M, g_M^2, which again have to be determined to sufficient depths. At leading order, $p_M \sim m_E^3 T$, $g_M^2 \sim g_E^2$. In addi-

tion, there are also higher order operators in Eq. (2.15). The lowest ones can be obtained by imagining again that we apply at least two covariant derivatives to Eq. (2.15), together with at least one factor g_E^2 brought in by the interactions with the massive modes. This leads to an operator

$$\delta\mathcal{L}_M \sim g_E^2 \frac{D_k D_l}{m_E^3} \mathcal{L}_M. \tag{2.16}$$

The only dynamical scale in the effective theory being $\sim g^2 T$, dimensional analysis indicates that we then obtain a contribution of the order

$$\frac{\delta p_{\text{QCD}}(T)}{T} \sim \delta\mathcal{L}_M \sim g_E^2 \frac{(g^2 T)^2}{m_E^3} (g^2 T)^3 \sim g^9 T^3. \tag{2.17}$$

Therefore, higher dimensional operators can again be omitted, if we are only interested in the order $\mathcal{O}(g^6 T^4)$ for $p_{\text{QCD}}(T)$.

After the two reduction steps, there still remains a contribution from the scale $g^2 T$:

$$p_G(T) \equiv \frac{T}{V} \ln \int \mathcal{D}A_k^a \exp(-S_M), \tag{2.18}$$

with S_M in Eqs. (2.14), (2.15). Since $\mathcal{L}_M$ only has one parameter, and it is dimensionful, the contribution is of the form

$$p_G(T) \sim T g_M^6. \tag{2.19}$$

The coefficient of this contribution is, however, nonperturbative [1,2].

In the following sections, we proceed in the opposite direction with regard to the presentation above, from the "bottom" scale $g^2 T$, producing $p_G(T)$, through the "middle" scale gT, producing $p_M(T)$, back to the "top" scale $2\pi T$, producing $p_E(T)$. We collect on the way all contributions up to order $g^6 T^4$ to obtain $p_{\text{QCD}}(T) = p_E(T) + p_M(T) + p_G(T)$.

III. CONTRIBUTIONS FROM THE SCALE $g^2 T$

The contribution to $p_{\text{QCD}}(T)$ from the scale $p \sim g^2 T$ is obtained by using the theory $\mathcal{L}_M$ in Eq. (2.15) in order to compute $p_G(T)$, as defined by Eq. (2.18). As is well known [1,2], the computation involves infrared divergent integrals, starting at the 4-loop level. This is a reflection of the fact that $\mathcal{L}_M$ defines a confining field theory. Therefore, $p_G(T)$ cannot be evaluated in perturbation theory.

What can be evaluated, however, is the logarithmic ultraviolet divergence contained in $p_G(T)$. For dimensional reasons, the nonperturbative answer would have to be of the form

$$\frac{p_G(T)}{T\mu^{-2\epsilon}} = d_A C_A^3 \frac{g_M^6}{(4\pi)^4} \left[\alpha_G \left(\frac{1}{\epsilon} + 8\ln\frac{\bar{\mu}}{2m_M} \right) + \beta_G + \mathcal{O}(\epsilon) \right], \tag{3.1}$$

where $m_M \equiv C_A g_M^2$. Now, because of the super-renormalizability of $\mathcal{L}_M$, the coefficient α_G can be computed in 4-loop perturbation theory, even if the constant part β_G cannot [29].

Of course, if we just carry out the 4-loop computation in strict dimensional regularization, then the result vanishes, because there are no perturbative mass scales in the problem. This means that ultraviolet and infrared divergences (erroneously) cancel against each other. Therefore, we have to be more careful in order to determine α_G.

To regulate the infrared divergences we introduce by hand a mass scale, m_G^2, into the gauge field (and ghost) propagators. This computation is described in detail in [9]. Individual diagrams contain then higher order poles, like $1/\epsilon^2$, as well as a polynomial of degree up to nine in the gauge parameter ξ. However, terms of both of these types cancel in the final result, which serves as a nice check of the procedure.

As a result, we obtain

$$\frac{p_G(T)}{T\mu^{-2\epsilon}} \approx d_A C_A^3 \frac{g_M^6}{(4\pi)^4} \left[\alpha_G \left(\frac{1}{\epsilon} + 8\ln\frac{\bar{\mu}}{2m_G} \right) + \tilde{\beta}_G(\xi) + \mathcal{O}(\epsilon) \right], \tag{3.2}$$

where "$\approx$" is used to denote that only the coefficient α_G multiplying $1/\epsilon$ is physically meaningful, as it contains the desired gauge independent ultraviolet divergence, defined in Eq. (3.1). The value of the coefficient, obtained by extensive use of techniques of symbolic computation (implemented [17] in FORM [18]), is [9]

$$\alpha_G = \frac{43}{96} - \frac{157}{6144}\pi^2 \approx 0.195715. \tag{3.3}$$

On the contrary, the constant part $\tilde{\beta}_G(\xi)$ depends on the gauge parameter ξ, because the introduction of m_G^2 breaks gauge invariance, and has nothing to do with β_G in Eq. (3.1).

IV. CONTRIBUTIONS FROM THE SCALE gT

We next proceed to include the contribution from the scale gT, contained in $p_M(T)$, as defined by Eq. (2.13). By construction, Eq. (2.13) assumes that all the infrared divergences of the expression on the left-hand side are contained in $p_G(T)$, defined in Eq. (2.18), and determined in Eq. (3.1). Therefore, if we compute the functional integral $(T/V)\ln[\int \mathcal{D}A_i^a \mathcal{D}A_0^a \exp(-S_E)]$ using strict dimensional regularization (i.e., without introducing by hand any mass m_G for the gauge field A_i), whereby $p_G(T)$ vanishes due to the cancellation between infrared and ultraviolet divergences mentioned above, we are guaranteed to obtain just the infrared insensitive matching coefficient $p_M(T)$. This is exactly the computation we need, and carry out in [10,19]. It may be mentioned that we have checked explicitly the infrared in-

sensitivity of the result, by giving an equal mass to both A_0 and A_i in the 4-loop expression for the functional integral, and then subtracting the graphs responsible for $p_G(T)$, with the same infrared regularization. This result is also independent of the gauge parameter.

Keeping terms up to order $\mathcal{O}(g^6 T^4)$, the full outcome for $p_M(T)$ is

$$
\frac{p_M(T)}{T\mu^{-2\epsilon}} = \frac{1}{(4\pi)} d_A m_E^3 \left[\frac{1}{3} + \mathcal{O}(\epsilon) \right]
$$

$$
+ \frac{1}{(4\pi)^2} d_A C_A g_E^2 m_E^2 \left[-\frac{1}{4\epsilon} - \frac{3}{4} - \ln\frac{\bar{\mu}}{2m_E} + \mathcal{O}(\epsilon) \right]
$$

$$
+ \frac{1}{(4\pi)^3} d_A C_A^2 g_E^4 m_E
$$

$$
\times \left[-\frac{89}{24} - \frac{1}{6}\pi^2 + \frac{11}{6}\ln 2 + \mathcal{O}(\epsilon) \right]
$$

$$
+ \frac{1}{(4\pi)^4} d_A C_A^3 g_E^6 \left[\alpha_M \left(\frac{1}{\epsilon} + 8\ln\frac{\bar{\mu}}{2m_E} \right) + \beta_M + \mathcal{O}(\epsilon) \right]
$$

$$
+ \frac{1}{(4\pi)^2} d_A (d_A + 2) \lambda_E^{(1)} m_E^2 \left[-\frac{1}{4} + \mathcal{O}(\epsilon) \right]
$$

$$
+ \frac{1}{(4\pi)^2} d_A \frac{2d_A - 1}{N_c} \lambda_E^{(2)} m_E^2 \left[-\frac{1}{4} + \mathcal{O}(\epsilon) \right], \quad (4.1)
$$

where [10]

$$
\alpha_M = \frac{43}{32} - \frac{491}{6144}\pi^2 \approx 0.555017. \quad (4.2)
$$

The finite constant β_M can be expressed in terms of a number of finite coefficients related to 4-loop vacuum scalar integrals [10], but we do not need it here.

In addition to $p_M(T)$, we also need to specify the effective parameter g_M^2 appearing in $\mathcal{L}_M$, to complete contributions from the scale gT. It is of the form

$$
g_M^2 = g_E^2 [1 + \mathcal{O}(g_E^2/m_E)], \quad (4.3)
$$

where the next-to-leading order correction is known (see, e.g., [20]), but not needed here.

V. CONTRIBUTIONS FROM THE SCALE $2\pi T$

The contributions from the scale $2\pi T$ are contained in the expressions for the parameters of the previous effective theories, as well as in $p_E(T)$. We write these as

$$
\mu^{2\epsilon} p_E(T) = T^4 \left(\alpha_{E1} + g^2 [\alpha_{E2} + \mathcal{O}(\epsilon)] + \frac{g^4}{(4\pi)^2} [\alpha_{E3} + \mathcal{O}(\epsilon)] \right.
$$

$$
\left. + \frac{g^6}{(4\pi)^4} [\beta_{E1} + \mathcal{O}(\epsilon)] + \mathcal{O}(g^8) \right), \quad (5.1)
$$

$$
m_E^2 = T^2 \left(g^2 [\alpha_{E4} + \alpha_{E5}\epsilon + \mathcal{O}(\epsilon^2)] \right.
$$

$$
\left. + \frac{g^4}{(4\pi)^2} [\alpha_{E6} + \beta_{E2}\epsilon + \mathcal{O}(\epsilon^2)] + \mathcal{O}(g^6) \right), \quad (5.2)
$$

$$
g_E^2 = T \left(g^2 + \frac{g^4}{(4\pi)^2} [\alpha_{E7} + \beta_{E3}\epsilon + \mathcal{O}(\epsilon^2)] + \mathcal{O}(g^6) \right), \quad (5.3)
$$

$$
\lambda_E^{(1)} = T \left(\frac{g^4}{(4\pi)^2} [\beta_{E4} + \mathcal{O}(\epsilon)] + \mathcal{O}(g^6) \right), \quad (5.4)
$$

$$
\lambda_E^{(2)} = T \left[\frac{g^4}{(4\pi)^2} [\beta_{E5} + \mathcal{O}(\epsilon)] + \mathcal{O}(g^6) \right], \quad (5.5)
$$

where g^2 is the renormalized coupling. We have named explicitly (α_E, β_E) the coefficients needed up to order $\mathcal{O}(g^6)$. The actual values for those needed at order $\mathcal{O}[g^6\ln(1/g)]$, denoted by α_E, are given in Appendix A. The additional coefficients needed at the full order $\mathcal{O}(g^6)$ are denoted by β_E; some of these are also known (for β_{E4}, β_{E5}, e.g., see [21]). The rest of the terms contribute only beyond $\mathcal{O}(g^6)$.

The expression for $p_E(T)$ is simply the functional integral in Eq. (2.7), calculated to the 4-loop level in the modified minimal subtraction ($\overline{\text{MS}}$) scheme, but without any resummations. The only physical scale entering is thus $2\pi T$. The calculation has so far been carried out only to three loops [6,11] so that β_{E1} is not known. Even when performed with the fully renormalized theory, the results in general contain uncancelled $1/\epsilon$ poles, as explicitly seen in the 3-loop expression in Eq. (A3) for α_{E3}. These only cancel when a physical fully resummed quantity is evaluated, i.e., in the sum $p_{QCD} = p_E + p_M + p_G$. Similarly, $m_E^2, g_E^2, \lambda_E^{(i)}$ can be obtained, for instance, from suitable 2-, 3-, and 4-point functions, respectively.

VI. THE COMPLETE RESULT

Combining now the results of Secs. III, IV, V and expanding in g, we arrive at

$$\frac{p_{\rm QCD}(T)}{T^4\mu^{-2\epsilon}}=\frac{p_{\rm E}(T)+p_{\rm M}(T)+p_{\rm G}(T)}{T^4\mu^{-2\epsilon}}$$

$$=g^0\{\alpha_{\rm E1}\}+g^2\{\alpha_{\rm E2}\}+\frac{g^3}{(4\pi)}\left\{\frac{d_A}{3}\alpha_{\rm E4}^{3/2}\right\}+\frac{g^4}{(4\pi)^2}\left\{\alpha_{\rm E3}-d_AC_A\left[\alpha_{\rm E4}\left(\frac{1}{4\epsilon}+\frac{3}{4}+\ln\frac{\bar{\mu}}{2gT\alpha_{\rm E4}^{1/2}}\right)+\frac{1}{4}\alpha_{\rm E5}\right]\right\}$$

$$+\frac{g^5}{(4\pi)^3}\left\{d_A\alpha_{\rm E4}^{1/2}\left[\frac{1}{2}\alpha_{\rm E6}-C_A^2\left(\frac{89}{24}+\frac{\pi^2}{6}-\frac{11}{6}\ln2\right)\right]\right\}+\frac{g^6}{(4\pi)^4}\left\{\beta_{\rm E1}-\frac{1}{4}d_A\alpha_{\rm E4}\left[(d_A+2)\beta_{\rm E4}+\frac{2d_A-1}{N_c}\beta_{\rm E5}\right]\right.$$

$$-d_AC_A\left[\frac{1}{4}(\alpha_{\rm E6}+\alpha_{\rm E5}\alpha_{\rm E7}+3\alpha_{\rm E4}\alpha_{\rm E7}+\beta_{\rm E2}+\alpha_{\rm E4}\beta_{\rm E3})+(\alpha_{\rm E6}+\alpha_{\rm E4}\alpha_{\rm E7})\left(\frac{1}{4\epsilon}+\ln\frac{\bar{\mu}}{2gT\alpha_{\rm E4}^{1/2}}\right)\right]$$

$$\left.+d_AC_A^3\left[\beta_{\rm M}+\beta_{\rm G}+\alpha_{\rm M}\left(\frac{1}{\epsilon}+8\ln\frac{\bar{\mu}}{2gT\alpha_{\rm E4}^{1/2}}\right)+\alpha_{\rm G}\left(\frac{1}{\epsilon}+8\ln\frac{\bar{\mu}}{2g^2TC_A}\right)\right]\right\}+\mathcal{O}(g^7)+\mathcal{O}(\epsilon). \tag{6.1}$$

Utilizing the expressions in Appendix A, the terms up to order $\mathcal{O}(g^5)$ reproduce the known result in [7].

For the contribution at order $\mathcal{O}(g^4)$, the $1/\epsilon$ divergence in $\alpha_{\rm E3}$ [cf. Eq. (A3)] and the $1/\epsilon$ divergence from $p_{\rm M}(T)$, shown explicitly in Eq. (6.1), cancel. This must happen since $p_{\rm QCD}(T)$ is a physical quantity. The associated $\bar{\mu}$'s also cancel, but a physical effect $\ln[m_{\rm E}/(2\pi T)]\sim\ln(g\alpha_{\rm E4}^{1/2})$ remains [5].

For the contribution at order $\mathcal{O}(g^6)$, a number of unknown coefficients remain (the $\beta_{\rm E}$'s, $\beta_{\rm M}$, $\beta_{\rm G}$), but a similar cancellation is guaranteed to take place. In addition, the result must be scale independent to the order it has been computed. The first point can be achieved by $\beta_{\rm E1}$ (the other $\beta_{\rm E}$'s are finite), so that it has to have the structure

$$\beta_{\rm E1}\equiv d_AC_A(\alpha_{\rm E6}+\alpha_{\rm E4}\alpha_{\rm E7})\frac{1}{4\epsilon}-d_AC_A^3(\alpha_{\rm M}+\alpha_{\rm G})\frac{1}{\epsilon}+\beta_{\rm E6}, \tag{6.2}$$

where $\beta_{\rm E6}$ does not contain any $1/\epsilon$ poles. The latter point can be achieved by adding and subtracting $\ln[\bar{\mu}/(2\pi T)]$'s, such that $\bar{\mu}$ gets effectively replaced by $2\pi T$ in the logarithms visible in the $\mathcal{O}(g^6)$ term in Eq. (6.1). The $\ln[\bar{\mu}/(2\pi T)]$'s left over, together with those coming from the $\beta_{\rm E}$'s, serve to cancel the effects from the 2-loop running of $g^2(\bar{\mu})$ and 1-loop running of $g^4(\bar{\mu})$ in the lower order contributions, without introducing large logarithms.

This general information is enough to fix the contributions of order $\mathcal{O}(g^6\ln(1/g))$ to $p_{\rm QCD}(T)$. Indeed, after inserting Eq. (6.2) and reorganizing the logarithms appearing in the $\beta_{\rm E}$'s as mentioned, there remains a logarithmic 4-loop term,

$$\left.\frac{p_{\rm QCD}(T)}{T^4\mu^{-2\epsilon}}\right|_{g^6\ln(1/g)}=g^6\frac{d_AC_A}{(4\pi)^4}\{(\alpha_{\rm E6}+\alpha_{\rm E4}\alpha_{\rm E7})\ln(g\alpha_{\rm E4}^{1/2})$$
$$-8C_A^2[\alpha_{\rm M}\ln(g\alpha_{\rm E4}^{1/2})+2\alpha_{\rm G}\ln(gC_A^{1/2})]\}, \tag{6.3}$$

where $\alpha_{\rm E4}$ is in Eq. (A4), $\alpha_{\rm E6}$ is in Eq. (A6), $\alpha_{\rm E7}$ is in Eq. (A7), $\alpha_{\rm M}$ is in Eq. (4.2), and $\alpha_{\rm G}$ is in Eq. (3.3). Note that there are logarithms of two types, with different non-analytic dependences on group theory factors inside them. Equation (6.3) is our main result.

Following [7,11], let us finally insert $N_c=3$, and give also the numerical values for the various coefficients, for an arbitrary N_f. We obtain

$$p_{\rm QCD}(T)=\frac{8\pi^2}{45}T^4\left[\sum_{i=0}^{6}p_i\left(\frac{\alpha_s(\bar{\mu})}{\pi}\right)^{i/2}\right], \tag{6.4}$$

where

$$p_0=1+\frac{21}{32}N_f, \tag{6.5}$$

$$p_1=0, \tag{6.6}$$

$$p_2=-\frac{15}{4}\left(1+\frac{5}{12}N_f\right), \tag{6.7}$$

$$p_3=30\left(1+\frac{1}{6}N_f\right)^{3/2}, \tag{6.8}$$

$$p_4=237.2+15.96N_f-0.4150N_f^2$$
$$+\frac{135}{2}\left(1+\frac{1}{6}N_f\right)\ln\left[\frac{\alpha_s}{\pi}\left(1+\frac{1}{6}N_f\right)\right]$$
$$-\frac{165}{8}\left(1+\frac{5}{12}N_f\right)\left(1-\frac{2}{33}N_f\right)\ln\frac{\bar{\mu}}{2\pi T}, \tag{6.9}$$

$$p_5 = \left(1 + \frac{1}{6}N_f\right)^{1/2}\left[-799.1 - 21.96N_f - 1.926N_f^2\right.$$

$$\left. + \frac{495}{2}\left(1 + \frac{1}{6}N_f\right)\left(1 - \frac{2}{33}N_f\right)\ln\frac{\bar{\mu}}{2\pi T}\right], \qquad (6.10)$$

$$p_6 = \left[-659.2 - 65.89N_f - 7.653N_f^2 + \frac{1485}{2}\left(1 + \frac{1}{6}N_f\right)\right.$$

$$\left.\times\left(1 - \frac{2}{33}N_f\right)\ln\frac{\bar{\mu}}{2\pi T}\right]\ln\left[\frac{\alpha_s}{\pi}\left(1 + \frac{1}{6}N_f\right)\right]$$

$$- 475.6\ln\frac{\alpha_s}{\pi} + q_a(N_f)\ln^2\frac{\bar{\mu}}{2\pi T} + q_b(N_f)\ln\frac{\bar{\mu}}{2\pi T}$$

$$+ q_c(N_f), \qquad (6.11)$$

where $q_a(N_f)$, $q_b(N_f)$, $q_c(N_f)$ are α_s-independent polynomials in N_f. Two of them, $q_a(N_f)$, $q_b(N_f)$, can already be written down because they just cancel the $\bar{\mu}$ dependence arising from the terms of orders $\alpha_s(\bar{\mu})$, $\alpha_s^2(\bar{\mu})$:

$$q_a(N_f) = -\frac{1815}{16}\left(1 + \frac{5}{12}N_f\right)\left(1 - \frac{2}{33}N_f\right)^2, \qquad (6.12)$$

$$q_b(N_f) = 2932.9 + 42.83N_f - 16.48N_f^2 + 0.2767N_f^3. \qquad (6.13)$$

The third one, $q_c(N_f)$, remains, however, unknown.

VII. THE NUMERICAL CONVERGENCE

This section is devoted to a numerical discussion of the result. Since the $\mathcal{O}(g^6\ln(1/g))$ term cannot be given an unambiguous numerical meaning until the $\mathcal{O}(g^6)$ term is specified, we have to present the result for various choices of the latter. In the relevant range of $T/\Lambda_{\overline{MS}}$ the outcome will de-

pend sensitively, even qualitatively, on this uncomputed term. One choice will be seen to agree with 4D lattice data down to about $T/\Lambda_{\overline{MS}} \sim 2\ldots 3$. Since, however, dimensional reduction, that is, an effective description of QCD via the theory in Eq. (2.10), is known to break down at about this point, and we have only kept a finite number of terms in the expansion following from Eq. (2.10), this cannot really be considered a prediction, even if the eventual computation of the $\mathcal{O}(g^6)$ term gave just the appropriate value. It is just an observation that a smooth transition from the domain of validity of our results to a domain of different approximations should be possible.

A standard procedure in the discussion of perturbative results would be to take the expansion in Eq. (6.4) and to study whether its scale dependence is reduced when further orders of perturbation theory are included. As is well known since [6], this fails for the pressure, unless $T \gg \Lambda_{\overline{MS}}$. Related to this, the numerical convergence of the perturbative expansion is known to be quite poor for any fixed scale choice, at least for temperatures below the electroweak scale [7,11,12]. The new term we have computed does not change this general pattern. But the culprit is known: it is $p_M(T) + p_G(T)$ emerging from the 3D sector of the theory, where the expansion parameter is only $g_E^2/(\pi m_E) \sim g/\pi$. In contrast, for $p_E(T)$ as well as for, say, jet physics, the expansion parameter is α_s/π, and there are good reasons to expect numerical convergence to be much better.

For these reasons, we will only discuss the sensitivity of the result on the so far unknown $\mathcal{O}(g^6)$ coefficient, as well as the slow convergence of the 3D sector, in the following. For simplicity, we only consider the case $N_c = 3$, $N_f = 0$ here.

As in [14], the actual form we choose for plotting contains $p_M(T) + p_G(T)$ [Eqs. (4.1)+(3.1)] in an "unexpanded" form, that is, with m_E, g_E^2 inserted from Eqs. (5.2), (5.3), and g_M^2 from Eq. (4.3). This means that we are effectively summing up higher orders: the $\mathcal{O}(g^3)$ term is really $\mathcal{O}(g^2 + g^4)^{3/2}$, while the $\mathcal{O}(g^6\ln(1/g))$ term contains a

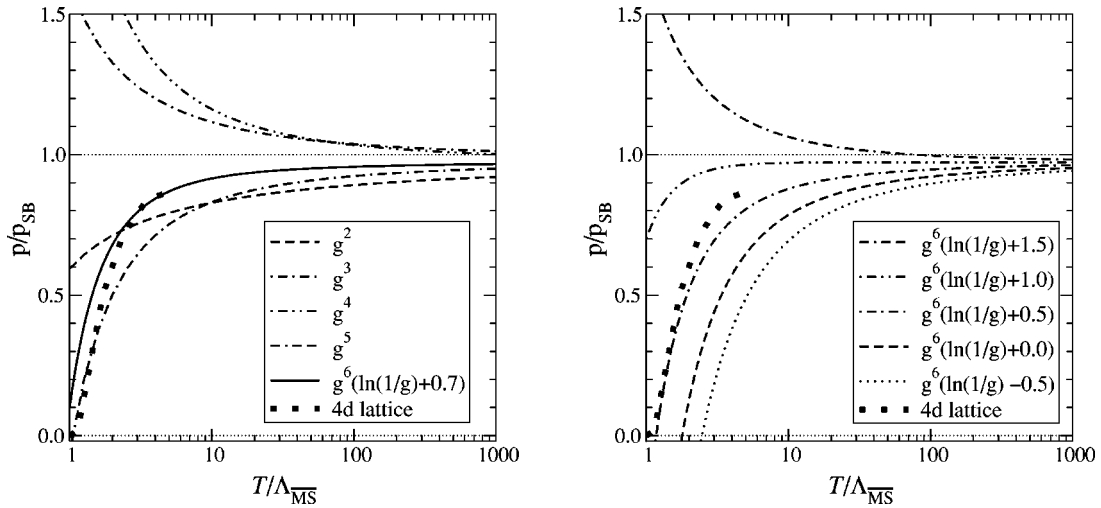FIG. 1. Left: perturbative results at various orders (the precise meanings thereof are explained in Sec. VII), including $\mathcal{O}(g^6)$ for an optimal constant, normalized to the non-interacting Stefan-Boltzmann value p_{SB}. Right: the dependence of the $\mathcal{O}(g^6)$ result on the (not yet computed) constant, which contains both perturbative and nonperturbative contributions. The 4D lattice results are from [22].

resummed coefficient, being then effectively $\mathcal{O}((g^2 + g^4)^3 \ln(1/g))$. We proceed in this way because then a comparison with numerical determinations [14] of the slowly convergent part $p_M(T) + p_G(T)$ is more straightforward, and also because the resummations carried out reduce the $\bar{\mu}$ dependence of the outcome. However, we have checked that the practical conclusions remain the same even if we plot directly the expression in Eqs. (6.4)–(6.11) (but with a larger scale dependence).

To be specific, the genuine $\mathcal{O}(g^6 \ln(1/g) + g^6)$ contribution, which collects the effects from all the terms involving the β_E's, β_M, β_G, α_M, and α_G in Eq. (6.1), is now written in the form (specific for $N_c = 3$, $N_f = 0$, where $m_E/g_E^2 \sim 1/g$),

$$\delta\left[\frac{p_{QCD}(T)}{T\mu^{-2\epsilon}}\right]_{g^6\ln(1/g)} \equiv 8d_A C_A^3 \frac{g_E^6}{(4\pi)^4}$$

$$\times \left[(\alpha_M + 2\alpha_G)\ln\frac{m_E}{g_E^2} + \delta\right],$$

$$(7.1)$$

while the remaining $\mathcal{O}(g^6)$ terms of Eq. (6.1) are contained in the resummed lower order contributions. The results are shown in Fig. 1 for various values of δ. The power of g labelling the curves indicates the leading magnitude of the highest order resummed contribution appearing. The scale is chosen as $\bar{\mu} \approx 6.7T$, as suggested by the next-to-leading order expression for g_E^2 [12]. We observe that for a specific value of δ, the curve extrapolates well to 4D lattice data.

While Fig. 1 looks tempting, the question still remains whether the good match to 4D lattice data with a specific value of the constant is simply a coincidence. This issue can be fully settled only once the constant is actually computed. However, we can already inspect how the slowly convergent part of the pressure, $p_M + p_G$, really behaves.

The different finite terms in $(p_M + p_G)/(Tg_E^6)$ are plotted in Fig. 2. The $\lambda_E^{(i)}$ contributions are negligible. The results depend then essentially only on m_E^2/g_E^4, which for $N_c = 3$, $N_f = 0$ is $m_E^2/g_E^4 \approx 0.32\log_{10}(T/\Lambda_{\overline{MS}}) + 0.29$. We observe that the leading 1-loop term $\mathcal{O}(g^3)$ is dominant for $T/\Lambda_{\overline{MS}} \gtrsim 10$, the 3-loop term $\mathcal{O}(g^5)$ is rather big, bigger in absolute value than the 2-loop term $\mathcal{O}(g^4)$ within the T-range of the figure, while the 4-loop term is always very small. Therefore, while it is quite possible that there is again a big "odd" $\mathcal{O}(g^7)$ contribution, it is perhaps not completely outrageous either to hope that the convergence could also already be reasonable, once the full $\mathcal{O}(g^6)$ contribution is included. If this were the case, then all higher order contributions would have to sum up to a small number.

Finally, it is perhaps interesting to remark that at the time of the numerical lattice Monte Carlo study in Ref. [14], nothing was known about the coefficient β_{E1}, which was therefore set to zero [cf. Eq. (4) in [14]], while the part $p_M(T) + p_G(T)$ was determined nonperturbatively. But this means
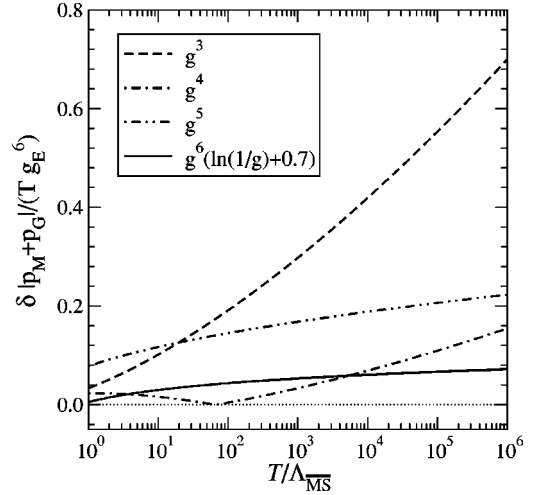
FIG. 2. The absolute values of the various terms of the slowly convergent expansion for $p_M(T) + p_G(T)$, normalized by Tg_E^6.

that a logarithmic term coming from the scale $2\pi T$, $\sim -g^6(\alpha_M + \alpha_G)\ln[\bar{\mu}/(2\pi T)]$, was missed. With the scale choice $\bar{\mu} \equiv \bar{\mu}_E = g_E^2$ within results obtained with $\mathcal{L}_E$, this converted to a missing $\mathcal{O}(g^6 \ln(1/g))$ contribution $g^6(2\alpha_M + 2\alpha_G)\ln(1/g)$. With the same scale choice the nonperturbative part, on the other hand, contributed $-g^6\alpha_M\ln(1/g)$ and led to the wrong curvature of the pressure seen at small $T/\Lambda_{\overline{MS}}$. Adding the missing part, which now has been computed, leads to a total of $g^6(\alpha_M + 2\alpha_G)\ln(1/g)$, with the opposite sign and the correct (i.e., the one seen in 4D lattice measurements) curvature in Fig. 1 (for small values of δ). Therefore the $\mathcal{O}(g^6 \ln(1/g))$ terms are indeed physically very relevant.

VIII. CONCLUSIONS

We have addressed in this paper the 4-loop logarithmic contributions to the pressure of hot QCD. Physical (regularization independent) logarithms can only arise from a ratio of two scales. Since there are three parametrically different scales in the system, $2\pi T$, gT, $g^2 T$, there are then various types of perturbatively computable logarithms in the 4-loop expression for the pressure:

(1) Logarithms of the type $g^6\ln[(2\pi T)/(g^2 T)]$. The coefficient of these is computed in [9], and given in Eq. (3.3).

(2) Logarithms of the type $g^6\ln[(2\pi T)/(gT)]$. The coefficient of these is computed in [10], and given in Eq. (4.2).

(3) Logarithms related to the running of the coupling constant in the 3-loop expression of order $\mathcal{O}(g^4\ln[(2\pi T)/(gT)])$. Their $\overline{MS}$ coefficient can be seen in the first term in Eq. (6.3), but it depends on the scheme, and can in principle even be chosen to vanish.

Logarithms of the first and second types can be written in many ways: it may be more intuitive, for instance, to reorganize them as

$$g^6\alpha_G\ln\left(\frac{2\pi T}{g^2 T}\right)+g^6\alpha_M\ln\left(\frac{2\pi T}{gT}\right)$$

$$=g^6(\alpha_M+\alpha_G)\ln\left(\frac{2\pi T}{gT}\right)+g^6\alpha_G\ln\left(\frac{gT}{g^2 T}\right).$$

$$(8.1)$$

The existence of three kinds of logarithms is somewhat specific to non-Abelian gauge theory. In QED, in particular, none of the logarithms appear. This is due to the fact that the effective theories we have used for their computation, Eqs. (2.10), (2.15), are non-interacting [apart from a term $\sim A_0^4$ in Eq. (2.10), which does not lead to logarithms]. Therefore we have nothing to add to the known $\mathcal{O}(g^5)$ QED result obtained in [23]. In the ϕ^4 scalar theory, on the other hand, there is a logarithm of the second type, and also one somewhat analogous to the third type. Their coefficients were already computed in [24].

There are interesting checks that can be made on the various logarithms mentioned, using methods completely different from those employed here. For instance, logarithms of the first and second types could in principle be seen with 3D lattice Monte Carlo methods [25,26], as well as with stochastic perturbation theory [27]. A very interesting analytical check would be to compute the 4-loop free energy directly in 4D in strict dimensional regularization, but without any re-summation. By definition, this computation produces the coefficient β_{E1} in Eq. (5.1) [11], and one check is that the result must contain the $1/\epsilon$ divergences shown in Eq. (6.2).

To complete the free energy from the current level $\mathcal{O}(g^6\ln(1/g))$ to the full level $\mathcal{O}(g^6)$ would require significantly more work than the computation presented here. More specifically, there are contributions from all the scales in the problem, ranging from $2\pi T$ (the coefficients $\beta_{E1},\ldots,\beta_{E5}$), through gT (the coefficient β_M), down to the non-perturbative scale $g^2 T$ (the coefficient β_G). This then requires carrying out 4-loop finite temperature sum-integrals, 4-loop vacuum integrals in $d=3-2\epsilon$, 4-loop vacuum integrals in 3D lattice regularization, and lattice simulations of the pure 3D gauge theory in Eq. (2.15). Nevertheless, given the potentially important combined effect of all these contributions, as indicated by Fig. 1, such computations would clearly be well motivated.

ACKNOWLEDGMENTS

APPENDIX: MATCHING COEFFICIENTS

In Eqs. (5.1)–(5.5) we have defined a number of matching coefficients, the α_E's and β_E's. For the α_E's, the following

expressions can be extracted from [11,15,28]:

$$\alpha_{E1}=\frac{\pi^2}{180}(4d_A+7d_F),\tag{A1}$$

$$\alpha_{E2}=-\frac{d_A}{144}\left(C_A+\frac{5}{2}T_F\right),\tag{A2}$$

$$\alpha_{E3}=\frac{d_A}{144}\left[C_A^2\left(\frac{12}{\epsilon}+\frac{194}{3}\ln\frac{\bar{\mu}}{4\pi T}+\frac{116}{5}+4\gamma+\frac{220}{3}\frac{\zeta'(-1)}{\zeta(-1)}\right.\right.$$
$$\left.-\frac{38}{3}\frac{\zeta'(-3)}{\zeta(-3)}\right)$$
$$+C_A T_F\left(\frac{12}{\epsilon}+\frac{169}{3}\ln\frac{\bar{\mu}}{4\pi T}+\frac{1121}{60}-\frac{157}{5}\ln2+8\gamma\right.$$
$$\left.+\frac{146}{3}\frac{\zeta'(-1)}{\zeta(-1)}-\frac{1}{3}\frac{\zeta'(-3)}{\zeta(-3)}\right)$$
$$+T_F^2\left(\frac{20}{3}\ln\frac{\bar{\mu}}{4\pi T}+\frac{1}{3}-\frac{88}{5}\ln2+4\gamma+\frac{16}{3}\frac{\zeta'(-1)}{\zeta(-1)}\right.$$
$$\left.-\frac{8}{3}\frac{\zeta'(-3)}{\zeta(-3)}\right)+C_F T_F\left(\frac{105}{4}-24\ln2\right)\right],\tag{A3}$$

$$\alpha_{E4}=\frac{1}{3}\ (C_A+T_F),\tag{A4}$$

$$\alpha_{E5}=\frac{2}{3}\left[C_A\left(\ln\frac{\bar{\mu}}{4\pi T}+\frac{\zeta'(-1)}{\zeta(-1)}\right)\right.$$
$$\left.+T_F\left(\ln\frac{\bar{\mu}}{4\pi T}+\frac{1}{2}-\ln2+\frac{\zeta'(-1)}{\zeta(-1)}\right)\right],\tag{A5}$$

$$\alpha_{E6}=C_A^2\left(\frac{22}{9}\ln\frac{\bar{\mu}e^\gamma}{4\pi T}+\frac{5}{9}\right)+C_A T_F\left(\frac{14}{9}\ln\frac{\bar{\mu}e^\gamma}{4\pi T}-\frac{16}{9}\ln2+1\right)$$
$$+T_F^2\left(-\frac{8}{9}\ln\frac{\bar{\mu}e^\gamma}{4\pi T}-\frac{16}{9}\ln2+\frac{4}{9}\right)-2C_F T_F,\tag{A6}$$

$$\alpha_{E7}=C_A\left(\frac{22}{3}\ln\frac{\bar{\mu}e^\gamma}{4\pi T}+\frac{1}{3}\right)-T_F\left(\frac{8}{3}\ln\frac{\bar{\mu}e^\gamma}{4\pi T}+\frac{16}{3}\ln2\right).\tag{A7}$$

Note that with our notation, the 1-loop running of the renormalized coupling constant goes as

$$g^2(\bar{\mu})=g^2(\bar{\mu}_0)-\frac{2}{3}\ (11C_A-4T_F)\frac{g^4(\bar{\mu}_0)}{(4\pi)^2}\ln\frac{\bar{\mu}}{\bar{\mu}_0}.\tag{A8}$$

[1] A.D. Linde, Phys. Lett. **96B**, 289 (1980).

[2] D.J. Gross, R.D. Pisarski, and L.G. Yaffe, Rev. Mod. Phys. **53**, 43 (1981).

[3] E.V. Shuryak, Zh. Éksp. Teor. Fiz. **74**, 408 (1978) [Sov. Phys. JETP **47**, 212 (1978)]; S.A. Chin, Phys. Lett. **78B**, 552 (1978).

[4] J.I. Kapusta, Nucl. Phys. **B148**, 461 (1979).

[5] T. Toimela, Phys. Lett. **124B**, 407 (1983).

[6] P. Arnold and C. Zhai, Phys. Rev. D **50**, 7603 (1994); *ibid.* **51**, 1906 (1995).

[7] C. Zhai and B. Kastening, Phys. Rev. D **52**, 7232 (1995).

[8] G.D. Moore, J. High Energy Phys. **10**, 055 (2002); A. Ipp, G.D. Moore, and A. Rebhan, *ibid.* **01**, 037 (2003).

[9] Y. Schröder, "Logarithmic divergence in the energy density of the three-dimensional Yang-Mills theory," in preparation.

[10] K. Kajantie, M. Laine, K. Rummukainen, and Y. Schröder, "Four-loop vacuum energy density of the SU(N_c)+adjoint Higgs theory," hep-ph/0304048.

[11] E. Braaten and A. Nieto, Phys. Rev. D **53**, 3421 (1996).

[12] K. Kajantie, M. Laine, K. Rummukainen, and M. Shaposhnikov, Nucl. Phys. **B503**, 357 (1997).

[13] P. Ginsparg, Nucl. Phys. **B170**, 388 (1980); T. Appelquist and R.D. Pisarski, Phys. Rev. D **23**, 2305 (1981).

[14] K. Kajantie, M. Laine, K. Rummukainen, and Y. Schröder, Phys. Rev. Lett. **86**, 10 (2001).

[15] K. Kajantie, M. Laine, K. Rummukainen, and M. Shaposhnikov, Nucl. Phys. **B458**, 90 (1996).

[16] S. Chapman, Phys. Rev. D **50**, 5308 (1994).

[17] Y. Schröder, Nucl. Phys. B (Proc. Suppl.) **116**, 402 (2003).

[18] J.A.M. Vermaseren, math-ph/0010025; http://www.nikhef.nl/~form/

[19] K. Kajantie, M. Laine, and Y. Schröder, Phys. Rev. D **65**, 045008 (2002).

[20] K. Farakos, K. Kajantie, K. Rummukainen, and M.E. Shaposhnikov, Nucl. Phys. **B425**, 67 (1994).

[21] S. Nadkarni, Phys. Rev. D **38**, 3287 (1988); N.P. Landsman, Nucl. Phys. **B322**, 498 (1989).

[22] G. Boyd *et al.*, Nucl. Phys. **B469**, 419 (1996); A. Papa, *ibid.* **B478**, 335 (1996); B. Beinlich, F. Karsch, E. Laermann, and A. Peikert, Eur. Phys. J. C **6**, 133 (1999); CP-PACS Collaboration, M. Okamoto *et al.*, Phys. Rev. D **60**, 094510 (1999).

[23] R.R. Parwani, Phys. Lett. B **334**, 420 (1994); *ibid.* **342**, 454(E) (1995); R.R. Parwani and C. Corianò, Nucl. Phys. **B434**, 56 (1995).

[24] E. Braaten and A. Nieto, Phys. Rev. D **51**, 6990 (1995).

[25] F. Karsch, M. Lütgemeier, A. Patkós, and J. Rank, Phys. Lett. B **390**, 275 (1997).

[26] K. Kajantie, M. Laine, K. Rummukainen, and Y. Schröder, Nucl. Phys. B (Proc. Suppl.) **106**, 525 (2002); hep-lat/0209072.

[27] F. Di Renzo, E. Onofri, G. Marchesini, and P. Marenzoni, Nucl. Phys. **B426**, 675 (1994).

[28] S. Huang and M. Lissia, Nucl. Phys. **B438**, 54 (1995).

[29] The constant part β_G could be determined by measuring a suitable observable on the lattice and converting then the result from lattice regularization to the $\overline{\text{MS}}$ scheme by a perturbative 4-loop matching computation.

Four–loop vacuum energy density of the SU(N_c) + adjoint Higgs theory

Four-loop vacuum energy density of the $\mathrm{SU}(N_c)$ + adjoint Higgs theory

Keijo Kajantie

Department of Physical Sciences
P.O.Box 64, FIN-00014 University of Helsinki, Finland
E-mail: `keijo.kajantie@helsinki.fi`

Mikko Laine

Theory Division, CERN
CH-1211 Geneva 23, Switzerland
E-mail: `mikko.laine@cern.ch`

Kari Rummukainen

Department of Physical Sciences and Helsinki Institute of Physics
P.O.Box 64, FIN-00014 University of Helsinki, Finland
E-mail: `kari.rummukainen@helsinki.fi`

York Schröder

Center for Theoretical Physics, MIT
Cambridge, MA 02139, USA
E-mail: `yorks@lns.mit.edu`

ABSTRACT: We compute the dimensionally regularised four-loop vacuum energy density of the $\mathrm{SU}(N_c)$ gauge + adjoint Higgs theory, in the disordered phase. "Scalarisation", or reduction to a small set of master integrals of the type appearing in scalar field theories, is carried out in d dimensions, employing general partial integration identities through an algorithm developed by Laporta, while the remaining master integrals are evaluated in $d = 3 - 2\epsilon$ dimensions, by expanding in $\epsilon \ll 1$ and evaluating a number of coefficients. The results have implications for the thermodynamics of finite temperature QCD, allowing to determine perturbative contributions of orders $\mathcal{O}(g^6 \ln(1/g))$, $\mathcal{O}(g^6)$ to the pressure, while the general methods are applicable also to studies of critical phenomena in QED-like statistical physics systems.

`http://jhep.sissa.it/archive/papers/jhep042003036/jhep042003036.pdf`

Contents

1. Introduction

The theory we study in this paper is the euclidean $SU(N_c)$ gauge + adjoint Higgs theory, defined in continuum dimensional regularisation by the action

$$S_{\rm E} \equiv \int {\rm d}^d x\, \mathcal{L}_{\rm E}\,, \tag{1.1}$$

$$\mathcal{L}_{\rm E} \equiv \frac{1}{2}\,{\rm Tr}\,F_{kl}^2 + {\rm Tr}[D_k, A_0]^2 + m^2\,{\rm Tr}\,A_0^2 + \lambda({\rm Tr}\,A_0^2)^2\,, \tag{1.2}$$

where $k, l = 1, \ldots, d$, $D_k = \partial_k - igA_k$, $A_k = A_k^a T^a$, $A_0 = A_0^a T^a$, $F_{kl} = (i/g)[D_k, D_l]$, and T^a are the hermitean generators of $SU(N_c)$, normalised as ${\rm Tr}\,T^a T^b = \delta^{ab}/2$. Summation over repeated indices is understood. We could have taken the scalar potential also in the form $\lambda_1({\rm Tr}\,A_0^2)^2 + \lambda_2\,{\rm Tr}\,A_0^4$, but the two quartic terms are independent only for $N_c \geq 4$ and thus, to avoid further proliferation of formulae, we will set $\lambda_2 = 0$ here, denoting $\lambda \equiv \lambda_1$. For the moment we keep d general, but later on we write $d = 3 - 2\epsilon$, and expand in $\epsilon \ll 1$.

The observable we would like to compute for the theory in eq. (1.2) is its partition function, or "vacuum energy density",

$$f(m^2, g^2, \lambda) \equiv - \lim_{V \to \infty} \frac{1}{V} \ln \int \mathcal{D}A_k \mathcal{D}A_0 \exp(-S_{\mathrm{E}}). \qquad (1.3)$$

Here V is the d-dimensional volume. The phase diagram of the system described by S_{E} has a "disordered", or symmetric phase and, depending on N_c, various kinds of symmetry broken phases [1, 2]. Our aim is to determine the perturbative expansion for f up to 4-loop order in the symmetric phase, expanding around $A_0^a = A_k^a = 0$; the 3-loop result is known already [3, 4]. The result will depend on N_c through $d_A \equiv N_c^2 - 1, C_A \equiv N_c$.

The main motivation for the exercise described comes from finite temperature QCD. Indeed, the simplest physical observable there, the free energy density or minus the pressure, has been computed perturbatively up to resummed 3-loop level [5, 6], but the expansion converges very slowly, requiring probably temperatures $T \gg \mathrm{TeV}$ to make any sense at all [5, 6, 3, 7]. Moreover, at the 4-loop level the expansion breaks down completely [8, 9]. Multiloop computations are not useless, though: these infrared problems can be isolated into the three-dimensional (3d) effective field theory in eq. (1.2) [10], and studied non-perturbatively there with simple lattice simulations [4]. However, to convert the results from lattice regularisation to 3d continuum regularisation, and from the 3d continuum theory to the original 4d physical theory, still necessitates a number of perturbative multiloop "matching" computations.

The way our computation enters this setup has been described in [11]. Combining our results with those of another paper [12] allows one to determine, as explained in [11], all the logarithmic ultraviolet and infrared divergences entering the 4-loop free energy of QCD. This not only fixes the last perturbatively computable contribution to the free energy of hot QCD [11], of order $\mathcal{O}(g^6 \ln(1/g)T^4)$, but is also a step towards renormalising the non-perturbative contributions, as determined with lattice methods [4, 13]. Some other applications of our results are discussed in section 8.

2. Outline of the general procedure

The first step of the perturbative computation is the generation of the Feynman diagrams. At 4-loop level, this is no longer a completely trivial task. In order to make the procedure tractable, we employ an algorithm whereby the graphs are generated in two sets: two-particle-irreducible "skeleton" graphs, as well as various types of "ring" diagrams, containing all possible self-energy insertions. The resulting sets, with the relevant symmetry factors, were provided explicitly in [14].

It actually turns out that some of the generic graphs shown in [14] do not contribute in the present computation. There are two reasons for this. First, once the Feynman rules for the interactions of gauge bosons and adjoint scalars are taken into account, some of the graphs vanish at the point of colour contractions. This concerns particularly the "non-planar" topologies [15]. Second, all vacuum graphs which do not contain at least one massive (adjoint scalar) line, vanish in strict dimensional regularisation. In some
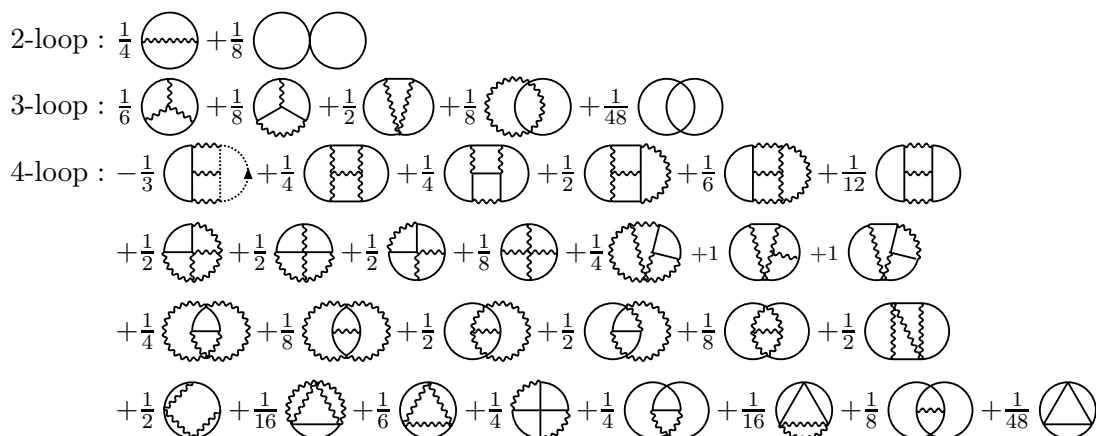
Figure 1: The skeleton diagrams contributing in eq. (1.3), after subtraction of those which obviously vanish because of colour contractions or specific properties of dimensional regularisation. Solid lines represent the adjoint scalar A_0, wavy lines the gauge boson A_i, and dotted lines the ghosts. The complete sets of skeleton diagrams have been enumerated and written down in ref. [14], whose overall sign conventions we also follow.

cases such a vanishing may be due to an unphysical cancellation between ultraviolet and infrared divergences, as we will recall in section 7, but for the moment we accept the vanishing literally. The remaining skeleton graphs are then as shown in figure 1. For the ring diagrams, which by far outnumber the skeleton graphs, we find it simpler to treat the full sets as shown in [14], letting the two types of cancellations mentioned above come out automatically in the actual computation. For completeness, the ring diagrams are reproduced in figure 2.

The Feynman rules for the vertices and propagators appearing are the standard ones. We employ covariant gauge fixing, with a general gauge fixing parameter, denoted here by

$$\xi \equiv \xi_{\text{here}} \equiv 1 - \xi_{\text{standard}} \,, \tag{2.1}$$

where ξ_{standard} is the gauge fixing parameter of the standard covariant gauges. Therefore, Feynman gauge corresponds here to $\xi = 0$, Landau gauge to $\xi = 1$. We keep everywhere ξ completely general, however, and verify explicitly that it cancels in all the results.

The graphs having been identified and the Feynman rules specified, we program them [16] in the symbolic manipulation package FORM [17], for further treatment.

After the colour contractions, the next step is to "scalarise" the remaining integrals. That is, we want to remove all scalar products from the numerators of the momentum integrations, such that only integrations of the type appearing in scalar field theories remain. This problem can be solved by using general partial integration identities [18]. The full power of the identities can be conveniently made use of through an algorithm developed by Laporta [19]. We discuss some aspects of our implementation of this algorithm, together with the results obtained, in section 3.
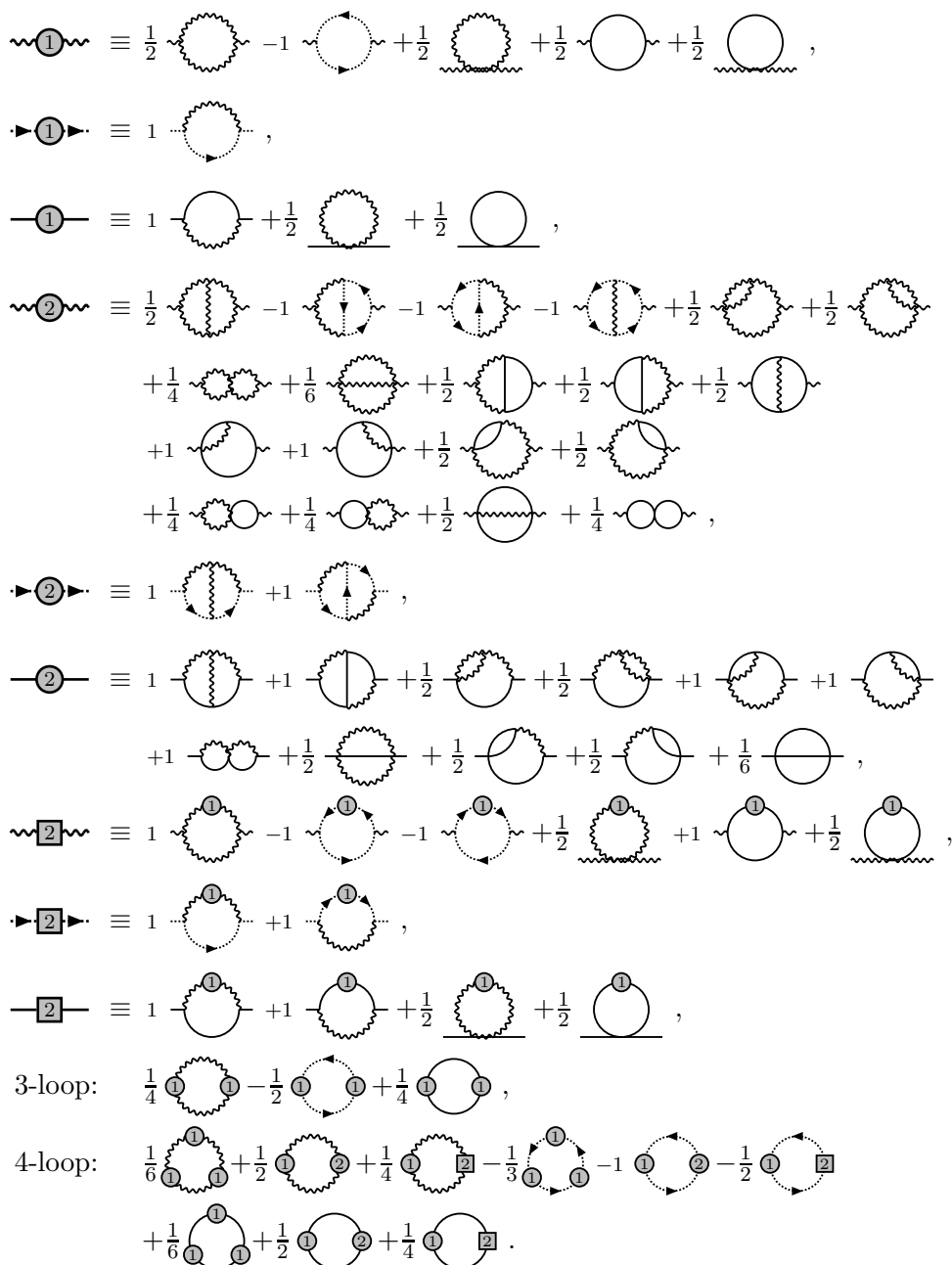
Figure 2: The ring diagrams contributing in eq. (1.3) [14]. The notation is as in figure 1.

After the reduction to scalar integrals, we are faced with their evaluation. At this point one has to specify the dimension d of the spacetime, in order to make further progress. We write $d = 3 - 2\epsilon$, expand in $\epsilon \ll 1$, and evaluate the various scalar integrals appearing to a certain (integral-dependent) depth in this expansion, such that a specified order is achieved for the overall result. For the new 4-loop contributions, the overall order for which we have either analytic or numerical expressions is $\mathcal{O}(1)$. The scalar integrals needed for this are discussed in section 4.
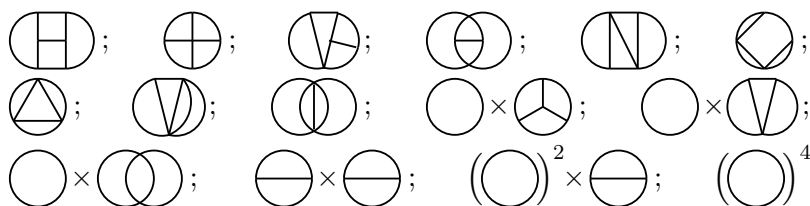
Figure 3: The 15 general types of 4-loop integrations remaining, in terms of momentum flow (momentum conservation is assumed at the vertices), after taking into account that colour contractions remove the non-planar topologies. Any line could contain a propagator to some power $n \geq 1$, and there is also an unspecified collection of scalar products of the integration momenta in the numerator.

There is one remaining step to be taken before we have the final result: the renormalisation of the parameters m^2, g^2, λ in eq. (1.2). In other words, the results presented up to this point were in terms of the bare parameters, and we now want to re-expand them in terms of the renormalised parameters. This step is also specific to the dimension, and turns out to be particularly simple for $d = 3 - 2\epsilon$, since only the mass parameter gets renormalised. The conversion of the bare parameters to the renormalised ones is discussed in section 5, and the final form of the results is then shown in section 6.

Having completed the straightforward computation, we discuss the conceptual issue of infrared divergences in section 7. We mention in this context also some checks of our results, based on largely independent computations. We end with a list of some applications in section 8.

3. Scalarisation in d dimensions

After inserting the Feynman rules and carrying out the colour contractions, there remains, at 4-loop level, a $4d$-dimensional momentum integration to be carried out. The different types of integrations emerging can be illustrated in graphical notation in the standard way. Without specifying the fairly complicated numerators, involving all possible kinds of scalar products of the integration momenta, the graphs are of the general types shown in figure 3.

There are a few simple tricks available in order to try and simplify the scalar products appearing in the numerators [16]. For instance, one can find relabelings of the integration variables such that the denominators appearing in the graph remain the same, while the scalar products in the numerators may get simplified, after symmetrising between such relabelings. Some scalar products in the numerators can also be completed into sums of squares, such that they cancel against the denominators. Furthermore, we can make use of various special properties of dimensional regularisation: any closed massless 1-loop tadpole integral vanishes; and any 1-loop massive bubble diagram with at most one external momentum is easily scalarised explicitly, in the sense of removing the loop momentum from all the scalar products appearing in the numerators. However, while such simple tricks are sufficient at, say, 2-loop level, this is no longer the case at 4-loop level.
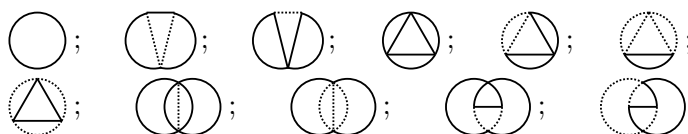
Figure 4: The 1-loop, 3-loop and 4-loop "master" topologies remaining after "scalarisation". There are no numerators left in these graphs. A solid line is a massive propagator, $1/(p^2 + m^2)$, and a dotted line a massless one, $1/p^2$, where p is the euclidean momentum flowing through the line. Note that no independent 2-loop representative appears.

To scalarise the 4-loop integrations, we have to make full use of the identities provided by general partial integrations [18]. To systematically employ all such identities, we implement the algorithm presented by Laporta [19] using the "tables" routines of FORM [17]. This leads to a complete solution of our problem. The main technical details of our implementation were discussed in [16].

After the scalarisation, the master integrals remaining are those shown in figure 4. This basis is, of course, not unique. As an example, one could have chosen a different basis for the 3-loop master integrals, employing identities following from partial integrations [20],

$$
\bigcirc\!\!\!\bigcirc = \frac{1}{m^2}\left(\bigcirc\right)^3\left[-\frac{(d-2)^2}{(d-3)(3d-8)}\right] + m^2\,\bigcirc\!\!\!\bigvee\left[\frac{4(d-3)}{(3d-8)}\right], \tag{3.1}
$$

$$
\bigcirc\!\!\!\bigcirc = \frac{1}{m^2}\left(\bigcirc\right)^3\left[-\frac{2(d-2)^2}{(d-3)(3d-8)}\right] + m^2\,\bigvee\!\!\!\bigvee\left[-\frac{4(d-4)}{(3d-8)}\right], \tag{3.2}
$$

where

$$
\bigcirc \equiv \int \frac{\mathrm{d}^d p}{(2\pi)^d}\frac{1}{p^2 + m^2}\,, \tag{3.3}
$$

and correspondingly for the higher loop integrals. Therefore, the 3-loop master integrals we are using, appearing on the right-hand-sides of eqs. (3.1), (3.2), could be exchanged in favour of the 3-loop integrals on the left-hand-sides of eqs. (3.1), (3.2).

To display the full result after scalarisation, we introduce the shorthand notations

$$
f(m^2, g^2, \lambda) \equiv -d_A \sum_{\ell=1}^{\infty}(g^2 C_A)^{\ell-1}\hat{p}_\ell\,, \qquad \bar{\lambda} \equiv \frac{\lambda(d_A + 2)}{g^2 C_A}\,. \tag{3.4}
$$

We then obtain the following expressions:

$$
\hat{p}_1 = m^2\,\bigcirc\left[-\frac{1}{d}\right], \tag{3.5}
$$

$$
\hat{p}_2 = \left(\bigcirc\right)^2\left[\frac{(d-1)}{4(d-3)} - \frac{1}{4}\bar{\lambda}\right], \tag{3.6}
$$

$$
\hat{p}_3 = \frac{1}{m^2}\left(\bigcirc\right)^3 \times
$$
$$
\times\left\{\left[-\frac{(d-2)(608 - 1064d + 654d^2 - 155d^3 + 12d^4)}{8(d-6)(d-4)(2d-7)(3d-8)}\right] + \right.
$$

$$+ \bar{\lambda}\left[\frac{(d-2)(d-1)}{4(d-3)}\right] +$$

$$+ \bar{\lambda}^2\left[-\frac{(d-2)}{8} - \frac{(d-2)^2}{2(d_A+2)(d-3)(3d-8)}\right]\Bigg\} +$$

$$+ m^2 \,\bigcirc\hspace{-0.9em}\vee\, \left[\frac{(d-2)^3(3d-11)}{(d-4)(2d-7)(3d-8)}\right] +$$

$$+ m^2 \,\bigcirc\hspace{-0.9em}\vee\hspace{-0.5em}\vee\, \left[-\frac{(16-18d+3d^2)}{2(d-6)(d-4)(3d-8)} - \bar{\lambda}^2\frac{(d-4)}{(d_A+2)(3d-8)}\right], \tag{3.7}$$

$$\hat{p}_4 = \frac{1}{m^4}\left(\bigcirc\right)^4 \times$$

$$\times\Bigg\{ \frac{(d-2)\alpha_1}{96(d-9)(d-7)(d-6)(d-5)(d-4)^2(d-3)^3} \times$$

$$\times \frac{1}{(d-1)(2d-9)(2d-7)(3d-13)(3d-11)(3d-10)(3d-8)} +$$

$$+ \bar{\lambda}\left[-\frac{(d-2)(2904-7150d+7097d^2-3581d^3+964d^4-131d^5+7d^6)}{8(d-6)(d-4)(d-3)^2(2d-7)} -\right.$$

$$\left.- \frac{5(d-5)(d-2)^3}{4(d_A+2)(d-4)^2(d-3)(3d-11)}\right] +$$

$$+ \bar{\lambda}^2\left[\frac{(d-2)(d-1)(2d-5)}{8(d-3)} + \frac{(d-2)^2(-32+56d-25d^2+3d^3)}{4(d_A+2)(d-4)(d-3)^2(3d-8)}\right] +$$

$$+ \bar{\lambda}^3\left[-\frac{(d-2)(2d-5)}{24} - \frac{(d-2)^2}{4(d_A+2)(d-3)}\right]\Bigg\} +$$

$$+ \left(\bigcirc\right) \times \left(\bigcirc\hspace{-0.9em}\vee\right) \times$$

$$\times\Bigg\{ \left[-\frac{(d-2)^2\alpha_2}{24(d-5)(d-4)^2(d-3)(d-1)(2d-9)(2d-7)(3d-11)(3d-10)(3d-8)}\right] +$$

$$+ \bar{\lambda}\left[\frac{(d-2)^3(3d-11)}{2(d-4)(2d-7)}\right]\Bigg\} +$$

$$+ \left(\bigcirc\right) \times \left(\bigcirc\hspace{-0.9em}\vee\hspace{-0.5em}\vee\right) \times$$

$$\times\Bigg\{ \frac{\alpha_3}{24(d-9)(d-7)(d-6)(d-5)(d-4)(d-3)} \times$$

$$\times \frac{1}{(d-1)(2d-9)(3d-13)(3d-11)(3d-8)} +$$

$$+ \bar{\lambda}\left[-\frac{16-18d+3d^2}{4(d-6)(d-4)} - \frac{5(d-6)(d-2)}{(d_A+2)(d-4)(3d-11)}\right] +$$

$$+ \bar{\lambda}^2\left[\frac{-32+56d-25d^2+3d^3}{2(d_A+2)(d-3)(3d-8)}\right] +$$

$$+ \bar{\lambda}^3\left[-\frac{(d-4)}{2(d_A+2)}\right]\Bigg\} +$$

$$+ \triangle\hspace{-0.9em}\bigcirc \times$$

$$\times \left\{ \frac{\alpha_4}{144(d-9)(d-7)(d-5)(d-4)^2(d-1)(3d-13)(3d-11)} + \right.$$

$$+ \bar{\lambda} \left[-\frac{5(96 - 64d + 7d^2 + d^3)}{12(d_A + 2)(d-4)^2(3d-11)} \right] +$$

$$+ \bar{\lambda}^2 \left[\frac{d}{6(d_A+2)(d-4)} \right] +$$

$$\left. + \bar{\lambda}^3 \left[-\frac{(d_A + 8)}{6(d_A + 2)^2} \right] \right\} +$$

$$+ \, \text{} \, \times$$

$$\times \left\{ \left[-\frac{8136 - 18176d + 14438d^2 - 5370d^3 + 984d^4 - 81d^5 + 2d^6}{16(d-5)(d-4)^2(d-1)(2d-9)} \right] + \right.$$

$$\left. + \bar{\lambda} \left[-\frac{5(20 - 10d + d^2)}{4(d_A+2)(d-4)} \right] \right\} +$$

$$+ \, \text{} \, \left[-\frac{(d-2)(-2656 + 5672d - 4072d^2 + 1302d^3 - 186d^4 + 9d^5)}{16(d-4)(d-1)(3d-11)(3d-10)} \right] +$$

$$+ \, \text{} \, \left[-\frac{4(d-2)(-9482 + 13225d - 7306d^2 + 1992d^3 - 267d^4 + 14d^5)}{9(d-4)^2(2d-7)(3d-11)(3d-10)} \right] +$$

$$+ \frac{1}{m^2} \, \text{} \, \times$$

$$\times \left\{ \left[-\frac{(d-2)(2d-5)\alpha_5}{24(d-4)^2(d-3)(d-1)(2d-9)(2d-7)} \right] + \right.$$

$$\left. + \bar{\lambda}^2 \left[-\frac{(d-2)(2d-5)}{2(d_A+2)(d-4)(d-3)} \right] \right\} +$$

$$+ \frac{1}{m^2} \, \text{} \, \left[\frac{(d-2)(2d-5)\alpha_6}{3(d-4)^3(d-3)^2(d-1)(2d-7)(3d-11)(3d-10)} \right] +$$

$$+ m^2 \, \text{} \, \left\{ \left[-\frac{3(11 - 7d + d^2)}{(d-4)(2d-9)} \right] + \bar{\lambda} \left[-\frac{10(d-3)}{(d_A+2)(d-4)} \right] \right\} +$$

$$+ m^2 \, \text{} \, \left[\frac{2(d-3)(d-2)}{(d-4)(2d-7)} \right], \tag{3.8}$$

where

$$\alpha_1 = -121583669760 + 2691971008704d - 13463496742176d^2 + 33122892972480d^3 -$$
$$- 50028680189824d^4 + 51445267135192d^5 - 38155599595406d^6 + 21131958532365d^7 -$$
$$- 8925676618775d^8 + 2909006141441d^9 - 734705333783d^{10} + 143430052519d^{11} -$$
$$- 21428725861d^{12} + 2402935979d^{13} - 195570319d^{14} +$$
$$+ 10896768d^{15} - 371376d^{16} + 5832d^{17}, \tag{3.9}$$

$$\alpha_2 = -14081760 + 11237380d + 64451424d^2 - 140115669d^3 + 129957772d^4 -$$
$$- 69456108d^5 + 23323366d^6 - 5020699d^7 + 674926d^8 - 51720d^9 + 1728d^{10}, \tag{3.10}$$

$$\alpha_3 = 508742208 - 1725645240d + 2236030380d^2 - 1426818168d^3 +$$
$$+ 436152106d^4 - 14158652d^5 - 36636937d^6 + 13713052d^7 -$$

$$-2491870d^8 + 254770d^9 - 13967d^{10} + 318d^{11} \,, \tag{3.11}$$

$$\alpha_4 = -1266048 - 122112d + 1785942d^2 - 1171982d^3 +$$
$$+307185d^4 - 35512d^5 + 1400d^6 + 6d^7 + d^8 \,, \tag{3.12}$$

$$\alpha_5 = 5112 - 11321d + 10618d^2 - 5358d^3 + 1489d^4 - 212d^5 + 12d^6 \,, \tag{3.13}$$

$$\alpha_6 = 171232 - 492404d + 584218d^2 - 380046d^3 +$$
$$+149811d^4 - 36924d^5 + 5595d^6 - 480d^7 + 18d^8 \,. \tag{3.14}$$

It is worth stressing that eqs. (3.5)–(3.14) were obtained with an arbitrary ξ, which just exactly cancelled once all the graphs were summed together, for a general d, and before inserting any properties of the master integrals. This is a consequence of the fact that the master integrals constitute really a linearly independent basis for the present problem.

4. Integrals in $d = 3 - 2\epsilon$ dimensions

A set of master scalar integrals having been identified, the next step is to compute them. As already mentioned, we do this by writing $d = 3 - 2\epsilon$, expanding in $\epsilon \ll 1$, and evaluating a number of coefficients in the series.

In order to display the results, we first choose a convenient integration measure. To this end, we introduce an $\overline{\text{MS}}$ scale parameter $\bar{\mu}$, by writing each integration as

$$\int \frac{\mathrm{d}^d p}{(2\pi)^d} \equiv \mu^{-2\epsilon} \left[\bar{\mu}^{2\epsilon} \left(\frac{e^\gamma}{4\pi} \right)^\epsilon \int \frac{\mathrm{d}^d p}{(2\pi)^d} \right] \,, \tag{4.1}$$

where $\mu = \bar{\mu}(e^\gamma/4\pi)^{1/2}$, and the expression in square brackets has integer dimensionality. This square bracket part of an ℓ-loop integration is then written as

$$\left[\prod_{i=1}^{\ell} \left\{ \bar{\mu}^{2\epsilon} \left(\frac{e^\gamma}{4\pi} \right)^\epsilon \int \frac{\mathrm{d}^d p_i}{(2\pi)^d} \right\} \right] g(p_1, \ldots, p_\ell, m) =$$
$$= \frac{1}{(4\pi)^\ell} m^{3\ell - 2k} \left(\frac{\bar{\mu}}{2m} \right)^{2\epsilon\ell} \left\{ \prod_{i=1}^{\ell} \left[4\pi \left(\frac{e^\gamma}{\pi} \right)^\epsilon \int \frac{\mathrm{d}^{3-2\epsilon} p_i}{(2\pi)^{3-2\epsilon}} \right] g(p_1, \ldots, p_\ell, 1) \right\} \,, \tag{4.2}$$

where k counts the number of propagators, or lines, in the graphical representation of the function g. From now on we assume that the loop integrations are computed with the dimensionless measure in the curly brackets in eq. (4.2), while the constants in front of the curly brackets, together with the explicit powers of m as they appear in eqs. (3.5)–(3.8), are to be provided in trivial prefactors (cf. eq. (4.14) below).

With such conventions, the loop integrals remaining are functions of ϵ only, and read:

$$\bigcirc = -1 - 2\epsilon - \epsilon^2 \left(4 + \frac{1}{4}\pi^2 \right) + \epsilon^3 \gamma_1 + \mathcal{O}(\epsilon^4) \,, \tag{4.3}$$

$$\ominus = \frac{\pi^2}{12} + \epsilon \gamma_2 + \mathcal{O}(\epsilon^2) \,, \tag{4.4}$$

$$\ominus = \ln 2 + \epsilon \gamma_3 + \mathcal{O}(\epsilon^2) \,, \tag{4.5}$$

$$\triangle = \frac{\pi^2}{32\epsilon} + \gamma_4 + \mathcal{O}(\epsilon) \,, \tag{4.6}$$

$$\triangle = \frac{\pi^2}{32\epsilon} + \gamma_5 + \mathcal{O}(\epsilon) \,, \tag{4.7}$$

$$\triangle = \frac{\pi^2}{32\epsilon} + \gamma_6 + \mathcal{O}(\epsilon) \,, \tag{4.8}$$

$$\triangle = \frac{\pi^2}{32\epsilon} + \gamma_7 + \mathcal{O}(\epsilon) \,, \tag{4.9}$$

$$\bigcirc = \frac{7}{4\epsilon} - 8\ln 2 + 21 + \epsilon\,\gamma_8 + \mathcal{O}(\epsilon^2) \,, \tag{4.10}$$

$$\bigcirc = \frac{3}{8\epsilon} + \frac{9}{2} + \epsilon\Big(\frac{75}{2} + \frac{11}{8}\pi^2\Big) + \epsilon^2\,\gamma_9 + \mathcal{O}(\epsilon^3) \,, \tag{4.11}$$

$$\bigcirc = \gamma_{10} + \mathcal{O}(\epsilon) \,, \tag{4.12}$$

$$\bigcirc = \mathcal{O}(1) \,. \tag{4.13}$$

As we will see, the terms shown explicitly are needed for determining the $1/\epsilon$-poles in the 4-loop expression for f, the constants γ_n are needed for determining the finite 4-loop contribution to f, and the higher order terms only contribute at the level $\mathcal{O}(\epsilon)$. Analytic results for $\gamma_1, \ldots, \gamma_9$, as well as a numerical determination of γ_{10}, are presented in appendix A.

It is now convenient to combine the conventions in eqs. (3.4), (4.1), (4.2) and write

$$f(m^2, g^2, \lambda) = -d_A \frac{\mu^{-2\epsilon}}{4\pi} \sum_{\ell=1}^{\infty} m^{4-\ell} \left(\frac{\bar{\mu}}{2m}\right)^{2\epsilon\ell} \left(\frac{\mu^{-2\epsilon} g^2 C_A}{4\pi}\right)^{\ell-1} \tilde{p}_\ell \,. \tag{4.14}$$

Substituting eqs. (4.3)–(4.13) into eqs. (3.5)–(3.8) and expanding in ϵ, the results then read, up to $\mathcal{O}(\epsilon)$ corrections:

$$\tilde{p}_1 = +\frac{1}{3} \,, \tag{4.15}$$

$$\tilde{p}_2 = -\frac{1}{4}\left(\frac{1}{\epsilon} + 3 + \bar{\lambda}\right) \,, \tag{4.16}$$

$$\tilde{p}_3 = -\frac{89}{24} + \frac{11}{6}\ln 2 - \frac{1}{6}\pi^2 + $$
$$+ \frac{\bar{\lambda}}{4}\left(\frac{1}{\epsilon} + 3\right) + \frac{\bar{\lambda}^2}{4}\left[\frac{1}{2} - \frac{1}{d_A+2}\left(\frac{1}{\epsilon} + 8 - 4\ln 2\right)\right] \,, \tag{4.17}$$

$$\tilde{p}_4 = +\frac{1}{\epsilon}\left(\frac{43}{32} - \frac{491}{6144}\pi^2\right) + \frac{85291}{768} - \frac{1259}{32}\ln 2 + \frac{5653}{1536}\pi^2 - $$
$$- \frac{1}{4}\gamma_1 + \frac{5}{3}\gamma_2 - \frac{19}{6}\gamma_3 - \frac{157}{192}\gamma_4 - \frac{13}{64}(\gamma_5 + \gamma_6) - \frac{4}{9}\gamma_7 - \frac{19}{48}\gamma_8 - \frac{1}{6}\gamma_9 + \gamma_{10} + $$
$$+ \bar{\lambda}\left[-\frac{1}{16\epsilon^2} - \frac{1}{8\epsilon}\left(1 + \frac{5}{(d_A+2)}\Big(\frac{\pi^2}{8} - 1\Big)\right) + \right.$$
$$\left. + \frac{37}{24} - \frac{11}{12}\ln 2 + \frac{\pi^2}{48} + \frac{1}{d_A+2}\left(-\frac{5}{2} - \frac{15}{2}\ln 2 + \frac{115}{192}\pi^2 - \frac{5}{4}(\gamma_4 + \gamma_5)\right)\right] + $$
$$+ \bar{\lambda}^2\left[\frac{1}{16\epsilon^2}\frac{1}{d_A+2} - \frac{1}{8\epsilon}\left(1 + \frac{1}{d_A+2}\Big(\frac{\pi^2}{8} - 5\Big)\right) - \right.$$

$$-\frac{1}{8} + \frac{1}{d_A + 2}\left(46 - \frac{51}{2}\ln 2 + \frac{13}{24}\pi^2 - 2\gamma_3 - \frac{1}{2}\gamma_4 - \frac{1}{4}\gamma_8\right)\Bigg] +$$

$$+\bar{\lambda}^3\Bigg[\frac{1}{\epsilon}\left(\frac{1}{8}\frac{1}{d_A + 2} - \frac{\pi^2}{192}\frac{(d_A + 8)}{(d_A + 2)^2}\right) -$$

$$-\frac{1}{24} + \frac{1}{2(d_A + 2)}(1 - \ln 2) - \frac{1}{6}\frac{(d_A + 8)}{(d_A + 2)^2}\,\gamma_4\Bigg]. \tag{4.18}$$

It is interesting to note that while single diagrams contributing to $\tilde{p}_3$ do have $1/\epsilon$-poles (cf. appendix B), they sum to zero in the term without $\bar{\lambda}$, but not in the terms proportional to $\bar{\lambda}$, $\bar{\lambda}^2$. This structure is related to counterterm contributions from lower orders, as discussed in the next section. Similarly, single diagrams contributing to $\tilde{p}_4$ have both $1/\epsilon^2$ and $1/\epsilon$-poles, but the former ones sum to zero in the term without any $\bar{\lambda}$'s.

Of course, single diagrams contain also ξ-dependence. In our computation ξ cancelled at the stage of eqs. (3.5)–(3.14), but one could alternatively express single diagrams in terms of the same basis of master integrals, this time with ξ-dependent coefficients, and let the ξ's sum to zero only in the end. For completeness, we again illustrate the general structure of such expressions at the 3-loop level, in appendix B.

5. Counterterm contributions

The computation so far has been in terms of the bare parameters of the lagrangian in eq. (1.2). As a final step the result is, however, to be converted into an expansion in terms of the renormalised parameters.

The conversion is particularly simple in low dimensions such as close to $d = 3$, since then the theory in eq. (1.2) is super-renormalisable. In fact, the only parameter requiring renormalisation is the mass parameter m^2. We write it as

$$m^2 \equiv m_{\text{bare}}^2 = m^2(\bar{\mu}) + \delta m^2, \tag{5.1}$$

$$\delta m^2 = 2(d_A + 2)\frac{1}{(4\pi)^2}\frac{\mu^{-4\epsilon}}{4\epsilon}\left(-g^2\lambda C_A + \lambda^2\right). \tag{5.2}$$

This exact counterterm [21, 22] guarantees that all n-point Green's functions computed with the theory are ultraviolet finite. Note that as far as dimensional reasons and single diagrams are concerned, there could also be divergences of the form g^4/ϵ, but they sum to zero in the counterterm appearing in eq. (5.2).

Inserting now eqs. (5.1), (5.2) into the 1-loop and 2-loop expressions for $f(m^2, g^2, \lambda)$, we get contributions of the same order as the 3-loop and 4-loop vacuum graphs, respectively, from $\delta m^2 \cdot \partial_{m^2}f(m^2(\bar{\mu}), g^2, \lambda)$. We need to use here eqs. (3.5), (3.6), since $\mathcal{O}(\epsilon)$-terms, not shown in eqs. (4.15), (4.16), contribute as well, being multiplied by the $1/\epsilon$ in δm^2. Explicitly, the terms to be added to eqs. (4.17), (4.18), once the prefactors in eq. (4.14) are expressed in terms of the renormalised parameter $m(\bar{\mu})$ rather than m, are

$$\delta\tilde{p}_3 = \left(\frac{\bar{\mu}}{2m(\bar{\mu})}\right)^{-4\epsilon}\left(\frac{1}{4\epsilon} + \frac{1}{2}\right)\left(-\bar{\lambda} + \frac{1}{d_A + 2}\bar{\lambda}^2\right), \tag{5.3}$$

$$\delta\tilde{p}_4 = \left(\frac{\bar{\mu}}{2m(\bar{\mu})}\right)^{-4\epsilon}\left(-\frac{1}{8}\right)\left(\frac{1}{\epsilon^2} + \frac{1}{\epsilon}(1 + \bar{\lambda}) + \frac{1}{2}(4 + \pi^2) + 2\bar{\lambda}\right)\left(-\bar{\lambda} + \frac{1}{d_A + 2}\bar{\lambda}^2\right). \tag{5.4}$$

The 3-loop $1/\epsilon$-contributions in eq. (5.3) cancel against the $1/\epsilon$-terms in eq. (4.17). Indeed, genuine vacuum divergences can only appear in $\tilde{p}_2, \tilde{p}_4$, since such divergences must be analytic in the parameters m^2, g^2, λ appearing in the lagrangian, while $\tilde{p}_3$ comes with a coefficient $\sim (m^2(\bar{\mu}))^{1/2}$ (cf. eq. (4.14)). Another point to note is that $1/\epsilon^2$-terms appear in $\delta \tilde{p}_4$ only with coefficients $\bar{\lambda}, \bar{\lambda}^2$, just as in eq. (4.18), although there is no complete cancellation.

6. The final result

We can now collect together the full result for $f(m^2, g^2, \lambda)$, in terms of the renormalised parameters of the theory. For dimensional reasons, its structure is,

$$
\begin{aligned}
f(m^2, g^2, \lambda) = \frac{\mu^{-2\epsilon}}{4\pi} & \left[\tilde{f}_{1,0} \right] m^3(\bar{\mu}) + \\
& + \frac{\mu^{-4\epsilon}}{(4\pi)^2} \left[\tilde{f}_{2,0}\, g^2 + \tilde{f}_{2,1}\, \lambda \right] m^2(\bar{\mu}) + \\
& + \frac{\mu^{-6\epsilon}}{(4\pi)^3} \left[\tilde{f}_{3,0}\, g^4 + \tilde{f}_{3,1}\, g^2 \lambda + \tilde{f}_{3,2}\, \lambda^2 \right] m(\bar{\mu}) + \\
& + \frac{\mu^{-8\epsilon}}{(4\pi)^4} \left[\tilde{f}_{4,0}\, g^6 + \tilde{f}_{4,1}\, g^4 \lambda + \tilde{f}_{4,2}\, g^2 \lambda^2 + \tilde{f}_{4,3}\, \lambda^3 \right] + \cdots,
\end{aligned} \tag{6.1}
$$

where $\tilde{f}_{\ell,i} = \tilde{f}_{\ell,i}(\epsilon, \bar{\mu}/m(\bar{\mu}))$ are dimensionless numbers, with ℓ indicating the loop order, and i the number of λ's appearing:

$$
\tilde{f}_{1,0} = d_A \left(-\frac{1}{3} + \mathcal{O}(\epsilon) \right), \tag{6.2}
$$

$$
\tilde{f}_{2,0} = d_A C_A \left(\frac{1}{4\epsilon} + \ln \frac{\bar{\mu}}{2m(\bar{\mu})} + \frac{3}{4} + \mathcal{O}(\epsilon) \right), \tag{6.3}
$$

$$
\tilde{f}_{2,1} = d_A (d_A + 2) \left(\frac{1}{4} + \mathcal{O}(\epsilon) \right), \tag{6.4}
$$

$$
\tilde{f}_{3,0} = d_A C_A^2 \left(\frac{89}{24} - \frac{11}{6} \ln 2 + \frac{\pi^2}{6} + \mathcal{O}(\epsilon) \right), \tag{6.5}
$$

$$
\tilde{f}_{3,1} = d_A C_A (d_A + 2) \left(-\ln \frac{\bar{\mu}}{2m(\bar{\mu})} - \frac{1}{4} + \mathcal{O}(\epsilon) \right), \tag{6.6}
$$

$$
\tilde{f}_{3,2} = d_A (d_A + 2) \left(\ln \frac{\bar{\mu}}{2m(\bar{\mu})} + \frac{3}{2} - \ln 2 + \mathcal{O}(\epsilon) \right) + d_A (d_A + 2)^2 \left(-\frac{1}{8} + \mathcal{O}(\epsilon) \right), \tag{6.7}
$$

$$
\begin{aligned}
\tilde{f}_{4,0} = d_A C_A^3 \Bigg[& \left(\frac{43}{32} - \frac{491}{6144} \pi^2 \right) \left(-\frac{1}{\epsilon} - 8 \ln \frac{\bar{\mu}}{2m(\bar{\mu})} \right) - \\
& - \frac{85291}{768} + \frac{1259}{32} \ln 2 - \frac{5653}{1536} \pi^2 + \frac{1}{4} \gamma_1 - \frac{5}{3} \gamma_2 + \frac{19}{6} \gamma_3 + \\
& + \frac{157}{192} \gamma_4 + \frac{13}{64} (\gamma_5 + \gamma_6) + \frac{4}{9} \gamma_7 + \frac{19}{48} \gamma_8 + \frac{1}{6} \gamma_9 - \gamma_{10} + \mathcal{O}(\epsilon) \Bigg],
\end{aligned} \tag{6.8}
$$

$$
\begin{aligned}
\tilde{f}_{4,1} = d_A C_A^2 \Bigg[& \left(\frac{5}{8} - \frac{5}{64} \pi^2 \right) \left(-\frac{1}{\epsilon} - 8 \ln \frac{\bar{\mu}}{2m(\bar{\mu})} \right) + \\
& + \frac{5}{2} + \frac{15}{2} \ln 2 - \frac{115}{192} \pi^2 + \frac{5}{4} (\gamma_4 + \gamma_5) + \mathcal{O}(\epsilon) \Bigg] +
\end{aligned}
$$

$$+ d_A C_A^2 (d_A + 2) \left(-\frac{1}{16\epsilon^2} + \ln^2 \frac{\bar\mu}{2m(\bar\mu)} + \frac{1}{2} \ln \frac{\bar\mu}{2m(\bar\mu)} - \right.$$
$$\left. - \frac{43}{24} + \frac{11}{12} \ln 2 - \frac{1}{12}\pi^2 + \mathcal{O}(\epsilon) \right), \tag{6.9}$$

$$\tilde{f}_{4,2} = d_A C_A (d_A + 2) \left[\frac{1}{16\epsilon^2} - \frac{32 - \pi^2}{64\epsilon} - \ln^2 \frac{\bar\mu}{2m(\bar\mu)} - \left(\frac{36 - \pi^2}{8} \right) \ln \frac{\bar\mu}{2m(\bar\mu)} - \right.$$
$$\left. - \frac{183}{4} + \frac{51}{2} \ln 2 - \frac{23}{48}\pi^2 + 2\gamma_3 + \frac{1}{2}\gamma_4 + \frac{1}{4}\gamma_8 + \mathcal{O}(\epsilon) \right] +$$
$$+ d_A C_A (d_A + 2)^2 \left(\frac{1}{2} \ln \frac{\bar\mu}{2m(\bar\mu)} - \frac{1}{8} + \mathcal{O}(\epsilon) \right), \tag{6.10}$$

$$\tilde{f}_{4,3} = d_A (d_A + 2)(d_A + 8) \left[\left(\frac{\pi^2}{192} \right) \left(\frac{1}{\epsilon} + 8 \ln \frac{\bar\mu}{2m(\bar\mu)} \right) + \frac{1}{6}\gamma_4 + \mathcal{O}(\epsilon) \right] +$$
$$+ d_A (d_A + 2)^2 \left(-\frac{1}{2} \ln \frac{\bar\mu}{2m(\bar\mu)} - \frac{1}{4} + \frac{1}{2} \ln 2 + \mathcal{O}(\epsilon) \right) +$$
$$+ d_A (d_A + 2)^3 \left(\frac{1}{24} + \mathcal{O}(\epsilon) \right). \tag{6.11}$$

In particular, following the notation of ref. [11] and writing

$$\tilde{f}_{4,0} \equiv -d_A C_A^3 \left[\alpha_{\rm M} \left(\frac{1}{\epsilon} + 8 \ln \frac{\bar\mu}{2m(\bar\mu)} \right) + \beta_{\rm M} \right], \tag{6.12}$$

we read from eq. (6.8) that

$$\alpha_{\rm M} = \frac{43}{32} - \frac{491}{6144}\pi^2 \approx 0.555017, \tag{6.13}$$

$$\beta_{\rm M} = \frac{85291}{768} - \frac{1259}{32} \ln 2 + \frac{5653}{1536}\pi^2 - \frac{1}{4}\gamma_1 + \frac{5}{3}\gamma_2 - \frac{19}{6}\gamma_3 -$$
$$- \frac{157}{192}\gamma_4 - \frac{13}{64}(\gamma_5 + \gamma_6) - \frac{4}{9}\gamma_7 - \frac{19}{48}\gamma_8 - \frac{1}{6}\gamma_9 + \gamma_{10}$$
$$= -\frac{311}{256} - \frac{43}{32} \ln 2 - \frac{19}{6} \ln^2 2 + \frac{77}{9216}\pi^2 - \frac{491}{1536}\pi^2 \ln 2 + \frac{1793}{512}\zeta(3) + \gamma_{10}$$
$$\approx -1.391512. \tag{6.14}$$

In eq. (6.14) we used values for $\gamma_1, \ldots, \gamma_{10}$ from appendix A.5 and appendix A.6. The coefficient $\alpha_{\rm M}$ gives a contribution of order $\mathcal{O}(g^6 \ln(1/g) T^4)$ and $\beta_{\rm M}$ a perturbative contribution of order $\mathcal{O}(g^6 T^4)$ to the pressure of hot QCD [11].

The expression in eq. (6.1), with the coefficients in eqs. (6.2)–(6.11), contains a number of $1/\epsilon^2$ and $1/\epsilon$-poles. Once our computation is embedded into some physical setting, such as in [11], a vacuum counterterm is automatically generated (denoted by $p_{\rm E}(T)$ in [11]), which eventually cancels all the UV-poles, such that physical observables remain finite for $\epsilon \to 0$. The nature of the poles in eqs. (6.2)–(6.11) is analysed in detail in the next section.

7. Infrared insensitivity of the results

The result shown in the previous section contains a number of $1/\epsilon^2$ and $1/\epsilon$-divergences. Since dimensional regularisation regulates at the same time both ultraviolet (UV) and

infrared (IR) divergences, we may ask of what type are those obtained? The purpose of this section is to show that the divergences are of purely UV origin, and the result is thus IR insensitive, *if interpreted properly*. There are two ways of showing this, firstly an effective theory approach in which one understands that all the IR divergences are contained in the SU(N_c) pure Yang-Mills theory obtained by integrating out the A_0-field, secondly a pragmatic one in which one shields away the IR divergences by giving the gluon and ghost fields a mass.

Conceptually the best way to analyse the IR sensitivity is to dress the problem in an effective theory language. In the present context, such an analysis was carried out in [10]. The idea is that since the field A_0 has a mass scale, it can be integrated out. The integration out is an ultraviolet procedure, thus by construction not sensitive to IR physics. The effective low-energy theory that emerges is a 3d pure gauge theory. Its partition function, on the other hand, does contain IR divergences, starting at 4-loop level [8, 9].

Therefore, we expect that all results up to 3-loop level should be IR insensitive. At 4-loop level there is a part of the result, that is the diagrams which can be constructed fully inside the pure SU(N_c) theory, which can be both IR and UV divergent. Since in dimensional regularisation, however, these graphs are set to zero, the non-zero result we have obtained should again be insensitive to any mass scales in the gluon and ghost propagators.

Apart from the issue mentioned, there is also another possible source of IR problems, namely that of overlapping divergences. Indeed, while IR divergences appear for vacuum graphs at 4-loop level only, they appear for self-energy graphs already at the 2-loop level (see, e.g., [10]). However, 2-loop self-energy insertions do appear also as subgraphs in the 4-loop "ring diagrams", making the divergence structure of such 4-loop graphs "doubly" problematic. We return to this issue presently, but first finish the discussion of IR divergences at lower than 4-loop level.

To be very explicit, let us introduce a fictitious mass parameter $m_{\rm G}$ for all massless lines (gluons and ghosts), hence giving the function $f(m^2, g^2, \lambda)$ a further functional dependence on the mass ratio $x = m_{\rm G}/m$. Let us denote by AH ("Adjoint Higgs") graphs with at least one A_0-line, and by YM ("Yang-Mills") graphs with none at all. The general structure of the bare $f(m^2, g^2, \lambda)$ can then be expressed as (cf. eq. (4.14))

$$f(m^2, g^2, \lambda) = \sum_{\ell=1}^{\infty} \Big(\frac{\mu^{-2\epsilon}}{4\pi}\Big)^{\ell} \Big(\frac{\bar{\mu}}{2m}\Big)^{2\epsilon\ell} (g^2)^{\ell-1} m^{4-\ell} \Big[\tilde{f}_{\ell}^{\rm AH}(x, \epsilon, \xi, \bar{\lambda}) + x^{4-\ell-2\epsilon\ell} \tilde{f}_{\ell}^{\rm YM}(\epsilon, \xi) \Big], \tag{7.1}$$

where $\tilde{f}_{\ell}^{\rm AH}, \tilde{f}_{\ell}^{\rm YM}$ are dimensionless functions. While the treatment above corresponds to setting $x = 0$ first and then computing the expansion in ϵ, we now keep a non-zero x through the entire calculation, being interested in the limit of small x only in the end:

$$\overline{\rm MS}: \quad \lim_{\epsilon \to 0} \lim_{x \to 0} \tilde{f}_{\ell}^{\rm AH}(x, \epsilon, \xi, \bar{\lambda}), \tag{7.2}$$

$$\text{IR-regulator}: \quad \lim_{x \to 0} \lim_{\epsilon \to 0} \tilde{f}_{\ell}^{\rm AH}(x, \epsilon, \xi, \bar{\lambda}). \tag{7.3}$$

These two limits do not in general commute for single diagrams, but should commute for the sum. Possible power IR divergences in single diagrams would show up as poles in x, while logarithmic ones correspond to $\ln x$.

The main technical differences in the IR regularised procedure with respect to the $\overline{\text{MS}}$ computation are a more complicated scalarisation, in the absence of low-level routines specific to the presence of massless lines, such as the so-called "triangle rule", and an enlarged set of master integrals. Furthermore, some additional diagrams contribute, which were set to zero from the outset in the $\overline{\text{MS}}$ calculation, due to the absence of any mass scale (in some subdiagram).

As a roundup, it turns out that, starting at the 3-loop level, individual diagrams *do* indeed contain logarithmic as well as powerlike IR divergences, which then cancel in the sum, proving *a posteriori* the validity of the dimensionally regularised $\overline{\text{MS}}$ calculation. For completeness, we illustrate this issue in appendix B.

We now return to the 4-loop level. According to the discussion above, the full set of graphs can be divided into four sub-classes, having potentially different IR properties: pure Yang–Mills graphs (YM) and those with at least one A_0-line (AH), with both sets further divided into skeletons (figure 1) and ring diagrams (figure 2). The properties of the pure Yang–Mills diagrams are discussed in [12], and we only state here that they contain both logarithmic UV as well as IR divergences, which however exactly cancel in strict dimensional regularisation (but not in regularisations which only regulate the UV, such as lattice regularisation). Here we then just discuss the skeletons and rings containing at least one massive A_0-line. For simplicity, we discuss explicitly only terms without a quartic coupling λ.

We have computed the $1/\epsilon$-divergence in the sum of such AH-skeletons with in total three different mass spectra:

1. As described above, whereby the A_0-lines carry the mass parameter m^2, while the gluon and ghost lines are massless.

2. By giving an equal mass to all the fields: A_0, gluons, and ghosts. The computation proceeds in complete analogy with the one described in [12].

3. By setting all masses to zero, picking some line in the 4-loop vacuum graph, integrating the massless 3-loop 2-point function connected to that line in d dimensions,[1] and regulating the remaining single integral by shielding the IR with a mass and regulating the UV via dimensional regularization.

All three methods give the same result for the $1/\epsilon$-pole in AH-skeletons, confirming its expected IR finiteness. Expressed as a contribution to $\tilde{p}_4$ in eq. (4.18), the divergence appearing in the result reads

$$\delta[\tilde{p}_4] = \frac{1}{3072\epsilon}\left[3(696 - 56\xi - 6\xi^2 - 5\xi^3) - \frac{\pi^2}{4}(832 - 144\xi + 81\xi^2 - 15\xi^3 + 3\xi^4)\right]. \quad (7.4)$$

For the AH-rings, on the other hand, the third method does not work. This is due to the overlapping divergences mentioned above: a 2-loop 2-point function of gluons alone

---

[1]This problem has been solved a long time ago via integration by parts; for a discussion as well as an algorithmic implementation, see [23].

leads to logarithmic UV and IR divergences, and trying to carry out the final integration by some recipe, gives generically an outcome $\sim 1/\epsilon^2$, but with a coefficient dependent on what the recipe precisely was. To cancel the $1/\epsilon^2$-pole, not to mention to get the correct coefficient for the remaining $1/\epsilon$-pole, is a very delicate problem, which can only be guaranteed to have been solved by employing a fully systematic procedure. Our non-abelian case is therefore qualitatively different from a pure scalar theory, where the problem of overlapping divergences does not emerge [24]. For a discussion of the cancellation of the analogue of the $1/\epsilon^2$-pole in cutoff regularisation in the pure $\mathrm{SU}(N_c)$ theory, see [15].

On the contrary, the AH-rings can be systematically computed with the 1st and 2nd types of mass spectra. Both procedures give the same result, confirming its IR insensitivity. Summing together with eq. (7.4), we recover the ξ-independent $1/\epsilon$-pole on the first row in eq. (4.18).

In summary, we have verified explicitly that the only possible IR divergence appearing in our computation is that of the pure $\mathrm{SU}(N_c)$ gauge theory, contained in the YM-graphs. It is addressed further in ref. [12].

8. Discussion and conclusions

The main point of this paper has been the discussion of formal analytic techniques for, and actual results from, the evaluation of the 4-loop partition function of the 3d $\mathrm{SU}(N_c)$ + adjoint Higgs theory using dimensional regularisation. The final result is shown in eqs. (6.1)–(6.11). We have also demonstrated that if interpreted as a matching coefficient — that is, if the pure Yang-Mills graphs, without any adjoint scalar lines, are dropped, as is automatically the case in strict dimensional regularisation — then the result is IR finite. Therefore, all IR divergences are contained in the pure Yang-Mills theory. We would now like to end by recalling that such techniques and results have also practical applications.

Perhaps the most important application is that our results provide two specific new *perturbative* contributions to the free energy of hot QCD, of orders $g^6 \ln(1/g)T^4$, $g^6 T^4$ [11]. Similarly, they provide also new perturbative contributions to quark number susceptibilities [25]. Once the parameters of the 3d theory are expressed in terms of the parameters of the physical finite temperature QCD via dimensional reduction, and once other contributions of the same parametric magnitudes are added, this allows for instance to re-estimate the convergence properties of QCD perturbation theory at high temperatures [11, 25, 26]. Our present computation also contributes to the $\overline{\mathrm{MS}}$ scheme renormalisation of the simplest 3d gauge-invariant local condensates, obtained by partial derivatives of the action with respect to various parameters [21], and thus in principle helps in non-perturbative studies of the pressure of high-temperature QCD [4, 13]. It may also allow for refined analytic estimates such as Padé resummations [27] for the observable in eq. (1.3).

Let us mention that there has recently been significant interest in somewhat more phenomenological approaches to QCD perturbation theory at high temperatures (for reviews see, e.g., [28]). As far as we can tell our results are of no immediate use in such settings.

Another application is that our general procedure is relevant for studies of critical phenomena in some statistical physics systems. In this context one may either study

directly the three-dimensional physical system, or carry out computations first in $d = 4 - \epsilon$ dimensions, expand in ϵ, and then take the limit $\epsilon \to 1$. For instance, some properties of the Ginzburg–Landau theory of superconductivity have been addressed in the former setup up to 2-loop level (see, e.g., [29]–[32]), and in the latter setup, in the disordered phase, up to 3-loop level [33]. The integrals arising in the disordered phase are "QED-like" just as in our study, so that scalarisation and the sets of master integrals are essentially the same as the present ones [16]. Moreover, in the case $d = 4 - \epsilon$, the master integrals can be evaluated to a high accuracy utilising the techniques introduced in [34], while for $d = 3 - 2\epsilon$ most master integrals have been evaluated in this paper. Our methods could therefore help in reaching the 4-loop order.

Acknowledgments

A. Master integrals

We discuss in this appendix the determination of the scalar master integrals of eqs. (4.3)–(4.13). They depend on one mass-scale m only and are thus "QED-like" in the generalised sense that the number of massive lines at each vertex is even. Since the dependence on m is trivial and has been absorbed into the coefficients, see eq. (4.2), $m = 1$ in most of what follows. One obtains particularly simple expansions in $3 - 2\epsilon$ dimensions by using the integration measure $\int_p = \frac{(4\pi e^\gamma)^\epsilon}{2\pi^2} \int \mathrm{d}^{3-2\epsilon} p$, in accordance with eq. (4.2).

We first discuss briefly the various general techniques we have employed for the evaluation of these integrals. The list of techniques includes: partial integration relations between various scalar integrals, in analogy with those derived at 3-loop level in [20] (appendix A.1); graphs with only two massive lines, which can often be evaluated exactly (appendix A.2); graphs with two or three vertices, which can be evaluated to a sufficient depth in ϵ using configuration space methods (appendix A.3); and some remaining graphs, which were evaluated in momentum space (appendix A.4). We combine the results from the various techniques in appendix A.5, showing the actual expansions for the master integrals to the depths specified in eqs. (4.3)–(4.11). There is one finite integral remaining which we have not been able to evaluate analytically, corresponding to eq. (4.12); its numerical value is determined in appendix A.6.

A.1 Partial integration identities

Implementing systematically all identities following from partial integrations, as discussed in section 3, allows not only to express all integrals in terms of a few scalar ones, which do not contain any non-trivial numerators, but produces also a set of relations between the

scalar integrals. As a simple example, we may recall that the identity

$$0 = \sum_{k=1}^{d} \int_{p,q} \frac{\partial}{\partial p_k} \left[\frac{p_k - q_k}{(p^2 + m^2)(q^2 + m^2)(p - q)^2} \right], \tag{A.1}$$

leads to the relation

$$\int_{p,q} \frac{1}{(p^2 + m^2)(q^2 + m^2)(p - q)^2} = \frac{1}{d - 3} \int_p \frac{1}{(p^2 + m^2)^2} \int_q \frac{1}{(q^2 + m^2)}. \tag{A.2}$$

Taking furthermore into account that in dimensional regularisation the two integrals on the right-hand-side of eq. (A.2) are related, we obtain

$$\bigcirc\!\!\!\cdots\!\!\!\bigcirc = \frac{1}{m^2} \left(\bigcirc \right)^2 \left[-\frac{(d - 2)}{2(d - 3)} \right]. \tag{A.3}$$

Examples of similar relations at 3-loop level were shown in eqs. (3.1), (3.2), and a complete 3-loop analysis can be found in [20] (see also [6]).

At 4-loop level, there are obviously many more identities than at 3-loop level. Rather than showing a complete list we give here, as an example, one of the relations:

$$\bigoplus = \frac{1}{m^2} \bigcirc \times \bigcirc\!\!\!\bigcirc \left[-\frac{d - 2}{2(d - 3)} \right] + \frac{1}{m^2} \bigcirc\!\!\!\bigcirc \left[\frac{2d - 5}{4(d - 3)} \right]. \tag{A.4}$$

It turns out that this relation is convenient for the determination of the 4-loop integral on the right-hand-side.

A.2 Integrals known exactly

A few of the integrals appearing can be evaluated exactly in d dimensions. This holds particularly for cases where only two massive propagators appear. As an example, we show how this can be done in configuration space. The massive propagator can be written as

$$G(x; m_i) \equiv \int \frac{\mathrm{d}^{3-2\epsilon} p}{(2\pi)^{3-2\epsilon}} \frac{e^{ip \cdot x}}{p^2 + m_i^2} = \frac{1}{(2\pi)^{\frac{3}{2}-\epsilon}} \left(\frac{m_i}{x} \right)^{\frac{1}{2}-\epsilon} K_{\frac{1}{2}-\epsilon}(m_i x), \tag{A.5}$$

where K is a modified Bessel function, and x denotes, depending on the context, either a d-dimensional vector or its modulus. On the other hand, the massless part of the graph converts in configuration space to

$$\int \frac{\mathrm{d}^{3-2\epsilon} p}{(2\pi)^{3-2\epsilon}} \frac{e^{ip \cdot x}}{p^\nu} = \frac{\Gamma(\frac{3}{2} - \frac{\nu}{2} - \epsilon)}{\Gamma(\frac{\nu}{2})} \frac{1}{2^\nu \pi^{\frac{3}{2}-\epsilon} x^{3-\nu-2\epsilon}}. \tag{A.6}$$

We can then employ the identity

$$\int_0^\infty \mathrm{d}x \, x^\lambda K_\mu^2(x) = \frac{2^{\lambda-2}}{\Gamma(1 + \lambda)} \Gamma\left(\frac{1 + \lambda + 2\mu}{2} \right) \Gamma^2\left(\frac{1 + \lambda}{2} \right) \Gamma\left(\frac{1 + \lambda - 2\mu}{2} \right). \tag{A.7}$$

With this result, the following expressions are easily derived (using the integration measure inside the curly brackets in eq. (4.2)):

$$\text{\Large ⊚} = \left(-\frac{1}{2\epsilon}\right)\frac{(4e^\gamma)^{3\epsilon}\,\Gamma(\tfrac{1}{2}+\epsilon)\Gamma(\tfrac{1}{2}-\epsilon)\Gamma(\tfrac{1}{2}+3\epsilon)\Gamma^2\,(1+2\epsilon)}{(1-2\epsilon)(1-6\epsilon)\Gamma^3(\tfrac{1}{2})\Gamma\,(1+4\epsilon)} \tag{A.8}$$

$$= -\frac{1}{2\epsilon} - 4 - \left(26+\frac{25}{24}\pi^2\right)\epsilon - \left(160+\frac{25}{3}\pi^2-\frac{47}{2}\zeta(3)\right)\epsilon^2 + \mathcal{O}(\epsilon^3), \tag{A.9}$$

$$\text{\Large ⊖} = \frac{\pi^2}{32\epsilon}\,(4e^\gamma)^{4\epsilon}\,\frac{\Gamma^2(\tfrac{1}{2}+\epsilon)\Gamma^3(\tfrac{1}{2}-\epsilon)\Gamma^2(\tfrac{1}{2}+3\epsilon)\Gamma(\tfrac{1}{2}-3\epsilon)\Gamma\,(1+4\epsilon)}{(1-2\epsilon)\Gamma^8(\tfrac{1}{2})\Gamma^2(1-2\epsilon)\Gamma\,(1+6\epsilon)} \tag{A.10}$$

$$= \frac{\pi^2}{32}\left[\frac{1}{\epsilon}+2+4\ln 2+\left(4+\frac{17}{3}\pi^2+8\ln 2\,(1+\ln 2)\right)\epsilon + \mathcal{O}(\epsilon^2)\right], \tag{A.11}$$

$$\text{\Large ⊘} = \frac{3}{8\epsilon}\,(4e^\gamma)^{4\epsilon}\,\frac{\Gamma^2(\tfrac{1}{2}-\epsilon)\Gamma^2(\tfrac{1}{2}+3\epsilon)\Gamma\,(1+2\epsilon)\,\Gamma\,(1+4\epsilon)}{(1-2\epsilon)(1-4\epsilon)(1-6\epsilon)\Gamma^4(\tfrac{1}{2})\Gamma\,(1+6\epsilon)} \tag{A.12}$$

$$= \frac{3}{8\epsilon} + \frac{9}{2} + \left(\frac{75}{2}+\frac{11}{8}\pi^2\right)\epsilon + \left(270+\frac{33}{2}\pi^2-\frac{55}{2}\zeta(3)\right)\epsilon^2 + \mathcal{O}(\epsilon^3). \tag{A.13}$$

Obviously we also know ($\int_p$ is again according to the curly brackets in eq. (4.2)):

$$\text{\Large ◯} = \int_p \frac{1}{p^2+1} = -\frac{(4e^\gamma)^\epsilon}{1-2\epsilon}\frac{\Gamma(\tfrac{1}{2}+\epsilon)}{\Gamma(\tfrac{1}{2})} \tag{A.14}$$

$$= -1 - 2\epsilon - \left(4+\frac{\pi^2}{4}\right)\epsilon^2 - \left(8+\frac{\pi^2}{2}-\frac{7}{3}\zeta(3)\right)\epsilon^3 + \mathcal{O}(\epsilon^4). \tag{A.15}$$

A.3 Configuration space evaluations

Even when configuration space does not allow for an exact evaluation of the integral, like in appendix A.2, it may allow for the most straightforward way of obtaining a number of coefficients in an expansion of the result in ϵ. This is the case particularly if there are only two vertices in the graph.

At ℓ-loop level, the graphs in this class are of the form

$$_1\!\text{\Large (}_2\text{\Large (}\cdots\text{\Large)}\text{\Large)}_{\ell+1} = \left[4\pi\left(\frac{e^\gamma}{\pi}\right)^\epsilon\right]^\ell\frac{2\pi^{\frac{3}{2}-\epsilon}}{\Gamma(\tfrac{3}{2}-\epsilon)}\int_0^\infty \mathrm{d}x\,x^{2-2\epsilon}\prod_{i=1}^{\ell+1}G(x;m_i), \tag{A.16}$$

where $G(x;m_i)$ is from eq. (A.5). The idea (see, e.g., [24]) is to split the integration into two parts: $\int_0^\infty \mathrm{d}x(\ldots) = \int_0^r \mathrm{d}x(\ldots) + \int_r^\infty \mathrm{d}x(\ldots)$. The first part is performed in $d=3-2\epsilon$ dimensions but by using the asymptotic small-x form of $G(x;m_i)$,

$$G(x;m_i) = \frac{\Gamma(\tfrac{1}{2}-\epsilon)}{4\pi^{\frac{3}{2}-\epsilon}}\frac{1}{x^{1-2\epsilon}}\left[1-\left(\frac{m_i x}{2}\right)^{1-2\epsilon}\frac{\Gamma(\tfrac{1}{2}+\epsilon)}{\Gamma(\tfrac{3}{2}-\epsilon)}+\left(\frac{m_i x}{2}\right)^2\frac{\Gamma(\tfrac{1}{2}+\epsilon)}{\Gamma(\tfrac{3}{2}+\epsilon)}+\cdots\right], \tag{A.17}$$

while the latter part, which is finite, is performed by expanding first in ϵ and then carrying out the remaining integrals is $d=3$ dimensions. For instance,

$$G(x;m_i) = \frac{e^{-m_i x}}{4\pi x}\left[1-\epsilon\left(\ln\frac{m_i^2 e^\gamma}{4\pi}+m_i x\int_1^\infty \mathrm{d}y\ln(y^2-1)e^{(1-y)m_i x}\right)+\mathcal{O}(\epsilon^2)\right]. \tag{A.18}$$

When the two parts are summed together and the limit $r\to 0$ is taken, the dependence on r cancels, and we obtain the desired result.

In the evaluation of such integrals, dilogarithms will in general appear. Their properties have been summarised, e.g., in [35]. For completeness, let us recall here that one can shift the argument of

$$\text{Li}_2(x) = -\int_0^x \mathrm{d}t\, \frac{\ln(1-t)}{t} = \sum_{n>0} \frac{x^n}{n^2} \tag{A.19}$$

from the intervals $[-\infty\ldots-1]$, $[-1\ldots0]$, $[1/2\ldots1]$ to the interval $[0\ldots1/2]$ via

$$\text{Li}_2(x) = \text{Li}_2\left(\frac{1}{1-x}\right) - \ln(1-x)\ln(-x) + \frac{1}{2}\ln^2(1-x) - \frac{\pi^2}{6}, \tag{A.20}$$

$$\text{Li}_2(x) = -\text{Li}_2\left(-\frac{x}{1-x}\right) - \frac{1}{2}\ln^2(1-x), \tag{A.21}$$

$$\text{Li}_2(x) = -\text{Li}_2(1-x) - \ln(1-x)\ln x + \frac{\pi^2}{6}, \tag{A.22}$$

respectively. As follows from here, the dilogarithms satisfy, for $x > 0$,

$$\text{Li}_2(-x) + \text{Li}_2\left(-\frac{1}{x}\right) = -\frac{1}{2}\ln^2 x - \frac{\pi^2}{6}. \tag{A.23}$$

Special values include

$$\text{Li}_2(-1) = -\frac{\pi^2}{12}, \qquad \text{Li}_2(0) = 0, \qquad \text{Li}_2\left(\frac{1}{2}\right) = \frac{\pi^2}{12} - \frac{1}{2}\ln^2 2, \qquad \text{Li}_2(1) = \frac{\pi^2}{6}. \tag{A.24}$$

Using these identities, and denoting $M = m_1 + m_2 + m_3$, we obtain for the 2-loop case

$$\overset{1}{\underset{3}{\overset{2}{\bigcirc}}} = \left(\frac{2}{M}\right)^{4\epsilon}\left\{\frac{1}{4\epsilon} + \frac{1}{2} + \epsilon\left[1 - \frac{\pi^2}{24} + \sum_{i=1}^{3}\text{Li}_2\left(1 - \frac{2m_i}{M}\right)\right] + \mathcal{O}(\epsilon^2)\right\}. \tag{A.25}$$

For the 3-loop case, now denoting $M = m_1 + m_2 + m_3 + m_4$, we obtain

$$ _1\!\left(2\!\bigcirc\!3\right)\!_4 = -M\left(\frac{2}{M}\right)^{6\epsilon}\left\{\frac{1}{4\epsilon} + 2 + \frac{1}{2}\sum_{i=1}^{4}\frac{m_i}{M}\ln\frac{M}{2m_i} + \right.$$
$$+ \epsilon\left[13 + \frac{3}{16}\pi^2 + \sum_{i=1}^{4}\left(\left(1 - \frac{2m_i}{M}\right)\text{Li}_2\left(1 - \frac{2m_i}{M}\right) + 4\frac{m_i}{M}\ln\frac{M}{2m_i} + \right.\right.$$
$$\left.\left.+ \frac{1}{2}\frac{m_i}{M}\ln^2\frac{M}{2m_i}\right)\right] + \mathcal{O}(\epsilon^2)\bigg\}. \tag{A.26}$$

In particular, if all masses are equal,

$$\bigcirc\!\!\bigcirc = -\frac{1}{\epsilon} - 8 + 4\ln 2 - 4\epsilon\left(13 + \frac{17}{48}\pi^2 - 8\ln 2 + \ln^2 2\right) + \mathcal{O}(\epsilon^2). \tag{A.27}$$

The case of two massless and two massive lines can be checked against eq. (A.9).

The 4-loop case has only been worked out to order $\mathcal{O}(1)$, rather than $\mathcal{O}(\epsilon)$. Denoting now $M = m_1 + m_2 + m_3 + m_4 + m_5$,

$$_1\!\left(2\bar{3}\bar{0}\bar{4}\right)\!_5 = M^2\left(\frac{2}{M}\right)^{8\epsilon}\left[\frac{1}{16\epsilon} + \frac{3}{4} + \sum_{i\neq j}\frac{m_i m_j}{2M^2}\left(\frac{1}{8\epsilon} + \frac{3}{2} + \ln\frac{M}{2m_i}\right) + \mathcal{O}(\epsilon)\right]. \tag{A.28}$$

The case of three massless and two massive lines can be checked against eq. (A.13). The next order, $\mathcal{O}(\epsilon)$, could also be worked out and is indeed needed for γ_8 in eq. (4.10), but we choose to use another way to determine it, based on eq. (A.4).

When there are more than two vertices in the graph, the configuration space technique gets rapidly more complicated, due to the difficult structure of the angular integrals. There is one graph we are interested in, however, whose divergent and, most incredibly, also the constant part [36] can still be obtained analytically:

$$2\left(\!\!\begin{array}{c}1\\3\,4\,5\end{array}\!\!\right)6= \left[4\pi\left(\frac{e^\gamma}{\pi}\right)^\epsilon\right]^4 \int \mathrm{d}^{3-2\epsilon}x \int \mathrm{d}^{3-2\epsilon}y \; G(x-y;m_1)\prod_{i=2}^{3} G(x;m_i)\prod_{j=4}^{6} G(y;m_j)\,. \quad \text{(A.29)}$$

Employing the angular integral [37]

$$\int \mathrm{d}\Omega_y \frac{K_\lambda(|x-y|)}{|x-y|^\lambda} = \frac{(2\pi)^{\lambda+1}}{(xy)^\lambda}\Big[\theta(x-y)K_\lambda(x)I_\lambda(y)+\theta(y-x)K_\lambda(y)I_\lambda(x)\Big]\,, \quad \text{(A.30)}$$

where $\lambda = \frac{1}{2}-\epsilon$ and on the right-hand-side $x \equiv |x|$, $y \equiv |y|$, one is left with two independent radial integrations which can be handled as above [36], by splitting the integrations as $\int_0^\infty \mathrm{d}x(\ldots) = \int_0^r \mathrm{d}x(\ldots) + \int_r^\infty \mathrm{d}x(\ldots)$. Denoting $M_{123} = m_1 + m_2 + m_3$, $M_{23456} = m_2 + m_3 + m_4 + m_5 + m_6$, the outcome is

$$2\left(\!\!\begin{array}{c}1\\3\,4\,5\end{array}\!\!\right)6= \left(\frac{2}{M_{123}}\right)^{8\epsilon}\frac{1}{32}\left[\frac{1}{\epsilon^2}+\frac{8}{\epsilon}+4\,\phi\left(\frac{M_{123}}{M_{23456}},\frac{2m_2}{M_{123}},\frac{2m_1}{M_{123}}-1\right)+\mathcal{O}(\epsilon)\right], \quad \text{(A.31)}$$

where

$$\phi(x,y,z) = 13 + \frac{7}{12}\pi^2 - 4\ln^2 x +$$
$$+2\mathrm{Li}_2(1-y)+2\mathrm{Li}_2(y+z)+2\mathrm{Li}_2(-z)+8\frac{1-x}{x(1+z)}\mathrm{Li}_2(1-x)+$$
$$+8\left(1+\frac{1-x}{x(1+z)}\right)\left(\mathrm{Li}_2(-xz)+\ln x\ln(1+xz)-\frac{\pi^2}{6}\right). \quad \text{(A.32)}$$

In particular,

$$\left(\!\!\bigcirc\!\!\!\!\!\! D\right) = \frac{1}{32}\left[\frac{1}{\epsilon^2}+\frac{8}{\epsilon}+4\left(13-8\ln^2 2-\frac{13}{12}\pi^2\right)+\mathcal{O}(\epsilon)\right]\,. \quad \text{(A.33)}$$

A.4 Momentum space evaluations

When the graph has more than two vertices, the configuration space method is in general no longer practical. Some of these graphs are, however, rather easily evaluated in momentum space. This is the case particularly for the "triangle" topology, shown in eq. (A.38) below.

The triangle graph consists of three consecutive 1-loop self-energy insertions,

$$\int \frac{\mathrm{d}^{3-2\epsilon}q}{(2\pi)^{3-2\epsilon}}\frac{1}{[q^2+m_1^2][(q+p)^2+m_2^2]} = \frac{\Gamma(\frac{1}{2}+\epsilon)}{(4\pi)^{\frac{3}{2}-\epsilon}p^{1+2\epsilon}}B(p,m_1,m_2,\epsilon)\,, \quad \text{(A.34)}$$

where $B(p, m_1, m_2, \epsilon)$ is a one-dimensional integral over a Feynman parameter. It has the properties

$$B(0, m_1, m_2, \epsilon) = 0, \tag{A.35}$$

$$B(p, 0, 0, \epsilon) = \lim_{p \to \infty} B(p, m_1, m_2, \epsilon) = \frac{\Gamma^2(\frac{1}{2} - \epsilon)}{\Gamma(1 - 2\epsilon)}, \tag{A.36}$$

$$B(p, m_1, m_2, 0) = 2 \arctan \frac{p}{m_1 + m_2}. \tag{A.37}$$

The triangle graph is then just a one-dimensional integration over the modulus of p. Carrying out one partial integration and expanding in ϵ, one obtains [36]

$$\begin{array}{c}{}^1\!\!\!\!\bigtriangleup^3 \\[-4pt] {}_5\end{array}{}^4 = \left(\frac{2}{m_1 + m_2} \right)^{8\epsilon} \frac{\pi^2}{32} \left[\frac{1}{\epsilon} + 2 + 4 \ln 2 - \chi \left(\frac{m_3 + m_4}{m_1 + m_2}, \frac{m_5 + m_6}{m_1 + m_2} \right) + \mathcal{O}(\epsilon) \right], \tag{A.38}$$

where

$$\chi(x, y) = \frac{64}{\pi^3} \int_0^\infty \mathrm{d}p \ln p \, \frac{\mathrm{d}}{\mathrm{d}p} \left[\arctan(p) \arctan \left(\frac{p}{x} \right) \arctan \left(\frac{p}{y} \right) \right], \tag{A.39}$$

$$\chi(1, 1) = \frac{84}{\pi^2} \zeta(3), \qquad \chi(1, 0) = \frac{56}{\pi^2} \zeta(3), \qquad \chi(0, 0) = 0. \tag{A.40}$$

A.5 Summary of expansions for master integrals

Given the results of the previous sections, we can collect together the expressions for the constants $\gamma_1, \ldots, \gamma_9$ defined in eqs. (4.3)–(4.11). From eq. (A.15),

$$\gamma_1 = -8 - \frac{\pi^2}{2} + \frac{7}{3} \zeta(3). \tag{A.41}$$

Combining eq. (3.1) with eq. (A.9),

$$\gamma_2 = \frac{1}{6} \pi^2 - \frac{5}{2} \zeta(3). \tag{A.42}$$

Combining eq. (3.2) with eq. (A.27),

$$\gamma_3 = -\frac{1}{6} \pi^2 - \ln^2 2. \tag{A.43}$$

From eqs. (A.38), (A.40) (or, for γ_6, from eq. (A.11)),

$$\gamma_4 = \frac{\pi^2}{32} \left(2 + 4 \ln 2 - \frac{84}{\pi^2} \zeta(3) \right), \tag{A.44}$$

$$\gamma_5 = \frac{\pi^2}{32} \left(2 + 4 \ln 2 - \frac{56}{\pi^2} \zeta(3) \right), \tag{A.45}$$

$$\gamma_6 = \frac{\pi^2}{32} \left(2 + 4 \ln 2 \right), \tag{A.46}$$

$$\gamma_7 = \frac{\pi^2}{32} \left(2 + 12 \ln 2 - \frac{84}{\pi^2} \zeta(3) \right). \tag{A.47}$$

Combining eqs. (A.33), (A.4),

$$\gamma_8 = 175 - 96 \ln 2 + 16 \ln^2 2 + \frac{53}{12} \pi^2. \tag{A.48}$$

Finally, from eq. (A.13),

$$\gamma_9 = 270 + \frac{33}{2} \pi^2 - \frac{55}{2} \zeta(3). \tag{A.49}$$

A.6 Numerical evaluation of γ_{10}

It can easily be verified that the integrals in eqs. (4.12), (4.13) are both infrared and ultraviolet finite. They can therefore be evaluated directly in $d = 3$ dimensions. For the present application we only need γ_{10}, defined by eq. (4.12).

There is no obvious partial integration relation whereby γ_{10} could be reduced to a simpler integral. Due to the fact that there are four vertices, it is also not easily treated in configuration space. The most straightforward approach seems then to be to combine the self-energy of eqs. (A.34), (A.37) with the 2-loop self-energy

$$\qquad\qquad(A.50)$$

for which a one-dimensional integral representation has been given in [38]. This leads to a simple two-dimensional integral representation:

$$\gamma_{10} = \frac{2}{\pi} \int_0^\infty \mathrm{d}p \, p \, \arctan \frac{p}{2} \cdot \Pi_2(p) \,, \qquad (A.51)$$

where [38]

$$\Pi_2(p) = \frac{1}{p^3} \int_{x_-(p)}^1 \frac{\mathrm{d}x}{\sqrt{p^2 x^2 - (1 - x^2)^2}} \times$$
$$\times \left\{ \frac{p}{1-x^2} \left[(1+x^2) \arctan \frac{p}{2} - 2(1-x+x^2) \arctan \frac{p}{1+x} + \frac{\pi}{2}(1-x)^2 \right] + \right.$$
$$\left. + x \ln \left[1 + \frac{p^2}{(1+x)^2} \right] \right\} \,, \qquad (A.52)$$

and $x_-(p) \equiv (1 + p^2/4)^{\frac{1}{2}} - p/2$. We may note that in eq. (A.52) it is numerically advantageous to change the integration variable from x to $y \equiv \sqrt{x - x_-(p)}$. The final result reads

$$\gamma_{10} \approx 0.171007009753(1) \,, \qquad (A.53)$$

where the number in parentheses indicates the uncertainty in the last digit.

B. Three-loop results with and without an IR cutoff

As discussed in section 7, starting at the 3-loop level single graphs are considerably more infrared sensitive than the total sum: the limits in eqs. (7.2), (7.3) commute only for the latter. Let us recall that there $x = m_{\mathrm{G}}/m$, where m_{G} is a fictitious mass given to the gluons and ghosts:

$$\langle A_k^a(p) A_l^b(-p) \rangle \equiv \frac{\delta^{ab}}{p^2 + m_{\mathrm{G}}^2} \left(\delta_{kl} - p_k p_l \frac{\xi}{p^2 + m_{\mathrm{G}}^2} \right), \qquad \langle c^a(p) \bar{c}^b(p) \rangle \equiv \frac{\delta^{ab}}{p^2 + m_{\mathrm{G}}^2} \,, \quad (B.1)$$

where $A_k^a, c^a, \bar{c}^b$ are the gluon, ghost, and anti-ghost fields, respectively. We illustrate the general structures appearing here with a few specific examples.
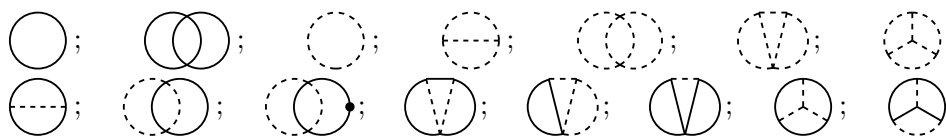
Figure 5: A possible choice for 1-loop, 2-loop and 3-loop "master" topologies, in the case that gluons and ghosts are treated as particles with a mass $m_{\rm G}$. There are no numerators left in these graphs. A solid line is a propagator of the form $1/(p^2 + m^2)$, and a dashed line of the form $1/(p^2 + m_{\rm G}^2)$, where p is the euclidean momentum flowing through the line. A line with a blob on it indicates a squared propagator, $1/(p^2 + m^2)^2$.

In the presence of the two mass scales $m, m_{\rm G}$, the set of master integrals is more complicated than when gluons and ghosts are massless. The master integrals that can appear in principle are shown in figure 5, up to 3-loop level.

It turns out that the skeleton diagrams are better behaved in the IR than the ring diagrams: power and logarithmic IR divergences appear only in single rings, but they cancel in their sum. A rather typical example, with both an UV pole $1/\epsilon$ and an IR divergence $\ln(m_{\rm G}/m)$, is given by the gluon ring with a scalar and ghost bubble attached to it. Carrying out scalarisation to the master integrals shown in figure 5, denoting $x = m_{\rm G}/m$, and normalising as in eq. (3.7), we obtain

$$
\begin{aligned}
-\frac{1}{4} \left. \text{\Large⬭} \right|_{x\neq 0} =\ & \frac{1}{m^2} \left(\bigcirc\right)^2 \times \left(\bigcirc\right) \left[-\frac{(d-2)}{8(d-1)x^2}\right] + \\
& + \frac{1}{m^2} \left(\bigcirc\right) \times \left(\bigcirc\right)^2 \left[\frac{(d-2)}{432(d-1)x^2}\right] \times \\
& \times \left(54 + 54d + 18\xi - 18d^2\xi - 14\xi^2 + 14d\xi^2 - d^2\xi^2 + d^3\xi^2\right) + \\
& + \left(\bigcirc\right) \times \left(\bigcirc\right) \left[\frac{(20 - 8d - 6x^2 + 3dx^2)}{16(d-1)x^2}\right] + \\
& + \left(\bigcirc\right) \times \left(\bigcirc\right) \left[\frac{1}{1296(d-1)}\right] \times \\
& \times \left(1134 - 459d + 54d^2 + 108\xi - 90d\xi - 18d^3\xi - 84\xi^2 + \right. \\
& \left. + 76d\xi^2 + 5d^2\xi^2 + 2d^3\xi^2 + d^4\xi^2\right) + \\
& + \left(\bigcirc\right) \left[-\frac{(32 - 12d - 6x^2 + 3dx^2)}{32(d-1)x^2}\right] + \\
& + m^2 \left(\bigcirc\right) \left[-\frac{(-1 + x^2)}{2(d-1)x^2}\right] + \\
& + m^2 \left(\bigcirc\right) \left[-\frac{(44 - 8d - 14x^2 + 5dx^2)}{32(d-1)}\right] .
\end{aligned}
\tag{B.2}
$$

According to eq. (7.3), the first step is now to expand in $\epsilon \ll 1$. The integrals emerging

are all known [6, 38]. Changing the normalisation to be according to eq. (4.17), we obtain

$$
\begin{aligned}
\delta\tilde{p}_3|_{x\neq0} = {}& -\frac{1}{32\epsilon}(\xi-1)^2 + \frac{20+x^2}{128x}\left[-\mathrm{Li}_2\left(\frac{3x}{2(1+x)}\right) - \mathrm{Li}_2\left(-\frac{x}{2+x}\right) - \right.\\
& \left. - \ln\left(1-\frac{x}{2}\right)\ln\frac{3x}{2(1+x)} - \frac{1}{2}\ln^2(1+x) + \frac{1}{2}\ln\left(1+\frac{x}{2}\right)\ln\frac{9x^2}{2(2+x)}\right] - \\
& - \frac{4-3x^2}{32x}\ln\left(1+\frac{x}{2}\right) - \frac{(1+x)(3x-4)}{32x}\ln(1+x) + \frac{3x}{32} + \\
& + \frac{1}{32}(2\xi-3)(2\xi-1)\ln\frac{3x}{2} - \frac{837-954\xi+409\xi^2}{2592} + \mathcal{O}(\epsilon).
\end{aligned}
\tag{B.3}
$$

The second step is then to expand in $x \ll 1$:

$$
\delta\tilde{p}_3|_{\text{eq. (7.3)}} = -\frac{1}{32\epsilon}(\xi-1)^2 + \frac{2-2\xi+\xi^2}{8}\ln\frac{3x}{2} - \frac{1080-954\xi+409\xi^2}{2592} + \mathcal{O}(x,\epsilon). \tag{B.4}
$$

We observe that there is a gauge-parameter dependent UV-divergence in the form of $1/\epsilon$, and a gauge-parameter dependent logarithmic IR divergence in the form of $\ln x$.

Proceeding according to eq. (7.2), on the other hand, leads to

$$
-\frac{1}{4}\,\Bigg\langle\!\!\Bigg\langle\Bigg|_{x=0} = \frac{1}{m^2}\left(\bigcirc\right)^3\left[-\frac{(d-2)^2}{16(d-3)(2d-7)(3d-8)}\right] + \\
+ m^2\,\bigcirc\left[\frac{(d-3)}{4(2d-7)(3d-8)}\right], \tag{B.5}
$$

in terms of the master integrals in figure 4. Expanding in $\epsilon \ll 1$,

$$
\delta\tilde{p}_3|_{\text{eq. (7.2)}} = \frac{1}{32\epsilon} + \frac{1}{8} + \mathcal{O}(\epsilon). \tag{B.6}
$$

Clearly eqs. (B.4), (B.6) do not agree.[2] Summing all the graphs together, however, both procedures lead to the gauge-parameter independent and UV and IR finite $\tilde{p}_3$ on the first row in eq. (4.17): in other words, ξ, $1/\epsilon$ and $\ln x$ all cancel.

Some other rings lead also to $1/x$-divergences. Let us show, as an example,

$$
\frac{1}{16}\,\Bigg\langle\!\!\Bigg|_{x\neq0} \Rightarrow \delta\tilde{p}_3|_{\text{eq. (7.3)}} = \frac{1}{x}\frac{24-12\xi+5\xi^2}{64} - \frac{5}{24} + \frac{1}{3}\ln 2 + \mathcal{O}(x,\epsilon), \tag{B.7}
$$

while

$$
\frac{1}{16}\,\Bigg\langle\!\!\Bigg|_{x=0} \Rightarrow \delta\tilde{p}_3|_{\text{eq. (7.2)}} = -\frac{5}{24} + \frac{1}{3}\ln 2 + \mathcal{O}(\epsilon). \tag{B.8}
$$

Again, the $1/x$-divergences of the type in eq. (B.7) cancel when gluon rings with all possible 1-loop scalar insertions are summed together.

As a comparison of eqs. (B.4) and (B.6), or eqs. (B.7) and (B.8) shows, the computation carried out with an IR cutoff leads in general to a more pronounced gauge-parameter

---

[2]The first two terms in eq. (B.4) can be written as $(2-2\xi+\xi^2)[\ln(3x/2)-1/(4\epsilon)]/8 + 1/(32\epsilon)$, showing that the result of eq. (B.6) arises after a cancellation of IR and UV divergences in dimensional regularisation.

dependence for single graphs than the computation carried out according to eq. (7.2), just because the introduction of a mass according to eq. (B.1) breaks gauge invariance. The results of eqs. (B.6), (B.8) are anomalously simple, however: in general there is certainly gauge-parameter dependence left over in single graphs also with the procedure of eq. (7.2). For example,

$$\frac{1}{8}\left.\bigcirc\!\!\!\!\!\!\bigcirc\right|_{x=0} \Rightarrow \left.\delta\tilde{p}_3\right|_{\text{eq. (7.2)}} = \frac{1}{32\epsilon}(13 - 4\xi + \xi^2) + \frac{40 - 28\xi + 5\xi^2}{32} + \mathcal{O}(\epsilon), \quad \text{(B.9)}$$

and ξ cancels only in the sum.

References

[1] S. Bronoff, R. Buffa and C.P. Korthals Altes, *Phase diagram of 3d* SU(3) *gauge-adjoint Higgs system*, `hep-ph/9809452`;
S. Bronoff and C.P. Korthals Altes, *Phase diagram of 3d* SU(3) *gauge-adjoint Higgs system and C-violation in hot QCD*, *Phys. Lett.* **B 448** (1999) 85 [`hep-ph/9811243`].

[2] A. Rajantie, SU(5) + *adjoint Higgs model at finite temperature*, *Nucl. Phys.* **B 501** (1997) 521 [`hep-ph/9702255`];
K. Kajantie, M. Laine, A. Rajantie, K. Rummukainen and M. Tsypin, *The phase diagram of three-dimensional* SU(3) + *adjoint Higgs theory*, *J. High Energy Phys.* **11** (1998) 011 [`hep-lat/9811004`].

[3] E. Braaten and A. Nieto, *Free energy of QCD at high temperature*, *Phys. Rev.* **D 53** (1996) 3421 [`hep-ph/9510408`].

[4] K. Kajantie, M. Laine, K. Rummukainen and Y. Schröder, *How to resum long-distance contributions to the QCD pressure?*, *Phys. Rev. Lett.* **86** (2001) 10 [`hep-ph/0007109`].

[5] P. Arnold and C.-X. Zhai, *The three loop free energy for pure gauge QCD*, *Phys. Rev.* **D 50** (1994) 7603 [`hep-ph/9408276`]; *The three loop free energy for high temperature QED and QCD with fermions*, *Phys. Rev.* **D 51** (1995) 1906 [`hep-ph/9410360`].

[6] C.-X. Zhai and B. Kastening, *The free energy of hot gauge theories with fermions through g^5*, *Phys. Rev.* **D 52** (1995) 7232 [`hep-ph/9507380`].

[7] K. Kajantie, M. Laine, K. Rummukainen and M.E. Shaposhnikov, *3d* SU(N) + *adjoint Higgs theory and finite-temperature QCD*, *Nucl. Phys.* **B 503** (1997) 357 [`hep-ph/9704416`].

[8] A.D. Linde, *Infrared problem in thermodynamics of the Yang-Mills gas*, *Phys. Lett.* **B 96** (1980) 289.

[9] D.J. Gross, R.D. Pisarski and L.G. Yaffe, *QCD and instantons at finite temperature*, *Rev. Mod. Phys.* **53** (1981) 43.

[10] P. Ginsparg, *First order and second order phase transitions in gauge theories at finite temperature*, *Nucl. Phys.* **B 170** (1980) 388;
T. Appelquist and R.D. Pisarski, *High-temperature Yang-Mills theories and three-dimensional Quantum Chromodynamics*, *Phys. Rev.* **D 23** (1981) 2305.

[11] K. Kajantie, M. Laine, K. Rummukainen and Y. Schröder, *The pressure of hot QCD up to g^6 ln(1/g)*, `hep-ph/0211321`.

[12] Y. Schröder, *Logarithmic divergence in the energy density of the three-dimensional Yang-Mills theory*, in preparation.

[13] K. Kajantie, M. Laine, K. Rummukainen and Y. Schröder, *Measuring infrared contributions to the QCD pressure*, Nucl. Phys. **106** *(Proc. Suppl.)* (2002) 525 [`hep-lat/0110122`]; *Four-loop logarithms in 3d gauge + Higgs theory*, `hep-lat/0209072`.

[14] K. Kajantie, M. Laine and Y. Schröder, *A simple way to generate high order vacuum graphs*, Phys. Rev. **D 65** (2002) 045008 [`hep-ph/0109100`].

[15] M. Achhammer, *The QCD partition function at high temperatures*, Ph.D. thesis, University of Regensburg, July 2000, Logos-Verlag, Berlin 2001.

[16] Y. Schröder, *Automatic reduction of four-loop bubbles*, Nucl. Phys. **116** *(Proc. Suppl.)* (2003) 402 [`hep-ph/0211288`].

[17] J.A.M. Vermaseren, *New features of form*, `math-ph/0010025`, `http://www.nikhef.nl/~form/`.

[18] K.G. Chetyrkin and F.V. Tkachov, *Integration by parts: the algorithm to calculate beta functions in 4 loops*, Nucl. Phys. **B 192** (1981) 159;
F.V. Tkachov, *A theorem on analytical calculability of four loop renormalization group functions*, Phys. Lett. **B 100** (1981) 65.

[19] S. Laporta, *High-precision calculation of multi-loop Feynman integrals by difference equations*, Int. J. Mod. Phys. **A 15** (2000) 5087 [`hep-ph/0102033`].

[20] D.J. Broadhurst, *Three loop on-shell charge renormalization without integration: $\Lambda_{\text{QED}}^{\overline{\text{MS}}}$ to four loops*, Z. Physik **C 54** (1992) 599.

[21] K. Farakos, K. Kajantie, K. Rummukainen and M.E. Shaposhnikov, *3d physics and the electroweak phase transition: a framework for lattice Monte Carlo analysis*, Nucl. Phys. **B 442** (1995) 317 [`hep-lat/9412091`].

[22] M. Laine and A. Rajantie, *Lattice-continuum relations for 3d $SU(N)$ + Higgs theories*, Nucl. Phys. **B 513** (1998) 471 [`hep-lat/9705003`].

[23] S.A. Larin and J.A.M. Vermaseren, *The three loop QCD beta function and anomalous dimensions*, Phys. Lett. **B 303** (1993) 334 [`hep-ph/9302208`];
S.A. Larin, F.V. Tkachov and J.A.M. Vermaseren, *The FORM version of Mincer*, preprint NIKHEF-H-91-18.

[24] E. Braaten and A. Nieto, *Effective field theory approach to high temperature thermodynamics*, Phys. Rev. **D 51** (1995) 6990 [`hep-ph/9501375`].

[25] A. Vuorinen, *Quark number susceptibilities of hot QCD up to $g^6 \ln(g)$*, `hep-ph/0212283`.

[26] J.P. Blaizot, E. Iancu and A. Rebhan, *On the apparent convergence of perturbative QCD at high temperature*, `hep-ph/0303045`.

[27] G. Cvetič and R. Kögerler, *Resummations of free energy at high temperature*, Phys. Rev. **D 66** (2002) 105009 [`hep-ph/0207291`].

[28] M. Strickland, *Reorganizing finite temperature field theory*, Int. J. Mod. Phys. **A 16S1C** (2001) 1277;
E. Braaten, *Thermodynamics of hot QCD*, Nucl. Phys. **A 702** (2002) 13;
A. Peshier, *Resummation of the QCD thermodynamic potential*, Nucl. Phys. **A 702** (2002) 128 [`hep-ph/0110342`];

J.O. Andersen, *Hard thermal loops and QCD thermodynamics*, `hep-ph/0210195`;
J.-P. Blaizot, E. Iancu and A. Rebhan, *Thermodynamics of the high-temperature quark gluon plasma*, `hep-ph/0303185`.

[29] K. Farakos, K. Kajantie, K. Rummukainen and M.E. Shaposhnikov, *3d physics and the electroweak phase transition: perturbation theory*, *Nucl. Phys.* **B 425** (1994) 67 [`hep-ph/9404201`].

[30] P.-N. Tan, B. Tekin and Y. Hosotani, *Maxwell-Chern-Simons scalar electrodynamics at two loops*, *Nucl. Phys.* **B 502** (1997) 483 [`hep-th/9703121`].

[31] J.O. Andersen, *3d effective field theory for finite temperature scalar electrodynamics*, *Phys. Rev.* **D 59** (1999) 065015 [`hep-ph/9709418`].

[32] K. Kajantie, M. Karjalainen, M. Laine and J. Peisa, *Three-dimensional* U(1) *gauge + Higgs theory as an effective theory for finite temperature phase transitions*, *Nucl. Phys.* **B 520** (1998) 345 [`hep-lat/9711048`].

[33] B. Kastening, H. Kleinert and B. Van den Bossche, *Three-loop ground-state energy of* $O(N)$-*symmetric Ginzburg-Landau theory above* T_c *in 4-ϵ dimensions with minimal subtraction*, *Phys. Rev.* **B 65** (2002) 174512 [`cond-mat/0109372`].

[34] S. Laporta, *High-precision ϵ-expansions of massive four-loop vacuum bubbles*, *Phys. Lett.* **B 549** (2002) 115 [`hep-ph/0210336`].

[35] A. Devoto and D.W. Duke, *Table of integrals and formulae for Feynman diagram calculations*, *Riv. Nuovo Cim.* **7N6** (1984) 1.

[36] A. Vuorinen, *Four-loop Feynman diagrams in three dimensions*, Master's Thesis, Helsinki University, 2001 (unpublished)
`http://ethesis.helsinki.fi/julkaisut/mat/fysii/pg/vuorinen/fourloop.pdf`.

[37] S. Groote, J.G. Korner and A.A. Pivovarov, *Configuration space based recurrence relations for sunset-type diagrams*, *Eur. Phys. J.* **C 11** (1999) 279 [`hep-ph/9903412`].

[38] A.K. Rajantie, *Feynman diagrams to three loops in three-dimensional field theory*, *Nucl. Phys.* **B 480** (1996) 729 [`hep-ph/9606216`], erratum *ibid.* **513** (1996) 761.

[YS6]

Tackling the infrared problem of thermal QCD

Tackling the infrared problem of thermal QCD

Y. Schröder [a]

[a]Center for Theoretical Physics, MIT, Cambridge, MA 02139, USA

Perturbative calculations of corrections to the behavior of an ideal gas of quarks and gluons, the limit that is formally realized at infinite temperature, are obstructed by severe infrared divergences. The limits to computability that the infrared problem poses can be overcome in the framework of dimensionally reduced effective theories. Here, we give details on the evaluation of the highest perturbative coefficient needed for this setup, in the continuum.

1. INTRODUCTION

The theory of strong interactions, Quantum Chromodynamics (QCD), is guaranteed to be accessible to perturbative methods once one of its parameters, the temperature T, is increased towards asymptotically high values. This general statement relies solely on the well-known property of asymptotic freedom.

In practice, however, calculations of corrections to the behavior of an ideal gas of quarks and gluons, the limit that is formally realized at infinite T, are obstructed by severe infrared (IR) divergences [1]: for every observable, there exists an order of the perturbative expansion to which an infinite number of Feynman diagrams contribute. No method is known how to re-sum these infinite classes of diagrams, a fact that seriously obstructs progress in the field of thermal QCD.

It is known how to evade this obstruction using dimensionally reduced effective theories. The key idea is to map the infrared sector of thermal QCD onto a three-dimensional pure gauge theory [1–4], whose contribution, being a pure number, could be extracted numerically by Monte-Carlo simulations. While the expansion of the QCD pressure in the effective theory framework, up to the order where IR contributions are relevant, is now known analytically [4], realizing the numerical extraction of the yet-unknown number emerging from the IR sector is a challenging open problem, with the main complication that high-order matching between lattice and continuum regularization schemes is necessary [5].

2. SETUP

Let us now switch gears and focus on one of the main building blocks of the procedure, while for a detailed description of the setup as well as notation and further references, we refer to [4]. In particular, we want to compute the (negative) 3d vacuum energy density of a pure SU(N) gauge theory,

$$\lim_{V \to \infty} \frac{1}{V} \ln \int \mathcal{D}A_i \, \exp\left(- \int \mathrm{d}^d x \, \frac{1}{2} \mathrm{Tr} F_{ij}^2 \right) \,, \quad (1)$$

which in a weak-coupling expansion can be written as the sum of all connected vacuum graphs containing gluons and ghosts. Since the theory is confining, the computation involves IR divergent integrals (starting at the 4-loop level here), forbidding a perturbative evaluation of the full vacuum energy. One can however obtain its logarithmic ultraviolet divergence.

Note that in 3d the coupling constant g is dimensionful, hence the full answer must be of the form

$$d_A C_A^3 \frac{g^6}{(4\pi)^4} \left[\alpha_G \left(\frac{1}{\epsilon} + 8 \ln \frac{\bar\mu}{2m_M} \right) + \beta_G + \mathcal{O}(\epsilon) \right] \,,$$

where $m_M \equiv C_A g^2$ is a dynamically generated infrared scale in the confining theory, and $C_A = N$ and $d_A = N^2 - 1$ are the Casimir and the dimension of the adjoint representation, respectively. Because of super-renormalizability, the coefficient α_G can then be computed in 4-loop perturbation theory, even if the constant part β_G cannot.

If we just carry out the 4-loop computation in strict dimensional regularisation, the result van-

ishes, because there are no perturbative mass scales in the problem. This means that UV and IR divergences (erroneously) cancel against each other. Therefore, we have to be more careful in order to determine α_G. To regulate the IR divergences, we introduce by hand a mass scale, m^2, into the gauge field (and ghost) propagators. One has to keep in mind, however, that now only the coefficient α_G multiplying $1/\epsilon$ is physically meaningful, as it contains the desired gauge independent ultraviolet divergence. On the contrary, the constant part depends on the gauge parameter ξ, because the introduction of m^2 breaks gauge invariance, and has nothing to do with β_G.

Note that e.g. diagrams with self-energy insertions can have IR sub-divergences, since IR divergences are known to be present in the 3d 2-loop gluon propagator. To avoid the problem of overlapping IR divergences from the outset, we have hence chosen to employ the mass parameter rigorously, i.e. by rewriting every $1/p^2$ as $1/(p^2+m^2)$.

This leaves us within the class of fully massive integrals. The computation can be divided in three parts. Roughly, those are (1) diagram generation [6], specification of Feynman rules and color algebra, (2) reduction to master integrals [7,8], (3) expansion in $d = 3 - 2\epsilon$ dimensions.

We will refrain from commenting on the first two parts of the computation here, since they are well documented in the references given above. Due to the complexity of the computation, both steps are automatized, allowing for the handling of a large set of diagrams.

3. MASTER INTEGRAL REPRESENTATION

Let us now give a little more detail on part (3) of the computation. At this point, all diagrams are expressed in terms of 19 scalar master integrals, which are enumerated in [8]. The general structure is

$$d_A C_A^3 \frac{g^6}{(4\pi)^4} \sum_{i=1}^{19} \frac{\text{poly}_i(d,\xi)}{\text{poly}_i(d)} \text{Master}_i(d) \,, \qquad (2)$$

where d is still an arbitrary (space-time) dimension. Only now do we need to specify $d = 3 - 2\epsilon$.

While it is trivial to expand the polynomial

prefactor in ϵ, considerable effort has to be put into obtaining the expansion for the master integrals to the depth required. Since we need the ϵ-poles only, it would seem sufficient to compute the divergent parts of all master integrals. It turns out, however, that the prefactor develops poles as well around 3 dimensions, having terms proportional to $1/(d-3)$ multiplying 10 of the master integrals, and even double poles in 4 of those cases.

A crucial simplification can be made by exploiting the freedom of choosing the basis of master integrals to represent the sum of diagrams Eq. (2). Going back to the tabulated relations between integrals that were derived by partial integration and used in part (2), we found two most useful relations:

$$= -\frac{8(d-3)}{5} \text{ } -\frac{(d-3)(3d-8)}{5} \text{ } +\frac{(2d-7)(2d-5)}{25} \text{ } -\frac{(d-2)^2}{10} \left(\text{ } \right)^2 \text{ } , \qquad (3)$$

$$= -\frac{2}{3} \text{ } -\frac{3d-10}{6} \text{ } +\frac{1}{3} \text{ } +\frac{d-3}{9} \text{ } . \qquad (4)$$

Notation: each line represents a massive scalar propagator, a dot on a line means an extra power, vertices have no structure. Trading the two master integrals on the lhs of the above equations for the first ones on the rhs respectively (all others are already included in the basis), the d-dimensional representation Eq. (2) of course still holds, albeit with a 'primed' version of the basis,

$$d_A C_A^3 \frac{g^6}{(4\pi)^4} \sum_{i=1}^{19} \frac{\text{poly}_i'(d,\xi)}{\text{poly}_i'(d)} \text{Master}_i'(d) \,. \qquad (5)$$

In this new basis, none of the prefactors has a double pole in 3d, while only 7 members of the new 'primed' basis are multiplied by a single pole. It is not excluded that there exists a choice of basis for which the prefactors never get singular, but this choice is currently not known to us.

4. EXPANSION

It turns out that (almost) all integrals are known analytically to the order needed for obtaining the poles in the sum of all diagrams. Lower loop cases have been treated in [10], while analytic results for the divergences of all 3d 4-loop master integrals as well as numerical and some analytic results for their constant parts as well as the $\mathcal{O}(\epsilon)$ term of the 2-loop sunset integral can be found in [11]. By an amusing relation specific to 3d, namely the fact that the leading term of the 3d 1-loop scalar 2-point integral is an arctan, whose derivative with respect to a mass looks like a propagator with double mass, it is furthermore possible to relate the leading term of one of the 4-loop master integrals to a 3-loop case [12]:

$$\left.\bigoplus\right|_{\mathrm{const}} = \frac{1}{2}\left.\bigoplus^{2m}\right|_{\mathrm{const}}. \qquad (6)$$

There are however 2 master integrals (out of the 7 which get multiplied by a $1/\epsilon$ from the prefactor) whose constant term we do not yet know analytically. Let us denote their leading parts by x_2 and x_3 (by naive power-counting, it is easy to see that both are UV finite),

$$\bigoplus = x_2 + \mathcal{O}(\epsilon) \quad , \quad \bigoplus = x_3 + \mathcal{O}(\epsilon) \qquad (7)$$

Filling in the known expansions for the master integrals as well as expanding the prefactors, higher poles cancel in the sum of diagrams, and we are left with a single pole only:

$$d_A C_A^3 \frac{g^6}{(4\pi)^4}\left(\frac{\bar{\mu}}{2m}\right)^{8\epsilon}\left(\frac{p(\xi)}{\epsilon} + \mathcal{O}(\epsilon^0)\right). \qquad (8)$$

The polynomial p is of order 6 in the gauge parameter ξ and contains, besides a collection of numbers like π^2, $\ln 2$ and dilogarithms, the two unknowns x_2 and x_3. Clearly, in order for the result to be gauge independent, all ξ-dependence has to vanish once x_2 and x_3 are known. We can now reverse the argument and try to fix these constants by requiring gauge independence. Inspecting the polynomial, it turns out to have a very simple structure:

$$p(\xi) = \alpha_G + (x_2 - 6x_3 - b)\sum_{i=0}^{6} c_i\,\xi^i \qquad (9)$$

$$\alpha_G = \frac{43}{96} - \frac{157}{6144}\,\pi^2 \approx 0.195715\ldots, \qquad (10)$$

where the c_i are pure numbers and $b = \mathrm{Li}_2\frac{1}{4} + \mathrm{Li}_2\frac{1}{5} - 3\mathrm{Li}_2\frac{2}{5} + 2(\ln 2)^2 - \frac{3}{2}(\ln 3)^2 - (\ln 5)^2 - 2\ln 2\ln 5 + 3\ln 3\ln 5 + \frac{\pi^2}{8}$. We have checked by numerical integration that

$$x_2 - 6x_3 = b \approx -0.00200966335\ldots \qquad (11)$$

to nine significant digits, hence establishing Eq. (10) as our main result for the logarithmic divergence of 3d pure gauge theory.

REFERENCES

1. A.D. Linde, Phys. Lett. B **96** (1980) 289; D.J. Gross, R.D. Pisarski and L.G. Yaffe, Rev. Mod. Phys. 53 (1981) 43.
2. P. Ginsparg, Nucl. Phys. B 170 (1980) 388; T. Appelquist and R.D. Pisarski, Phys. Rev. D 23 (1981) 2305.
3. E. Braaten and A. Nieto, Phys. Rev. Lett. 76 (1996) 1417.
4. K. Kajantie, M. Laine, K. Rummukainen and Y. Schröder, Phys. Rev. D **67** (2003) 105008.
5. F. DiRenzo et. al., these proceedings.
6. K. Kajantie, M. Laine and Y. Schröder, Phys. Rev. D 65 (2002) 045008.
7. S. Laporta, Int. J. Mod. Phys. A 15 (2000) 5087.
8. Y. Schröder, Nucl. Phys. Proc. Suppl. **116** (2003) 402.
9. J.A.M. Vermaseren, math-ph/0010025.
10. A.K. Rajantie, Nucl. Phys. B 480 (1996) 729; *ibid.* B 513 (1996) 761 (E); D. J. Broadhurst, Eur. Phys. J. C **8** (1999) 363.
11. K. Kajantie, M. Laine, K. Rummukainen and Y. Schröder, JHEP **0304** (2003) 036; A. Vuorinen, Master's Thesis, Helsinki University, 2001.
12. M. Laine, private notes.

[YS7]

High-precision evaluation of four-loop vacuum bubbles in three dimensions

High-precision evaluation of four-loop vacuum bubbles
in three dimensions

Y. Schröder[a], A. Vuorinen[b]

[a] *Center for Theoretical Physics, MIT, Cambridge, MA 02139, USA*
[b] *Department of Physical Sciences and Helsinki Institute of Physics*
P.O Box 64, FIN-00014 University of Helsinki, Finland

Abstract

In this letter we present a high-precision evaluation of the expansions in $\epsilon = (3-d)/2$ of (up to) four-loop scalar vacuum master integrals, using the method of difference equations developed by Laporta. We cover the complete set of fully massive master integrals.

PACS numbers: 11.10.Kk, 12.20.Ds, 12.38.Bx

1   Introduction

Higher-order perturbative computations have become a necessity in many areas of theoretical physics, be it for high-precision tests of QED, QCD and the standard model, or for studying critical phenomena in condensed matter systems.

Most recent investigations employ a highly automated approach, utilizing algorithms that can be implemented on computer algebra systems, in order to handle the growing numbers of diagrams as well as integrals which occur at higher loop orders.

Computations can be divided into four key steps. First, the complete set of diagrams including symmetry factors has to be generated. For a detailed description of an algorithm for this step for the case of vacuum topologies, see [1]. Second, after specifying the Feynman rules, the color- and Lorentz-algebra has to be worked out. Third, within dimensional regularization, massive use of the integration-by-parts (IBP) technique [2] to derive linear relations between different Feynman integrals in conjunction with an ordering prescription can be used to reduce the (typically large number of) integrals to a basis of (typically a few) master integrals [3]. Practical notes as well as a classification of vacuum master integrals is given in [4]. Fourth, the master integrals have to be solved, either fully analytically, or in an expansion around the space-time dimension d of interest.

It is the fourth step that we wish to address here. While most work has been and is being devoted to $d = 4$, perturbative results in lower dimensions are needed for applications in condensed matter systems, as well as in the framework of dimensionally reduced effective field theories for thermal QCD, where recent efforts have made four-loop contributions an issue [5].

A very important subset of master integrals are fully massive vacuum (bubble) integrals, since they constitute a main building block in asymptotic expansions (see e.g. [6]). They are also useful for massless

theories, when a propagator mass is introduced as an intermediate infrared regulator [7].

The main purpose of this note is to numerically compute the complete set of fully massive vacuum master integrals in terms of a high-precision ϵ-expansion in $d = 3 - 2\epsilon$ dimensions, in complete analogy with the four-dimensional work of S. Laporta [8].

The plan of the paper is as follows. In Section 2, we give a brief review of the method of difference equations applied to vacuum integrals. In Section 3, we discuss the actual implementation of the algorithm. In Section 4, we display our numerical results for the truncated power series expansions in ϵ of all fully massive master integrals, up to four-loop level, in $d = 3 - 2\epsilon$.

2 The evaluation of master integrals through difference equations

The method we have chosen to compute the coefficients of the truncated power series expansions of the master integrals is based on constructing difference equations for the integrals and then solving them numerically using factorial series. This approach was recently developed in Ref. [3], and below we briefly summarize its basic concepts following the notation of the original paper, which contains a much more detailed presentation on the subject. While the method is completely general as it applies to arbitrary kinematics, masses and topologies [9], our brief summary is somewhat adapted to the specific case of massive vacuum integrals.

The main idea is to attach an arbitrary power x to one of the lines of a master integral U,

$$U(x) \equiv \int \frac{1}{D_1^x D_2 ... D_N}, \tag{1}$$

where the $D_i = (p_i^2 + 1)$ denote inverse scalar propagators. In our case all of these share the same mass m, which we have therefore set to 1, noting that it can be restored in the end as a trivial dimensional prefactor of each integral. The original integral is then just $U = U(1)$. Depending on the symmetry properties of the integral, there can be different choices for the 'special' line with the arbitrary power x, but in the limit $x = 1$ they all reduce to the original integral U. This degeneracy can (and will later) be used for non-trivial checks of the method.

Employing IBP identities in a systematic way, it is possible to derive a linear difference equation obeyed by the generalized master integral $U(x)$,

$$\sum_{j=0}^{R} p_j(x) U(x + j) = F(x), \tag{2}$$

where R is a finite positive integer and the coefficients p_j are polynomials in x (and the space-time dimension d). The function F on the r.h.s. is a linear combination of functions analogous to $U(x)$ but derived from simpler master integrals, i.e. integrals containing a smaller number of loops and/or propagators.

The general solution of this kind of an equation is the sum of a special solution of the full equation, $U_0(x)$, and all solutions of the homogeneous equation ($F = 0$),

$$U(x) = U_0(x) + \sum_{j=1}^{R} U_j(x), \tag{3}$$

where each ($j = 0, ..., R$)

$$U_j(x) = \mu_j^x \sum_{s=0}^{\infty} a_j(s) \frac{\Gamma(x+1)}{\Gamma(x+1+s-K_j)} \tag{4}$$

is a factorial series[1]. Substituting into Eq. (2), one obtains the coefficients μ and K (the latter being a function of d), as well as recursion relations for the x-independent coefficients $a(s)$ (being functions of d as

---

[1]For a rigorous definition of the concept as well as a motivation for this kind of an ansatz, we refer the reader to Ref. [3].

well) for each solution. For the homogeneous solutions, these recursion relations relate all coefficients to their value at $s = 0$, $a_j(s) = c_j(s) \, a_j(0)$, where the $c_j(s)$ are rational functions (of d as well). For the special solution, the $a_0(s)$ are completely fixed in terms of the inhomogeneous part $F(x)$, consisting of 'simpler' integrals which are assumed to already be known in terms of their factorial series expansions.

What remains to be done is to fix the x- and s-independent constants $a_j(0)$, $j \neq 0$, in order to determine the weights of the different homogeneous solutions. To this end, it is most useful to study the behavior of $U(x)$ at large x, where the first factor in

$$U(x) \;\; = \;\; \int \frac{1}{(p_1^2 + 1)^x} \; g(p_1) \tag{5}$$

peaks strongly around $p_1^2 = 0$. Hence, the large-x behavior of the modified master integral is determined by the small-momentum expansion of the two-point function $g(p_1)$, which has one loop less than the original vacuum integral. In fact, for all cases we cover here, the first coefficient in the asymptotic expansion suffices. This is furthermore particularly simple, since it factorizes into a one-loop bubble carrying the large power x and a lower-loop vacuum bubble $g(0)$, which corresponds to $U(x)$ with its 'special' line cut away,

$$\lim_{x \to \infty} U(x) \;\; = \;\; \left[\int \frac{1}{(p_1^2 + 1)^x} \right] \times \left[g(0) \right] \; \sim \; (1)^x x^{-d/2} g(0) \,. \tag{6}$$

A comparison with the large-x behavior of Eqs. (3), (4), proportional to $\sum_j \mu_j^x a_j(0) x^{K_j}$, can now be used to fix the $a_j(0)$, of which maximally one will turn out to be non-zero for our set of integrals.

Having the full solution at hand, we have in principle completed our entire task, as in the limit $x = 1$ we recover from $U(x)$ the value of the initial integral. Let us, however, add a couple of practical remarks here. What is still to be done is to perform the summation of the factorial series of Eq. (4), which means truncating the infinite sum at some $s_{\max}$. Studying the convergence behavior of these sums, one notices that even in the cases where they do converge down to $x \sim 1$, their convergence properties usually strongly decline with decreasing x. This means that in practical computations, where one aims at obtaining a maximal number of correct digits for $U(1)$ with as little CPU time as possible, the optimal strategy is to evaluate the integral $U(x)$ with the factorial series approach at some $x_{\max} \gg 1$ and then use the recurrence relation of Eq. (2) to obtain the desired result at $x = 1$. The price to pay is, however, a loss of numerical accuracy at each 'pushdown' ($x \to x - 1$) step due to possible cancellations, which makes the use of a very high $x_{\max}$ impossible. In practice the strategy is to determine an optimal value for the ratio $s_{\max}/x_{\max}$. To give an example, for the four-loop integrals of Section 4 we have found that $s_{\max}/x_{\max} \sim 50$ is a good value, while we used a range of $s_{\max} \sim 1350 \ldots 2000$.

3 Implementation of the algorithm

As is apparent from the preceding section, there are three main steps involved in obtaining the desired numerical coefficients in the ϵ-expansion of each master integral: deriving the difference equations obeyed by each integral, solving them in terms of factorial series, and finally performing the ϵ-expansion and numerically evaluating the sum of Eq. (4) (truncated at $s_{\max}$) to the precision needed. We will briefly address each of them in the following.

For the first step, we slightly generalized the IBP algorithm we had used for reducing generic 4-loop bubble integrals to master integrals, which follows the setup given in [3], and whose implementation in FORM [10] is documented in [4]. The main difference is an enlarged representation for the integrals, keeping track of the line which carries the extra powers x, as well as the fact that there are now two independent variables (d, x), requiring factorization (and inversion) of bivariate polynomials, as opposed to univariate polynomials in the original version.

Second, staying within FORM for convenience, we implemented routines that straightforwardly solve the difference equations in terms of factorial series, along the lines of [3]. This is done starting with the

3

simplest one-loop master integral, and working the way up to the most complicated (most lines) four-loop integral, ensuring that at each step, the 'simpler' terms constituting the inhomogeneous parts of the difference equation are already known. The output are then plain ascii files specifying each solution in the form of Eq. (4) as well as containing recursion relations for the coefficients $a(s)$. Note that these first two steps are performed exactly, in d dimensions.

Third, once the recursion relations for the coefficients $a(s)$ were known, we used a Mathematica program to obtain their numerical values at each s to a predefined precision, and to perform the summation of the factorial series. While this procedure is in principle very straightforward, there are some twists that we employed to help reduce the running times significantly, most of which are probably quite specific to our use of Mathematica. To avoid a rapid loss of significant digits in solving the recursion steps that relate each $a(s)$ to $a(0)$, especially those for the homogeneous coefficients, we first solved the relations analytically and only in the end substituted the numerical value (actually the truncated ϵ-expansion) of the first non-zero coefficient. In fact, we found Mathematica to operate quite efficiently with operations like multiplication of two truncated power series, so that we relied heavily on it. Furthermore, since — not surprisingly — the most time-consuming part in the summation of the series turned out to be the ϵ-expansion of Γ-functions, we achieved a notable speed-up by substituting the Γ-functions with large arguments by suitable products of linear factors times Γ-functions of smaller arguments. Finally, a vital step in avoiding an excessive loss in the depth of the ϵ-expansions when going from one integral to the next, was to apply the 'Chop' command to remove from the results and coefficients excess unphysical poles, whose coefficients were of the order of, say, 10^{-50} or less.

4   Numerical results

Below we list the Laurent expansions in $\epsilon = (3 - d)/2$ of the 1+1+3+13 fully massive vacuum master integrals up to four loops. We use an intuitive graphical notation, in which each line represents a massive scalar propagator, while dot on a line means it carries an extra power. The integral measure we have chosen here is

$$\int_p \;\equiv\; \frac{1}{\Gamma(3/2 + \epsilon)} \int \frac{\mathrm{d}^{3-2\epsilon}p}{\pi^{3/2-\epsilon}}\,. \tag{7}$$

In each case[2] we provide the first 8 ϵ-orders keeping the accuracy at 50 significant digits for the 1-, 2-, and 3-loop master integrals and at 22-25 for the 4-loop ones. To obtain more ϵ-orders and significant digits is merely a matter of additional CPU time.

$$
\begin{aligned}
= \; & -\,4.00000000000000000000000000000000000000000000000000 \\
& -\,16.0000000000000000000000000000000000000000000000000 \,\epsilon^2 \\
& -\,64.0000000000000000000000000000000000000000000000000 \,\epsilon^4 \\
& -\,256.000000000000000000000000000000000000000000000000 \,\epsilon^6 + \mathcal{O}\left(\epsilon^8\right) \tag{8}
\end{aligned}
$$

$$
\begin{aligned}
= \; & +\,4.00000000000000000000000000000000000000000000000000 \,\epsilon^{-1} \\
& -\,14.8744172973063011164820984742958618515184677540 0 \\
& +\,41.495035953369978394225958244504121655360756728405 \,\epsilon \\
& -\,107.49752321579967383991953818365893067117808339742 \,\epsilon^2
\end{aligned}
$$

$$+\,263.49878761720606330238135348797499506915058750280\,\epsilon^3$$
$$-\,623.49940078392000186832902635721463645559035022216\,\epsilon^4$$
$$+\,1439.49970268698795739684495246995578749622978882621\,\epsilon^5$$
$$-\,3263.49985208606447262255429193999438959434910311166\,\epsilon^6 + \mathcal{O}\left(\epsilon^7\right) \qquad (9)$$

$$\text{(diagram)} \;=\; -\,64.00000000000000000000000000000000000000000000000\,\epsilon^{-1}$$
$$+\,49.44567822334599921081142309329320142732803439623$$
$$-\,1981.20773622951353403009368321442227834841666 1525\,\epsilon$$
$$-\,235.70771709267187520954743749080980061362043562 28\,\epsilon^2$$
$$-\,63521.71508871044639640714223746384514019533126715\,\epsilon^3$$
$$-\,33675.11111780076696716334804652776927940758434016\,\epsilon^4$$
$$-\,2213147.07127551125111364024784487794833409141970 0\,\epsilon^5$$
$$-\,1414250.72871759347405327238754119665201377398423 6\,\epsilon^6 + \mathcal{O}\left(\epsilon^7\right) \qquad (10)$$

$$\text{(diagram)} \;=\; +\,32.85977004392350373882717273153253694744854744899 6$$
$$-\,365.41238154175547388711920818936800707879030719734\,\epsilon$$
$$+\,2803.79404025231670471502938584399854720959661182 07\,\epsilon^2$$
$$-\,18727.18739210814430160727984405852741837883694398 8\,\epsilon^3$$
$$+\,117794.3587313330613973487896062630796215004348049 8\,\epsilon^4$$
$$-\,721386.6330030556992091543818595111261178054310704 4\,\epsilon^5$$
$$+\,4366100.1639736899128559563097848872427318803864 139\,\epsilon^6$$
$$+\,26291285.7084548338323062427664398116619775834408 14\,\epsilon^7 + \mathcal{O}\left(\epsilon^8\right) \qquad (11)$$

$$\text{(diagram)} \;=\; +\,1.39120488529602194181204813692532774091046670639 0$$
$$-\,4.89815245525180066603264116860819094244694433375 8\,\epsilon$$
$$+\,12.98842503803858164353982398007130232261458098462\,\epsilon^2$$
$$-\,30.39637625288207454078370310227949470365033235457\,\epsilon^3$$
$$+\,66.67957617359017942652215661267829752624475575093\,\epsilon^4$$
$$-\,140.99749457088454138122148243154603147486056900 42\,\epsilon^5$$
$$+\,291.72876322681791384421997423986141477339266246 89\,\epsilon^6$$
$$-\,595.70062754494022666956752823759322295091027997 33\,\epsilon^7 + \mathcal{O}\left(\epsilon^8\right) \qquad (12)$$

$$\text{(diagram)} \;=\; +\,720.000000000000000000000\,\epsilon^{-1} - 52.13034199729620858728708$$
$$+\,33748.69042965137616701638\,\epsilon + 10819.60558535024688749473\,\epsilon^2$$
$$+\,1311729.690542895866693548\,\epsilon^3 + 615270.7589383441011319577\,\epsilon^4$$
$$+\,48899219.67276170476701364\,\epsilon^5 + 24885879.11003549349511900\,\epsilon^6 + \mathcal{O}\left(\epsilon^7\right) \quad (13)$$

$$\text{(diagram)} \;=\; -\,32.000000000000000000000\,\epsilon^{-1} + 21.28521367989184834349148$$
$$-\,945.47646178622579501025 33\,\epsilon - 500.9879407913869195081538\,\epsilon^2$$
$$-\,29027.99548541518650323471\,\epsilon^3 - 34796.65982174097113175672\,\epsilon^4$$

$$- 993306.5068744076465770453 \, \epsilon^5 - 1406349.173668893367086333 \, \epsilon^6 + \mathcal{O}\left(\epsilon^7\right) \quad (14)$$

$$\bigcirc\!\!\!\!\!\vee \;\; = \;\; + 8.000000000000000000000000 \, \epsilon^{-2} - 25.9497669189225204659284 \, \epsilon^{-1}$$
$$- 152.5193565764658289654545 + 2653.873458838396323815566 \, \epsilon$$
$$- 23471.0591030962644740639 \, \epsilon^2 + 169839.2007120049515774452 \, \epsilon^3$$
$$- 1124117.877397355450165203 \, \epsilon^4 + 7116455.837989754857686241 \, \epsilon^5 + \mathcal{O}\left(\epsilon^6\right) \quad (15)$$

$$\bigtriangleup \;\; = \;\; + 78.95683520871486895067593 \, \epsilon^{-1} - 1062.608419332108844057560$$
$$+ 9340.076804859596283223881 \, \epsilon - 68699.47293187699594375521 \, \epsilon^2$$
$$+ 462145.6926820632806821051 \, \epsilon^3 - 2963063.672524354359852913 \, \epsilon^4$$
$$+ 18494675.22629230338091457 \, \epsilon^5 - 113673206.9834859509114931 \, \epsilon^6 + \mathcal{O}\left(\epsilon^7\right) \quad (16)$$

$$\bigcirc\!\!\!\!\diamond \;\; = \;\; + 33.05150971425671642138224 - 358.4595946559340238066389 \, \epsilon$$
$$+ 2451.469078369636793421997 \, \epsilon^2 - 13564.14170819716549262162 \, \epsilon^3$$
$$+ 66602.55178881628657891800 \, \epsilon^4 - 303915.1384697444382333780 \, \epsilon^5$$
$$+ 1323370.670112542076081095 \, \epsilon^6 - 5589978.086026239748023404 \, \epsilon^7 + \mathcal{O}\left(\epsilon^8\right) \quad (17)$$

$$\bigcirc\!\!\!\!\mathbb{N} \;\; = \;\; + 27.57584879577521927818358 - 291.4075344540614879796315 \, \epsilon$$
$$+ 1956.162997112043390446958 \, \epsilon^2 - 10678.5639091187201818981 \, \epsilon^3$$
$$+ 51925.38887990077059709 28 \, \epsilon^4 - 235296.36309585614167636 \, \epsilon^5$$
$$+ 1019555.9650538012793966 \, \epsilon^6 - 4292011.3101269758990557 \, \epsilon^7 + \mathcal{O}\left(\epsilon^8\right) \quad (18)$$

$$\bigoplus \;\; = \;\; + 19.84953756526739935782082 - 200.9768306606422068619864 \, \epsilon$$
$$+ 1308.883448000100198800887 \, \epsilon^2 - 6990.225621000635371 85149 \, \epsilon^3$$
$$+ 33456.83269024832144 17013 \, \epsilon^4 - 149903.6970327312215100 18 \, \epsilon^5$$
$$+ 644404.61801211590204150 \, \epsilon^6 - 2697912.0878890801856234 \, \epsilon^7 + \mathcal{O}\left(\epsilon^8\right) \quad (19)$$

$$\bigoplus\!\!{}^{\bullet} \;\; = \;\; + 3.141336279450209755917806 - 19.78740273338730374386071 \, \epsilon$$
$$+ 83.81604328128850410126511 \, \epsilon^2 - 295.3496021971085625102731 \, \epsilon^3$$
$$+ 934.2247995435558122394582 \, \epsilon^4 - 2751.318523476274628869 09 \, \epsilon^5$$
$$+ 7700.18972963585089750348 \, \epsilon^6 - 20740.97694743651451 16212 \, \epsilon^7 + \mathcal{O}\left(\epsilon^8\right) \quad (20)$$

$$\bigvee\!\!\!\!\bigcirc \;\; = \;\; + 2.012584635078182771827701 - 10.76814227797251921324485 \, \epsilon$$
$$+ 39.40636857271936487899035 \, \epsilon^2 - 121.0015646826735646109733 \, \epsilon^3$$
$$+ 335.6942965583773421544251 \, \epsilon^4 - 872.0097737555522247813 19 \, \epsilon^5$$
$$+ 2163.887072219868 80315576 \, \epsilon^6 - 5193.512491885938504830 93 \, \epsilon^7 + \mathcal{O}\left(\epsilon^8\right) \quad (21)$$

$$\bigoplus \;\; = \;\; + 1.272270541849894199397 88 - 5.679912939948535790366 83 \, \epsilon$$
$$+ 17.67972389481737323437 88 \, \epsilon^2 - 46.57218466495432618640 19 \, \epsilon^3$$
$$+ 111.6585221762143853635 68 \, \epsilon^4 - 252.46396390100217743236 \, \epsilon^5$$

$$+ 549.30166596161426941705\,\epsilon^6 - 1164.5120588971521623546\,\epsilon^7 + \mathcal{O}\left(\epsilon^8\right) \qquad (22)$$

 $= +0.29779072668375265186 5168 - 0.70989638569914343012 6726\,\epsilon$
$$+ 1.4053554947268313237 0135\,\epsilon^2 - 2.4572190850925667344 0117\,\epsilon^3$$
$$+ 4.0099803600576445970 7090\,\epsilon^4 - 6.2518071963546459390 185\,\epsilon^5$$
$$+ 9.4402506572040685160 665\,\epsilon^6 - 13.924465979877416801887\,\epsilon^7 + \mathcal{O}\left(\epsilon^8\right) \qquad (23)$$

 $= +0.23392393258030320647 0057 - 0.48523164074102176840 584\,\epsilon$
$$+ 0.8855574440150372957 7888\,\epsilon^2 - 1.4380198713684102418 10\,\epsilon^3$$
$$+ 2.1987253504407907556 08\,\epsilon^4 - 3.2319747943817196797 29\,\epsilon^5 + \mathcal{O}\left(\epsilon^6\right) \qquad (24)$$

 $= +0.19590640134123879990 5792 - 0.37006152907989745845 214\,\epsilon$
$$+ 0.6522827381814630213 0509\,\epsilon^2 - 1.0292881525141438711 18\,\epsilon^3$$
$$+ 1.5424845094385067108 08\,\epsilon^4 + \mathcal{O}\left(\epsilon^5\right) \qquad (25)$$

We have performed various checks in order to test the correctness of our recursion relations as well as to verify the number of exact digits contained in our results Eqs. (8)-(25). The first task we have completed by exploiting the fact that the recursion relations are not specific to $d = 3 - 2\epsilon$, but can easily be applied to any dimension, such as $d = 4 - 2\epsilon$. We have successfully verified the results of Ref. [8] to somewhat lower accuracy and depth in ϵ. Note that our choice of a basis for 4-loop master integrals differs slightly from the one made in [8]. The relations needed for a basis transformation are listed in [4]. An immediate advantage in the light of difference equations is that with our choice, the above results Eqs. (14),(20) and (23) follow 'for free' from their counterparts without dots.

The accuracy of our three-dimensional results we have on the other hand examined in three independent ways:

- by comparing the numerical results to existing analytic calculations; they can be found in [11] (divergent and constant parts of Eqs. (9)-(11)), [12] (leading term of Eq. (12)), [13] (divergence of Eq. (16)) and [14,15] (all divergences and some constant parts of 4-loop integrals, as well as some $\mathcal{O}(\epsilon)$ terms of lower-loop cases).

- by comparing the results obtained by raising topologically inequivalent lines to the power x,

- by analyzing the convergence properties of the factorial series, i.e. by checking the stability of our results with respect to varying $s_{\max}$.

The first method is of course exact, but is only available for a few low (in ϵ) orders for approximately half of the integrals considered. The second one, on the other hand, has the advantage of covering all the different powers of ϵ, but is inapplicable for those integrals, in which all propagators are equivalent (e.g. the basketball-topology). The third method is then the most widely applicable one, but has the downside of providing no evidence for the correctness of our results, rather giving only the number of digits stable in the variation of the cut-off of the factorial series. For the integral of Eq. (25) only the last method is available, but in addition we have verified the leading term in the result to 3 digits using a Monte Carlo integration of an 8-dimensional integral representation derived for this integral in Ref. [14].

One might be concerned about the rapid growth with increasing ϵ-orders of most of the coefficients. This is, as was pointed out in [8], caused by poles that the integrals (seen as functions of d) develop near $d = 3$, e.g. at $d = 7/2, 4$, etc. It is to be expected that factoring out the first few of these nearby poles in each case will improve the apparent convergence in ϵ considerably.

7

In principle, having a method at hand that is capable of generating coefficients to very high accuracy, even to a couple of hundred digits, one could now use the algorithm PSLQ [16] combined with an educated guess of the number content of some of the yet-unknown constant terms, in order to search for analytic representations of the numerical results. These could then in turn be used as an inspiration to find useful transformations of the integral representation of the original integral, which might allow for a fully analytic solution in those cases where it could not yet be achieved. We have not made any attempts in that direction, since the numerical accuracy of the results Eqs. (8)-(25) should be sufficient for all practical purposes.

Acknowledgments

References

[1] K. Kajantie, M. Laine and Y. Schröder, Phys. Rev. D **65** (2002) 045008 [hep-ph/0109100].

[2] K. G. Chetyrkin and F. V. Tkachov, Nucl. Phys. B **192** (1981) 159; F. V. Tkachov, Phys. Lett. B **100** (1981) 65.

[3] S. Laporta, Int. J. Mod. Phys. A **15** (2000) 5087 [hep-ph/0102033].

[4] Y. Schröder, Nucl. Phys. Proc. Suppl. **116** (2003) 402 [hep-ph/0211288].

[5] K. Kajantie, M. Laine, K. Rummukainen and Y. Schröder, Phys. Rev. D **67** (2003) 105008 [hep-ph/0211321].

[6] M. Misiak and M. Münz, Phys. Lett. B **344** (1995) 308 [hep-ph/9409454].

[7] Y. Schröder, hep-lat/0309112.

[8] S. Laporta, Phys. Lett. B **549** (2002) 115 [hep-ph/0210336].

[9] S. Laporta, Phys. Lett. B **523** (2001) 95 [hep-ph/0111123].

[10] J. A. M. Vermaseren, math-ph/0010025.

[11] A. K. Rajantie, Nucl. Phys. B **480** (1996) 729 [Erratum-ibid. B **513** (1998) 761] [hep-ph/9606216].

[12] D. J. Broadhurst, hep-th/9806174.

[13] E. Braaten and A. Nieto, Phys. Rev. D **51** (1995) 6990 [hep-ph/9501375].

[14] A. Vuorinen, Master's Thesis, University of Helsinki (2001),
http://ethesis.helsinki.fi/julkaisut/mat/fysii/pg/vuorinen/fourloop.pdf

[15] K. Kajantie, M. Laine, K. Rummukainen and Y. Schröder, JHEP **0304** (2003) 036 [hep-ph/0304048].

[16] H. R. P. Ferguson, D. H. Bailey and S. Arno, Math. Comput. **68** (1999) 351.

[YS8]

3-d lattice Yang-Mills free energy to four loops

3-d lattice Yang-Mills free energy to four loops

Francesco Di Renzo, Andrea Mantovi, Vincenzo Miccio

Dipartimento di Fisica, Università di Parma, and
INFN, Gruppo Collegato di Parma, Parma, Italy
E-mail: `direnzo@fis.unipr.it`, `mantovi@fis.unipr.it`, `miccio@fis.unipr.it`

York Schröder

Center for Theoretical Physics, MIT
Cambridge, MA, U.S.A.
E-mail: `yorks@lns.mit.edu`

ABSTRACT: We compute the expansion of the 3-d Lattice Yang-Mills free energy to four-loop order by means of Numerical Stochastic Perturbation Theory. The first and second order are already known and are correctly reproduced. The third- and fourth-order coefficients are new results. The known logarithmic divergence in the fourth order is correctly identified. We comment on the relevance of our computation in the context of dimensionally reduced finite temperature QCD.

Contents

1. Introduction

The QCD free energy density (or the pressure of the quark-gluon plasma) is a good observable to study the deconfinement phase transition [1]. The goal is to study the transition between the realm of low-temperature hadronic matter, where confinement is the main physical phenomenon, and the quark-gluon plasma phase that is realized at high temperatures, which in turn is governed by asymptotic freedom. In the latter phase the pressure is given by the Stefan-Boltzmann limit of an ideal gas of non-interacting particles, $p \propto T^4$. Ideally, one would like to undertake lattice simulations across the phase transition up to temperatures at which the pressure exhibits a purely perturbative behavior. In practice, however, the convergence properties of the perturbative expansion are poor at temperatures which are not asymptotically large [2], while on the other hand computational resources limit the highest temperatures at which lattice simulations can be performed (a fair limit is some $4 \div 5$ times the transition temperature $T_c \sim 200\,\text{MeV}$).

Dimensional reduction [3] is a strategy to fill the gap one is facing, and in fact has been applied to the problem in question [4]. The setup is as follows. One starts with the full theory ($4d$ QCD) and as a first step matches this to a $3d\,\text{SU}(3)$ gauge theory coupled to a Higgs field in the adjoint representation. This theory can then be matched to $3d$ pure gauge $\text{SU}(3)$, which captures the ultrasoft degrees of freedom. Both these reductions have been successfully performed in a continuum (perturbative) scheme, i.e. $\overline{\text{MS}}$. $3d$ pure gauge $\text{SU}(3)$ then has to be treated non-perturbatively, the only practical method being lattice measurements.

In order to incorporate these lattice measurements into the reduction setup, it is essential to know the relation between the two regularization schemes. This is the point where Lattice Perturbation Theory (LPT) comes into play. Due to the superrenormalizable nature of the $3d$ theory, *all* divergences can be computed perturbatively. This allows a clean matching of the schemes in the continuum. Computing at high orders in LPT is not a simple task (in the present case we need g^8 order — note that this means four loops for the free energy, but three loops for the plaquette), and that is why we make use of Numerical Stochastic Perturbation Theory (NSPT) [5].

We recall the definition of the free energy density f

$$Z = \int DU \, e^{-S_W[U]} = e^{-\frac{V}{T}f}, \tag{1.1}$$

where the (Wilson) pure gauge action reads

$$S_W = \beta_0 \sum_P (1 - \Pi_P), \tag{1.2}$$

with $\beta_0 = 2N_c/(a^{4-d}g_0^2)$ denoting the standard dimensionless (bare) lattice inverse coupling in d dimensions, while Π_P is the basic plaquette

$$\Pi_P = \frac{1}{N_c} \operatorname{Re}(\operatorname{Tr} U_P), \tag{1.3}$$

which is to be computed at any point on any independent plane according to

$$U_P = U_{\mu\nu}(n) = U_\mu(n)U_\nu(n+\mu)U_\mu^\dagger(n+\nu)U_\nu^\dagger(n). \tag{1.4}$$

To compute the free energy one can now revert to the computation of the plaquette

$$\langle 1 - \Pi_P \rangle = Z^{-1} \int DU \, e^{-S_W[U]} (1 - \Pi_P) = -\frac{2\,a^d}{d(d-1)V} \frac{\partial}{\partial\beta_0} \ln Z = \frac{2\,a^d}{d(d-1)} \frac{\partial}{\partial\beta_0} \left(\frac{1}{T}f\right). \tag{1.5}$$

Hence, given a weak-coupling expansion of the plaquette

$$\langle 1 - \Pi_P \rangle = \frac{c_1(N_c,d)}{\beta_0} + \frac{c_2(N_c,d)}{\beta_0^2} + \frac{c_3(N_c,d)}{\beta_0^3} + \frac{c_4(N_c,d)}{\beta_0^4} + \cdots \tag{1.6}$$

it follows that

$$\frac{2\,a^d}{d(d-1)} \left(\frac{1}{T}f\right) = c_0(N_c,d) + c_1(N_c,d) \ln\beta_0 - \frac{c_2(N_c,d)}{\beta_0} - \frac{c_3(N_c,d)}{2\beta_0^2} - \frac{c_4(N_c,d)}{3\beta_0^3} - \cdots . \tag{1.7}$$

We now specialize to $N_c = 3$ and $d = 3$ dimensions, where $g_0^2 \sim a^{-1}$ and hence $\beta_0 = 6/(ag_0^2)$. The previous formula reads (from here on, $c_i \equiv c_i(N_c = 3, d = 3)$)

$$\frac{2}{6}\frac{1}{T}f = a^{-3}(c_0 + c_1 \ln\beta_0) - a^{-2}\frac{c_2}{6}g_0^2 - a^{-1}\frac{c_3}{72}g_0^4 - \frac{\tilde{c}_4}{648}g_0^6 + O(a). \tag{1.8}$$

In order to control the matching to continuum one then needs the first four coefficients in the expansion of the basic plaquette. Note however that it is already known from a computation in the continuum that at four loop level there is a logarithmic infrared (IR) divergence [6]. One of the aims of our computation is to recover the scheme-independent coefficient of this logarithm, while fixing the lattice constant which is left over once an IR regulator has been chosen. In eq. (1.8) we have put a tilde on c_4 to denote that the IR divergence has to be isolated and subtracted in a convenient scheme. Later on, the lattice size L will act as the IR regulator. Going back to the lattice coefficients themselves, the first and the second ones are already known [7]. We will give them in section 3. The third and the fourth ones are the goal of the present work, a task which one can manage within our computational scheme.[1]

---

[1]In $4d$ the expansion of the plaquette is known via NSPT up to a much higher order. It is interesting to compare the two different situations. In $3d$ there is the additional subtlety of the IR divergence. On the other hand, the dimensionful nature of the coupling in $3d$ makes it possible to single out the different divergent contributions in Perturbation Theory. The situation is much more involved in $4d$ (see [8]).

2. Computational setup

Our computational tool is NSPT. Computing to β_0^{-4} order requires to expand the field up to β^{-4} order [5], that is

$$U_\mu(n) = 1 + \sum_{i=1}^{8} \beta_0^{-\frac{i}{2}} U_\mu^{(i)}(n). \tag{2.1}$$

We write the expansion in terms of the U_μ field. One could also express everything in terms of the Lie algebra field $A_\mu(n) = \sum_{i=1}^{8} \beta_0^{-\frac{i}{2}} A_\mu^{(i)}(n)$, the relation being $U_\mu(n) = \exp(A_\mu(n))$. Whichever one uses, one should keep in mind that perturbation theory amounts in any case to decompactifying the formulation of lattice gauge theory. The expansion in terms of the $U_\mu^{(i)}(n)$ is easier to manage from the point of view of computer data organization. Eq. (2.1) is the expansion to be inserted in the Langevin equation

$$\partial_t U_\eta = [-i\nabla S[U_\eta] - i\eta]U_\eta, \tag{2.2}$$

η being a gaussian noise. The equation has to be integrated in a convenient (time) discretization scheme. Our choice is the Euler scheme as it was proposed in [9]. This amounts to introducing a time step ϵ. As usual, the solution is recovered by working in a region where the time step corrections are linear (Euler scheme is a first order scheme) and extrapolating to $\epsilon \to 0$. We computed the expansion in eq. (1.6) for $\langle 1 - \Pi_P \rangle$ on different lattice sizes ranging from $L = 5$ to $L = 16$ (up to three loops we also performed the computations on a $L = 18$ lattice)

$$\langle 1 - \Pi_P \rangle^{(L)} = \frac{c_1^{(L)}}{\beta_0} + \frac{c_2^{(L)}}{\beta_0^2} + \frac{c_3^{(L)}}{\beta_0^3} + \frac{c_4^{(L)}}{\beta_0^4} + \cdots. \tag{2.3}$$

We then extrapolated the infinite lattice size results according to

$$
\begin{aligned}
c_1^{(L)} &= c_1 + \frac{d_1}{L^3} \\
c_i^{(L)} &= c_i + \sum_{j=j_i}^{J_i} \sum_{k=0}^{i-1} d_i^{(j,k)} \frac{\ln^k L}{L^j} \qquad (i = 2, 3) \\
c_4^{(L)} &= c_4^{(ln)} \ln L^3 + c_4 + \sum_{j=j_4}^{J_4} \sum_{k=0}^{3} d_4^{(j,k)} \frac{\ln^k L}{L^j}.
\end{aligned} \tag{2.4}
$$

These asymptotic forms are basically dictated by Symanzik's analysis [10]. In particular they include the contribution from subleading logarithms (they are suppressed by inverse powers of L). For each i the index k runs up to $i - 1$, which equals the number of loops (remember that in terms of the plaquette we are computing up to three loops, i.e. $i = 1$ is the tree level). The index j counts the subleading contributions coming from inverse powers of L. As it appears from the last line of the previous formula, the finite volume also acts as the IR regulator needed at order β_0^{-4} (this is instead a leading logarithm). Some comments are in order at this point. The final errors on infinite volume results are dominated by this extrapolation process.

Trying to assess the effect of the subleading logarithms, it turns out that both the range of our data and our statistical errors do not allow to distinguish between a logarithm and a constant. Hence we will only give (effective) extrapolations based on pure power-like fits. The spread of the results comes from the indetermination on the (inverse) powers to be included in the fit. This is not surprising, since in NSPT there is no control on what in the language of Feynman diagrams would be contributions coming from different diagrams (i.e. sums). We then try different choices of the powers and then compare the corresponding χ^2's. This process does not select a definite set of powers: the better choices (see figure 2) turn out to be comparable with respect to the resulting χ^2. The quoted values for the c_i ($i > 1$) together with the associated errors embrace the range of the outcomes.

Most of the computer simulations have been performed on a PC cluster the Parma group installed one year ago. This is made of ten bi-processor Athlon MP2200. A programming environment for NSPT for Lattice Gauge Theory was set up in C++. This was in part inspired by the TAO codes we use on the APE machines and for a large fraction based on the use of (C++ specific) *classes* and *methods* to handle lattice and algebraic structures. Needless to say, this part of the work will be useful in other applications of NSPT. The results we report come out of 6 months of runs on the above mentioned cluster. Some more statistics came from another PC cluster more recently installed in Parma. The latter is a *blade* system based on 14 Intel Xeon 2.0 GHz.

3. Results

In table 1 we present the results we obtained for the coefficients $c_i^{(L)}$ at various values of L. As in eq. (1.6) and eq. (2.3), we only give the coefficients of order β_0^{-n}: the coefficients odd in g_0 (i.e. of order $\beta_0^{-(2n+1)/2}$) were verified to be zero within errors. In the last line one can read the values extrapolated to infinite volume. For the fourth order we present both the bare coefficients $c_4^{(L)}$ and the subtracted ones $c_4^{(L)} - c_4^{(ln)} \ln L^3$; the latter is the finite quantity one is interested in at $L = \infty$.

In figure 1 we plot the values of the coefficients at the various lattice sizes together with the interpolating finite size corrections. Again, for the fourth order we plot both the bare coefficients $c_4^{(L)}$ and the subtracted ones $c_4^{(L)} - c_4^{(ln)} \ln L^3$. An obvious benchmark for our computations is the first order, whose value is $c_1^{(L)} = 8/3 * (1 - 1/L^3)$. In this (trivial) case one knows the result both at finite and at infinite volume. That is why in figure 1 we also plot the known finite size corrections for c_1.

Another benchmark is the second coefficient, which is also found in agreement with the diagrammatic studies in [7]. From ref. [11] one reads $c_2 = 1.9486$, however without an error estimate.

As it was already pointed out, for orders higher than the trivial one, the quoted errors of the infinite volume-extrapolated values are dominated by the form of the fitting polynomials in eq. (2.4). Still, the final errors are acceptable. Note the asymmetric error for c_3. The more conservative lower bound takes into account a choice for the subleading powers of L which results in a worse χ^2, see figure 2. It is interesting to compare the result

L	$c_1^{(L)}$	$c_2^{(L)}$	$c_3^{(L)}$	$c_4^{(L)}$	$c_4^{(L)} - c_4^{(ln)} \ln L^3$
5	2.6455(13)	1.8682(45)	5.990(26)	25.99(18)	21.28(18)
6	2.6536(8)	1.8968(31)	6.200(19)	27.66(14)	22.41(14)
7	2.6580(8)	1.9095(30)	6.307(21)	28.68(15)	22.98(15)
8	2.6615(6)	1.9226(23)	6.408(16)	29.66(14)	23.57(14)
9	2.6630(6)	1.9288(22)	6.484(18)	30.44(16)	24.00(16)
10	2.6638(4)	1.9340(15)	6.519(13)	30.91(13)	24.16(13)
11	2.6645(4)	1.9381(14)	6.574(11)	31.53(14)	24.51(14)
12	2.6650(3)	1.9413(12)	6.591(11)	31.67(15)	24.39(15)
13	2.6653(3)	1.9423(12)	6.621(11)	32.27(18)	24.76(18)
14	2.6656(3)	1.9436(12)	6.288(11)	32.37(16)	24.64(16)
15	2.6662(2)	1.9455(10)	6.652(10)	32.84(19)	24.91(19)
16	2.6657(2)	1.9442(8)	6.658(9)	33.28(19)	25.16(19)
18	2.6663(2)	1.9489(7)	6.715(8)	–	–
$\vdots$					
∞	2.6666(1)	1.955(2)	$6.90^{(2)}_{(12)}$		25.8(4)

Table 1: The coefficients $c_i^{(L)}$ at the various lattice sizes and their infinite volume extrapolations c_i. For the last order we report both $c_4^{(L)}$ and $c_4^{(L)} - c_4^{(ln)} \ln L^3$; the latter is the quantity to be extrapolated. For the error on c_3 see text and figure 2.

c_3 (our first original result) with the one conjectured in [11] from the hypothesis of the dominance of a given contribution: $c_3 \approx 7.02$. This conjecture turned out to be not too far from the result.

Let us now discuss the IR divergence at order β_0^{-4}. As is well known, it is difficult to recognize the presence of a logarithm. Still, we obtain some evidence for it. By this we mean the following. One can take different approaches to the fit of the last line of eq. (2.4). One possibility is to include no logarithmic correction at all. A second one is to include a logarithmic correction whose prefactor $c_4^{(ln)}$ is a fitting parameter. A third possibility is to include a logarithmic correction whose prefactor $c_4^{(ln)}$ equals the result which has already been obtained in the continuum computation of [6]: $c_4^{(ln)} = 81 \, (688 - 157\pi^2/4)/(4\pi)^4 = 0.9765$. By varying the choice of the inverse powers included in the fit, the first case (no log) yields values of χ^2 which are only slightly, but systematically worse than in the other two cases (of the order of 0.5 vs 0.4). By fitting both c_4 and $c_4^{(ln)}$ we obtained $c_4 = 24.5(2.0)$ and $c_4^{(ln)} = 1.1(2)$, a result fully consistent with [6], which gives us some more confidence in the presence of the log. In the third case (see figure 3) we obtain $c_4 = 25.8(4)$, getting a smaller error like expected. For the meaning of the quoted errors, see the discussion in section 2.

4. Conclusions and perspectives

We computed the first four coefficients in the expansion eq. (1.8) of the plaquette in $3d$ pure gauge SU(3) theory, from which one can trivially obtain the expansion of the free energy at four loops. For the first two coefficients the already known results have been correctly
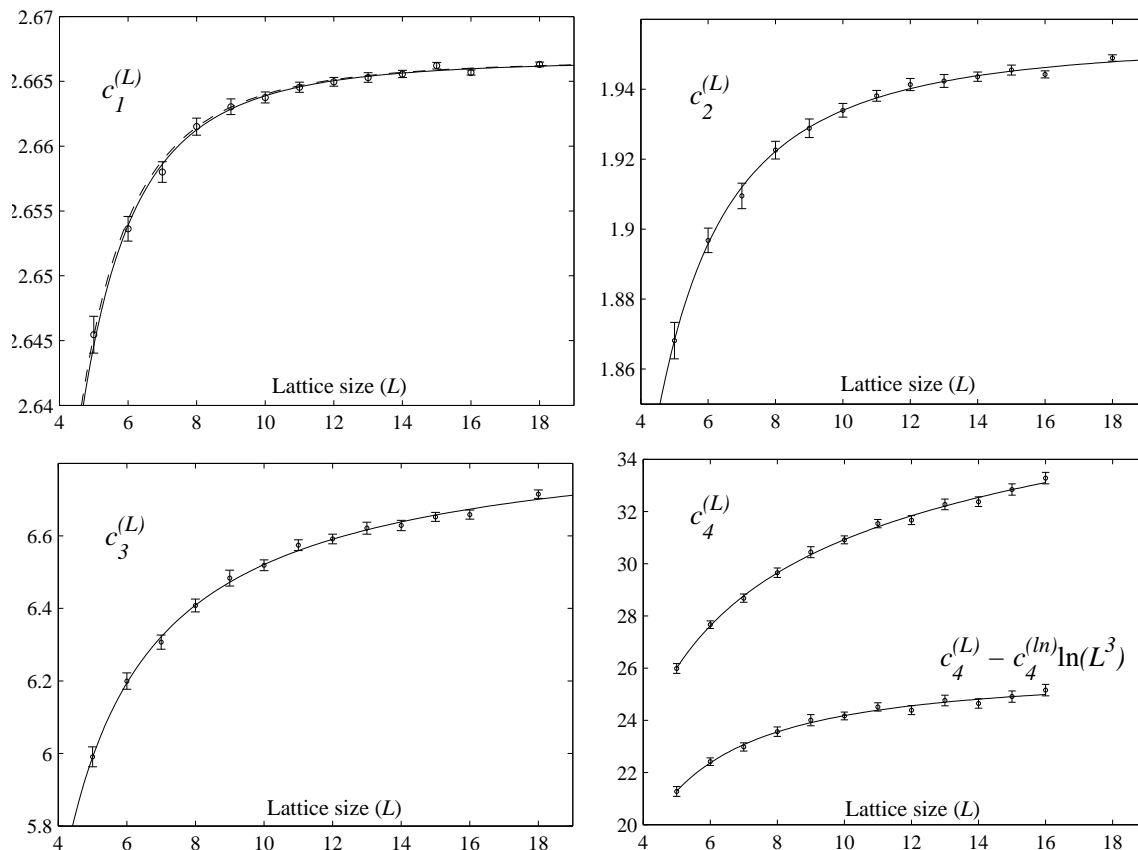
Figure 1: The coefficients $c_i^{(L)}$ together with the interpolating finite size corrections (solid lines). For the first order we also plot the (known) analytic finite volume corrections (dashed line). For the last order we plot both $c_4^{(L)}$ and $c_4^{(L)} - c_4^{(ln)} \ln L^3$.

reproduced. The third coefficient (the first original result of this paper) is connected with the mildest power divergence to be subtracted from simulations data for a lattice determination of the free energy.

The fourth coefficient was known to be logarithmically divergent, a result that was reproduced. Let us further comment on this point. A priori one can use any IR regulator in order to extract a finite part for the four loop contribution: the finite volume (the one we used in the present work), a mass (a very popular IR cutoff in the continuum) or the coupling itself (since it is dimensionful in $3d$). Notice that the latter is in a sense the natural choice for computer simulations. Obviously each choice defines a scheme of its own. While the coefficient of the logarithm is universal, there are of course specific constants relating the different schemes. As already pointed out, the coupling itself is the most natural regulator for computer simulations, even if there is no simple way to take it as the cutoff in perturbation theory. Ultimately, we are interested in the matching between the lattice and a continuum perturbative scheme (to be definite, $\overline{\text{MS}}$). The idea is to take the same IR regulator both in continuum and in lattice perturbation theory, which most naturally would be a common mass for all tree-level propagators. Since the same mismatch will be present in both computations with respect to the data coming from
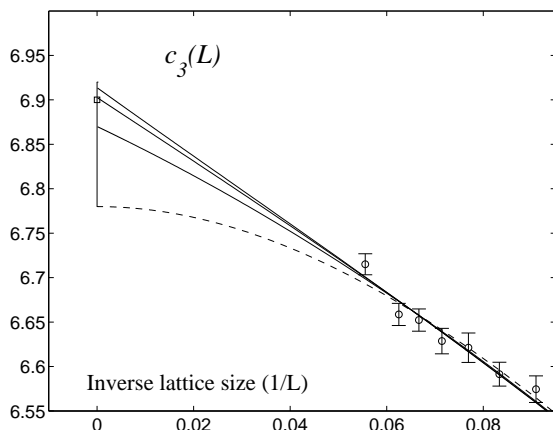
Figure 2: Different fits for $c_3^{(L)}$, showing the infinite-volume result (open square). The upper curves take $1/L$ as the leading power, while the lower (dashed) one takes $1/L^2$. The latter results in a higher χ^2 (0.7 vs 0.55).
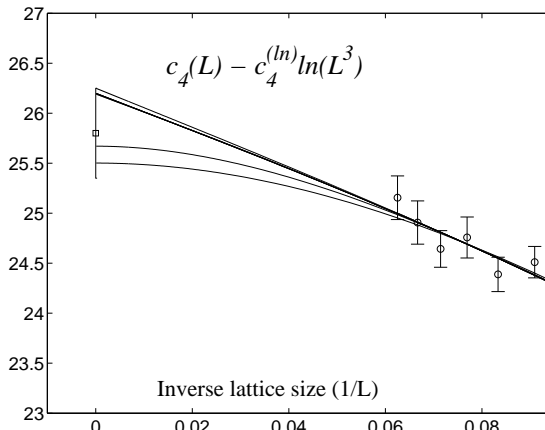
Figure 3: Different fits for $c_4^{(L)} - c_4^{(ln)} \ln L^3$, showing the infinite-volume result. In these fits the value for $c_4^{(ln)}$ is fixed to be the analytically known one. Within the range of the data the fits almost coincide.

computer simulations, that mismatch will cancel in the matching. Employing massive propagators in NSPT will therefore be the natural extension of the approach presented here.

Acknowledgments

References

[1] A. Papa, SU(3) *thermodynamics on small lattices, Nucl. Phys.* **B 478** (1996) 335 [hep-lat/9605004];
B. Beinlich, F. Karsch, E. Laermann and A. Peikert, *String tension and thermodynamics with tree level and tadpole improved actions, Eur. Phys. J.* **C 6** (1999) 133 [hep-lat/9707023].

[2] C.-x. Zhai and B. Kastening, *The free energy of hot gauge theories with fermions through g^5, Phys. Rev.* **D 52** (1995) 7232 [hep-ph/9507380].

[3] P.H. Ginsparg, *First order and second order phase transitions in gauge theories at finite temperature, Nucl. Phys.* **B 170** (1980) 388;
T. Appelquist and R.D. Pisarski, *High-temperature Yang-Mills theories and three-dimensional quantum chromodynamics, Phys. Rev.* **D 23** (1981) 2305.

[4] E. Braaten and A. Nieto, *Free energy of QCD at high temperature, Phys. Rev.* **D 53** (1996) 3421 [hep-ph/9510408];

K. Kajantie, M. Laine, K. Rummukainen and Y. Schroder, *How to resum long-distance contributions to the QCD pressure?*, *Phys. Rev. Lett.* **86** (2001) 10 [`hep-ph/0007109`].

[5] F. Di Renzo, E. Onofri, G. Marchesini and P. Marenzoni, *Four loop result in* SU(3) *lattice gauge theory by a stochastic method: lattice correction to the condensate*, *Nucl. Phys.* **B 426** (1994) 675 [`hep-lat/9405019`].

[6] K. Kajantie, M. Laine, K. Rummukainen and Y. Schroder, *The pressure of hot QCD up to* $g^6 \ln(1/g)$, *Phys. Rev.* **D 67** (2003) 105008 [`hep-ph/0211321`].

[7] U.M. Heller and F. Karsch, *One loop perturbative calculation of Wilson loops on finite lattices*, *Nucl. Phys.* **B 251** (1985) 254.

[8] F. Di Renzo and L. Scorzato, *A consistency check for renormalons in lattice gauge theory:* β^{-10} *contributions to the* SU(3) *plaquette*, *J. High Energy Phys.* **10** (2001) 038 [`hep-lat/0011067`];
For a different point of view see ,R. Horsley, P.E.L. Rakow and G. Schierholz, *Separating perturbative and non-perturbative contributions to the plaquette*, *Nucl. Phys.* **106** *(Proc. Suppl.)* (2002) 870 [`hep-lat/0110210`].

[9] G.G. Batrouni et al., *Langevin simulations of lattice field theories*, *Phys. Rev.* **D 32** (1985) 2736.

[10] M. Lüscher and P. Weisz, *Efficient numerical techniques for perturbative lattice gauge theory computations*, *Nucl. Phys.* **B 266** (1986) 309.

[11] F. Karsch, M. Lutgemeier, A. Patkos and J. Rank, *The* $O(g^6)$ *coefficient in the thermodynamic potential of hot* SU(N) *gauge theories and mqcd*, *Phys. Lett.* **B 390** (1997) 275 [`hep-lat/9605031`].

[YS9]

Plaquette expectation value and gluon condensate in three dimensions

Plaquette expectation value and gluon condensate in three dimensions

Ari Hietanen,[a] **Keijo Kajantie,**[a] **Mikko Laine,**[b] **Kari Rummukainen**[cde] **and York Schröder**[b]

[a] *Theoretical Physics Division, Department of Physical Sciences*
   P.O.Box 64, FI-00014 University of Helsinki, Finland
[b] *Faculty of Physics, University of Bielefeld*
   D-33501 Bielefeld, Germany
[c] *Department of Physics, Theory Division, CERN*
   CH-1211 Geneva 23, Switzerland
[d] *Department of Physics, University of Oulu*
   P.O.Box 3000, FI-90014 Oulu, Finland
[e] *Helsinki Institute of Physics*
   P.O.Box 64, FI-00014 University of Helsinki, Finland
   E-mail: `ari.hietanen@helsinki.fi`, `keijo.kajantie@helsinki.fi`,
   `laine@physik.uni-bielefeld.de`, `kari.rummukainen@cern.ch`,
   `yorks@physik.uni-bielefeld.de`

ABSTRACT: In three dimensions, the gluon condensate of pure SU(3) gauge theory has ultraviolet divergences up to 4-loop level only. By subtracting the corresponding terms from lattice measurements of the plaquette expectation value and extrapolating to the continuum limit, we extract the finite part of the gluon condensate in lattice regularization. Through a change of regularization scheme to $\overline{\rm MS}$ and (inverse) dimensional reduction, this result would determine the first non-perturbative coefficient in the weak-coupling expansion of hot QCD pressure.

Contents

1. Introduction

As non-abelian gauge theories in three and four dimensions are confining, their properties need, in general, to be studied non-perturbatively. If the observables considered involve momenta or masses (M) large compared with the confinement scale, however, then the conceptual framework of the operator product expansion [1] may allow to isolate the non-perturbative dynamics into only a few (gluon) condensates, while the rest of the answer can be computed by perturbative means. A classic example is the mass of a heavy quark–anti-quark bound state [2]. The task faced by numerical lattice simulations might then get significantly simplified, as local condensates are simpler to measure with controlled systematic errors than correlation functions of heavy states.

On the other hand, the physical interpretation of a "bare" lattice measurement of a gluon condensate is non-trivial. The reason is that the condensate is represented by the expectation value of a dimensionful singlet operator and, in general, contains ultraviolet divergences of the same degree as its dimension. Operator product expansion type relations are often derived employing dimensional regularization, since the system then only contains one large parameter (M) rather than two (M and the momentum cutoff), which simplifies the derivation considerably. Making use of lattice results in such a context requires then a transformation from lattice to continuum regularization. While in principle a well-defined perturbative problem (see, e.g., refs. [3]), this is in practice somewhat problematic in four dimensions, given that there are contributions from all orders in the loop expansion.

The observable we consider in this paper is the (lowest-dimensional) singlet gluon condensate in three dimensions (3d), measured with pure SU(3) gauge theory. As 3d pure Yang-Mills theory is super-renormalisable, the problem of changing the regularization scheme becomes solvable: there are ultraviolet divergences up to 4-loop level only [4]. Furthermore, as we will elaborate in the following, all the divergences have been determined recently. These advances allow us to obtain a finite "subtracted" continuum value for the gluon condensate in lattice regularization. A conversion to the $\overline{\text{MS}}$ scheme, amounting to the (perturbative) computation of the constant c_4' in eq. (2.12) below, remains however a future challenge.

There might be various physics settings where the 3d gluon condensate finds practical applications. The one that motivated us, is that this condensate appears in high-temperature physics, where the temperature T plays the role of the mass scale M mentioned above. Indeed 3d pure Yang-Mills theory determines the leading non-perturbative contribution to the weak-coupling expansion of the pressure (and a number of other quantities) of physical QCD [5, 6], through a conceptual counterpart of the operator product expansion, called finite-temperature dimensional reduction [7, 8, 9]. Other applications might exist as well.

The plan of this paper is the following. In section 2, we specify the observables considered and discuss the theoretical setting of our study. Numerical results from lattice Monte Carlo simulations are reported in section 3, and we conclude in section 4.

2. Theoretical setting

We start this section by formulating the observables that we are interested in, in the formal continuum limit of the theory. The ultraviolet (UV) divergences appearing in loop contributions are at this stage regulated through the use of dimensional regularization. Later on we go over to lattice regularization, in order to give a precise non-perturbative meaning to the observables introduced, allowing for their numerical determination.

The euclidean continuum action of pure $SU(N_c)$ Yang-Mills theory can be written as

$$S_E = \int d^d x \, \mathcal{L}_E, \qquad \mathcal{L}_E = \frac{1}{2g_3^2} \text{Tr}[F_{kl}^2] . \tag{2.1}$$

Here $d = 3 - 2\epsilon$, g_3^2 is the gauge coupling, $k, l = 1, \ldots, d$, $F_{kl} = i[D_k, D_l]$, $D_k = \partial_k - iA_k$, $A_k = A_k^a T^a$, T^a are the hermitean generators of $SU(N_c)$, normalised as $\text{Tr}[T^a T^b] = \delta^{ab}/2$, and repeated indices are assumed to be summed over. Leaving out for brevity gauge fixing and Faddeev-Popov terms, the "vacuum energy density" reads

$$f_{\overline{MS}} \equiv - \lim_{V \to \infty} \frac{1}{V} \ln \left[\int \mathcal{D}A_k \exp\left(-S_E\right) \right]_{\overline{MS}}, \tag{2.2}$$

where V is the d-dimensional volume, $\mathcal{D}A_k$ a suitable (gauge-invariant) functional integration measure, and we have assumed the use of the $\overline{MS}$ dimensional regularization scheme to remove any $1/\epsilon$ poles from the expression. We note that $f_{\overline{MS}}$ has the dimensionality $[\text{GeV}]^d$.

In strict dimensional regularization, $f_{\overline{MS}}$ of course vanishes order by order in the loop expansion, due to the absence of any mass scales in the propagators. This behaviour is unphysical, however, and due to an exact cancellation between UV and infrared (IR) divergences; for an explicit discussion at 3-loop level in a related case, see appendix B of ref. [10]. In fact non-perturbatively the structure of $f_{\overline{MS}}$ is rather

$$f_{\overline{MS}} = -g_3^6 \frac{d_A N_c^3}{(4\pi)^4} \left[\left(\frac{43}{12} - \frac{157}{768}\pi^2 \right) \ln \frac{\bar{\mu}}{2N_c g_3^2} + B_G + \mathcal{O}(\epsilon) \right], \tag{2.3}$$

where $d_A \equiv N_c^2 - 1$, and we have introduced an $\overline{MS}$ scheme scale parameter $\bar{\mu}$. The coefficient of the logarithm in eq. (2.3) has been determined in ref. [11] with a perturbative

4-loop computation, by regulating all the propagators by a small mass scale m_{G}, and sending $m_{\mathrm{G}} \to 0$ only after the computation (see also ref. [12]). The non-perturbative constant part B_{G},[1] which actually is a function of N_{c}, is what we would ultimately like to determine.

One direct physical application of B_{G} is that it determines the first non-perturbative contribution to the weak-coupling expansion of the pressure p of QCD at high temperatures [5, 6]. To be precise, this contribution is of the form $\delta p = d_A N_{\mathrm{c}}^3 g^6 T^4 B_{\mathrm{G}}/(4\pi)^4$, where g^2 is the renormalised QCD gauge coupling. Terms up to order $\mathcal{O}(g^6 \ln(1/g))$ are, in contrast, perturbative, and all known by now [12].

For future reference, we note that given $f_{\overline{\mathrm{MS}}}$, we immediately obtain the gluon condensate:

$$\frac{1}{2g_3^2} \left\langle \mathrm{Tr}[F_{kl}^2] \right\rangle_{\overline{\mathrm{MS}}} \equiv -g_3^2 \frac{\partial}{\partial g_3^2} f_{\overline{\mathrm{MS}}} \tag{2.4}$$

$$= 3g_3^6 \frac{d_A N_{\mathrm{c}}^3}{(4\pi)^4} \left[\left(\frac{43}{12} - \frac{157}{768}\pi^2 \right) \left(\ln \frac{\bar{\mu}}{2N_{\mathrm{c}} g_3^2} - \frac{1}{3} \right) + B_{\mathrm{G}} + \mathcal{O}(\epsilon) \right]. \tag{2.5}$$

We now go to the lattice. In the standard Wilson discretization, the lattice action, S_a, corresponding to eq. (2.1), reads

$$S_a = \beta \sum_{\mathbf{x}} \sum_{k<l} \left(1 - \frac{1}{N_{\mathrm{c}}} \mathrm{Re}\,\mathrm{Tr}[P_{kl}(\mathbf{x})] \right), \tag{2.6}$$

where $P_{kl}(\mathbf{x}) = U_k(\mathbf{x}) U_l(\mathbf{x}+k) U_k^{-1}(\mathbf{x}+l) U_l^{-1}(\mathbf{x})$ is the plaquette, $U_k(\mathbf{x})$ is a link matrix, $\mathbf{x} + k \equiv \mathbf{x} + a\hat{\epsilon}_k$, where a is the lattice spacing and $\hat{\epsilon}_k$ is a unit vector, and

$$\beta \equiv \frac{2N_{\mathrm{c}}}{g_3^2 a}. \tag{2.7}$$

Note that the gauge coupling does not get renormalised in 3d, and the parameters g_3^2 appearing in eqs. (2.1), (2.7) can hence be assumed finite and equivalent. The observable we consider is still the vacuum energy density, eq. (2.2), which in lattice regularization reads

$$f_a \equiv -\lim_{V\to\infty} \frac{1}{V} \ln\left[\int \mathcal{D}U_k \exp\left(-S_a\right) \right], \tag{2.8}$$

where $\mathcal{D}U_k$ denotes integration over link matrices with the gauge-invariant Haar measure.

Now, being in principle physical quantities, the values of $f_{\overline{\mathrm{MS}}}$ and f_a must agree, provided that suitable vacuum counterterms are added to the theory. Due to super-renormalizability, there can be such counterterms up to 4-loop level only [4], and correspondingly

$$\Delta f \equiv f_a - f_{\overline{\mathrm{MS}}} \tag{2.9}$$

$$= C_1 \frac{1}{a^3} \left(\ln \frac{1}{a g_3^2} + C_1' \right) + C_2 \frac{g_3^2}{a^2} + C_3 \frac{g_3^4}{a} + C_4 \, g_3^6 \left(\ln \frac{1}{a\bar{\mu}} + C_4' \right) + \mathcal{O}(g_3^8 a), \tag{2.10}$$

---

[1]In ref. [12], B_{G} was denoted by β_{G}, but we prefer to introduce a new notation here, in order to avoid confusion with the coupling constant β appearing in eq. (2.6). The subscript G might refer to gluons.

where the C_i are dimensionless functions of N_c. The values of C_1, C_2, C_3, C_4 are known, as we will recall presently; C'_1 is related to the precise normalisation of the Haar integration measure and void of physical significance; and C'_4 is unknown as of today.

Correspondingly, the gluon condensates, i.e. the logarithmic derivatives of $f_{\overline{MS}}$, f_a with respect to g_3^2, can also be related by a perturbative 4-loop computation. Noting that three-dimensional rotational and translational symmetries and the reality of S_a allow us to write

$$-g_3^2 \frac{\partial}{\partial g_3^2} f_a = \frac{3\beta}{a^3} \left\langle 1 - \frac{1}{N_c} \mathrm{Tr}[P_{12}] \right\rangle_a , \qquad (2.11)$$

and employing eqs. (2.5), (2.10), we obtain finally the master relation

$$8 \frac{d_A N_c^6}{(4\pi)^4} B_G = \lim_{\beta \to \infty} \beta^4 \left\{ \left\langle 1 - \frac{1}{N_c} \mathrm{Tr}[P_{12}] \right\rangle_a - \left[\frac{c_1}{\beta} + \frac{c_2}{\beta^2} + \frac{c_3}{\beta^3} + \frac{c_4}{\beta^4} \left(\ln \beta + c'_4 \right) \right] \right\}. \qquad (2.12)$$

The values of the constants $c_1, \ldots, c'_4$ are trivially related to those of $C_1, \ldots, C'_4$ in eq. (2.10).

Now, a straightforward 1-loop computation yields

$$c_1 = \frac{d_A}{3} \approx 2.66666667 , \qquad (2.13)$$

where the numerical value applies for $N_c = 3$.

The 2-loop term is already non-trivial: it was first computed in four dimensions in ref. [13], and in three dimensions in ref. [14]. The 3d result can be written in the form

$$c_2 = -\frac{2}{3} \frac{d_A N_c^2}{(4\pi)^2} \left(\frac{4\pi^2}{3N_c^2} + \frac{\Sigma^2}{4} - \pi\Sigma - \frac{\pi^2}{2} + 4\kappa_1 + \frac{2}{3}\kappa_5 \right) = 1.951315(2) , \qquad (2.14)$$

where the coefficients Σ, κ_1 can be found in refs. [4, 15], and we have defined

$$\kappa_5 = \frac{1}{\pi^4} \int_{-\pi/2}^{\pi/2} \mathrm{d}^3 x \, \mathrm{d}^3 y \frac{\sum_i \sin^2 x_i \sin^2(x_i + y_i) \sin^2 y_i}{\sum_i \sin^2 x_i \sum_i \sin^2(x_i + y_i) \sum_i \sin^2 y_i} = 1.013041(1) . \qquad (2.15)$$

The numbers in parentheses in eqs. (2.14), (2.15) indicate the uncertainties of the last digits.

The 3-loop term is well known in four dimensions since a long time ago [16], but the same computation has been carried out in three dimensions only very recently [17]:

$$c_3 = 6.8612(2) . \qquad (2.16)$$

This value improves on a previous estimate $c_3 = 6.90^{+0.02}_{-0.12}$ [18], obtained through the evaluation of the 3-loop graphs with the method of stochastic perturbation theory [19].

The value of c_4 follows by a comparison of eqs. (2.3) and (2.10): there is no $\bar{\mu}$-dependence in f_a, so that the one in $f_{\overline{MS}}$ determines the coefficient of the logarithm in Δf. Consequently,

$$c_4 = 8 \frac{d_A N_c^6}{(4\pi)^4} \left(\frac{43}{12} - \frac{157}{768}\pi^2 \right) \approx 2.92942132 . \qquad (2.17)$$

β	volumes
12	24^3, 32^3, 48^3
16	24^3, 32^3, 48^3, 64^3
20	24^3, 32^3, 48^3
24	$\{12^3,\ 14^3,\ 16^3,\ 20^3,\ 24^3\}$, 32^3, 48^3, 64^3
32	$\{14^3,\ 16^3,\ 20^3,\ 24^3,\ 32^3\}$, 48^3, 64^3, 96^3
40	$\{32^3\}$, 48^3, 64^3, 96^3
50	$\{20^3,\ 24^3,\ 26^3,\ 28^3,\ 32^3,\ 48^3\}$, 64^3, 96^3, 128^3, 320^3
64	$\{48^3,\ 64^3\}$, 96^3, 128^3, 320^3
80	$\{64^3\}$, 128^3, 320^3
[100	128^3, 192^3, 320^3]
[140	$\{128^3\}$, 192^3, 320^3]
[180	$\{192^3\}$, 320^3]

Table 1: The lattice spacings (parametrised by β, cf. eq. (2.7)) and the volumes (in lattice units, N^3, so that $V = N^3 a^3$) studied. On each lattice we have collected $\sim 10^4 \ldots 10^6$ independent measurements. The lattices in curly brackets have been left out from the infinite-volume extrapolations, while for the lattices in square brackets the significance loss due to the ultraviolet subtractions in eq. (2.12) is so large (six orders of magnitude or more) that the subtracted values have little effect on our final fit (see below).

The knowledge of c_1, c_2, c_3, c_4 allows us to subtract all the divergent contributions from the gluon condensate. A finite 4-loop term, parametrised by c'_4 in eq. (2.12), however still remains. It could in principle be determined by extending either the method of ref. [17] or of ref. [18] to 4-loop level. There is the additional complication, though, that intermediate steps of the computation require the use of an IR cutoff, which then cancels once the lattice and $\overline{\text{MS}}$ results are subtracted, in eq. (2.10). This computation has not been carried out yet, and therefore we will not be able to determine B_G in this paper. We can determine, however, the non-perturbative input needed for it (cf. eq. (3.1) below), the purely perturbative determination of c'_4 then remaining a future challenge.

3. Lattice measurements

The goal of the numerical study is to measure the plaquette expectation value, $\langle 1 - \frac{1}{3}\text{Tr}[P_{12}]\rangle_a$, as a function of β, such that the extrapolation in eq. (2.12) can be carried out. For each β, the infinite-volume limit needs to be taken. Given that the theory has a mass gap, we expect that finite-volume effects are exponentially small, if the length of the box L is large compared with the confinement scale, $\sim 1/g_3^2$. Writing $L = Na$, where N is the number of lattice sites, the requirement $L \gg 1/g_3^2$ converts to $\beta/N \ll 6$ (cf. eq. (2.17)). Detailed studies with other observables show that in practice the finite-volume effects are invisible as soon as $\beta/N < 1$ [20]. The values of β and N that we have employed are shown in table 1. Earlier lattice measurements of the same observable were carried out with a volume $N^3 = 32^3$, with values of β up to $\beta = 30$ [21].
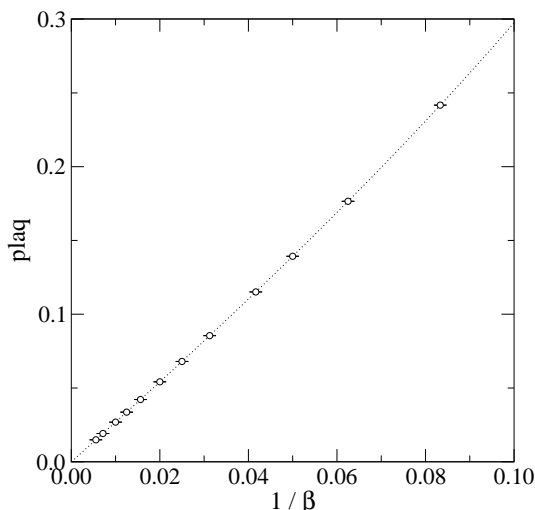
Figure 1: The plaquette expectation value, "plaq" $\equiv \langle 1 - \frac{1}{3}\,\mathrm{Tr}[P_{12}]\rangle_a$, as a function of $1/\beta$. Statistical errors are (much) smaller than the symbol sizes. The dotted curve contains the four known terms $c_1/\beta + c_2/\beta^2 + c_3/\beta^3 + c_4 \ln\beta/\beta^4$ from eq. (2.12), together with terms of the type $1/\beta^4$, $1/\beta^5$ and $1/\beta^6$ with fitted coefficients.

It is important to stress that the subtractions in eq. (2.12) lead to a major significance loss. Essentially, we need to evaluate numerically the fourth derivative with respect to β^{-1} of the function $\langle 1 - \frac{1}{3}\,\mathrm{Tr}[P_{12}]\rangle_a$, at the point $\beta^{-1} = 0$. Another way to express the problem is that as the numbers $c_1, \ldots, c_4$ are of order unity (cf. eqs. (2.13)–(2.17)), the dominant term, c_1/β, is about six orders of magnitude larger than the effect we are interested in, $\sim 1/\beta^4$, if $\beta \sim 100$. Therefore the relative error of our lattice measurements should be smaller than one part in a million. We also need to know the coefficients c_i with good precision.

Lattice-measured values of $\langle 1 - \frac{1}{3}\,\mathrm{Tr}[P_{12}]\rangle_a$ are shown in figure 1, as a function of $1/\beta$. In order to demonstrate the accuracy requirements we are faced with, figure 2 shows $\beta^4 \langle 1 - \frac{1}{3}\,\mathrm{Tr}[P_{12}]\rangle_a$, before and after the various subtractions. It is observed from figure 2 that after all the subtractions, this function indeed appears to have a finite limit for $\beta \to \infty$, or $1/\beta \to 0$.

For each β, we have carried out simulations at a number of different lattice extents N; examples are shown in figure 3. No significant volume dependence is observed for $\beta/N < 1$, and we thus estimate the infinite-volume limit by fitting a constant to data in this range.

Given the infinite-volume estimates, we extrapolate the data to the continuum limit, $\beta \to \infty$. In figure 4 we show the functions $\beta^4\{\langle 1 - \frac{1}{3}\,\mathrm{Tr}[P_{12}]\rangle_a - [c_1/\beta + c_2/\beta^2 + c_3/\beta^3]\}$ and $\beta^4\{\langle 1 - \frac{1}{3}\,\mathrm{Tr}[P_{12}]\rangle_a - [c_1/\beta + c_2/\beta^2 + c_3/\beta^3 + c_4 \ln\beta/\beta^4]\}$. It is observed how even the 4-loop logarithmic divergence is visible in the data, as some upwards curvature for $1/\beta \lesssim 0.06$. On the other hand, for $1/\beta \leq 0.01$ the significance loss due to the subtractions grows rapidly and the error bars become quite large, so that these data points have little effect on the fit.

The continuum extrapolation is carried out by fitting a function $d_1 + d_2/\beta + d_3/\beta^2$ to the infinite-volume extrapolated data for $\beta^4\{\langle 1 - \frac{1}{3}\,\mathrm{Tr}[P_{12}]\rangle_a - [c_1/\beta + c_2/\beta^2 + c_3/\beta^3 +$
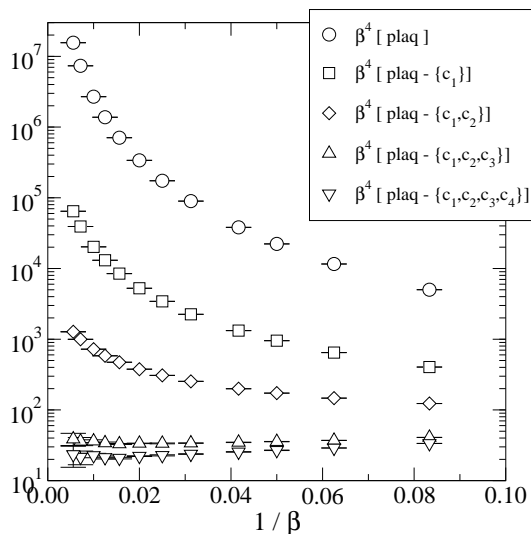
Figure 2: The significance loss due to the subtractions of the various ultraviolet divergent contributions in the gluon condensate. Here again "plaq" $\equiv \langle 1 - \frac{1}{3} \text{Tr}[P_{12}] \rangle_a$, and the symbols c_i in the curly brackets indicate which subtractions of eq. (2.12) have been taken into account.
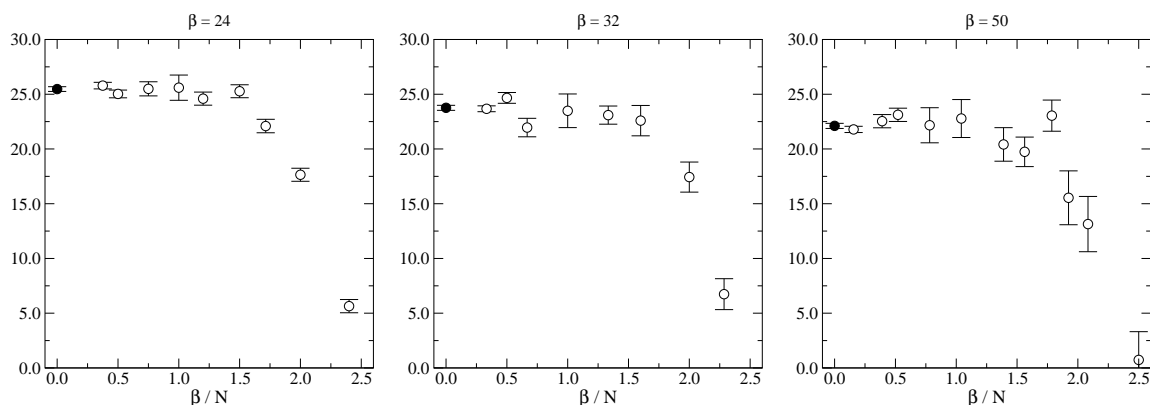
Figure 3: Finite-volume values for $\beta^4 \{\langle 1 - \frac{1}{3} \text{Tr}[P_{12}] \rangle_a - [c_1/\beta + c_2/\beta^2 + c_3/\beta^3 + c_4 \ln \beta/\beta^4] \}$, as a function of the physical extent $\beta/N = 6/g_3^2 L$ of the box. The solid symbols indicate the infinite-volume estimates, obtained by fitting a constant to data in the range $\beta/N < 1$.

$c_4 \ln \beta/\beta^4]\}$, in the range $0.01 < 1/\beta < 0.10$. We find that this functional form describes the data very well. The fitted values are $d_1 = 19.4 \ldots 20.7$, $d_2 = 110 \ldots 63$, $d_3 = 717 \ldots 1101$, with $\chi^2/\text{dof} = 5.8/6$, where the intervals indicate the projections of the 68% confidence level contour (i.e. the surface where $\chi^2 = \chi^2_{\text{min}} + 3.53$) onto the various axes, from one end of the elongated ellipse to the other.[2] We have also estimated the systematic errors from the effect of higher order terms in the fit ansatz, and found that they are of the same order as these intervals, which we thus consider as our combined error estimates. Returning back

---

[2]If the three largest β's are included in the fit, the parameters remain essentially the same, $d_1 = 19.4 \ldots 20.8$, $d_2 = 107 \ldots 62$, $d_3 = 733 \ldots 1117$, while $\chi^2/\text{dof} = 7.0/9$ has decreased due to the large error bars at these β's.
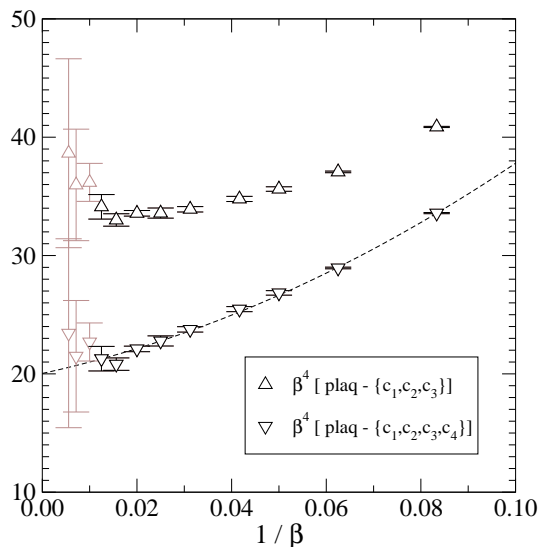
Figure 4: The infinite-volume extrapolated data, plotted as in figure 2. The effect of the 4-loop logarithmic divergence is to cause additional upwards "curvature" in the upper data set. The lower set includes all the subtractions, and should thus have a finite continuum limit. The continuum extrapolation (as described in the text) is indicated with the dashed line. The gray points have error bars so large that they are insignificant as far as the fit is concerned.

to eq. (2.12), we then obtain our final result,

$$B_{\rm G} + \left(\frac{43}{12} - \frac{157}{768}\pi^2 \right) c'_4 = \left(\frac{2\pi^2}{27} \right)^2 \times (20.0 \pm 0.7) = 10.7 \pm 0.4 \,, \qquad (3.1)$$

where we have inserted $N_{\rm c} = 3$.

4. Conclusions

The purpose of this paper has been to study the expectation value of the elementary plaquette in pure SU(3) lattice gauge theory in three dimensions, as well as to outline how the $\overline{\rm MS}$ scheme gluon condensate of the continuum theory can be extracted from it. To achieve this goal, we have carried out high precision numerical Monte Carlo simulations close to the continuum limit, corresponding to lattice spacings $0.05 \lesssim ag_3^2 \lesssim 0.5$, where g_3^2 is the gauge coupling.

When the leading perturbative terms, up to 4-loop level, are subtracted from the plaquette expectation value, and the result is divided by $(ag_3^2)^4$, a finite quantity remains (the right-hand side of eq. (2.12), without c'_4) which can be taken as the definition of a renormalised gluon condensate in lattice regularization (in certain units). We have carried out the subtractions and the extrapolation $ag_3^2 \to 0$, and shown that our data appear to be precise enough to determine the remainder with less than 5% errors, cf. figure 4 and eq. (3.1).

To relate this number to the gluon condensate in some continuum scheme, say $\overline{\rm MS}$, a further perturbative 4-loop matching computation remains to be completed, fixing the

constant c_4' in eqs. (2.12), (3.1). Our study should provide a strong incentive for finalising this challenging but feasible task, and there indeed is work in progress with this goal. The $\overline{\text{MS}}$ scheme conversion is also needed in order to apply our result in the context of finite temperature physics, particularly for determining the $\mathcal{O}(g^6 T^4)$ contribution to the pressure of hot QCD, since the other parts of that computation have been formulated in the $\overline{\text{MS}}$ scheme [12].

Acknowledgments

References

[1] K.G. Wilson, *Non-lagrangian models of current algebra*, *Phys. Rev.* **179** (1969) 1499.

[2] M.B. Voloshin, *On dynamics of heavy quarks in non-perturbative QCD vacuum*, *Nucl. Phys.* **B 154** (1979) 365; *Precoulombic asymptotics for energy levels of heavy quarkonium*, *Sov. J. Nucl. Phys.* **36** (1982) 143;
H. Leutwyler, *How to use heavy quarks to probe the QCD vacuum*, *Phys. Lett.* **B 98** (1981) 447.

[3] A. Hasenfratz and P. Hasenfratz, *The connection between the Λ parameters of lattice and continuum QCD*, *Phys. Lett.* **B 93** (1980) 165;
R.F. Dashen and D.J. Gross, *The relationship between lattice and continuum definitions of the gauge theory coupling*, *Phys. Rev.* **D 23** (1981) 2340.

[4] K. Farakos, K. Kajantie, K. Rummukainen and M.E. Shaposhnikov, *3d physics and the electroweak phase transition: a framework for lattice Monte Carlo analysis*, *Nucl. Phys.* **B 442** (1995) 317 [`hep-lat/9412091`].

[5] A.D. Linde, *Infrared problem in thermodynamics of the Yang-Mills gas*, *Phys. Lett.* **B 96** (1980) 289.

[6] D.J. Gross, R.D. Pisarski and L.G. Yaffe, *QCD and instantons at finite temperature*, *Rev. Mod. Phys.* **53** (1981) 43.

[7] P.H. Ginsparg, *First order and second order phase transitions in gauge theories at finite temperature*, *Nucl. Phys.* **B 170** (1980) 388;
T. Appelquist and R.D. Pisarski, *High-temperature Yang-Mills theories and three-dimensional quantum chromodynamics*, *Phys. Rev.* **D 23** (1981) 2305.

[8] K. Kajantie, M. Laine, K. Rummukainen and M.E. Shaposhnikov, *Generic rules for high temperature dimensional reduction and their application to the Standard Model*, *Nucl. Phys.* **B 458** (1996) 90 [`hep-ph/9508379`].

[9] E. Braaten and A. Nieto, *Free energy of QCD at high temperature*, *Phys. Rev.* **D 53** (1996) 3421 [`hep-ph/9510408`].

[10] K. Kajantie, M. Laine, K. Rummukainen and Y. Schröder, *Four-loop vacuum energy density of the* SU(N_c) + *adjoint Higgs theory*, *J. High Energy Phys.* **04** (2003) 036 [`hep-ph/0304048`].

[11] Y. Schröder, *Tackling the infrared problem of thermal QCD*, *Nucl. Phys.* **129** *(Proc. Suppl.)* (2004) 572 [`hep-lat/0309112`];
Logarithmic divergence in the energy density of the three-dimensional Yang-Mills theory, in preparation.

[12] K. Kajantie, M. Laine, K. Rummukainen and Y. Schröder, *The pressure of hot QCD up to* $g^6 \ln(1/g)$, *Phys. Rev.* **D 67** (2003) 105008 [`hep-ph/0211321`].

[13] A. Di Giacomo and G.C. Rossi, *Extracting* $\langle (\alpha/\pi) \sum_{a,\mu\nu} G^a_{\mu\nu} G^a_{\mu\nu} \rangle$ *from gauge theories on a lattice*, *Phys. Lett.* **B 100** (1981) 481.

[14] U.M. Heller and F. Karsch, *One loop perturbative calculation of Wilson loops on finite lattices*, *Nucl. Phys.* **B 251** (1985) 254.

[15] M. Laine and A. Rajantie, *Lattice-continuum relations for 3d* SU(N)+*Higgs theories*, *Nucl. Phys.* **B 513** (1998) 471 [`hep-lat/9705003`].

[16] B. Allés, M. Campostrini, A. Feo and H. Panagopoulos, *The three loop lattice free energy*, *Phys. Lett.* **B 324** (1994) 433 [`hep-lat/9306001`];
B. Allés, A. Feo and H. Panagopoulos, *Asymptotic scaling corrections in QCD with Wilson fermions from the 3-loop average plaquette*, *Phys. Lett.* **B 426** (1998) 361 [`hep-lat/9801003`] erratum *ibid.* **B 553** (2003) 337.

[17] H. Panagopoulos and A. Tsapalis, in preparation.

[18] F. Di Renzo, A. Mantovi, V. Miccio and Y. Schröder, *3-d lattice Yang-Mills free energy to four loops*, *J. High Energy Phys.* **05** (2004) 006 [`hep-lat/0404003`].

[19] F. Di Renzo, E. Onofri, G. Marchesini and P. Marenzoni, *Four loop result in* SU(3) *lattice gauge theory by a stochastic method: lattice correction to the condensate*, *Nucl. Phys.* **B 426** (1994) 675 [`hep-lat/9405019`].

[20] M.J. Teper, SU(N) *gauge theories in 2+1 dimensions*, *Phys. Rev.* **D 59** (1999) 014512 [`hep-lat/9804008`];
M. Laine and O. Philipsen, *The non-perturbative QCD Debye mass from a Wilson line operator*, *Phys. Lett.* **B 459** (1999) 259 [`hep-lat/9905004`].

[21] F. Karsch, M. Lütgemeier, A. Patkós and J. Rank, *The* $\mathcal{O}(g^6)$ *coefficient in the thermodynamic potential of hot* SU(N) *gauge theories and MQCD*, *Phys. Lett.* **B 390** (1997) 275 [`hep-lat/9605031`].

[YS10]

Two-loop static QCD potential for general colour state

Two-loop static QCD potential for general colour state

B.A. Kniehl [a], A.A. Penin [b,c], Y. Schröder [d], V.A. Smirnov [a,e], M. Steinhauser [b]

[a] *II. Institut für Theoretische Physik, Universität Hamburg, Luruper Chaussee 149, 22761 Hamburg, Germany*
[b] *Institut für Theoretische Teilchenphysik, Universität Karlsruhe, 76128 Karlsruhe, Germany*
[c] *Institute for Nuclear Research, Russian Academy of Sciences, 60th October Anniversary Prospect 7a, 117312 Moscow, Russia*
[d] *Fakultät für Physik, Universität Bielefeld, 33501 Bielefeld, Germany*
[e] *Institute for Nuclear Physics, Moscow State University, 119992 Moscow, Russia*

Abstract

In this Letter, we extend the known results for the QCD potential between a static quark and its antiquark by computing the two-loop corrections to the colour-octet state.
© 2004 Elsevier B.V. All rights reserved.

PACS: 12.38.Bx; 12.38.-t

The QCD potential between a static quark and its antiquark has for a long time been used as a probe of the fundamental properties of the strong interactions such as asymptotic freedom and confinement [1]. Historically, the potential for a quark–antiquark pair in the colour-singlet state attracted the most attention because it is a basic ingredient in the theory of heavy quarkonium and, therefore, of primary phenomenological interest. Nowadays, however, there is growing interest in its colour-octet counterpart. The latter naturally appears in effective-theory calculations of high-order corrections to the heavy-quarkonium spectrum and decay rates through the so-called ultrasoft contribution [2]. Moreover, it determines the properties of glueballinos and is necessary for the analysis of gluino–antigluino threshold production [3,4]. It is also used in lattice QCD for studying the behavior of strong interactions at long distances and the interplay between perturbative and non-perturbative physics [3]. This requires knowledge of the corresponding perturbative corrections which, in contrast to the colour-singlet case, are not available beyond one loop. In the present Letter, we fill this gap and compute the $\mathcal{O}(\alpha_s^2)$ correction to the colour-octet static potential.

The perturbative expansion of the colour-singlet potential reads

$$V(|\mathbf{q}|) = -\frac{4\pi C_F \alpha_s(|\mathbf{q}|)}{\mathbf{q}^2}$$
$$\times \left[1 + \frac{\alpha_s(|\mathbf{q}|)}{4\pi} a_1 + \left(\frac{\alpha_s(|\mathbf{q}|)}{4\pi}\right)^2 a_2 \right.$$
$$\left. + \left(\frac{\alpha_s(|\mathbf{q}|)}{4\pi}\right)^3 \left(a_3 + 8\pi^2 C_A^3 \ln\frac{\mu^2}{\mathbf{q}^2}\right) + \cdots \right]$$
$$(1)$$

where the first term corresponds to the Coulomb potential. The one-loop coefficient,

$$a_1 = \frac{31}{9} C_A - \frac{20}{9} T_F n_l, \tag{2}$$

has been known for a long time [5,6], while the two-loop coefficient, a_2, has only recently been found [7–9]. In Ref. [9], the result of Ref. [8] was confirmed,

$$a_2 = \left[\frac{4343}{162} + 4\pi^2 - \frac{\pi^4}{4} + \frac{22}{3}\zeta(3)\right] C_A^2$$
$$- \left[\frac{1798}{81} + \frac{56}{3}\zeta(3)\right] C_A T_F n_l$$
$$- \left[\frac{55}{3} - 16\zeta(3)\right] C_F T_F n_l + \left(\frac{20}{9} T_F n_l\right)^2, \quad (3)$$

where ζ is Riemann's zeta function, with value $\zeta(3) = 1.202057\ldots$. Here, $C_A = N$ and $C_F = (N^2-1)/(2N)$ are the eigenvalues of the quadratic Casimir operators of the adjoint and fundamental representations of the $SU(N)$ colour gauge group, respectively, $T_F = 1/2$ is the index of the fundamental representation, and n_l is the number of light-quark flavours. The modified minimal-subtraction ($\overline{\mathrm{MS}}$) scheme for the renormalization of α_s is implied. The logarithmic term of $\mathcal{O}(\alpha_s^3)$ in Eq. (1) reflects the infrared divergence of the static potential [10]. The particular form of the logarithmic term corresponds to dimensional regularization [11]. The corresponding infrared-divergent term is cancelled against the ultraviolet-divergent one of the ultra-soft contribution [2] in the calculation of the physical heavy-quarkonium spectrum [11,12]. The non-logarithmic third-order term, a_3, is still unknown.

The perturbative expansion of the potential for the colour-octet state can be cast in the form

$$V^o(|\mathbf{q}|) = \frac{4\pi\alpha_s(|\mathbf{q}|)}{\mathbf{q}^2}\left(\frac{C_A}{2} - C_F\right)$$
$$\times \left[1 + \frac{\alpha_s(|\mathbf{q}|)}{4\pi} a_1^o + \left(\frac{\alpha_s(|\mathbf{q}|)}{4\pi}\right)^2 a_2^o \right.$$
$$+ \left(\frac{\alpha_s(|\mathbf{q}|)}{4\pi}\right)^3$$
$$\left. \times \left(a_3^o + 8\pi^2 C_A^3 \ln\frac{\mu^2}{\mathbf{q}^2}\right) + \cdots \right], \tag{4}$$

where the one-loop coefficient is the same as in the colour-singlet case, $a_1^o = a_1$. The two-loop coefficient, however, differs by a finite renormalization-independent term,

$$a_2^o = a_2 + \delta a_2. \tag{5}$$

Our result is

$$\delta a_2 = C_A^2 \frac{3d - 11}{d - 5}$$
$$\times \left[\text{—}\!\bigcirc\!\!\bigcirc\!\text{—} - \frac{3(d-4)(d-1)}{d-5} \text{—}\!\bigcirc\!\!\!\bigcirc\!\text{—} \right]$$
$$= (\pi^4 - 12\pi^2) C_A^2 + \mathcal{O}(d-4), \tag{6}$$

where d is the space–time dimension, and we have introduced a graphical notation for the two master two-point integrals, where single and double lines represent the propagators $1/(k^2 + i\varepsilon)$ and $1/(k_0 + i\varepsilon)$, respectively. The non-logarithmic part of the three-loop coefficient, a_3^o, is still unknown. It is instructive to look at the numerical size of the corrections. For $N = 3$ one obtains $\delta a_2 = -189.2$. At the same time, we have $a_2 = 155.8(211.1, 268.8)$ and $a_1 = 4.778(5.889, 7.000)$ for $n_l = 5(4, 3)$. Thus, in the colour-octet case, the two-loop correction is significantly smaller than for the colour-singlet configuration. Depending on n_l, it even changes sign.

In the remaining part of this Letter, we wish to describe two independent ways that have been used to evaluate δa_2. The first method proceeds along the lines of the analysis [9,11] based on the threshold expansion [13]. In general, the threshold expansion is the proper framework for performing calculations involving a heavy quark–antiquark system. It provides rigorous power-counting rules and natural definitions of the formal expressions obtained in the perturbative analysis of the non-relativistic effective theory. The corrections to the static potential only arise from the

soft regions of the loop integrals, which are characterized by the following scaling of the loop momenta: $l_0 \sim |\mathbf{l}| \sim |\mathbf{q}|$. Thus, the calculation of the coefficients a_i and a_i^o can be performed in the static limit of NRQCD, $m_q \to \infty$.

Due to the exponentiation of the static potential [5], the coefficients a_i of the colour-singlet state only receive contributions from the maximally non-Abelian parts, leaving aside the terms involving n_l. The selection of these parts effectively retains the contributions of the soft region, as the appearance of the Abelian colour factor C_F indicates the presence of a Coulomb pinch and thus implies that at least one loop momentum is potential. The latter contributions just represent iterations of the lower-order potential and, therefore, should be excluded from the potential itself. In the non-relativistic effective theory, these iterations are taken into account in the perturbative solution of the Schrödinger equation about the Coulomb approximation. These contributions refer to dynamical rather than static heavy-quark and -antiquark fields, and the Coulomb pinch singularities we encounter in the static-limit calculations are resolved by keeping a finite mass in the non-relativistic heavy-quark propagator.

The analysis of the colour-octet state is more involved, since, in this case, the Coulomb pinches come with all possible colour factors and cannot be removed by selecting the maximum non-Abelian ones. Thus, the separation of the Coulomb pinches should be performed explicitly. They appear in the Feynman diagrams involving the product of the non-relativistic quark and antiquark propagators,

$$\frac{1}{k_0 - \mathbf{k}^2/(2m_q) + i\varepsilon} \frac{1}{k_0 + \mathbf{k}^2/(2m_q) - i\varepsilon}. \qquad (7)$$

In this case, after expanding the quark propagator in $1/m_q$, one obtains ill-defined products like

$$\frac{1}{(k_0 + i\varepsilon)^m} \frac{1}{(k_0 - i\varepsilon)^n}. \qquad (8)$$

Thus, separating the soft and potential regions is unavoidable.[1] In the soft region, the pole contributions

of the quark and antiquark propagators have to be excluded, and the product in Eq. (8) should actually be defined to be its principal value,

$$\frac{1}{2}\left[\frac{1}{(k_0 + i\varepsilon)^{m+n}} + \frac{1}{(k_0 - i\varepsilon)^{m+n}} \right]. \qquad (9)$$

In the potential region, the quark and antiquark propagator poles produce contributions of the form

$$-i\pi \frac{m_q}{\mathbf{k}^2 - i\varepsilon}\left[\delta\left(k_0 - \frac{\mathbf{k}^2}{2m_q}\right) + \delta\left(k_0 + \frac{\mathbf{k}^2}{2m_q}\right) \right], \qquad (10)$$

where the $1/v$ Coulomb singularity shows up explicitly. After integration over k_0, Eq. (10) yields the non-relativistic Green function of the free Schrödinger equation. Only Eq. (9) should be taken into account in the calculation of the static potential.

At one loop, there is only one diagram involving a Coulomb pinch, namely, the planar box, which has the colour factor C_F^2 for the colour-singlet state. Picking up the soft contribution, i.e., using the principal-value prescription of Eq. (9) to define Eq. (8), we find the planar box to cancel the C_F^2 part of the non-planar box, which in total is proportional to $C_F^2 - C_F C_A/2$. This explicitly demonstrates the exponentiation of the one-loop colour-singlet static potential in momentum space. However, we can also turn things around and express the planar box with Coulomb pinches through the well-defined non-planar box by actually requiring the cancellation of the C_F^2 terms in the sum of all one-loop diagrams, as is dictated by the exponentiation. The result for a_1^o as given above is then obtained by simply replacing the colour-singlet colour factor by the colour-octet one.

This strategy carries over to two loops. Here, we have diagrams with zero, one, or two Coulomb pinches. For the diagrams without Coulomb pinch, the contribution to a_2^o is obtained by adopting the correct colour factor. We divide the Feynman diagrams with Coulomb pinches into those that have two quark and two antiquark propagators (cf. Fig. 1) and the rest. The latter ones are treated directly using the principal-value prescription of Eq. (9). For the former, however, it is simpler to use the exponentiation, which requires that the diagrams contributing to the colour factors $C_A C_F^2$ and C_F^3 sum up to zero in the colour-singlet case. This leads to two equations for the diagrams suffering from Coulomb pinches, namely, those shown in

---

[1] Note that, for the diagrams without Coulomb pinches, the separation of the soft and potential regions is ambiguous and even gauge dependent. In such diagrams, the non-relativistic quark and antiquark propagators can be safely expanded in $1/m_q$.
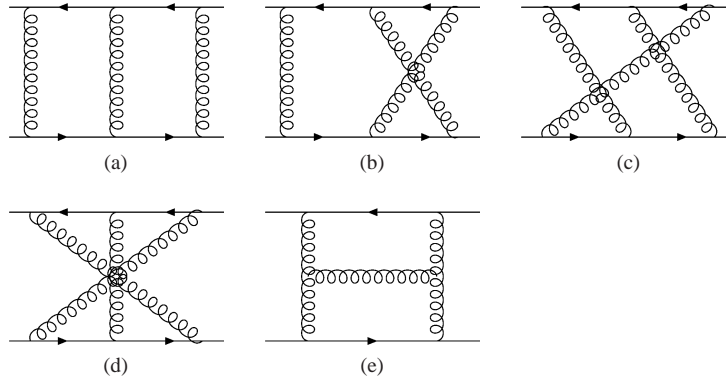
Fig. 1. Two-loop Feynman diagrams with ((a) and (b)) and without ((c)–(e)) Coulomb pinches that contribute to δa_2.

Fig. 1(a) and (b), which can be solved. This provides a result in terms of the diagrams in Fig. 1(c) and (d), which are free of pinches. After adopting the colour factors corresponding to the colour-octet configuration, one obtains the contributions to the results given in Eqs. (5) and (6). We wish to mention that the calculation was performed in the general covariant gauge and that the dependence on the gauge parameter was found to cancel out in the final result.

The second method to compute V^o proceeds along the lines of Ref. [8]. While in the above, we had to assume exponentiation of the colour-singlet potential, we will now relax that assumption. The reason is that, although exponentiation is plausible to all orders of perturbation theory, the proof given in Ref. [5] holds for the singlet potential in *Abelian* theories only.

As a starting point, we now expand the logarithm of the $(T \times R)$ Wilson loop spanned by the static quark–antiquark pair at distance R through $\mathcal{O}(\alpha_s^3)$. Taking the limit $T \to \infty$ (which, in a diagrammatic sense, 'cuts' the Wilson loop twice and restores translational invariance in the temporal direction, hence guaranteeing energy conservation at the vertices and leading to simple momentum-space Feynman rules) and inserting $SU(N)$ generators T^a into the purely spatial Wilson lines to obtain the colour-octet potential to this order (for a manifestly gauge-invariant definition, see Ref. [14]), we now explicitly keep disconnected as well as one-particle-reducible diagrams in our expansion.

At this point, the general structure of the expansion involves (products of) up to two-loop four-point functions of static quarks (cf. Fig. 1). After Fourier transforming to momentum-space, we can choose a special

point to evaluate these four-point functions, since the potential, of course, only knows about the distance R of the $q\bar{q}$ pair, which in a momentum-space representation translates into the momentum transfer $|\mathbf{q}|$ between the upper and lower lines in Fig. 1. Hence, effectively, we have to compute two-point functions with external static quarks, external momentum $q = (0, \mathbf{q})$, and internal static quarks, gluons, ghosts and light quarks, with the additional occurrence of a static (anti-)quark–gluon two-point vertex, resulting from the special kinematics.

After performing the colour algebra and exploiting symmetries of the integrals occurring in the expansion, all integrals which might give rise to pinch singularities, and had to be treated with caution in our first approach, cancel exactly. Thus, we are left with the task of computing a class of two-loop two-point integrals for which there exists a generic algorithm [8,15], based on integration by parts (IBP) [16]. The implementation in Ref. [15] (see also Chapter 6 of Ref. [17]) is based on Ref. [18].

Having generated the relevant set of diagrams and reduced the occurring Feynman integrals to the set of two-point functions described above, we now employ the reduction algorithm, which maps them to a (small) set of so-called master integrals, multiplied by rational functions in the dimension d. At this stage, we observe cancellation of the gauge-parameter dependence, serving as a check for the reduction. As an additional strong check, we use our implementation [19] of the strategy to solve a truncated set of IBP relations, based on lexicographic ordering of integrals [20].

The set of (massless, two-point) master integrals is known analytically in terms of gamma functions, for

generic dimension d, as given, e.g., in Ref. [8]. Expanding prefactors as well as master integrals about $d = 4 - 2\epsilon$ and renormalizing the gauge coupling, we again arrive at Eq. (6).

To conclude, we have evaluated the $\mathcal{O}(\alpha_s^2)$ correction to the colour-octet static potential using two independent techniques. Both evaluations are in agreement, giving us confidence in our main result, Eq. (6).

Acknowledgements

References

[1] L. Susskind, Coarse grained QCD, in: R. Balian, C.H. Llewellyn Smith (Eds.), Weak and Electromagnetic Interactions at High Energy, North-Holland, Amsterdam, 1977.

[2] B.A. Kniehl, A.A. Penin, Nucl. Phys. B 563 (1999) 200;
B.A. Kniehl, A.A. Penin, Nucl. Phys. B 577 (2000) 197;
N. Brambilla, A. Pineda, J. Soto, A. Vairo, Nucl. Phys. B 566 (2000) 275.

[3] G.S. Bali, A. Pineda, Phys. Rev. D 69 (2004) 094001, and references therein.

[4] J.H. Kühn, P.M. Zerwas, Phys. Rep. 167 (1988) 321.

[5] W. Fischler, Nucl. Phys. B 129 (1977) 157.

[6] A. Billoire, Phys. Lett. B 92 (1980) 343.

[7] M. Peter, Phys. Rev. Lett. 78 (1997) 602;
M. Peter, Nucl. Phys. B 501 (1997) 471.

[8] Y. Schröder, Phys. Lett. B 447 (1999) 321;
Y. Schröder, Ph.D. Thesis, Hamburg University, 1999, Report No. DESY-THESIS-1999-021.

[9] B.A. Kniehl, A.A. Penin, V.A. Smirnov, M. Steinhauser, Phys. Rev. D 65 (2002) 091503(R).

[10] T. Appelquist, M. Dine, I.J. Muzinich, Phys. Rev. D 17 (1978) 2074;
N. Brambilla, A. Pineda, J. Soto, A. Vairo, Phys. Rev. D 60 (1999) 091502.

[11] B.A. Kniehl, A.A. Penin, V.A. Smirnov, M. Steinhauser, Nucl. Phys. B 635 (2002) 357.

[12] A.A. Penin, M. Steinhauser, Phys. Lett. B 538 (2002) 335.

[13] M. Beneke, V.A. Smirnov, Nucl. Phys. B 522 (1998) 321;
V.A. Smirnov, Applied Asymptotic Expansions in Momenta and Masses, Springer Tracts in Modern Physics, vol. 177, Springer-Verlag, Heidelberg, 2001.

[14] N. Brambilla, A. Pineda, J. Soto, A. Vairo, Phys. Rev. D 63 (2001) 014023.

[15] V.A. Smirnov, M. Steinhauser, Nucl. Phys. B 672 (2003) 199.

[16] K.G. Chetyrkin, F.V. Tkachov, Nucl. Phys. B 192 (1981) 159;
F.V. Tkachov, Phys. Lett. B 100 (1981) 65.

[17] V.A. Smirnov, Evaluating Feynman Integrals, Springer Tracts in Modern Physics, vol. 211, Springer-Verlag, Heidelberg, 2004.

[18] P.A. Baikov, Phys. Lett. B 385 (1996) 404;
P.A. Baikov, Nucl. Instrum. Methods A 389 (1997) 347.

[19] Y. Schröder, Nucl. Phys. B (Proc. Suppl.) 116 (2003) 402;
K. Kajantie, M. Laine, K. Rummukainen, Y. Schröder, JHEP 0304 (2003) 036.

[20] S. Laporta, Int. J. Mod. Phys. A 15 (2000) 5087.

[YS11]

Two-loop QCD gauge coupling at high temperatures

Two-loop QCD gauge coupling at high temperatures

Mikko Laine and York Schröder

Faculty of Physics, University of Bielefeld
D-33501 Bielefeld, Germany
E-mail: `laine@physik.uni-bielefeld.de`, `yorks@physik.uni-bielefeld.de`

Abstract: We determine the 2-loop effective gauge coupling of QCD at high temperatures, defined as a matching coefficient appearing in the dimensionally reduced effective field theory. The result allows to improve on one of the classic non-perturbative probes for the convergence of the weak-coupling expansion at high temperatures, the comparison of full and effective theory determinations of an observable called the spatial string tension. We find surprisingly good agreement almost down to the critical temperature of the deconfinement phase transition. We also determine one new contribution of order $\mathcal{O}(g^6 T^4)$ to the pressure of hot QCD.

Keywords: Lattice Gauge Field Theories, Thermal Field Theory, QCD, NLO Computations.

Contents

1. Introduction

Indirect signs for rapid thermalisation after heavy ion collisions at RHIC energies, derived for instance from the fact that hydrodynamic models assuming local thermodynamic equilibrium appear to work very well [1], have underlined the need to understand the physics of thermal QCD at temperatures above a few hundred MeV.

Given asymptotic freedom, a natural tool for these studies is the weak-coupling expansion [2]. Alas, it has been known since a long time that the weak-coupling expansion converges very slowly at all realistic temperatures [3, 4]. It also has theoretically a non-trivial structure, with odd powers of the gauge coupling [5] and even coefficients that can only be determined non-perturbatively [6, 7].

On the other hand, the degrees of freedom responsible for the slow convergence can be identified [8–10]: they are the "soft" static colour-electric modes, parametrically $p \sim gT$ (leading to the odd powers in the gauge coupling), as well as the "ultrasoft" static colour-magnetic modes, parametrically $p \sim g^2 T$ (leading to the non-perturbative coefficients in the weak-coupling expansion). Here p denotes the characteristic momentum scale, g the gauge coupling and T the temperature. The belief has been that perturbation theory restricted to parametrically hard scales $p \sim 2\pi T$ alone should converge well, while the soft and the ultrasoft scales need to be treated either with "improved" analytic schemes, or then non-perturbatively. As a starting point for these demanding tasks one may take, however, either the dimensionally reduced effective field theory [11, 12] or the hard thermal loop effective theory [13], which have been obtained by integrating out the parametrically hard scales.

– 1 –

Quantitative evidence for this picture can be obtained by choosing simple observables which can be determined reliably both with four-dimensional (4d) lattice simulations and with the soft/ultrasoft effective theory. This forces us to restrict to static observables and, for the moment, mostly pure gauge theory. Various comparisons of this kind are summarised in references [14–16]. The most precise results are related to static correlation lengths in various quantum number channels [17], where good agreement has generally been found down to $T \sim 2T_c$, where T_c is the critical temperature of the deconfinement phase transition. The thermodynamic pressure of QCD is also consistent with this picture [10], even though that comparison is not unambiguous yet, due to the fact that the effective theory approach does not directly produce the physical number, but requires not-yet-determined ultraviolet matching coefficients for its interpretation [18].[1]

The purpose of this paper is to study another observable for which an unambiguous comparison is possible. The observable is the "spatial string tension", σ_s. 4d lattice determinations of σ_s in pure SU(3) gauge theory exist since a while already [22] but, as has most recently been stressed in reference [23], the comparison with effective theory results shows a clear discrepancy. In order to improve on the resolution on the effective theory side, we compute here the gauge coupling of the dimensionally reduced theory up to 2-loop order. Combining with other ingredients [24, 25], to be specified below, allows then for a precise comparison. We find that once the 2-loop corrections are included, the match to 4d lattice data improves quite significantly and supports the picture outlined above.

The plan of this paper is the following. In section 2 we present the 2-loop computation of the effective gauge coupling of the dimensionally reduced theory. In section 3 we discuss the numerical evaluation of this result. In section 4 we use the outcome for estimating the spatial string tension, and compare with 4d lattice data. We conclude in section 5.

2. Effective gauge coupling

We consider finite temperature QCD with the gauge group $SU(N_c)$, and N_f flavours of massless quarks. In dimensional regularisation the bare euclidean lagrangian reads, before gauge fixing,

$$S_{QCD} = \int_0^\beta d\tau \int d^d x \, \mathcal{L}_{QCD} \,, \tag{2.1}$$

$$\mathcal{L}_{QCD} = \frac{1}{4} F_{\mu\nu}^a F_{\mu\nu}^a + \bar{\psi}\gamma_\mu D_\mu \psi \,, \tag{2.2}$$

where $\beta = T^{-1}$, $d = 3 - 2\epsilon$, $\mu, \nu = 0, \ldots, d$, $F_{\mu\nu}^a = \partial_\mu A_\nu^a - \partial_\nu A_\mu^a + g_B f^{abc} A_\mu^b A_\nu^c$, $D_\mu = \partial_\mu - i g_B A_\mu$, $A_\mu = A_\mu^a T^a$, T^a are hermitean generators of $SU(N_c)$ normalised such that $\text{Tr}\,[T^a T^b] = \delta^{ab}/2$, $\gamma_\mu^\dagger = \gamma_\mu$, $\{\gamma_\mu, \gamma_\nu\} = 2\delta_{\mu\nu}$, g_B is the bare gauge coupling, and ψ carries Dirac, colour, and flavour indices. We use the standard symbols $C_A = N_c, C_F = (N_c^2 - 1)/(2N_c), T_F = N_f/2$ for the various group theory factors emerging.

---

[1] For the status regarding a few other observables, see references [19–21].

At high enough temperatures, the dynamics of eq. (2.2) is contained in a simpler, dimensionally reduced effective field theory [11, 12, 8]:

$$S_{\text{EQCD}} = \int \mathrm{d}^d x \mathcal{L}_{\text{EQCD}}\,, \tag{2.3}$$

$$\mathcal{L}_{\text{EQCD}} = \frac{1}{4}\, F_{ij}^a F_{ij}^a + \text{Tr}\,[D_i, B_0]^2 + m_{\text{E}}^2 \text{Tr}\,[B_0^2] + \lambda_{\text{E}}^{(1)}(\text{Tr}\,[B_0^2])^2 + \lambda_{\text{E}}^{(2)}\text{Tr}\,[B_0^4] + \cdots\,. \tag{2.4}$$

Here $i = 1, \ldots, d$, $F_{ij} = \partial_i B_j^a - \partial_j B_i^a + g_{\text{E}} f^{abc} B_i^b B_j^c$, and $D_i = \partial_i - ig_{\text{E}} B_i$. The fields B_μ^a have the dimension $[\text{GeV}]^{1/2-\epsilon}$, due to a trivial rescaling with $T^{1/2}$. Note also that the quartic couplings $\lambda_{\text{E}}^{(1)}$, $\lambda_{\text{E}}^{(2)}$ are linearly dependent for $N_c \leq 3$, since then $\text{Tr}\,[B_0^4] = \frac{1}{2}\,(\text{Tr}\,[B_0^2])^2$.

The theory in eq. (2.4) has been truncated to be super-renormalisable; that is, higher order operators [27] (see also references [28, 29] and references therein) have been dropped. The relative error thus induced has been discussed for generic Green's functions in reference [30], and for the particular case of the pressure of hot QCD in reference [10]. In the following we concentrate on an observable dynamically determined by the colour-magnetic scale $p \sim g^2 T$, and it is easy to see that in this case the higher order operators do not play any role at the order we are working.

The effective parameters in eq. (2.4) can be determined by matching, that is, by requiring that QCD and EQCD produce the same results, within the domain of validity of the latter theory. It is essential that infrared (IR) physics be treated in the same way in both theories at the matching stage and, as outlined in reference [8], the most convenient implementation of this requirement is to perform computations on both sides using "unresummed" propagators. We follow this procedure here.

The matching simplifies further by using the background field gauge (reference [31] and references therein). As this is essential for what follows, we start by briefly recalling the basic advantage of this approach. For a concise yet rigorous overview of the technique, see reference [32].

We denote the background gauge potential with B_μ^a, and the gauge-invariant combination following from $F_{\mu\nu}^a(B)F_{\mu\nu}^a(B)$ symbolically as $B^2 + gB^3 + g^2 B^4$. Now, the computation of the effective Lagrangian by integrating out the hard scales $p \sim 2\pi T$ produces, in general, an expression of the type

$$\mathcal{L}_{\text{eff}} \sim c_2 B^2 + c_3\, g B^3 + c_4 g^2 B^4 + \cdots\,, \tag{2.5}$$

where c_i are coefficients of the form $c_i = 1 + \mathcal{O}(g^2)$. As the next step we are free to define a canonically normalised effective field B_{eff} as $B_{\text{eff}}^2 \equiv c_2 B^2$. Then the effective Lagrangian obtains the form

$$\mathcal{L}_{\text{eff}} \sim B_{\text{eff}}^2 + c_3 c_2^{-3/2}\, g B_{\text{eff}}^3 + c_4 c_2^{-2}\, g^2 B_{\text{eff}}^4 + \cdots\,. \tag{2.6}$$

We can now read off the effective gauge coupling from the gauge-invariant structure:

$$g_{\text{eff}} = c_3 c_2^{-3/2}\, g = c_4^{1/2} c_2^{-1} g\,. \tag{2.7}$$

We observe that two independent computations are needed for the determination of g_{eff}, but we can choose whether to go through the 3-point or the 4-point function, in addition to the 2-point function (that is, using c_3 or c_4, in addition to c_2).
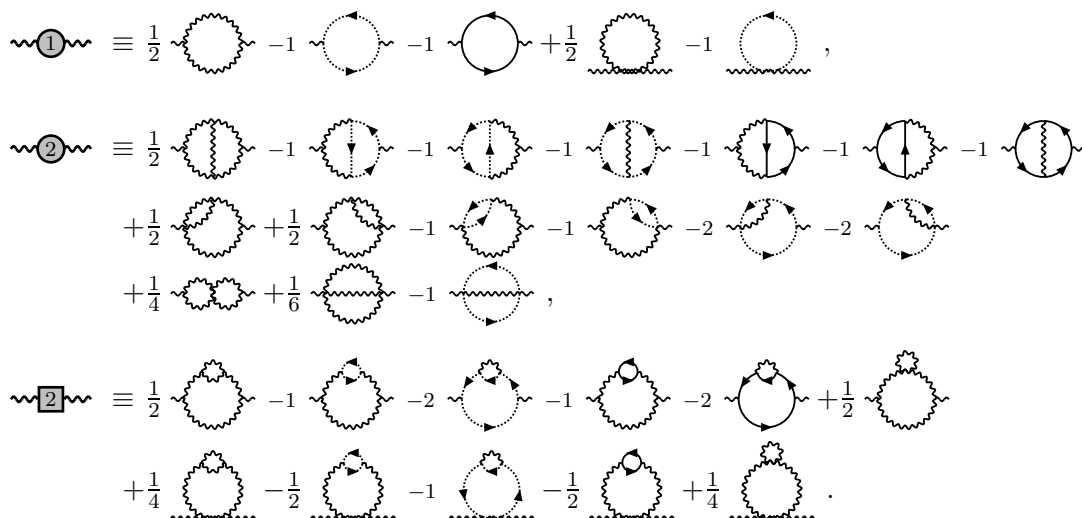
Figure 1: The 1-loop and 2-loop self-energy diagrams in the background field gauge. Wavy lines represent gauge fields, dotted lines ghosts, and solid lines fermions. The 2-loop graphs have been divided into two-particle-irreducible and two-particle-reducible contributions.

The background field gauge economises this setup. Indeed, the effective action is then gauge-invariant not only in terms of B_{eff}, but also in terms of the original field B [31]. Writing equation (2.5) as

$$\mathcal{L}_{\text{eff}} \sim c_2 \left[B^2 + c_3 c_2^{-1} g B^3 + c_4 c_2^{-1} g^2 B^4 \right] + \cdots, \tag{2.8}$$

gauge invariance in terms of B now tells us that $c_3 = c_2$ and $c_4 = c_2$. Combining with equation (2.7), we obtain

$$g_{\text{eff}} = c_2^{-1/2} g, \tag{2.9}$$

so that it is enough to carry out one single 2-point computation, in order to obtain g_{eff}. In our case, the role of g_{eff} is played by g_{E} (cf. equation (2.4)).

The class of background field gauges still allows for a general (bare) gauge parameter, ξ. As a cross-check we have carried out all computations with a general ξ, and verified that it cancels at the end. To be definite, we denote $(\xi)_{\text{here}} = 1 - (\xi)_{\text{standard}}$, so that the gauge field propagator reads

$$\left\langle A_\mu^a(q) A_\nu^b(-q) \right\rangle = \delta^{ab} \left[\frac{\delta_{\mu\nu}}{q^2} - \xi \frac{q_\mu q_\nu}{(q^2)^2} \right]. \tag{2.10}$$

In order to match the effective gauge coupling, we need to compute the 2-loop gluon self-energy, $\Pi_{\mu\nu}(p)$, for the background gauge potential B_μ^a. The graphs entering are shown in fig. 1. The external momentum p is taken purely spatial, $p = (0, \mathbf{p})$, while the heat bath is timelike, with euclidean four-velocity $u = (1, 0)$, so that $u \cdot u = 1, u \cdot p = 0$. In this case $\Pi_{\mu\nu}$ has three independent components (Π_{0i}, Π_{i0} vanish identically),

$$\Pi_{00}(\mathbf{p}) \equiv \Pi_{\text{E}}(\mathbf{p}^2), \qquad \Pi_{ij}(\mathbf{p}) \equiv \left(\delta_{ij} - \frac{p_i p_j}{\mathbf{p}^2} \right) \Pi_{\text{T}}(\mathbf{p}^2) + \frac{p_i p_j}{\mathbf{p}^2} \Pi_{\text{L}}(\mathbf{p}^2), \tag{2.11}$$

where $i, j = 1, \ldots, d$. In fact loop corrections to the spatially longitudinal part Π_{L} also vanish, so that only two non-trivial functions, $\Pi_{\text{E}}, \Pi_{\text{T}}$, remain.

Since we are carrying out a matching computation, any possible IR divergences cancel as we subtract the contribution of EQCD. Therefore we may Taylor-expand $\Pi_{\mu\nu}(p)$ to second order in $\mathbf{p}^2$. This leads to the nice simplification that the results on the EQCD side vanish identically in dimensional regularization, due to the absence of any mass scales in the propagators. Thus we only need to compute unresummed integrals on the QCD side.

After the Taylor-expansion, the 2-loop QCD integrals can all be cast in the form

$$I(i_1, i_2; j_1, j_2, j_3; k_1, k_2, k_3) \equiv \sum\!\!\!\!\!\!\!\!\int_{q,r} \frac{q_0^{i_1} r_0^{i_2} (\mathbf{q} \cdot \mathbf{p})^{j_1} (\mathbf{r} \cdot \mathbf{p})^{j_2} (\mathbf{q} \cdot \mathbf{r})^{j_3}}{[q_0^2 + \mathbf{q}^2]^{k_1} [r_0^2 + \mathbf{r}^2]^{k_2} [(q_0 + r_0)^2 + (\mathbf{q} + \mathbf{r})^2]^{k_3}} \,. \qquad (2.12)$$

The indices here are non-negative integers, and the measure is the standard Matsubara sum-integral (bosonic or fermionic), with the spatial part $\int \mathrm{d}^d\mathbf{q}/(2\pi)^d \int \mathrm{d}^d\mathbf{r}/(2\pi)^d$.

To reduce integrals of the type in eq. (2.12) to a small set of "master integrals", we employ symmetries following from exchanges of integration variables, as well as general partial integration identities for the spatial parts of the momentum integrations. The implementation of these identities follows the procedure outlined by Laporta [33], in analogy with reference [34]. We are lead both to very simple 1-loop recursion relations, such as

$$I(2i_1, 0; 0, 0, 0; k_1, 1, 0) = \frac{2k_1 - 2 - d}{2k_1 - 2} I(2i_1 - 2, 0; 0, 0, 0; k_1 - 1, 1, 0) \,, \qquad (2.13)$$

as well as well-known but less obvious 2-loop ones [35], like

$$I(0, 0; 0, 0, 0; 1_\mathrm{b}, 1_\mathrm{b}, 1_\mathrm{b}) = 0 \,, \qquad (2.14)$$

where the subscripts refer to bosonic four-momenta.

After this reduction, only six master integrals remain:

$$I_\mathrm{b}(n) = \sum\!\!\!\!\!\!\!\!\int_{q_\mathrm{b}} \frac{1}{(q^2)^n} \,, \qquad I_\mathrm{f}(n) = \sum\!\!\!\!\!\!\!\!\int_{q_\mathrm{f}} \frac{1}{(q^2)^n} \,, \qquad (2.15)$$

where $q_\mathrm{b}, q_\mathrm{f}$ refer to bosonic and fermionic Matsubara momenta, respectively, and $n = 1, 2, 3$. For a vanishing quark chemical potential, as we assume to be the case here, the fermionic integrals reduce further to the bosonic ones,

$$I_\mathrm{f}(n) = \left(2^{2n-d} - 1 \right) I_\mathrm{b}(n) \,, \qquad (2.16)$$

leaving only three master integrals. They are known explicitly,

$$I_\mathrm{b}(n) = \frac{2\pi^{d/2} T^{1+d}}{(2\pi T)^{2n}} \frac{\Gamma(n - d/2)}{\Gamma(n)} \zeta(2n - d) \,. \qquad (2.17)$$

This expression is easily expanded in ϵ and, in the following, we need terms up to $\mathcal{O}(\epsilon)$. For completeness, the relevant expansions are shown in appendix A.

Writing now the Taylor-expanded bare 2-point function Π_T of equation (2.11) as

$$\begin{aligned} \Pi_\mathrm{T}(\mathbf{p}^2) &\equiv \Pi_\mathrm{T}(0) + \mathbf{p}^2 \Pi_\mathrm{T}'(0) + \cdots \\ &\equiv \sum_{n=1}^{\infty} \Pi_\mathrm{Tn}(0)(g_B^2)^n + \mathbf{p}^2 \sum_{n=1}^{\infty} \Pi_\mathrm{Tn}'(0)(g_B^2)^n + \cdots \,, \end{aligned} \qquad (2.18)$$

where g_B is the bare gauge coupling, and correspondingly for Π_{E}, our results read

$$\Pi_{\mathrm{T}1}(0) = 0, \tag{2.19}$$

$$\Pi'_{\mathrm{T}1}(0) = \frac{d-25}{6}C_A I_{\mathrm{b}}(2) + \frac{4}{3}T_F I_{\mathrm{f}}(2), \tag{2.20}$$

$$\Pi_{\mathrm{T}2}(0) = 0, \tag{2.21}$$

$$\begin{aligned}
\Pi'_{\mathrm{T}2}(0) = \frac{(d-3)(d-4)}{d(d-2)(d-5)(d-7)}\Big\{ &2(4d^2-21d-7)C_A^2 I_{\mathrm{b}}^2(2) - \\
&- 8\Big[4C_F + (d^2-6d+1)C_A\Big]T_F I_{\mathrm{b}}(2)I_{\mathrm{f}}(2) - \\
&- \Big[(d^3-12d^2+39d-12)C_A - \\
&- 2(d^3-12d^2+41d-14)C_F\Big]T_F I_{\mathrm{f}}^2(2)\Big\} + \\
+ \frac{(d-1)}{3d(d-7)}\Big\{ &(d^2-31d+144)\Big[4T_F I_{\mathrm{f}}(1) - (d-1)C_A I_{\mathrm{b}}(1)\Big]C_A I_{\mathrm{b}}(3) - \\
&- 8(d-1)(d-6)C_F T_F\Big[I_{\mathrm{b}}(1) - I_{\mathrm{f}}(1)\Big]I_{\mathrm{f}}(3)\Big\},
\end{aligned} \tag{2.22}$$

$$\Pi_{\mathrm{E}1}(0) = -(d-1)\Big[4T_F I_{\mathrm{f}}(1) - (d-1)C_A I_{\mathrm{b}}(1)\Big], \tag{2.23}$$

$$\Pi'_{\mathrm{E}1}(0) = -\Big[\frac{d^2-5d+28}{6} + (d-3)\xi\Big]C_A I_{\mathrm{b}}(2) + \frac{2(d-1)}{3}T_F I_{\mathrm{f}}(2), \tag{2.24}$$

$$\begin{aligned}
\Pi_{\mathrm{E}2}(0) = (d-1)(d-3)\Big\{ &(1+\xi)\Big[4T_F I_{\mathrm{f}}(1) - (d-1)C_A I_{\mathrm{b}}(1)\Big]C_A I_{\mathrm{b}}(2) + \\
&+ 4C_F T_F\Big[I_{\mathrm{b}}(1) - I_{\mathrm{f}}(1)\Big]I_{\mathrm{f}}(2)\Big\}.
\end{aligned} \tag{2.25}$$

We leave out the lengthy expression for $\Pi'_{\mathrm{E}2}(0)$, as it is not needed in the following.

The bare results need still to be renormalised. The bare gauge coupling is written as $g_B^2 = g^2(\bar{\mu})Z_g$, where $g^2(\bar{\mu})$ is the renormalised gauge coupling, $\bar{\mu}$ is an $\overline{\mathrm{MS}}$ scheme scale parameter introduced through $\mu^2 \equiv \bar{\mu}^2 e^{\gamma_{\mathrm{E}}}/4\pi$, and the combination $\mu^{-2\epsilon}g^2(\bar{\mu})$ is dimensionless. Denoting

$$\beta_0 \equiv \frac{-22C_A + 8T_F}{3}, \tag{2.26}$$

$$\beta_1 \equiv \frac{-68C_A^2 + 40C_A T_F + 24C_F T_F}{3}, \tag{2.27}$$

the factor Z_g reads

$$Z_g = 1 + \frac{1}{(4\pi)^2}\frac{\beta_0}{2\epsilon}\mu^{-2\epsilon}g^2(\bar{\mu}) + \frac{1}{(4\pi)^4}\Big[\frac{\beta_1}{4\epsilon} + \frac{\beta_0^2}{4\epsilon^2}\Big]\mu^{-4\epsilon}g^4(\bar{\mu}) + \mathcal{O}(g^6), \tag{2.28}$$

and the renormalised gauge coupling satisfies, in the limit $\epsilon \to 0$,

$$\bar{\mu}\frac{\mathrm{d}}{\mathrm{d}\bar{\mu}}g^2(\bar{\mu}) = \frac{\beta_0}{(4\pi)^2}g^4(\bar{\mu}) + \frac{\beta_1}{(4\pi)^4}g^6(\bar{\mu}) + \mathcal{O}(g^8). \tag{2.29}$$

To proceed, we first cross-check our results for $\Pi_{\rm E}$ against known expressions. After the fields B_0^a of EQCD are normalised to their canonical form (cf. eq. (2.6)), $(B_0^a B_0^a)_{\rm E}\,\mathbf{p}^2 \equiv (B_0^a B_0^a)_{\rm 4d}\,\mathbf{p}^2[1 + \Pi'_{\rm E1}(0)]/T$, we obtain for the matching coefficient $m_{\rm E}^2$,

$$m_{\rm E}^2 = g_B^2\,\Pi_{\rm E1}(0) + g_B^4\left[\Pi_{\rm E2}(0) - \Pi'_{\rm E1}(0)\Pi_{\rm E1}(0)\right] + \mathcal{O}(g_B^6)\,. \tag{2.30}$$

Inserting eqs. (2.23)–(2.25), the ξ-dependence duly cancels. Re-expanding also g_B^2 in terms of the renormalised gauge coupling, and writing then [10]

$$m_{\rm E}^2 \equiv T^2\left\{g^2(\bar{\mu})\Big[\alpha_{\rm E4} + \alpha_{\rm E5}\epsilon\Big] + \frac{g^4(\bar{\mu})}{(4\pi)^2}\Big[\alpha_{\rm E6} + \beta_{\rm E2}\epsilon\Big] + \mathcal{O}(g^6,\epsilon^2)\right\}, \tag{2.31}$$

we recover the known values of $\alpha_{\rm E4}$, $\alpha_{\rm E5}$ and $\alpha_{\rm E6}$ [10] (for original derivations, see reference [8] and references therein). We also obtain

$$
\begin{aligned}
\beta_{\rm E2} = {}& \frac{1}{36}C_A^2\bigg\{264\ln^2\!\left(\frac{\bar{\mu}e^{\gamma_{\rm E}}}{4\pi T}\right) + \left[80 - 176\gamma_{\rm E} + 176\frac{\zeta'(-1)}{\zeta(-1)}\right]\ln\!\left(\frac{\bar{\mu}e^{\gamma_{\rm E}}}{4\pi T}\right) + \\
& + 8 + 11\pi^2 - 88\gamma_{\rm E}^2 - 40\gamma_{\rm E} - 176\gamma_1 + 40\frac{\zeta'(-1)}{\zeta(-1)}\bigg\} + \\
& + C_F T_F\bigg\{-8\ln\!\left(\frac{\bar{\mu}e^{\gamma_{\rm E}}}{4\pi T}\right) - 2 - \frac{20}{3}\ln 2 + 4\gamma_{\rm E} - 4\frac{\zeta'(-1)}{\zeta(-1)}\bigg\} + \\
& + \frac{1}{36}C_A T_F\bigg\{168\ln^2\!\left(\frac{\bar{\mu}e^{\gamma_{\rm E}}}{4\pi T}\right) + \left[232 - 432\ln 2 - 112\gamma_{\rm E} + 112\frac{\zeta'(-1)}{\zeta(-1)}\right]\ln\!\left(\frac{\bar{\mu}e^{\gamma_{\rm E}}}{4\pi T}\right) + \\
& + 28 + 7\pi^2 + 24\ln 2 - 64\ln^2 2 - 56\gamma_{\rm E}^2 - 72\gamma_{\rm E} + 128\gamma_{\rm E}\ln 2 - 112\gamma_1 + \\
& + 72\frac{\zeta'(-1)}{\zeta(-1)} - 128\ln 2\frac{\zeta'(-1)}{\zeta(-1)}\bigg\} + \\
& + \frac{1}{9}T_F^2\bigg\{-24\ln^2\!\left(\frac{\bar{\mu}e^{\gamma_{\rm E}}}{4\pi T}\right) + \left[8 - 48\ln 2 + 16\gamma_{\rm E} - 16\frac{\zeta'(-1)}{\zeta(-1)}\right]\ln\!\left(\frac{\bar{\mu}e^{\gamma_{\rm E}}}{4\pi T}\right) + \\
& + 4 - \pi^2 - 8\ln 2 + 16\ln^2 2 + 8\gamma_{\rm E}^2 - 8\gamma_{\rm E} + 32\gamma_{\rm E}\ln 2 + 16\gamma_1 + \\
& + 8\frac{\zeta'(-1)}{\zeta(-1)} - 32\ln 2\frac{\zeta'(-1)}{\zeta(-1)}\bigg\}.
\end{aligned} \tag{2.32}
$$

Here γ_1 is a Stieltjes constant, defined through the series $\zeta(s) = 1/(s-1) + \sum_{n=0}^{\infty}\gamma_n(-1)^n(s-1)^n/n!$. (Note that the Euler gamma-constant is $\gamma_{\rm E} \equiv \gamma_0$.) The result in eq. (2.32), first obtained in reference [37] by employing the results of reference [8], contributes to the pressure of hot QCD at $\mathcal{O}(g^6 T^4)$ [10]. We rewrite the expression here, since reference [37] employed an extremely compactified notation.

We then move to consider the transverse spatial part, $\Pi_{\rm T}(\mathbf{p}^2)$. According to eq. (2.9), this directly determines the effective gauge coupling:

$$g_{\rm E}^2 = T\left\{g_B^2 - g_B^4\Pi'_{T1}(0) + g_B^6\left[\left(\Pi'_{T1}(0)\right)^2 - \Pi'_{T2}(0)\right] + \mathcal{O}(g_B^8)\right\}. \tag{2.33}$$

Re-expanding again in terms of $g^2(\bar{\mu})$, we parameterise the result (following ref. [10]) as

$$g_{\rm E}^2 \equiv T\left\{g^2(\bar{\mu}) + \frac{g^4(\bar{\mu})}{(4\pi)^2}\left[\alpha_{\rm E7} + \beta_{\rm E3}\epsilon + \mathcal{O}(\epsilon^2)\right] + \frac{g^6(\bar{\mu})}{(4\pi)^4}\left[\gamma_{\rm E1} + \mathcal{O}(\epsilon)\right] + \mathcal{O}(g^8)\right\}. \tag{2.34}$$

We recover the known expression [36, 12] for α_{E7},

$$\alpha_{\mathrm{E7}} = -\beta_0 \ln\left(\frac{\bar{\mu}e^{\gamma_{\mathrm{E}}}}{4\pi T}\right) + \frac{1}{3} C_A - \frac{16}{3}T_F \ln 2 \,, \tag{2.35}$$

and obtain the new contributions

$$\beta_{\mathrm{E3}} = \frac{1}{12}C_A \left[88\ln^2\left(\frac{\bar{\mu}e^{\gamma_{\mathrm{E}}}}{4\pi T}\right) + 8\ln\left(\frac{\bar{\mu}e^{\gamma_{\mathrm{E}}}}{4\pi T}\right) + 11\pi^2 - 88\gamma_{\mathrm{E}}^2 - 176\gamma_1\right] -$$
$$- \frac{1}{3}T_F \left[8\ln^2\left(\frac{\bar{\mu}e^{\gamma_{\mathrm{E}}}}{4\pi T}\right) + 32\ln 2\ln\left(\frac{\bar{\mu}e^{\gamma_{\mathrm{E}}}}{4\pi T}\right) + \pi^2 + 16\ln^2 2 - 8\gamma_{\mathrm{E}}^2 - 16\gamma_1\right], \quad (2.36)$$

$$\gamma_{\mathrm{E1}} = -\beta_1 \ln\left(\frac{\bar{\mu}e^{\gamma_{\mathrm{E}}}}{4\pi T}\right) + \left[\beta_0 \ln\left(\frac{\bar{\mu}e^{\gamma_{\mathrm{E}}}}{4\pi T}\right) - \frac{1}{3} C_A + \frac{16}{3}T_F \ln 2\right]^2 -$$
$$- \frac{1}{18}\left\{C_A^2\left[-341 + 20\zeta(3)\right] + 4C_A T_F\left[43 + 24\ln 2 + 5\zeta(3)\right] +\right.$$
$$\left. + 6C_F T_F\left[23 + 80\ln 2 - 14\zeta(3)\right]\right\}. \tag{2.37}$$

The first one, β_{E3}, constitutes again an $\mathcal{O}(g^6T^4)$ contribution to the pressure of hot QCD [10], while the latter one is the desired finite 2-loop correction to the effective gauge coupling.

3. Numerical evaluation

We wish to compare numerically the 1-loop and 2-loop expressions for g_{E}^2, in the limit $\epsilon \to 0$. When carrying out such a comparison, it is important to specify the definitions of the $\Lambda_{\overline{\mathrm{MS}}}$-parameters. Following standard procedures, we solve eq. (2.29) exactly at 2-loop level, and define

$$\Lambda_{\overline{\mathrm{MS}}} \equiv \lim_{\bar{\mu}\to\infty} \bar{\mu} \left[b_0 g^2(\bar{\mu})\right]^{-b_1/2b_0^2} \exp\left[-\frac{1}{2b_0 g^2(\bar{\mu})}\right], \tag{3.1}$$

where $b_0 \equiv -\beta_0/2(4\pi)^2$, $b_1 \equiv -\beta_1/2(4\pi)^4$. For large $\bar{\mu}$ this leads to the usual behaviour

$$\frac{1}{g^2(\bar{\mu})} \approx 2b_0 \ln\frac{\bar{\mu}}{\Lambda_{\overline{\mathrm{MS}}}} + \frac{b_1}{b_0}\ln\left(2\ln\frac{\bar{\mu}}{\Lambda_{\overline{\mathrm{MS}}}}\right). \tag{3.2}$$

In the 1-loop case, we set $b_1 \equiv 0$ in eqs. (3.1), (3.2).

Through eqs. (2.34), (2.35), (2.37) and (3.2), g_{E}^2 is a function $\bar{\mu}/T$ and $\bar{\mu}/\Lambda_{\overline{\mathrm{MS}}}$. The dependence on $\bar{\mu}$ is formally of higher order than the computation. Numerically, of course, there is non-vanishing dependence, as illustrated in figure 2.

As usual, one may choose some "optimisation" criterion which should lead to a reduced $\bar{\mu}$-dependence and thus reasonable convergence. We fix $\bar{\mu}_{\mathrm{opt}}$ to be the point where the 1-loop coupling g_{E}^2 has vanishing slope ("principal of minimal sensitivity"), cf. figure 2, and vary then the scale in the range $\bar{\mu} = (0.5\ldots 2.0)\times\bar{\mu}_{\mathrm{opt}}$ around this point. Results are shown in fig. 3. The $\bar{\mu}$-dependence indeed decreases significantly as we go to the 2-loop level. The numerical 2-loop value is some 20% smaller than the 1-loop value. It is comforting that the 2-loop value is on the side to which the "error band" of the 1-loop result points, even though it does not in general lie within that band.
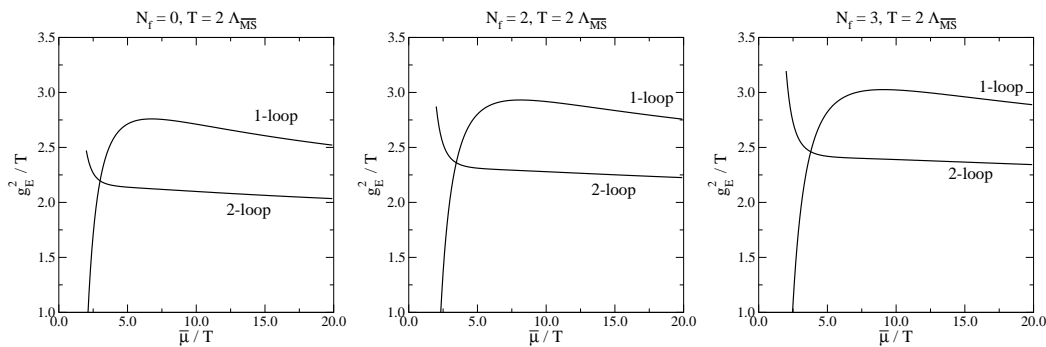
Figure 2: A comparison of 1-loop and 2-loop values for $g_{\rm E}^2/T$, as a function of $\bar{\mu}/T$, for a fixed $T/\Lambda_{\overline{\rm MS}} = 2.0$ and $N_{\rm f} = 0, 2, 3$.
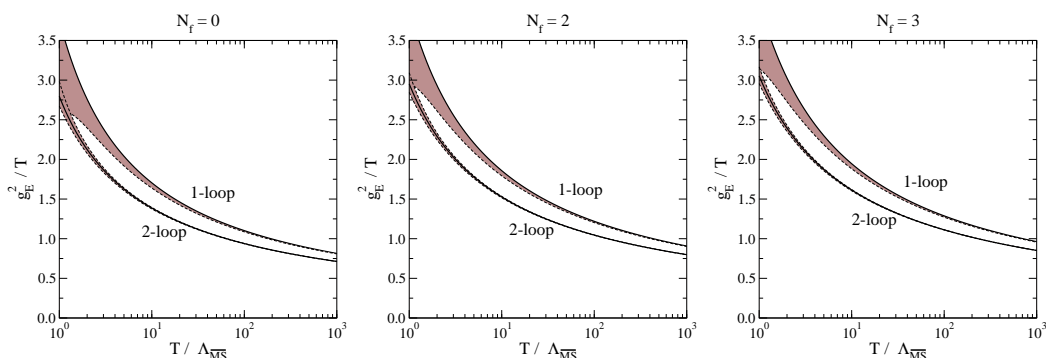
Figure 3: The 1-loop and 2-loop values for $g_{\rm E}^2/T$, as a function of $T/\Lambda_{\overline{\rm MS}}$ (solid lines). For each T the scale $\bar{\mu}$ has been fixed to the "principal of minimal sensitivity" point $\bar{\mu}_{\rm opt}$ following from the 1-loop expression, and varied then in the range $\bar{\mu} = (0.5 \dots 2.0) \times \bar{\mu}_{\rm opt}$ (the grey bands).

4. Spatial string tension

The computations in the previous sections can be given a "phenomenological" application, by considering lattice measurements of the so-called spatial string tension. The spatial string tension is obtained from a rectangular Wilson loop $W_s(R_1, R_2)$ in the (x_1, x_2)-plane, of size $R_1 \times R_2$. The potential $V_s(R_1)$ is defined through

$$V_s(R_1) = - \lim_{R_2 \to \infty} \frac{1}{R_2} \ln W_s(R_1, R_2) \,, \tag{4.1}$$

and the spatial string tension σ_s from the asymptotic behaviour of the potential,

$$\sigma_s \equiv \lim_{R_1 \to \infty} \frac{V_s(R_1)}{R_1} \,. \tag{4.2}$$

Since σ_s has the dimensionality GeV^2, it is often expressed [22] as the combination

$$\frac{\sqrt{\sigma_s}}{T} = \phi\Big(\frac{T}{T_{\rm c}}\Big) \,, \tag{4.3}$$

where ϕ is a (decreasing) dimensionless function, and $T_{\rm c}$ is the critical temperature of the deconfinement phase transition.

We now turn to how the result for g_E^2 that we have obtained in this paper, combined with other ingredients, allow us to obtain an independent prediction for the spatial string tension.

4.1 Three-dimensional prediction

The very same observable as in eq. (4.1), exists also in 3d SU(3) gauge theory, or "Magnetostatic QCD" (MQCD). Since the gauge coupling g_M^2 of MQCD is dimensionful, σ_s must have the form $\sigma_s = c \times g_M^4$, where c is a numerical proportionality constant. It has been determined with lattice Monte Carlo methods most recently in reference [24] where, after the continuum extrapolation, it was expressed as

$$\frac{\sqrt{\sigma_s}}{g_M^2} = 0.553(1)\,. \tag{4.4}$$

In order to compare eqs. (4.3), (4.4), we need a relation between T and g_M^2. In the previous section, we obtained a relation between T and g_E^2. The relation between g_E^2 and g_M^2 is also known, up to 2-loop order [25]:[2]

$$g_M^2 = g_E^2 \left[1 - \frac{1}{48} \frac{g_E^2 C_A}{\pi m_E} - \frac{17}{4608} \left(\frac{g_E^2 C_A}{\pi m_E} \right)^2 \right], \tag{4.5}$$

where the 1-loop part was determined already in reference [26].

It is worth stressing that the corrections in eq. (4.5) are in practice extremely small, even for values of m_E/g_E^2 corresponding to temperatures very close to the critical one. (For $N_c = 3$ and $N_f = 0$, $(m_E/g_E^2)^2 \approx 0.32 \log_{10}(T/\Lambda_{\overline{\rm MS}}) + 0.29$.) This seems by no means obvious *a priori*, given the observed slow convergence in the case of the vacuum energy density of EQCD [10]. In view of this fact, however, we can safely ignore all higher loop corrections in eq. (4.5).

Another source of errors in going from EQCD to MQCD are the higher order operators that have been truncated from the action of MQCD. As discussed in reference [10], they are expected to contribute at the relative order $\mathcal{O}(g_E^6/m_E^3)$, i.e. at the same order that 3-loop corrections enter eq. (4.5). From this consideration, one might expect them to again be numerically negligible. In principle one could avoid this assumption, however: the ratio $\sqrt{\sigma_s}/g_E^2$ has been estimated in reference [17] through direct numerical simulations in EQCD. Unfortunately the statistical and particularly the systematic errors appear to be non-vanishing (no continuum extrapolation was carried out for this quantity), so that we prefer to follow the line starting from eq. (4.4) in the following. Nevertheless it would be interesting to learn more about the importance of the higher order operators.

Now, as we know g_E^2/T as a function of $T/\Lambda_{\overline{\rm MS}}$ from fig. 3, eqs. (4.4) and (4.5) allow us to obtain $\sqrt{\sigma_s}/T$ as a function of the same variable. In order to compare with eq. (4.3), however, we still need to relate $\Lambda_{\overline{\rm MS}}$ to T_c. This problem has also been addressed with 4d lattice simulations, as we review in section 4.2.

---

[2]The 2-loop correction $\delta g_M^2/g_E^2 = -g_E^2 C_A[2(C_A C_F + 1)\lambda_E^{(1)} + (6C_F - C_A)\lambda_E^{(2)}]/384(\pi m_E)^2$ was ignored in reference [25], as it is of higher order according to 4d power counting and numerically insignificant.

4.2 Critical temperature in "perturbative units"

The determination of $T_c/\Lambda_{\overline{\text{MS}}}$ is a classic problem in lattice QCD. Two main lines have been followed, one going via the zero temperature string tension $\sqrt{\sigma}$, the other via the Sommer scale r_0 [38].

Values obtained for $T_c/\sqrt{\sigma}$ by various lattice collaborations are summarised in reference [39], Table 7. Traditionally the values were around $T_c/\sqrt{\sigma} = 0.630(5)$ [40], but reference [39] argues in favour of a slightly larger number in the continuum limit. Indeed the most precise estimate appears to come from reference [41], where $T_c/\sqrt{\sigma} = 0.646(3)$ is cited. Combining with $\Lambda_{\overline{\text{MS}}}/\sqrt{\sigma} = 0.555(19)$ from reference [42], we are lead to

$$\frac{T_c}{\Lambda_{\overline{\text{MS}}}} = 1.16(4)\,. \tag{4.6}$$

The error is dominated by the one in $\Lambda_{\overline{\text{MS}}}/\sqrt{\sigma}$.

A value for $r_0 T_c$, on the other hand, has been obtained in reference [43]: $r_0 T_c = 0.7498(50)$. Combining with $r_0 \Lambda_{\overline{\text{MS}}} = 0.602(48)$ from reference [44] (the value $r_0 \Lambda_{\overline{\text{MS}}} = 0.586(48)$ from a few lines below eq. (4.11) in reference [45] is well within error bars), one obtains

$$\frac{T_c}{\Lambda_{\overline{\text{MS}}}} = 1.25(10)\,. \tag{4.7}$$

This is consistent, within statistical errors, with eq. (4.6), if favouring a slightly larger central value. Again the error is dominated by the zero-temperature part, $r_0 \Lambda_{\overline{\text{MS}}}$ in this case. In general it might be expected, though, that systematic uncertainties are better under control in the extraction of r_0 than of $\sqrt{\sigma}$, since the static potential needs to be computed only up to intermediate distances.

Apart from going through $\sqrt{\sigma}$ and r_0, there is also a third possibility [46]. It is based on directly determining a (lattice) Λ-parameter from the scaling of a suitably defined renormalised gauge coupling at the critical point, and converting at the end to the $\overline{\text{MS}}$ scheme. The value obtained is

$$\frac{T_c}{\Lambda_{\overline{\text{MS}}}} = 1.15(5)\,, \tag{4.8}$$

consistent with eqs. (4.6) and (4.7).

To be conservative, we will consider the interval $T_c/\Lambda_{\overline{\text{MS}}} = 1.10 \ldots 1.35$ in the following, encompassing the central values as well as the error bars of eqs. (4.6)–(4.8).

4.3 Four-dimensional measurement

The spatial string tension of 4d pure SU(3) gauge theory at temperatures above the critical one, as a function of T/T_c, has been measured at $N_\tau = 8$ in reference [22] (cf. figure 11). There are, of course, systematic uncertainties, both from the lack of a continuum extrapolation as well as from how the string tension is extracted by fitting to the large-distance behaviour of the static potential. Nevertheless, we expect that the results are in the right ballpark.

Given the considerations in sections 4.1, 4.2, we can thus compare the 3d and the 4d determinations of $\sqrt{\sigma_s}/T$. The result is shown in fig. 4, where $T/\sqrt{\sigma_s}$ is plotted. We observe
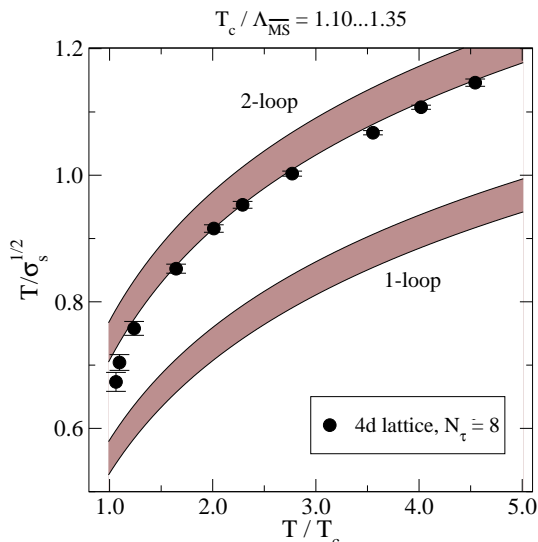
Figure 4: We compare 4d lattice data for the spatial string tension, taken from reference [22], with expressions obtained by combining 1-loop and 2-loop results for g_E^2 together with eq. (4.5) and the non-perturbative value of the string tension of 3d SU(3) gauge theory, eq. (4.4). The upper edges of the bands correspond to $T_c/\Lambda_{\overline{\rm MS}} = 1.35$, the lower edges to $T_c/\Lambda_{\overline{\rm MS}} = 1.10$.

a significant discrepancy at 1-loop level (as most recently pointed out in reference [23]), but a remarkable agreement once we go to 2-loop level. It is also noteworthy that the functional form of the 2-loop curve appears to match the behaviour of the lattice data down to low temperatures.

5. Conclusions

The main purpose of this paper has been the analytic computation of the 2-loop effective gauge coupling of QCD at finite temperatures, defined as a matching coefficient appearing in the dimensionally reduced effective theory, EQCD.[3] The result is given in eqs. (2.34)–(2.37). We have also determined a new contribution of order $\mathcal{O}(g^6T^4)$ to the pressure of hot QCD; the information is contained in eq. (2.36), and how it enters the pressure is explained in reference [10].

The 2-loop correction we find is numerically substantial, some 20% of the 1-loop expression. This indicates that while perturbation theory is in principle still under control, if restricted to the parametrically hard modes $p \sim 2\pi T$ only, it is important to push it to a sufficiently high order, in order to obtain precise results.

Our expression for the effective gauge coupling has a direct "phenomenological" application, in that it allows for a parameter-free comparison of 3d MQCD and 4d full theory results for an observable called the spatial string tension. We find that the 2-loop correction computed here improves the match between the two results quite significantly, down

---

[3]Other "effective gauge couplings" can of course also be defined; for a recent review, see reference [47]. The difference is that in these cases all momentum scales influence the effective gauge coupling, so that perturbation theory cannot be reliably applied for its computation.

to temperatures very close to the critical one. A small discrepancy still remains but, given that no continuum extrapolation was taken in 4d lattice simulations, that the extraction of the spatial string tension may involve systematic uncertainties due to large subleading terms in the r-dependence of the spatial static potential $V_s(r)$ [48], and that there also has to be some room for residual 3-loop corrections, as well as improvements in the matching between EQCD and MQCD, we do not consider this discrepancy to be worrying. We do believe that the discrepancy can be decreased by improving systematically on the various ingredients that enter the comparison.

These conclusions support a picture of thermal QCD according to which the *parametrically* "hard" scales, $p \sim 2\pi T$, can be treated perturbatively, almost as soon as we are in the deconfined phase, will the *parametrically* "soft" scales, $p \sim gT, g^2T$, require in general a non-perturbative analysis within one of the effective theories describing their dynamics. For the observable we considered here, in fact, even the colour-electric scale $p \sim gT$ could be integrated out perturbatively, but it is known that this is in general not the case. We should like to stress that this conclusion is rather non-trivial, as there *numerically* is little hierarchy between the scales $2\pi T, gT, g^2T$ at the realistic temperatures that we have been considering.

Acknowledgments

―――――――――――――――――――――

A. Expansions for master integrals

Using the notation introduced in the text, the master integrals of eq. (2.17) read, up to $\mathcal{O}(\epsilon)$:

$$I_{\rm b}(1) = \mu^{-2\epsilon} \frac{T^2}{12} \left\{ 1 + \epsilon \left[2\ln\left(\frac{\bar{\mu}e^{\gamma_{\rm E}}}{4\pi T}\right) + 2 - 2\gamma_{\rm E} + 2\frac{\zeta'(-1)}{\zeta(-1)} \right] \right\}, \tag{A.1}$$

$$I_{\rm b}(2) = \mu^{-2\epsilon} \frac{1}{(4\pi)^2} \left\{ \frac{1}{\epsilon} + 2\ln\left(\frac{\bar{\mu}e^{\gamma_{\rm E}}}{4\pi T}\right) + \epsilon \left[2\ln^2\left(\frac{\bar{\mu}e^{\gamma_{\rm E}}}{4\pi T}\right) + \frac{\pi^2}{4} - 2\gamma_{\rm E}^2 - 4\gamma_1 \right] \right\}, \tag{A.2}$$

$$I_{\rm b}(3) = \mu^{-2\epsilon} \frac{\zeta(3)}{128\pi^4 T^2} \left\{ 1 + \epsilon \left[2\ln\left(\frac{\bar{\mu}e^{\gamma_{\rm E}}}{4\pi T}\right) + 2 - 2\gamma_{\rm E} + 2\frac{\zeta'(3)}{\zeta(3)} \right] \right\}, \tag{A.3}$$

$$I_{\rm f}(1) = \mu^{-2\epsilon} \left(-\frac{T^2}{24}\right) \left\{ 1 + \epsilon \left[2\ln\left(\frac{\bar{\mu}e^{\gamma_{\rm E}}}{\pi T}\right) + 2 - 6\ln 2 - 2\gamma_{\rm E} + 2\frac{\zeta'(-1)}{\zeta(-1)} \right] \right\}, \tag{A.4}$$

$$I_{\rm f}(2) = \mu^{-2\epsilon} \frac{1}{(4\pi)^2} \left\{ \frac{1}{\epsilon} + 2\ln\left(\frac{\bar{\mu}e^{\gamma_{\rm E}}}{\pi T}\right) + \epsilon \left[2\ln^2\left(\frac{\bar{\mu}e^{\gamma_{\rm E}}}{\pi T}\right) + \frac{\pi^2}{4} - 4\ln^2 2 - 2\gamma_{\rm E}^2 - 4\gamma_1 \right] \right\}, \tag{A.5}$$

$$I_{\rm f}(3) = \mu^{-2\epsilon} \frac{7\zeta(3)}{128\pi^4 T^2} \left\{ 1 + \epsilon \left[2\ln\left(\frac{\bar{\mu}e^{\gamma_{\rm E}}}{\pi T}\right) + 2 - \frac{12}{7}\ln 2 - 2\gamma_{\rm E} + 2\frac{\zeta'(3)}{\zeta(3)} \right] \right\}. \tag{A.6}$$

References

[1] U.W. Heinz, *Thermalization at RHIC, AIP Conf. Proc.* **739** (2005) 163–180 [`nucl-th/0407067`].

[2] E.V. Shuryak, *Theory of hadronic plasma, Sov. Phys. JETP* **47** (1978) 212;
S.A. Chin, *Transition to hot quark matter in relativistic heavy ion collision, Phys. Lett.* **B 78** (1978) 552.

[3] P. Arnold and C. Zhai, *The three-loop free energy for pure gauge QCD, Phys. Rev.* **D 50** (1994) 7603 [`hep-ph/9408276`]; *The three-loop free energy for high-temperature QED and QCD with fermions, Phys. Rev.* **D 51** (1995) 1906 [`hep-ph/9410360`].

[4] C. Zhai and B.M. Kastening, *The free energy of hot gauge theories with fermions through g^5, Phys. Rev.* **D 52** (1995) 7232 [`hep-ph/9507380`].

[5] J.I. Kapusta, *Quantum chromodynamics at high temperature, Nucl. Phys.* **B 148** (1979) 461.

[6] A.D. Linde, *Infrared problem in thermodynamics of the Yang-Mills gas, Phys. Lett.* **B 96** (1980) 289.

[7] D.J. Gross, R.D. Pisarski and L.G. Yaffe, *QCD and instantons at finite temperature, Rev. Mod. Phys.* **53** (1981) 43.

[8] E. Braaten and A. Nieto, *Free energy of QCD at high temperature, Phys. Rev.* **D 53** (1996) 3421 [`hep-ph/9510408`].

[9] K. Kajantie, M. Laine, K. Rummukainen and M.E. Shaposhnikov, *$3d$ SU(N) + adjoint Higgs theory and finite-temperature QCD, Nucl. Phys.* **B 503** (1997) 357 [`hep-ph/9704416`].

[10] K. Kajantie, M. Laine, K. Rummukainen and Y. Schröder, *The pressure of hot QCD up to $g^6 \ln(1/g)$, Phys. Rev.* **D 67** (2003) 105008 [`hep-ph/0211321`].

[11] P.H. Ginsparg, *First order and second order phase transitions in gauge theories at finite temperature, Nucl. Phys.* **B 170** (1980) 388;
T. Appelquist and R.D. Pisarski, *High-temperature Yang-Mills theories and three-dimensional quantum chromodynamics, Phys. Rev.* **D 23** (1981) 2305.

[12] K. Kajantie, M. Laine, K. Rummukainen and M.E. Shaposhnikov, *Generic rules for high temperature dimensional reduction and their application to the standard model, Nucl. Phys.* **B 458** (1996) 90 [`hep-ph/9508379`].

[13] R.D. Pisarski, *Scattering amplitudes in hot gauge theories, Phys. Rev. Lett.* **63** (1989) 1129;
E. Braaten and R.D. Pisarski, *Simple effective lagrangian for hard thermal loops, Phys. Rev.* **D 45** (1992) 1827.

[14] M. Laine, *What is the simplest effective approach to hot QCD thermodynamics?*, `hep-ph/0301011`.

[15] E. Laermann and O. Philipsen, *Status of lattice QCD at finite temperature, Ann. Rev. Nucl. Part. Sci.* **53** (2003) 163 [`hep-ph/0303042`].

[16] C.P. Korthals Altes, *Forces, fluxes and quasi-particles in hot QCD*, `hep-ph/0308229`.

[17] M. Laine and O. Philipsen, *The non-perturbative QCD Debye mass from a Wilson line operator, Phys. Lett.* **B 459** (1999) 259 [`hep-lat/9905004`];
A. Hart and O. Philipsen, *The spectrum of the three-dimensional adjoint Higgs model and hot SU(2) gauge theory, Nucl. Phys.* **B 572** (2000) 243 [`hep-lat/9908041`];

A. Hart, M. Laine and O. Philipsen, *Static correlation lengths in QCD at high temperatures and finite densities*, *Nucl. Phys.* **B 586** (2000) 443 [hep-ph/0004060].

[18] A. Hietanen, K. Kajantie, M. Laine, K. Rummukainen and Y. Schröder, *Plaquette expectation value and gluon condensate in three dimensions*, *JHEP* **01** (2005) 013 [hep-lat/0412008].

[19] M. Laine and M. Vepsäläinen, *Mesonic correlation lengths in high-temperature QCD*, *JHEP* **02** (2004) 004 [hep-ph/0311268].

[20] P. Giovannangeli and C.P. Korthals Altes, *Spatial 't Hooft loop to cubic order in hot QCD*, hep-ph/0212298;
P. Giovannangeli and C.P. Korthals Altes, *Spatial 't Hooft loop to cubic order in hot QCD. II*, hep-ph/0412322.

[21] P. Bialas, A. Morel, B. Petersson, K. Petrov and T. Reisz, *High temperature 3d QCD: dimensional reduction at work*, *Nucl. Phys.* **B 581** (2000) 477 [hep-lat/0003004]; *QCD with adjoint scalars in 2d: properties in the colourless scalar sector*, *Nucl. Phys.* **B 603** (2001) 369 [hep-lat/0012019].

[22] G. Boyd et al., *Thermodynamics of* SU(3) *lattice gauge theory*, *Nucl. Phys.* **B 469** (1996) 419 [hep-lat/9602007].

[23] P. Giovannangeli, *Two loop renormalisation of the magnetic coupling in hot QCD and spatial Wilson loop*, hep-ph/0410346.

[24] M.J. Teper, SU(N) *gauge theories in* 2 + 1 *dimensions*, *Phys. Rev.* **D 59** (1999) 014512 [hep-lat/9804008];
B. Lucini and M. Teper, SU(N) *gauge theories in* 2 + 1 *dimensions: further results*, *Phys. Rev.* **D 66** (2002) 097502 [hep-lat/0206027].

[25] P. Giovannangeli, *Two loop renormalization of the magnetic coupling in hot QCD*, *Phys. Lett.* **B 585** (2004) 144 [hep-ph/0312307].

[26] K. Farakos, K. Kajantie, K. Rummukainen and M.E. Shaposhnikov, *3d physics and the electroweak phase transition: perturbation theory*, *Nucl. Phys.* **B 425** (1994) 67 [hep-ph/9404201].

[27] S. Chapman, *A new dimensionally reduced effective action for QCD at high temperature*, *Phys. Rev.* **D 50** (1994) 5308 [hep-ph/9407313].

[28] E. Megías, E. Ruiz Arriola and L.L. Salcedo, *The thermal heat kernel expansion and the one-loop effective action of QCD at finite temperature*, *Phys. Rev.* **D 69** (2004) 116003 [hep-ph/0312133].

[29] D. Diakonov and M. Oswald, *Gauge invariant effective action for the Polyakov line in the* SU(N) *Yang-Mills theory at high temperatures*, *Phys. Rev.* **D 70** (2004) 105016 [hep-ph/0403108].

[30] K. Kajantie, M. Laine, K. Rummukainen and M.E. Shaposhnikov, *High temperature dimensional reduction and parity violation*, *Phys. Lett.* **B 423** (1998) 137 [hep-ph/9710538].

[31] L.F. Abbott, *The background field method beyond one loop*, *Nucl. Phys.* **B 185** (1981) 189.

[32] M. Lüscher and P. Weisz, *Background field technique and renormalization in lattice gauge theory*, *Nucl. Phys.* **B 452** (1995) 213 [hep-lat/9504006].

[33] S. Laporta, *High-precision calculation of multi-loop Feynman integrals by difference equations*, *Int. J. Mod. Phys.* **A 15** (2000) 5087 [hep-ph/0102033].

[34] Y. Schröder, *Automatic reduction of four-loop bubbles*, *Nucl. Phys.* **116** *(Proc. Suppl.)* (2003) 402 [`hep-ph/0211288`].

[35] P. Arnold and O. Espinosa, *The effective potential and first-order phase transitions: beyond leading order*, *Phys. Rev.* **D 47** (1993) 3546 [`hep-ph/9212235`], erratum *ibid.* **50** (1994) 6662.

[36] S. Huang and M. Lissia, *The relevant scale parameter in the high temperature phase of QCD*, *Nucl. Phys.* **B 438** (1995) 54 [`hep-ph/9411293`].

[37] Y. Schröder, *Evading the infrared problem of thermal QCD*, `hep-ph/0410130`.

[38] R. Sommer, *A new way to set the energy scale in lattice gauge theories and its applications to the static force and α_s in* SU(2) *Yang-Mills theory*, *Nucl. Phys.* **B 411** (1994) 839 [`hep-lat/9310022`].

[39] M. Hasenbusch and S. Necco, SU(3) *lattice gauge theory with a mixed fundamental and adjoint plaquette action: lattice artefacts*, *JHEP* **08** (2004) 005 [`hep-lat/0405012`].

[40] B. Beinlich, F. Karsch, E. Laermann and A. Peikert, *String tension and thermodynamics with tree level and tadpole improved actions*, *Eur. Phys. J.* **C 6** (1999) 133 [`hep-lat/9707023`].

[41] B. Lucini, M. Teper and U. Wenger, *The high temperature phase transition in* SU(N) *gauge theories*, *JHEP* **01** (2004) 061 [`hep-lat/0307017`].

[42] G.S. Bali and K. Schilling, *Running coupling and the Λ parameter from* SU(3) *lattice simulations*, *Phys. Rev.* **D 47** (1993) 661 [`hep-lat/9208028`].

[43] S. Necco, *Universality and scaling behavior of RG gauge actions*, *Nucl. Phys.* **B 683** (2004) 137 [`hep-lat/0309017`].

[44] ALPHA collaboration, S. Capitani, M. Lüscher, R. Sommer and H. Wittig, *Non-perturbative quark mass renormalization in quenched lattice QCD*, *Nucl. Phys.* **B 544** (1999) 669 [`hep-lat/9810063`].

[45] S. Necco and R. Sommer, *The $N_f = 0$ heavy quark potential from short to intermediate distances*, *Nucl. Phys.* **B 622** (2002) 328 [`hep-lat/0108008`].

[46] S. Gupta, *A precise determination of T_c in QCD from scaling*, *Phys. Rev.* **D 64** (2001) 034507 [`hep-lat/0010011`].

[47] O. Kaczmarek and F. Zantow, *Running coupling of 2-flavor QCD at zero and finite temperature*, `hep-lat/0502012`.

[48] M. Lüscher and P. Weisz, *Quark confinement and the bosonic string*, *JHEP* **07** (2002) 049 [`hep-lat/0207003`].

[YS12]

High-precision ϵ expansions of single-mass-scale four-loop vacuum bubbles

High-precision epsilon expansions of single-mass-scale four-loop vacuum bubbles

York Schröder

Fakultät für Physik, Universität Bielefeld
33501 Bielefeld, Germany
E-mail: `yorks@physik.uni-bielefeld.de`

Aleksi Vuorinen

Department of Physics, P.O. Box 351560, University of Washington
Seattle, WA 98195, U.S.A.
E-mail: `vuorinen@phys.washington.edu`

ABSTRACT: In this article we present a high-precision evaluation of the expansions in $\epsilon = (4 - d)/2$ of (up to) four-loop scalar vacuum master integrals, using the method of difference equations developed by S. Laporta. We cover the complete set of 'QED-type' master integrals, i.e. those with a single mass scale only (i.e. $m_i \in \{0, m\}$) and an even number of massive lines at each vertex. Furthermore, we collect all that is known analytically about four-loop 'QED-type' masters, as well as about *all* single-mass-scale vacuum integrals at one-, two- and three-loop order.

Contents

1. Introduction

Higher-order perturbative computations have become a necessity in many areas of theoretical physics, be it for high-precision tests of QED, QCD and the standard model, or for studying critical phenomena in condensed matter systems.

Most recent investigations employ a highly automated approach, utilizing algorithms that can be implemented on computer algebra systems, in order to handle the growing numbers of diagrams as well as integrals which occur at higher loop orders.

Computations can be divided into four key steps. First, the complete set of diagrams including symmetry factors has to be generated. For a detailed description of an algorithm for this step for the case of vacuum topologies, see ref. [1]. Second, after specifying the Feynman rules, the color- and Lorentz-algebra has to be worked out. Third, within dimensional regularization, massive use of the integration-by-parts (IBP) technique [2] to derive linear relations between different Feynman integrals in conjunction with an ordering prescription [3] can be used to reduce the (typically large number of) integrals to a basis of (typically a few) master integrals. Practical notes as well as a classification of vacuum master integrals are given in ref. [4]. Fourth, the master integrals have to be solved, either fully analytically, or in an expansion around the space-time dimension d of interest. It is the fourth step that we wish to address here.

A very important subset of master integrals are fully massive vacuum (bubble) integrals, since they constitute a main building block in asymptotic expansions (see e.g. ref. [5]). They are also useful for massless theories, when a propagator mass is introduced as an intermediate infrared regulator [6]. In four dimensions, this class of master integrals has been given up to the 4-loop level in ref. [7]. As an application, these integrals are vital for computing the 4-loop QCD beta-function and anomalous dimensions [8]. In lower dimensions, perturbative results are needed for applications in condensed matter systems, as well as in the framework of dimensionally reduced effective field theories for thermal QCD, where recent efforts have made four-loop contributions an issue [9]. We have recently extended the work of ref. [7], to give the complete set of fully massive vacuum master integrals in three dimensions, again up to the 4-loop level [10].

The next larger set of scalar vacuum master integrals are those in which there is only one mass-scale m, i.e. the propagators $1/(p_i^2 + m_i^2)$ have masses $m_i \in \{0, m\}$. These integrals are needed for problems with widely separated mass scales, in which one then sets the masses of all heavy particles to m and those of all light particles to zero. As a well-defined subset of these single-mass-scale integrals, we here treat 'QED-type' vacuum integrals, i.e. those with an even number of massive lines at each vertex, at the 4-loop level. A recent application is in the computation of heavy-quark vacuum polarization [11].

The complete set of 'QED-type' vacuum master integrals up to the 4-loop level has already been identified in ref. [4]. The main purpose of this work is to numerically compute this set in terms of a high-precision ϵ-expansion in $d = 4 - 2\epsilon$ dimensions, and to present new analytic results for some low-order (in ϵ) coefficients. Furthermore, we have made an attempt to collect all presently known analytic results on 4d single-mass-scale vacuum integrals, up to four loops, in a coherent notation.

The plan of the paper is as follows. In section 2, we give a brief review of the method of difference equations applied to vacuum integrals. In section 3, we discuss the actual implementation of the algorithm. In section 4, we display our numerical results for the truncated power series expansions in ϵ of our master integrals, up to the four-loop level, in $d = 4 - 2\epsilon$. In section 5, we discuss one case of a master integral which we needed to solve via a Laplace transform of its difference equation. In section 6, we list analytic results [12].

2. The evaluation of master integrals through difference equations

The method we have chosen to compute the coefficients of the truncated power series expansions of the master integrals is based on constructing difference equations for the integrals and then solving them numerically using factorial series. This approach has recently been developed in ref. [3], and below we briefly summarize its basic concepts following the notation of the original paper, which contains a much more detailed presentation of the subject. While the method is completely general as it applies to arbitrary kinematics, masses and topologies [13], our brief summary is somewhat adapted to the specific case of vacuum integrals.

The main idea is to attach an arbitrary power x to one of the massive[1] lines of a master integral U,

$$U(x) \equiv \int \frac{1}{D_1^x D_2 \cdots D_N}, \qquad (2.1)$$

where the $D_i = (p_i^2 + m_i^2)$ denote inverse scalar propagators. In our case the mass parameter m_i has only two values, 0 and m, the latter of which we set to 1, noting that it can be restored in the end as a trivial dimensional pre-factor of each integral. The original master integral is then just $U = U(1)$. Depending on the symmetry properties of the integral, there can be different choices for the 'special' line with the arbitrary power x, but in the limit $x = 1$ they all reduce to the original master integral U. This degeneracy can (and will later) be used for non-trivial checks of the method.

Employing IBP identities in a systematic way, it is possible to derive a linear difference equation obeyed by the generalized master integral $U(x)$,

$$\sum_{j=0}^{R} p_j(x) U(x+j) = F(x), \qquad (2.2)$$

where R is a finite positive integer and the coefficients p_j are polynomials in x (and the space-time dimension d). The function F on the r.h.s. is a linear combination of functions analogous to $U(x)$ but derived from 'simpler' master integrals, i.e. integrals containing a smaller number of loops and/or propagators.

The general solution of this kind of an equation is the sum of a special solution to the full equation, $U_0(x)$, and the solutions to the homogeneous equation ($F = 0$),

$$U(x) = U_0(x) + \sum_{j=1}^{R} U_j(x), \qquad (2.3)$$

where each $(j = 0, \ldots, R)$

$$U_j(x) = \mu_j^x \sum_{s=0}^{\infty} a_j(s) \frac{\Gamma(x+1)}{\Gamma(x+1+s-K_j)} \qquad (2.4)$$

is a factorial series.[2] Substituting this form into eq. (2.2), one obtains the coefficients μ_j and K_j (the latter being a function of d), as well as recursion relations for the x-independent coefficients $a_j(s)$ (being functions of d as well) for each solution. For the homogeneous solutions, these recursion relations relate all coefficients with $s > 0$ to their (in principle arbitrary) value at $s = 0$, $a_j(s) = c_j(s) a_j(0)$, where the $c_j(s)$ are rational functions of d. For the special solution, all $a_0(s)$ are on the other hand completely fixed in terms of the inhomogeneous part $F(x)$, consisting of 'simpler' integrals which are assumed to be already known in terms of their factorial series expansions.

---

[1]The massiveness is crucial in order to avoid problems with the infrared behavior of the integral.

[2]For a rigorous definition of the concept as well as a motivation for this kind of an Ansatz, we refer the reader to ref. [3].

What clearly remains to be done is to fix the x- and s-independent constants $a_j(0)$, $j \neq 0$, in order to determine the weights of the different homogeneous solutions. To this end, it is most useful to study the behavior of $U(x)$ at large x. Writing the integral in the form

$$U(x) = \int \frac{1}{(p_1^2 + 1)^x} \, g(p_1) \,, \tag{2.5}$$

it is easy to see that its large-x behavior is determined by the small-momentum expansion of the two-point function $g(p_1)$, which has one loop less than the original vacuum integral.

In the case of integrals for which the limit $g(0)$ is well-defined and non-zero, the calculation becomes particularly simple. Then the large-x limit of $U(x)$ factorizes into a one-loop bubble carrying the large power x and a lower-loop vacuum bubble $g(0)$, which corresponds to $U(x)$ with its 'special' line cut away,

$$\lim_{x \to \infty} U(x) = \left[\int \frac{1}{(p_1^2 + 1)^x} \right] \times \left[g(0) \right] \sim (1)^x x^{-d/2} g(0) \,. \tag{2.6}$$

A comparison with the large-x behavior of eqs. (2.3), (2.4), proportional to $\sum_j \mu_j^x a_j(0) x^{K_j}$, can now be used to fix the $a_j(0)$, of which maximally one will turn out to be non-zero for our set of integrals.

If on the other hand $g(0) = 0$, the treatment of the small-p_1 limit of this function becomes more involved. Fortunately, the massless lines of the sub-diagram — which were responsible for the vanishing of its value at zero external momentum in the first place — also make its analytic evaluation more straightforward. Performing a careful analysis of the subgraph, one always ends up with an integral of the type

$$\lim_{x \to \infty} U(x) \sim \int \frac{(p_1^2)^\alpha}{(p_1^2 + 1)^x} \,, \tag{2.7}$$

from which the calculation proceeds just as above providing us with the values of the $a_j(0)$.

Having the full solution at hand, we have in principle completed our task, as in the limit $x = 1$ we recover from $U(x)$ the value of the initial integral. Let us, however, add a couple of practical remarks here. What is still to be done is to perform the summation of the factorial series of eq. (2.4), which in practice means truncating the infinite sum at some large but finite $s_{\max}$. Studying the convergence behavior of these sums, one notices that even in the cases where they do converge down to $x \sim 1$, their convergence properties usually strongly decline with decreasing x. This means that in practical computations, where one aims at obtaining a maximal number of correct digits for $U(1)$ with as little CPU time as possible, the optimal strategy is to evaluate the integrals $U(x_{\max} + 1)$, ..., $U(x_{\max} + R)$ with the factorial series approach at some $x_{\max} \gg 1$ and then use the recurrence relation of eq. (2.2) to obtain the desired result at $x = 1$. The price to pay is, however, a loss of numerical accuracy at each 'pushdown' ($x \to x - 1$) step due to possible cancellations, which makes the use of a very high $x_{\max}$ impossible. In practice the strategy is to determine an optimal value for the ratio $s_{\max}/x_{\max}$. To give an example, for the four-loop integrals of section 4 we have found that $s_{\max}/x_{\max} \sim 20 \dots 40$ is a good value, while we used a range

of $s_{\max} \sim 2000 \ldots 2500$. For a few special cases, for which additional numerical problems emerged, we were forced to limit the value of the parameters to roughly $s_{\max} \sim 200$ and $x_{\max} \sim 30$, which decreased the accuracy of the results significantly.

3. Implementation of the algorithm

As is apparent from the preceding section, there are three main steps involved in obtaining the desired numerical coefficients in the ϵ-expansion of each master integral: deriving the difference equations obeyed by each integral, solving them in terms of factorial series, and finally performing the ϵ-expansion and numerically evaluating the sum of eq. (2.4) (truncated at $s_{\max}$) to the precision needed. We will briefly address each of them in the following.

For the first step, we slightly generalized the IBP algorithm we had used for reducing generic 4-loop bubble integrals to master integrals, which follows the setup given in ref. [3], and whose implementation in FORM [14] is documented in ref. [4]. The main difference is an enlarged representation for the integrals, keeping track of the line which carries the extra powers x, as well as the fact that there are now two independent variables (d, x), requiring factorization (and inversion) of bivariate polynomials, as opposed to univariate polynomials in the original version.

Second, staying within FORM for convenience, we implemented routines that straight-forwardly solve the difference equations in terms of factorial series, along the lines of ref. [3]. This is done starting with the simplest one-loop master integral, and working the way up to the most complicated (most lines) four-loop integral, ensuring that at each step, the 'simpler' terms constituting the inhomogeneous parts of the difference equation are already known. The output are then plain ascii files specifying each solution in the form of eq. (2.4) as well as containing recursion relations for the coefficients $a(s)$. Note that these first two steps are performed exactly, in d dimensions.

Third, once the recursion relations for the coefficients $a(s)$ were known, we used a Mathematica program to obtain their numerical values at each s to a predefined precision, and to perform the summation of the factorial series. While this procedure is in principle straightforward, there are some twists that we employed to help reduce the running times significantly, most of which are probably quite specific to our use of Mathematica. To avoid a rapid loss of significant digits in solving the recursion steps that relate each $a(s)$ to $a(0)$, especially those for the homogeneous coefficients, we first solved the relations analytically and only in the end substituted the numerical value (actually the truncated ϵ-expansion) of the first non-zero coefficient. In fact, we found Mathematica to operate quite efficiently with operations like multiplication of two truncated power series, so that we relied heavily on it. Furthermore, since — not surprisingly — the most time-consuming part in the summation of the series turned out to be the ϵ-expansion of Γ-functions, we achieved a notable speed-up by substituting the Γ-functions with large arguments by suitable products of linear factors times Γ-functions of smaller arguments. Finally, a vital step in avoiding an excessive loss in the depth of the ϵ-expansions when going from one integral to the next, was to apply the 'Chop' command to remove from the results and coefficients excess unphysical poles,

whose coefficients were of the order of, say, 10^{-50} or less. In some cases we were in addition able to reduce the loss of precision in the pushdown steps by first analytically solving $U(1)$ as a function of $U(x_{\max})$, and only in the very end substituting the numerical value of the latter.

4. Numerical results

Below we list the Laurent expansions in $\epsilon = (4-d)/2$ of vacuum master integrals up to four loops. We use an intuitive graphical notation, in which each solid line represents a massive scalar propagator $1/(p^2+1)$ and a dashed line a massless one $1/p^2$. The integral measure we have chosen here is

$$\int_p \equiv \frac{1}{\Gamma(2+\epsilon)} \int \frac{\mathrm{d}^{4-2\epsilon}p}{\pi^{2-\epsilon}}, \tag{4.1}$$

which implies that the 1-loop tadpole is $J = \int_p \frac{1}{p^2+1} = \frac{-1}{\epsilon(1-\epsilon^2)} = -\sum_{n=0}^{\infty} \epsilon^{2n-1}$. In each case we provide the results to order ϵ^{10} keeping the accuracy at 50 significant digits for the 2- and 3-loop master integrals and at 40 for the 4-loop ones. There are two exceptions. For one of the 3-loop integrals (see eq. (4.6) below) the factorial series does not converge and hence the integral has to be treated by Laplace transform, see section 5. For one of the 4-loop integrals (see eq. (4.14) below) we only give the first seven ϵ-orders to 17 significant digits. To obtain more ϵ-orders and significant digits for all integrals listed here is merely a matter of additional CPU time.

We have produced numerical results for all single-mass-scale vacuum master integrals up to three loops (these are the master integrals entering the package of Avdeev [15] and MATAD [16]), and for all 'QED-type' vacuum master integrals at four loops. Here, we display only those numerical results which correspond neither to analytically solvable integrals (1 of 1 1-loop master, 1 of 2 2-loop masters, 3 of 12 3-loop masters, 2 of 10 4-loop masters, all of which are given analytically in section 6 below, and are listed in numerical form in the appendix), nor to fully massive cases (1 of 2 2-loop masters, 3 of 12 3-loop masters, which are given in section 9.3.1 of ref. [3]; 1 of 10 4-loop masters, which is given in eq. (4) of ref. [7]).

 $= + 1.00000000000000000000000000000000000000000000000000 \; \epsilon^{-3} +$
$+ 0.75000000000000000000000000000000000000000000000000 \; \epsilon^{-2} +$
$+ 2.87500000000000000000000000000000000000000000000000 \; \epsilon^{-1} +$
$+ 1.8362912870512825038535151499626234054646567716807 \; -$
$- 26.427828097688527267319254765120590367456377175480 \; \epsilon \; -$
$- 35.088051385481306364065961402117419432373775682177 \; \epsilon^2 \; -$
$- 512.75537623727044689027104289971864365971796649684 \; \epsilon^3 \; -$
$- 607.61494953927726782115473332930225595551912885034 \; \epsilon^4 \; -$
$- 5868.5987295458313170081280447224279031237930577453 \; \epsilon^5 \; -$

$$- 6835.6108788455114123641492279253803965001408075543 \; \epsilon^6 -$$
$$- 58194.090725773231428299235587057139067942816045554 \; \epsilon^7 -$$
$$- 67435.335245041201792055506063164867635607825896649 \; \epsilon^8 -$$
$$- 546094.78026628005592146280450252032502449454982782 \; \epsilon^9 -$$
$$- 631563.41278231233491152773645513360004834876043263 \; \epsilon^{10} +$$
$$+ \mathcal{O}\left(\epsilon^{11}\right) \tag{4.2}$$

 $= - 0.66666666666666666666666666666666666666666666666667 \; \epsilon^{-3} -$
$$- 1.6666666666666666666666666666666666666666666666667 \; \epsilon^{-2} -$$
$$- 5.1290732088140381005700717333376095855758453867530 \; \epsilon^{-1} -$$
$$- 26.359970069205366659319388577532454678949629074714 -$$
$$- 27.711175418518951962132692178901111387631205211816 \; \epsilon -$$
$$- 293.15661097603756640443665077615751632698451158842 \; \epsilon^2 -$$
$$- 142.70296384808301760189570443963964069968530061393 \; \epsilon^3 -$$
$$- 2882.1838924952422595902727649753356121323154437366 \; \epsilon^4 -$$
$$- 801.64629651874722343778241421866459175486305997074 \; \epsilon^5 -$$
$$- 26947.975116190322270468856280241915887082034700044 \; \epsilon^6 -$$
$$- 5202.1954102253813787831194867097139379256134207497 \; \epsilon^7 -$$
$$- 246612.58893683893330836716807041349553641918919392 \; \epsilon^8 -$$
$$- 38662.312198716830334636275721442722552625311137805 \; \epsilon^9 -$$
$$- 2235893.9169450155346378997842831790622571843918826 \; \epsilon^{10} +$$
$$+ \mathcal{O}\left(\epsilon^{11}\right) \tag{4.3}$$

 $= + 2.4041138063191885707994763230228999815299725846810 \; \epsilon^{-1} -$
$$- 13.125546202841586242894146861604104971473328745577 +$$
$$+ 58.026260003878655576719786597271170572487856789112 \; \epsilon -$$
$$- 215.15799420773251496754795359758001229751012774168 \; \epsilon^2 +$$
$$+ 741.02167568175382570477503744319405060687524908840 \; \epsilon^3 -$$
$$- 2422.8745603243623464433277838674972111388328822910 \; \epsilon^4 +$$
$$+ 7691.0946660371679072096695375419004253731139722117 \; \epsilon^5 -$$
$$- 23935.477541938694107878632636617038283240279946231 \; \epsilon^6 +$$
$$+ 73567.948130076321368433008921329180208448045889323 \; \epsilon^7 -$$
$$- 224259.22429731742234354745849077250951082319381698 \; \epsilon^8 +$$
$$+ 679949.06185664528482517935972319009053625673803897 \; \epsilon^9 -$$
$$- 2054250.6137900838709156880585181458050495843111626 \; \epsilon^{10} +$$
$$+ \mathcal{O}\left(\epsilon^{11}\right) \tag{4.4}$$

– 7 –

$$\text{(图)} = + 2.40411380631918857079947632302289998152997258468\,10\;\epsilon^{-1} -$$
$$- 10.073203643096893062671213536841941862151359216063 +$$
$$+ 46.082030897278984204342981632818973100797752268016\;\epsilon -$$
$$- 162.843215714725496046854279989294952475644526077\,77\;\epsilon^2 +$$
$$+ 563.025415990525499216909123033911424820565031939\,63\;\epsilon^3 -$$
$$- 1822.827841603937966179232299308506237990042143924\,4\;\epsilon^4 +$$
$$+ 5785.981512228647211870123880030386184363649237002\,8\;\epsilon^5 -$$
$$- 17968.847688521304415691142884872355494614421789034\;\epsilon^6 +$$
$$+ 55216.376506037509642111329809657803343085975716148\;\epsilon^7 -$$
$$- 168240.563077149874383285760617030421873489613552\,71\;\epsilon^8 +$$
$$+ 510052.278307608834920026669049630352681249513663\,79\;\epsilon^9 -$$
$$- 1540802.785840645652249959294427918373758314899733\,8\;\epsilon^{10} +$$
$$+ \mathcal{O}\left(\epsilon^{11}\right) \tag{4.5}$$

$$\text{(图)} = + 2.40411380631919\;\epsilon^{-1} - 6.09209302191832 +$$
$$+ 35.8130598712514\;\epsilon - 104.744695525740\;\epsilon^2 +$$
$$+ 394.7643404810\;\epsilon^3 - 1200.978166746\;\epsilon^4 + \mathcal{O}\left(\epsilon^5\right) \tag{4.6}$$

$$\text{(图)} = + 2.40411380631918857079947632302289998152997258468\,10\;\epsilon^{-1} -$$
$$- 10.239350912945217732184803670827657230740659540460 +$$
$$+ 46.310233388509835938575195677581891346572247104081\;\epsilon -$$
$$- 163.719036668462745879401608177675102512677988015\,63\;\epsilon^2 +$$
$$+ 564.309100694997914499178910531924831694144485238\,30\;\epsilon^3 -$$
$$- 1825.820669149058610133959291741425068355320841705\,6\;\epsilon^4 +$$
$$+ 5790.483050325622650038980184408733148190979917504\,3\;\epsilon^5 -$$
$$- 17977.329926014373828927297954140399343188401436964\;\epsilon^6 +$$
$$+ 55229.228709840982549894271961274899889724333654202\;\epsilon^7 -$$
$$- 168262.339848810394699003364155833832775065566826\,77\;\epsilon^8 +$$
$$+ 510085.272124680407815997873536174545161737821110\,15\;\epsilon^9 -$$
$$- 1540855.637920761521277754754593865788964539741247\,1\;\epsilon^{10} +$$
$$+ \mathcal{O}\left(\epsilon^{11}\right) \tag{4.7}$$

$$\text{(图)} = - 1.000000000000000000000000000000000000000\;\epsilon^{-4} -$$
$$- 0.500000000000000000000000000000000000000\;\epsilon^{-3} -$$
$$- 3.527777777777777777777777777777777777778\;\epsilon^{-2} -$$
$$- 1.995370370370370370370370370370370370370\;\epsilon^{-1} -$$
$$- 36.820216049382716049382716049382716049\,38 -$$
$$- 19.879208014511070350695756351563801015\,75\;\epsilon -$$

$$- 1809.0011266386371609338945077987817066682 \ \epsilon^2 -$$

$$- 941.24864982151354075297536146242545521594 \ \epsilon^3 -$$

$$- 49114.804042402752639408373706267476635512 \ \epsilon^4 -$$

$$- 25712.879446586062398883019313871953777680 \ \epsilon^5 -$$

$$- 1014742.5403373231089313967946997794706304 \ \epsilon^6 -$$

$$- 533925.93151851652218243121931171571357135164 \ \epsilon^7 -$$

$$- 18513953.445193284783606859981513200048728 \ \epsilon^8 -$$

$$- 9769845.1467152700074494284869530161222496 \ \epsilon^9 -$$

$$- 317669932.95156919762776583625967846951155 \ \epsilon^{10} + \mathcal{O}\left(\epsilon^{11}\right) \qquad (4.8)$$

 $= + 0.25000000000000000000000000000000000000000 \ \epsilon^{-4} +$

$$+ 0.50000000000000000000000000000000000000000 \ \epsilon^{-3} +$$

$$+ 1.0000000000000000000000000000000000000000 \ \epsilon^{-2} +$$

$$+ 1.8133698705373628550982980498244249399972 \ \epsilon^{-1} -$$

$$- 113.82245428361314613117625528439489456680 -$$

$$- 33.706920081218750827467307095493182925582 \ \epsilon -$$

$$- 3800.1311779523988333644680864867013103224 \ \epsilon^2 -$$

$$- 724.24839804598684355297859167065804155218 \ \epsilon^3 -$$

$$- 83243.751142113515576003512426035483109433 \ \epsilon^4 -$$

$$- 9962.2448747314710546906295542094497455080 \ \epsilon^5 -$$

$$- 1556494.3926815711769347584956681121116219 \ \epsilon^6 -$$

$$- 125852.92690070946307747809490021578838966 \ \epsilon^7 -$$

$$- 27026768.743241396910049258064204638655625 \ \epsilon^8 -$$

$$- 1619900.9859452311997604296185581311155494 \ \epsilon^9 -$$

$$- 451968203.17072642331268703265775073422793 \ \epsilon^{10} + \mathcal{O}\left(\epsilon^{11}\right) \qquad (4.9)$$

 $= + 0.66666666666666666666666666666666666666667 \ \epsilon^{-4} +$

$$+ 1.3333333333333333333333333333333333333333 \ \epsilon^{-3} +$$

$$+ 3.3333333333333333333333333333333333333333 \ \epsilon^{-2} -$$

$$- 2.9223631831488304778680631386056000049253 \ \epsilon^{-1} -$$

$$- 52.505297398427697569734877949455803028226 -$$

$$- 622.15489727085903760125156858803040779291 \ \epsilon -$$

$$- 1741.3929443462620522604059569171149277201 \ \epsilon^2 -$$

$$- 17196.126853309025827683400985542376368824 \ \epsilon^3 -$$

$$- 35037.764381407253718562939041917773844497 \ \epsilon^4 -$$

$$- 350040.60522854940167839120743404103655119 \ \epsilon^5 -$$

$$- 619669.77561600605005058840167044452111642 \ \epsilon^6 -$$

$$- 6316632.078794015469602341973684043315269 \; \epsilon^7 -$$
$$- 10420684.666262760453830102149282840 87492 \; \epsilon^8 -$$
$$- 107682720.99366560868072010024983134 47872 \; \epsilon^9 -$$
$$- 171175743.733478588931602649777435958 7050 \; \epsilon^{10} + \mathcal{O}\left(\epsilon^{11}\right) \qquad (4.10)$$

 $= - 0.166666666666666666666666666666666666667 \; \epsilon^{-4} -$
$$- 0.833333333333333333333333333333333333333 \; \epsilon^{-3} -$$
$$- 5.535390236492927618733071494844783324098 \; \epsilon^{-2} -$$
$$- 18.82211358179364443034084677047078519365 \; \epsilon^{-1} -$$
$$- 25.33131709639103630297934297632219102642 -$$
$$- 692.6253681383859207802291611352811358818 \; \epsilon +$$
$$+ 1304.406827189023173835521731683389467596 \; \epsilon^2 -$$
$$- 17597.62761742767175796342110253040416842 \; \epsilon^3 +$$
$$+ 43608.68478725040973761321535022863250602 \; \epsilon^4 -$$
$$- 356925.7947952212585233385307804100264907 \; \epsilon^5 +$$
$$+ 939175.5208936133499000732308171881559393 \; \epsilon^6 -$$
$$- 6467516.567931160982387324881460909595434 \; \epsilon^7 +$$
$$+ 17364082.00316543469946942544036134544207 \; \epsilon^8 -$$
$$- 110630064.0504718962799294108969364410321 \; \epsilon^9 +$$
$$+ 299555848.2967199841801845664112146544429 \; \epsilon^{10} + \mathcal{O}\left(\epsilon^{11}\right) \qquad (4.11)$$

 $= - 0.166666666666666666666666666666666666667 \; \epsilon^{-4} -$
$$- 0.833333333333333333333333333333333333333 \; \epsilon^{-3} -$$
$$- 4.934361784913130476033202414089058328716 \; \epsilon^{-2} -$$
$$- 16.20728580177089935860423675579773428042 \; \epsilon^{-1} -$$
$$- 66.26045267088253719950145322703822192330 -$$
$$- 375.8131807648258568590885739785987842170 \; \epsilon -$$
$$- 558.8684980291056611497739327005648555056 \; \epsilon^2 -$$
$$- 8005.909258052308131324607228836046381631 \; \epsilon^3 -$$
$$- 1919.455472313357401527573620257269458394 \; \epsilon^4 -$$
$$- 151678.4473872174906037102434226085312395 \; \epsilon^5 +$$
$$+ 45367.13703676553118943884640644928312337 \; \epsilon^6 -$$
$$- 2666691.771475554201053771443874777744895 \; \epsilon^7 +$$
$$+ 1469487.259313641787542428480707831779115 \; \epsilon^8 -$$
$$- 44948193.38776277686896804573212402472750 \; \epsilon^9 +$$
$$+ 30458142.54983328875970186426762508169587 \; \epsilon^{10} + \mathcal{O}\left(\epsilon^{11}\right) \qquad (4.12)$$

 $= + 5.1846387757168496316568274322851708402850 \; \epsilon^{-1} -$
$- 43.2761585693246406112018660531844001478700 \; +$
$+ 281.6878028207571441503294898731325032572 \; \epsilon \; -$
$- 1513.439498357334510783856768928671867962 \; \epsilon^2 \; +$
$+ 7425.188218180801392788420314778806091908 \; \epsilon^3 \; -$
$- 34157.28328369996440389044714608216014037 \; \epsilon^4 \; +$
$+ 150927.1863992836861076852919478736657397 \; \epsilon^5 \; -$
$- 648212.2200729992344766408701706025837197 \; \epsilon^6 \; +$
$+ 2730180.324952706549742379412290749026850 \; \epsilon^7 \; -$
$- 11339683.06464037751511038174569497508966 \; \epsilon^8 \; +$
$+ 46630964.11789747669532801502683952077042 \; \epsilon^9 \; -$
$- 190369535.4103429881202484621694879170262 \; \epsilon^{10} + \mathcal{O}\left(\epsilon^{11}\right)$ (4.13)

 $= + 1.80887954620833474 - 12.7814836099524403 \; \epsilon \; +$
$+ 71.046049240835262 \; \epsilon^2 - 334.59648933739741 \; \epsilon^3 \; +$
$+ 1467.5837602507405 \; \epsilon^4 - 6165.5621168597119 \; \epsilon^5 \; +$
$+ 25329.619267580422 \; \epsilon^6 + \mathcal{O}\left(\epsilon^7\right)$ (4.14)

Just as in the three-dimensional case [10], we have performed various checks on our results. These can be divided into two categories: first, we had to make sure that the difference equation, eq. (2.2), as well as the various parts of its solution, eqs. (2.3), (2.4), were in principle correct, and second, that we have reached the desired accuracy in the numerical part of our computation. For the first task, it was in general enough to ensure that the first few ϵ-orders we obtained for each integral coincided with the existing analytic results. Here the main difference to our previous three-dimensional computation laid in the fact that while at $d = 3 - 2\epsilon$ most of the integrals were either finite or their expansions started with a $1/\epsilon$ term, we now encountered in many cases (often analytically calculable) divergent terms up to $1/\epsilon^4$ order. The analytic results relevant to our graphs that we have found in the literature, as well as a few new ones, are collected in section 6. We have found agreement in all cases.

The comparisons with existing analytic results also provide an easy and reliable method to inspect the accuracy of the numerical results, since the number of correct digits usually stays roughly constant when moving from one ϵ-order to the next. Just as in our previous work [10], other methods we have employed to assess the accuracy question include comparing the results obtained by raising topologically inequivalent lines in a single integral to a higher power and analyzing the convergence properties of the factorial series, i.e. checking the stability of our results with respect to varying s_{max}. The results given in the preceding section have been observed to be stable to at least the number of digits shown.

One might be concerned about the rapid growth with increasing ϵ-orders of most of the coefficients. This is, as was pointed out in ref. [7], caused by poles that the integrals

(seen as functions of d) develop near $d = 4$, e.g. at $d = 7/2, 3$, etc. It is to be expected that factoring out the first few of these nearby poles in each case will improve the apparent convergence in ϵ considerably.

In principle, having a method at hand that is capable of generating coefficients to very high accuracy, even to a couple of hundred digits, one could now use the algorithm PSLQ [17] combined with an educated guess of the number content of some of the yet-unknown constant terms, in order to search for analytic representations of the numerical results. We have not made any systematic attempts in that direction, since the numerical accuracy of our results should be sufficient for all practical purposes. However, for a few leading coefficients we have successfully applied this method. The analytic values are given in section 6.

5. Laplace transform

As already mentioned in the above, we have encountered one case where the method of computing the ϵ-expansion via a factorial series representation does not work (or, more precisely, does not converge), namely for the 3-loop integral of eq. (4.6). Let us take this specific example as an opportunity to finally display a difference equation like eq. (2.2) in full detail and exhibit, following ref. [3], one method other than factorial series to solve it.

Defining the integral

$$M_2(x) \equiv \frac{\overbrace{}^{x}}{} = \frac{\overbrace{}^{x}}{J^3} \frac{2^{d-2}\Gamma(\frac{1}{2})}{\Gamma(\frac{3-d}{2})\Gamma(\frac{d}{2})}, \tag{5.1}$$

where the dot with the label x means that the corresponding propagator is raised to the x-th power, the difference equation eq. (2.2) it satisfies is of second order and reads

$$0 = -2(x+1)M_2(x+2) + 3\left(x+2-\frac{d}{2}\right)M_2(x+1) - (x+3-d)M_2(x) +$$

$$+ \frac{\Gamma(x+5-\frac{3d}{2})}{\Gamma(x+1)}\frac{3-d}{\Gamma(5-\frac{3d}{2})}M_2(0) + \frac{\Gamma(x+3-d)}{\Gamma(x+1)}\frac{1}{\Gamma(2-d)} -$$

$$- \frac{\Gamma(x+2-\frac{d}{2})}{\Gamma(x+1)}\frac{2}{\Gamma(1-\frac{d}{2})} + \frac{\Gamma(x+5-\frac{3d}{2})\Gamma(x+3-d)}{\Gamma(x)\Gamma(x+7-2d)}\frac{2}{\Gamma(1-\frac{d}{2})}, \tag{5.2}$$

with boundary conditions $M_2(x \gg 1) \sim x^{-\frac{d}{2}}$ (cf. eq. (2.6)) and

$$M_2(0) = \frac{\overbrace{}}{} = -\frac{\Gamma(\frac{3d}{2})\Gamma(1-\frac{3d}{2})\Gamma(\frac{d}{2}-1)\Gamma(\frac{d}{2})}{\Gamma(d)\Gamma(d-2)\Gamma(1-d)}. \tag{5.3}$$

We would like to know the master integral $M_2(1)$, or at least its ϵ-expansion in $d = 4-2\epsilon$ dimensions. Note that only the first two terms of that expansion are known, cf. eq. (6.32) below. Formally, it is of course possible to solve eq. (5.2) in terms of factorial series, following the recipe sketched in section 2. However, it turns out that the series does not converge in this (and only this, of all cases treated in this paper) case, such that in practice a different method of solving the difference equation is needed.

One way to tackle eq. (5.2) could be the iterative method used e.g. in ref. [18] (cf. eq. (11)ff therein): expand in ϵ, make Ansätze for the ϵ-coefficients of M_2 in terms of (sums of multiple) harmonic sums with unknown constants, write all ϵ-expansions of the Gamma functions in terms of harmonic sums, then rewrite everything in terms of a unique basis, and finally fix the constants by comparing coefficients. Unfortunately, there does not seem to exist an algorithm yet that automatizes the choice of Ansatz, hence requiring a fair amount of hand-work. For the basic literature on harmonic sums, see the references of ref. [18].

Another way of tackling eq. (5.2) is to transform it to a differential equation, which should then be solved by analytical or numerical methods, or by a combination of both. This is what we will do in the following, and this is how we have obtained the numerical values given in eq. (4.6).

We can use the Ansatz $M_2(x) = \int_0^1 dt\, t^{x-1} v(t)$ to Laplace transform the difference equation for M_2 into a first order differential equation $\Phi_0(t)v(t) - t\Phi_1(t)v'(t) = w(t)$, where $\Phi_0(t) = 3 - d - 3(1 - \frac{d}{2})t - 2t^2$ and $\Phi_1(t) = (1-t)(1-2t)$ [3].

The homogeneous equation is solved by $v_H(t) = c_H t^{3-d}(1-t)^{\frac{d}{2}-2}(1-2t)^{\frac{d}{2}-2}$, which however makes $M_2(x \gg 1)$ grow too fast at large x (it would grow like $x^{1-\frac{d}{2}}$, in conflict with the large-x boundary condition), such that $c_H \equiv 0$ and hence $M_2^H(x) = 0$.

For solving the inhomogeneous equation, note that the inhomogeneous piece has four terms $w(z) = \sum_{j=1}^4 w_j(z)$, which correspond to the last four terms of eq. (5.2), written as $T_j(x) = \int_0^1 dz\, z^{x-1} w_j(z)$. For $j = 1, 2, 3$ we therefore have $w_j(z) = \frac{b_j}{\Gamma(1-a_j)} z^{a_j}(1-z)^{-a_j}$, where $\vec{a} = (5 - \frac{3d}{2}, 3 - d, 2 - \frac{d}{2})$ and $\vec{b} = (\frac{(3-d)M_2(0)}{\Gamma(5-\frac{3d}{2})}, \frac{1}{\Gamma(2-d)}, -\frac{2}{\Gamma(1-\frac{d}{2})})$. For w_4, we know that it satisfies

$$\int_0^1 dz\, z^{x-1} w_4(z) = T_4(x) = \frac{\Gamma(x+5-\frac{3d}{2})\Gamma(x+3-d)}{\Gamma(x)\Gamma(x+7-2d)}\frac{2}{\Gamma(1-\frac{d}{2})}. \quad (5.4)$$

For the expression $T_4(x)$, we can immediately construct a simple first-order difference equation, $x(x+7-2d)T_4(x+1) = (x+5-\frac{3d}{2})(x+3-d)T_4(x)$, from which we get — in complete analogy to Laplace transforming eq. (5.2) – a differential equation for w_4:

$$0 = (d-3)(3d-10-4z)w_4(z) - z(14-5d+4z(d-2))w_4'(z) + 2z^2(1-z)w_4''(z). \quad (5.5)$$

To write its boundary condition eq. (5.4) in a (for numerical treatment) more useful form, note that the behavior of $w_4(z)$ at the singular point $z = 1$ is connected to the large-x limit of $T_4(x)$. Using Stirling's formula to write $\frac{\Gamma(x+a)}{\Gamma(x+b)} = x^{a-b}(1 + \frac{(a-b)(a+b-1)}{2x} + \mathcal{O}(x^{-2}))$, we can fix the three constants in the Ansatz $w_4(z \approx 1) = c_1(1-z)^{c_2}(1 + c_3(1-z) + \ldots)$, when comparing $\int_0^1 dz\, z^{x-1} w_4(z \approx 1)$ at large x with $T_4(x \gg 1)$. Hence, writing

$$w_4(z) = c_1(1-z)^{c_2}\frac{2z^{1-\frac{d}{2}}}{d-2}\bar{w}_4(z) = \frac{4(1-z)^{\frac{d}{2}-2}z^{1-\frac{d}{2}}\bar{w}_4(z)}{\Gamma(1-\frac{d}{2})\Gamma(\frac{d}{2}-1)(d-2)}$$

$$= \frac{2\sin\frac{\pi d}{2}}{\pi} z^{1-\frac{d}{2}}(1-z)^{\frac{d}{2}-2}\bar{w}_4(z), \quad (5.6)$$

we get simple boundary conditions $\bar{w}_4(1) = \frac{d-2}{2}$, $\bar{w}_4'(1) = \frac{d-2}{2}(\frac{d-2}{2} - c_3) = \frac{(d-4)^2}{2}$ for the new function $\bar{w}_4(z)$, which satisfies the differential equation

$$0 = -(d-4)^2 \bar{w}_4(z) + z(10 - 3d + 4z(d-3))\bar{w}_4'(z) + 2z^2(z-1)\bar{w}_4''(z). \quad (5.7)$$

We now get the non-homogeneous solution $v_{NH}(t)$ by varying the constant of the homogeneous solution. Due to the linearity of the differential equation, the full solution is simply the sum of four terms, which when plugged back into the definition of the Laplace transform gives a representation for the master M_2:

$$M_2(x) = \int_0^1 dt\, t^{x+2-d}(1-t)^{\frac{d}{2}-2}(1-2t)^{\frac{d}{2}-2} \int_t^1 dz\, z^{d-4}(1-z)^{1-\frac{d}{2}}(1-2z)^{1-\frac{d}{2}} \times$$

$$\times \left\{ \sum_{j=1}^3 \frac{b_j}{\Gamma(1-a_j)} z^{a_j}(1-z)^{-a_j} + w_4(z) \right\}. \quad (5.8)$$

The integral converges (in 4d) for $x > 1$, so one can use it to compute $M_2(2)$ and get $M_2(1)$ via eq. (5.2).

Unable to solve eq. (5.8) for generic d, let us now go to $d = 4 - 2\epsilon$ dimensions and start expanding. First, we need to solve the differential equation eq. (5.7). Writing $\bar{w}_4(z) = \sum_{n=0}^{\infty} \epsilon^n f_n(z)$, the boundary conditions translate into $f_0(1) = 1$, $f_1(1) = -1$, $f_{n>1}(1) = 0$ and $f_0'(1) = 0$, $f_1'(1) = 0$, $f_2'(1) = 2$, $f_{n>2}'(1) = 0$. The $f_n(z)$ satisfy the differential equations

$$0 = z(z-1)f_n''(z) + (2z-1)f_n'(z) + (3-4z)f_{n-1}'(z) - \frac{2}{z}f_{n-2}(z), \quad (5.9)$$

which have to be solved starting with $n = 0$ (setting $f_{n<0}(z) \equiv 0$).

One can e.g. solve eq. (5.9) in terms of multiple (nested) integrals. In fact, the Ansatz $f_n(z) = \delta_{n,0} - \delta_{n,1} + \int_1^z da\, g_n(a)$ respects the boundary conditions for $f_n(1)$ and transforms eq. (5.9) into a first order differential equation for $g_n(a)$, whose boundary conditions $g_n(1) = 2\delta_{n,2}$ incorporates those for $f_n'(1)$. The homogeneous solution is of the form $g_n^H(a) = \frac{c_n}{a(1-a)}$ and vanishes due to the boundary condition: $c_n \equiv 0$. The inhomogeneous solution now follows by variation of the constant, such that finally

$$f_n(z) = \delta_{n,0} - \delta_{n,1} + \int_1^z \frac{da}{a} \frac{h_n(a)}{1-a}, \quad (5.10)$$

$$h_n(a) = 2(\delta_{n,3} - \delta_{n,2})\ln(a) + \int_1^a \frac{db}{b} \frac{(3-4b)h_{n-1}(b)}{1-b} - 2\int_1^a \frac{db}{b} \int_1^b \frac{dc}{c} \frac{h_{n-2}(c)}{1-c}. \quad (5.11)$$

The strategy is now clear: $h_n(a) \to f_n(z) \to \bar{w}_4(z) \to w(z) \to M_2(2) \to M_2(1)$. All of these steps can be performed numerically, and there is a discussion of methods in ref. [3].

In practice, we numerically solved for the f_n using Mathematica, changed the order of integrations in eq. (5.8), dealt with the t-integration (semi-) analytically, and finally performed the z-integration numerically. The singular point at $z = 1/2$ was treated as a principal value integral, and the logarithmically divergent regions near $z = 1/2$ and $z = 1$ were split off and treated analytically via a series-expansion in z.

– 14 –

To check the setup, it is possible to start analytically. Solving eq. (5.11), the first couple of orders for h_n read $h_0(a) = 0$, $h_1(a) = 0$, $h_2(a) = -2\ln(a)$ and $h_3(a) = 2\ln(a) - 3\ln^2(a) + 2\text{Li}_2(1-a)$, where $\text{Li}_n(z) = \sum_{k=1}^{\infty} \frac{z^k}{k^2}$ is the polylogarithm.

Using eq. (5.10), this then implies $f_0(z) = 1$, $f_1(z) = -1$, $f_2(z) = -\ln^2 z - 2\text{Li}_2(1-z)$, $f_3(z) = (1 + 5\ln(1-z) - \ln(z))\ln^2(z) + 2(1 + \ln(z))\text{Li}_2(1-z) + 10\ln(z)\text{Li}_2(z) - 2\text{Li}_3(1-z) - 10\text{Li}_3(z) + 10\zeta_3$.

Knowing now $\bar{w}_4(z) = 1 - \epsilon + \epsilon^2 f_2(z) + \mathcal{O}(\epsilon^3)$ and using eq. (5.6) to get $w_4(z)$, we can expand the curly bracket of eq. (5.8). The two leading terms cancel, such that we obtain $\{\cdots\} = \frac{2\epsilon^3}{3z}[(z-1)(\pi^2 + 2\ln^2(1-z) - 6\ln z \ln(1-z)) + 3z\ln^2 z + 6\text{Li}_2(1-z)] + \mathcal{O}(\epsilon^4)$. Now $M_2(x) = \int_0^1 dt\, t^{x-2} \int_t^1 dz\, \frac{\{\cdots\}}{(1-z)(1-2z)} + \mathcal{O}(\epsilon^4) = \int_0^1 dz\, \frac{\{\cdots\}}{(1-z)(1-2z)} \frac{z^{x-1}}{x-1} + \mathcal{O}(\epsilon^4)$. We obtain $M_2(2) = 6\zeta_3\epsilon^3 + \mathcal{O}(\epsilon^4)$, which, using eq. (5.2) at $x = 0$, translates into $M_2(1) = \frac{4}{3(4-d)}M_2(2) = \frac{2}{3\epsilon}M_2(2) = 4\zeta_3\epsilon^2 + \mathcal{O}(\epsilon^3)$, in nice agreement with the first term of eq. (6.32).

6. Analytic results

For completeness we list here all existing analytic results applicable to our integrals that we are aware of [12]. Additionally, we give the analytic form of some new coefficients of 4-loop master integrals. These were extracted from our high-precision numerical results of section 4, with the help of the integer-relation finding algorithm PSLQ [17] combined with an educated guess of their number content.

Here, we normalize every integral with the appropriate power of the 1-loop tadpole, such that analytic results are independent of the integration measure. Also, recall that we have set $m = 1$.

We will use the following transcendentals:

$$\zeta_n = \sum_{k=1}^{\infty} \frac{1}{k^n}, \tag{6.1}$$

$$a_n = \sum_{k=1}^{\infty} \frac{1}{2^k k^n} = \text{Li}_n\left(\frac{1}{2}\right), \tag{6.2}$$

$$\text{Ls}_j(\theta) = -\int_0^\theta d\tau \ln^{j-1}\left|2\sin\frac{\tau}{2}\right|, \tag{6.3}$$

and abbreviate the log-sine integrals at their maximum value as $\text{Ls}_j(\frac{2\pi}{3}) \equiv \text{Ls}_j$ below.

6.1 1-loop

There is one 1-loop topology and one coloring by mass. The 1-loop tadpole is solved in terms of Gamma functions. With measure $\int d^d p$, $J = \int d^d p \frac{1}{p^2+1} = \pi^{d/2}\Gamma(1 - d/2)$.

$$\bigcirc \equiv J. \tag{6.4}$$

6.2 2-loop

There is one 2-loop topology and three colorings by mass. One of them reduces to simpler cases, while the other two are master integrals. One of the two master integrals has an

analytic solution in terms of Gamma functions. The other (fully massive) one can be written in terms of the hypergeometric function $_2F_1$ (see eqs. (4.12) and (4.13) in ref. [19]), or alternatively in terms of a one-dimensional integral (see eqs. (21), (15) and (16) in ref. [20]) which has a simple ϵ-expansion (for 4d in terms of log-sine integrals).

$$\bigcirc\!\!\!\cdots = -\frac{d-2}{2(d-3)}\left(\bigcirc\right)^2 \tag{6.5}$$

$$\frac{\ominus}{J^2} = \frac{\Gamma(\frac{3-d}{2})\Gamma(\frac{d}{2})}{2^{d-2}\Gamma(\frac{1}{2})} \tag{6.6}$$

$$\frac{\ominus}{J^2} = -\frac{3(d-2)}{4(d-3)}\left\{{}_2F_1\left(\frac{4-d}{2},1;\frac{5-d}{2};\frac{3}{4}\right) - 3^{\frac{d-5}{2}}\frac{2\pi\Gamma(5-d)}{\Gamma(\frac{4-d}{2})\Gamma(\frac{6-d}{2})}\right\} \tag{6.7}$$

$$= -\frac{3(d-2)}{4(d-3)}\left\{1 - 3^{\frac{d-3}{2}}(d-4)\int_0^{\frac{\pi}{3}} d\tau(2\sin(\tau))^{4-d} - 3^{\frac{d-5}{2}}\frac{2\pi\Gamma(5-d)}{\Gamma(\frac{4-d}{2})\Gamma(\frac{6-d}{2})}\right\} \tag{6.8}$$

$$\overset{d=n-2\epsilon}{=} -\frac{3(n-2-2\epsilon)}{4(n-3-2\epsilon)}\left\{1 + 3^{-\epsilon}\frac{\frac{n-4}{2}-\epsilon}{3^{\frac{3-n}{2}}}\sum_{j=0}^{\infty}\frac{(2\epsilon)^j}{j!}\mathrm{Ls}_{j+1}^{(4-n)} - \right.$$
$$\left. - 3^{-\epsilon}\frac{3^{\frac{n-5}{2}}2\pi\Gamma(5-n+2\epsilon)}{\Gamma(\frac{4-n}{2}+\epsilon)\Gamma(\frac{6-n}{2}+\epsilon)}\right\} \tag{6.9}$$

The numbers $\mathrm{Ls}_j^{(a)} = -\int_0^{\frac{2\pi}{3}} d\tau(2\sin\frac{\tau}{2})^a \ln^{j-1}|2\sin\frac{\tau}{2}|$ in the 4d ($n=4$) case are the log-sine integrals $\mathrm{Ls}_j^{(0)} = \mathrm{Ls}_j = \mathrm{Ls}_j(\frac{2\pi}{3})$ of eq. (6.3).

6.3 3-loop

There are three 3-loop topologies.

3-loop, 4 lines: there are four colorings by mass, all of which are master integrals. Two of them have an analytic solution in terms of Gamma functions. The third one (called $D_3(0,1,0,1,1,1)$ in the literature, according to the notation introduced in ref. [15]) can be written in terms of a single hypergeometric function $_3F_2$ (see eq. (4.33) of ref. [21], where also the first seven orders of its 4d ϵ-expansion were given in eq. (4.32)).[3] The first seven orders of the 4d ϵ-expansion of the fourth (fully massive) master (called $B_N(0,0,1,1,1,1)$ in the literature) can be deduced from the function B_4 introduced in ref. [24] using the reductions eqs. (6.26) and (6.27) given below. Two more orders could be obtained from B_4 as given in ref. [25], but we refrain from reproducing them here.

$$\frac{\bigcirc\!\!\!\bigcirc}{J^3} = -\frac{3\Gamma(\frac{6-3d}{2})\Gamma(3-d)\Gamma^2(\frac{d-2}{2})}{\Gamma^3(\frac{2-d}{2})} \tag{6.10}$$

---

[3]In some sense, the representation in terms of special types of hypergeometric functions can be called an all-order analytic ϵ-expansion, namely when their expansion can be written in terms of rapidly converging (multiple inverse binomial) sums, for which efficient algorithms exist [22]. The 3-loop integrals E_3, D_5 and D_4 [23] below belong to this class as well.

$$\frac{\bigcirc\hspace{-0.4em}\dotsc}{J^3} = \frac{2^{d-3}\Gamma(\frac{8-3d}{2})\Gamma(\frac{3-d}{2})\Gamma(\frac{d}{2})}{\Gamma(\frac{7-2d}{2})\Gamma(\frac{2-d}{2})} \tag{6.11}$$

$$\frac{\bigcirc\hspace{-0.4em}\dotsc}{J^3} \overset{d=4-2\epsilon}{=} -1 - \frac{3}{4}\epsilon + \frac{1}{8}\epsilon^2 + \left(\frac{91}{16} - \frac{9}{2}\sqrt{3}\mathrm{Ls}_2\right)\epsilon^3 +$$

$$+ \left(\frac{913}{32} - \frac{3}{4}\sqrt{3}(\pi^3 + 9(3-2\ln 3)\mathrm{Ls}_2 + 18\mathrm{Ls}_3)\right)\epsilon^4 +$$

$$+ \left(\frac{7027}{64} + \frac{1}{8}\sqrt{3}(9\pi^3(2\ln 3 - 3) + 64\mathrm{Ls}_4\left(\frac{\pi}{3}\right) - 9(67 - 54\ln 3 + 18\ln^2 3)\mathrm{Ls}_2 +\right.$$

$$\left. + 162(2\ln 3 - 3)\mathrm{Ls}_3 - 216\mathrm{Ls}_4 + 184\pi\zeta_3)\right)\epsilon^5 +$$

$$+ \left(\frac{48601}{128} +\right.$$

$$+ \sqrt{3}\left(-\frac{3}{16}\pi^3(67 + 18\ln 3(\ln 3 - 3)) - \frac{23}{36}\pi^5 + \frac{69}{2}\pi(3 - 2\ln 3)\zeta_3 +\right.$$

$$+ 81\pi\mathrm{Ls}_4' + \frac{9}{16}(-457 + 6\ln 3(67 + 3\ln 3(2\ln 3 - 9)))\mathrm{Ls}_2 -$$

$$- \frac{27}{8}(67 + 8\pi^2 + 18\ln 3(\ln 3 - 3))\mathrm{Ls}_3 + \frac{81}{2}(2\ln 3 - 3)\mathrm{Ls}_4 -$$

$$- \frac{81}{2}\mathrm{Ls}_5 + 12(3 - 2\ln 3)\mathrm{Ls}_4\left(\frac{\pi}{3}\right) +$$

$$\left.\left. + 49\mathrm{Ls}_5\left(\frac{\pi}{3}\right) - \frac{243}{4}\mathrm{Ls}_5'\right)\right)\epsilon^6 + \mathcal{O}\left(\epsilon^7\right) \tag{6.12}$$

$$\frac{\bigcirc\hspace{-0.4em}\bigcirc}{J^3} \overset{d=4-2\epsilon}{=} -2 - \frac{5}{3}\epsilon - \frac{1}{2}\epsilon^2 + \frac{103}{12}\epsilon^3 + \frac{7}{24}(163 - 128\zeta_3)\epsilon^4 +$$

$$+ \left(\frac{9055}{48} + \frac{136\pi^4}{45} + \frac{32}{3}\ln^2 2(\pi^2 - \ln^2 2) - 168\zeta_3 - 256a_4\right)\epsilon^5 +$$

$$+ \left(\frac{63517}{96} + \frac{16}{5}\ln^4 2(4\ln 2 - 15) - \frac{16}{3}\pi^2\ln^2 2(4\ln 2 - 9) - \frac{68}{15}\pi^4(4\ln 2 - 3) -\right.$$

$$\left. - \frac{1876}{3}\zeta_3 + 1240\zeta_5 - 1152a_4 - 1536a_5\right)\epsilon^6 + \mathcal{O}\left(\epsilon^7\right) \tag{6.13}$$

$\mathrm{Ls}_j' = -\int_0^{\frac{2\pi}{3}} d\tau\, \tau^{j-3}\ln^2\left|2\sin\frac{\tau}{2}\right|$ are special values of the generalized log-sine function [21].

3-loop, 5 lines: there are eleven colorings by mass. Eight of them reduce, while the remaining three are master integrals. One of the masters has an analytic solution in terms of Gamma functions. The second one (called E_3 in the literature) can be written in terms of the hypergeometric function $_2F_1$, cf. eq. (4.24) of ref. [21]. Its first six terms of the 4d ϵ-expansion (we will only reproduce the first five of them below) are given in eqs. (4.16), (4.18) of ref. [21]. The first five terms of the 4d ϵ-expansion of the third (fully massive) master integral (called D_5 in the literature) can be deduced from ref. [26] using the reduction given in eq. (6.25) below. One more term has recently been given in eq. (3.28) of ref. [27], but

we refrain from listing it here.

$$\text{(diagram)} = \frac{1}{6(d-3)}\left\{(3d-8)\,\text{(diagram)} - 3(d-2)\,\text{(diagram)}\right\} \tag{6.14}$$

$$\text{(diagram)} = \frac{1}{4(d-3)}\left\{(3d-8)\,\text{(diagram)} + \frac{(d-2)^2}{d-3}\left(\text{(diagram)}\right)^3\right\} \tag{6.15}$$

$$\text{(diagram)} = \frac{1}{2(d-3)}\left\{(3d-8)\,\text{(diagram)} - (d-2)\,\text{(diagram)}\right\} \tag{6.16}$$

$$\text{(diagram)} = -\frac{1}{4(d-4)}\left\{(3d-8)\,\text{(diagram)} + \frac{2(d-2)^2}{d-3}\left(\text{(diagram)}\right)^3\right\} \tag{6.17}$$

$$\text{(diagram)} = \frac{3d-8}{2}\,\text{(diagram)} - \frac{d-2}{2}\,\text{(diagram)} + \frac{(d-2)^2}{2(d-3)}\left(\text{(diagram)}\right)^3 \tag{6.18}$$

$$\text{(diagram)} = -\frac{3d-8}{4(2d-7)}\,\text{(diagram)} \tag{6.19}$$

$$\text{(diagram)} = \frac{3d-8}{d-2}\,\text{(diagram)} - 2\,\text{(diagram)} \tag{6.20}$$

$$\text{(diagram)} = -\frac{3d-8}{d-4}\,\text{(diagram)} \tag{6.21}$$

$$\frac{\text{(diagram)}}{J^3} = \frac{\pi^3}{\sin^2(\frac{\pi d}{2})\sin(\frac{3\pi d}{2})}\frac{\Gamma^2(\frac{d-2}{2})}{\Gamma^3(\frac{2-d}{2})\Gamma^2(d-2)\Gamma(\frac{d}{2})} \tag{6.22}$$

$$\frac{\text{(diagram)}}{J^3} \overset{d=4-2\epsilon}{=} \frac{2}{3} + \frac{5}{3}\epsilon + \left(5 + \frac{\pi^2}{6} - 3\sqrt{3}\text{Ls}_2\right)\epsilon^2 +$$

$$+ \left(\frac{44}{3} + \frac{\pi^2}{3} + \frac{1}{3}\zeta_3 - 3\sqrt{3}\left(\frac{5\pi^3}{162} + (2 - \ln 3)\text{Ls}_2 + \text{Ls}_3\right)\right)\epsilon^3 +$$

$$+ \left(\frac{128}{3} + \frac{5\pi^2}{6} - \frac{\pi^4}{60} + \frac{10}{3}\zeta_3 + \right. \tag{6.23}$$

$$+ \sqrt{3}\left(-\frac{1}{6}(2\pi^2 + 9\ln 3(10 + (\ln 3 - 4)\ln 3))\text{Ls}_2 + 3(\ln 3 - 2)\text{Ls}_3 - \right.$$

$$\left.\left. - 2\text{Ls}_4 - \frac{80}{27}\text{Ls}_4\left(\frac{\pi}{3}\right) + \frac{5\pi^3}{54}(\ln 3 - 2) + \frac{94}{27}\pi\zeta_3\right)\right)\epsilon^4 + \mathcal{O}\left(\epsilon^5\right)$$

$$\frac{\text{(diagram)}}{J^3} \overset{d=4-2\epsilon}{=} 1 + \frac{8}{3}\epsilon + \left(\frac{25}{3} - 6\sqrt{3}\text{Ls}_2\right)\epsilon^2 +$$

$$+ \left(\frac{76}{3} - 6\zeta_3 + \sqrt{3}\left(-\frac{\pi^3}{3} + 6(\ln 3 - 2)\text{Ls}_2 - 6\text{Ls}_3\right)\right)\epsilon^3 +$$

$$+ \left(76 - \frac{7\pi^4}{10} + 18\text{Ls}_2^2 - 12\pi\text{Ls}_3 + 18\text{Ls}_4' + \left(-\frac{92}{3} + 4\sqrt{3}\pi + 26\ln 3\right)\zeta_3 + \right.$$

$$+ \sqrt{3}\left(\frac{\pi^3}{3}(\ln 3 - 2) - 3(10 - 4\ln 3 + \ln^2 3)\text{Ls}_2 + \right.$$

$$\left.\left. + 6(\ln 3 - 2)\text{Ls}_3 - 4\text{Ls}_4\right)\right)\epsilon^4 + \mathcal{O}\left(\epsilon^5\right) \tag{6.24}$$

3-loop, 6 lines: there are ten colorings by mass. The first two terms of their 4d ϵ-

expansion are given in ref. [26]. Five of them reduce, while the remaining five are masters. The third term of the 4d ϵ-expansion of one of the masters (called D_4 in the literature) is given in eq. (4.10) of ref. [21].[4] The remaining four masters (called D_M, D_N, D_3 and D_6, respectively) are read from ref. [26].

$$\begin{aligned}
(\text{diagram}) &= -\frac{2(d-3)}{3(d-4)}(\text{diagram}) + \frac{3d-8}{12(d-4)}(\text{diagram}) - \frac{2(d-2)}{3(d-4)}(\text{diagram})\,(\text{diagram}) - \\
&\quad - \frac{(d-2)^2}{6(d-4)(d-3)}\Big((\text{diagram})\Big)^3
\end{aligned} \tag{6.25}$$

$$\begin{aligned}
(\text{diagram}) &= \frac{(3d-10)(3d-8)}{16(d-4)^2}\left((\text{diagram}) + \frac{4(d-4)}{2d-7}(\text{diagram})\right) + \\
&\quad + \frac{(d-2)^2(5d-18)}{8(d-4)^2(d-3)}\Big((\text{diagram})\Big)^3
\end{aligned} \tag{6.26}$$

$$(\text{diagram}) = -\frac{3(3d-10)(3d-8)}{16(d-4)(2d-7)}(\text{diagram}) - \frac{(d-2)^2}{8(d-4)(d-3)}\Big((\text{diagram})\Big)^3 \tag{6.27}$$

$$\begin{aligned}
(\text{diagram}) &= -\frac{(3d-10)(3d-8)}{(d-4)^2}\left((\text{diagram}) + \frac{d-4}{4(2d-7)}(\text{diagram})\right) + \\
&\quad + \frac{d-2}{d-4}(\text{diagram})\,(\text{diagram})
\end{aligned} \tag{6.28}$$

$$(\text{diagram}) = \frac{2(d-3)}{d-4}(\text{diagram}) + \frac{2(3d-10)(3d-8)}{(d-4)^2}(\text{diagram}) \tag{6.29}$$

$$\begin{aligned}
\frac{(\text{diagram})}{J^3} \overset{d=4-2\epsilon}{=} &-2\zeta_3\epsilon^2 + \left(\frac{77\pi^4}{1080} + \frac{27}{2}\mathrm{Ls}_2^2\right)\epsilon^3 + \\
&+ \left(-\frac{21}{8}\chi_5 + \frac{161}{54}\pi\mathrm{Ls}_4\left(\frac{\pi}{3}\right) - \frac{367}{216}\pi^3\mathrm{Ls}_2 - \right.\\
&\quad \left. - 7\pi\mathrm{Ls}_4 - 2\zeta_3 + \frac{2615}{432}\pi^2\zeta_3 - \frac{2047}{216}\zeta_5\right)\epsilon^4 + \mathcal{O}\left(\epsilon^5\right)
\end{aligned} \tag{6.30}$$

$$\frac{(\text{diagram})}{J^3} \overset{d=4-2\epsilon}{=} -2\zeta_3\epsilon^2 + \left(\frac{11\pi^4}{180} + 9\mathrm{Ls}_2^2\right)\epsilon^3 + \mathcal{O}\left(\epsilon^4\right) \tag{6.31}$$

$$\frac{(\text{diagram})}{J^3} \overset{d=4-2\epsilon}{=} -2\zeta_3\epsilon^2 + \left(\frac{7\pi^4}{60} + \frac{2}{3}\ln^2 2(\pi^2 - \ln^2 2) - 16a_4\right)\epsilon^3 + \mathcal{O}\left(\epsilon^4\right) \tag{6.32}$$

$$\frac{(\text{diagram})}{J^3} \overset{d=4-2\epsilon}{=} -2\zeta_3\epsilon^2 + \left(\frac{\pi^4}{24} + \frac{27}{2}\mathrm{Ls}_2^2\right)\epsilon^3 + \mathcal{O}\left(\epsilon^4\right) \tag{6.33}$$

$$\frac{(\text{diagram})}{J^3} \overset{d=4-2\epsilon}{=} -2\zeta_3\epsilon^2 + \left(\frac{17\pi^4}{90} + \frac{2}{3}\ln^2 2(\pi^2 - \ln^2 2) + 9\mathrm{Ls}_2^2 - 16a_4\right)\epsilon^3 + \mathcal{O}\left(\epsilon^4\right) \tag{6.34}$$

$\chi_5 = \sum_{n=1}^{\infty}\frac{(n!)^2}{(2n)!}\frac{1}{n^2}\left(\sum_{j=1}^{n-1}\frac{1}{j}\right)^3 \approx 0.0678269619272\ldots$ is a special case of a binomial sum [21].

---

[4]Note that there is a typo in eq. (4.10) of ref. [21]. The second-last term should read $-\frac{161}{54}\pi\mathrm{Ls}_4(\frac{\pi}{3})$, see also ref. [27].

6.4 4-loop

There are ten topologies.

4-loop QED-type cases, 5 lines: there is one topology, BB.

There are two QED-type colorings of BB. Both of them are masters. One is known analytically in terms of Gamma functions, while the other one is new.[5] Interestingly, the analytic value of the last two terms in eq. (6.36) were obtained in a physics computation in which this master integral contributed [29].

$$\frac{\bigcirc}{J^4} = 3(d-2)4^{d-3}\frac{\Gamma(5-2d)\Gamma(\frac{8-3d}{2})\Gamma(\frac{5-d}{2})\Gamma^2(\frac{d}{2})}{\Gamma(\frac{11-3d}{2})\Gamma^3(\frac{4-d}{2})} \tag{6.35}$$

$$\frac{\bigcirc}{J^4} \overset{d=4-2\epsilon}{=} -1 - \frac{1}{2}\epsilon + \frac{17}{36}\epsilon^2 + \frac{1}{216}\epsilon^3 - \frac{37207}{1296}\epsilon^4 + \left(-\frac{1976975}{7776} + \frac{1792}{9}\zeta_3\right)\epsilon^5 +$$
$$+ \left(-\frac{72443143}{46656} - \frac{4352\pi^4}{135} + \frac{1024}{9}\ln^2 2(\ln^2 2 - \pi^2) + \frac{8192}{3}a_4 + \frac{47488}{27}\zeta_3\right)\epsilon^6 +$$
$$+ \mathcal{O}\left(\epsilon^7\right) \tag{6.36}$$

4-loop QED-type cases, 6 lines: there are two topologies, T and G.

There are four QED-type colorings of T. All of them are masters. One of them is known analytically, while the first six orders of the 4d ϵ-expansion of two others were given in eq. (16) of ref. [7] and eq. (18) of ref. [11],[6] respectively. The fourth one is new.

$$\frac{\bigcirc}{J^4} = \frac{8^{d-3}\Gamma^3(\frac{1}{2})\Gamma(6-2d)\Gamma^3(\frac{d}{2})}{\sin(\frac{3\pi d}{2})\Gamma(\frac{11-3d}{2})\Gamma^2(\frac{4-d}{2})\Gamma^2(d-2)} \tag{6.37}$$

$$\frac{\bigcirc}{J^4} \overset{d=4-2\epsilon}{=} \frac{3}{2} + \frac{7}{2}\epsilon + \frac{9}{2}\epsilon^2 + \left(-\frac{39}{2} - 3\zeta_3\right)\epsilon^3 + \left(-208 - \frac{\pi^4}{20} + 109\zeta_3\right)\epsilon^4 +$$
$$+ \left(-1254 - \frac{547\pi^4}{60} + 32\ln^2 2(\ln^2 2 - \pi^2) + 768a_4 + 855\zeta_3 + 189\zeta_5\right)\epsilon^5 +$$
$$+ \mathcal{O}\left(\epsilon^6\right) \tag{6.38}$$

$$\frac{\bigcirc}{J^4} \overset{d=4-2\epsilon}{=} \frac{2}{3} + \frac{4}{3}\epsilon + \frac{2}{3}\epsilon^2 + \frac{4}{3}(-11 + 4\zeta_3)\epsilon^3 + \left(-116 - \frac{4\pi^4}{15} + \frac{200\zeta_3}{3}\right)\epsilon^4 +$$
$$+ \left(-\frac{1928}{3} - \frac{326\pi^4}{45} + \frac{64}{3}\ln^2 2(\ln^2 2 - \pi^2) + 512a_4 + \frac{1192\zeta_3}{3} + 96\zeta_5\right)\epsilon^5 +$$
$$+ \mathcal{O}\left(\epsilon^6\right) \tag{6.39}$$

$$\frac{\bigcirc}{J^4} \overset{d=4-2\epsilon}{=} \frac{1}{4} + \frac{1}{2}\epsilon + 0\cdot\epsilon^2 + \left(-8 + \frac{13}{2}\zeta_3\right)\epsilon^3 + \left(-\frac{241}{4} - \frac{5\pi^4}{8} + 4\zeta_3\right)\epsilon^4 +$$

---

[5]This integral has also been expanded in terms of 1-dimensional harmonic polylogarithms [28].

[6]Note that in ref. [11] the last term of eq. (6.39) involves a numerical coefficient $N_{10} \approx 5.3111546$, which we have determined to be $N_{10} = \frac{49\pi^4}{720} + \frac{1}{6}\ln^2 2\left(\pi^2 - \ln^2 2\right) - 4a_4$, using our high-precision result eq. (4.10) and PSLQ [17].

$$+\left(-\frac{669}{2}-\frac{\pi^4}{5}-36\zeta_3+\frac{693}{2}\zeta_5\right)\epsilon^5+\mathcal{O}\left(\epsilon^6\right) \tag{6.40}$$

There are five QED-type colorings of G. All of them reduce.

$$\text{(G diagram)}=\frac{2d-5}{4(d-3)}\,\text{(diagram)}-\frac{d-2}{2(d-3)}\,\text{(diagram)} \tag{6.41}$$

$$\text{(G diagram)}=\frac{2d-5}{4}\,\text{(diagram)}-\frac{d-2}{2}\,\text{(diagram)}+\frac{(d-2)^3}{8(d-3)^2}\left(\text{(diagram)}\right)^4 \tag{6.42}$$

$$\text{(G diagram)}=-\frac{2d-5}{6(d-3)}\,\text{(diagram)} \tag{6.43}$$

$$\text{(G diagram)}=-\frac{(2d-5)(3d-8)}{6(d-3)(d-4)}\,\text{(diagram)} \tag{6.44}$$

$$\text{(G diagram)}=\frac{2d-5}{2(d-3)}\,\text{(diagram)}-\frac{d-2}{2(d-3)}\,\text{(diagram)} \tag{6.45}$$

4-loop QED-type cases, 7 lines: there are three topologies, VB, N and U.

There are seven QED-type colorings of VB. Five of them reduce. There are two master integrals. Both are new.

$$\text{(VB diagram)}=\frac{(2d-5)(3d-10)(3d-8)}{3(d-4)^2(3d-11)}\,\text{(diagram)}+\frac{2(d-3)^2}{(d-4)(3d-11)}\,\text{(diagram)} \tag{6.46}$$

$$\text{(VB diagram)}=-\frac{(2d-5)(3d-8)}{3(d-4)^2}\,\text{(diagram)}-\frac{4(d-3)^2}{3(d-4)(3d-10)}\,\text{(diagram)}+$$
$$+\frac{(d-2)(3d-8)}{8(2d-7)(3d-10)}\,\text{(diagram)} \tag{6.47}$$

$$\text{(VB diagram)}=\frac{(2d-5)(3d-8)}{3(d-4)(d-3)}\,\text{(diagram)}-\frac{d-3}{d-4}\,\text{(diagram)}-\frac{(d-2)(3d-8)}{4(d-4)(d-3)}\,\text{(diagram)} \tag{6.48}$$

$$\text{(VB diagram)}=\frac{(2d-5)(3d-8)}{16(d-4)(d-3)}\,\text{(diagram)}-\frac{2(d-3)}{3(d-4)}\,\text{(diagram)}-\frac{(d-2)(3d-8)}{8(d-4)(d-3)}\,\text{(diagram)}-$$
$$-\frac{(d-2)^3}{32(d-4)(d-3)^2}\left(\text{(diagram)}\right)^4 \tag{6.49}$$

$$\text{(VB diagram)}=\frac{2}{3d-10}\left\{(d-3)\,\text{(diagram)}-\frac{3d-8}{2(d-3)}\left(\frac{2d-5}{3}\,\text{(diagram)}-\frac{d-2}{4}\,\text{(diagram)}\right)\right\} \tag{6.50}$$

$$\frac{\text{(diagram)}}{J^4}\overset{d=4-2\epsilon}{=}-\frac{1}{6}-\frac{5}{6}\epsilon-\left(\frac{11}{3}+\zeta_3\right)\epsilon^2+\left(-\frac{44}{3}-\frac{\pi^4}{60}+\frac{2}{3}\zeta_3\right)\epsilon^3+$$
$$+\left(-\frac{332}{6}-\frac{\pi^4}{6}+\frac{31}{3}\zeta_3+53\zeta_5\right)\epsilon^4+\mathcal{O}\left(\epsilon^5\right) \tag{6.51}$$

$$\frac{\text{(diagram)}}{J^4}\overset{d=4-2\epsilon}{=}-\frac{1}{6}-\frac{5}{6}\epsilon-\left(\frac{11}{3}+\frac{1}{2}\zeta_3\right)\epsilon^2+\left(-\frac{44}{3}-\frac{\pi^4}{120}+\frac{13}{6}\zeta_3\right)\epsilon^3+$$
$$+\left(-\frac{166}{3}-\frac{5\pi^4}{24}+\frac{29}{6}\zeta_3+\frac{43}{2}\zeta_5\right)\epsilon^4+\mathcal{O}\left(\epsilon^5\right) \tag{6.52}$$

There are five QED-type colorings of N. All of them reduce.

$$\text{(N diagram)}=\frac{(2d-5)(3d-8)}{6(d-3)^2}\,\text{(diagram)}-\frac{(d-2)(3d-8)}{4(d-3)^2}\,\text{(diagram)}-$$

$$-\frac{(d-2)^3}{8(d-3)^3}\left(\bigcirc\right)^4 \tag{6.53}$$

$$\text{⬭} = -\frac{(2d-5)(3d-8)}{6(d-4)(d-3)}\,\text{⬭} + \frac{(d-2)(3d-8)}{8(d-3)(2d-7)}\,\text{⬭}\,\bigcirc \tag{6.54}$$

$$\text{⬭} = \frac{(2d-5)(3d-8)}{6(d-4)(3d-11)}\,\text{⬭} \tag{6.55}$$

$$\text{⬭} = -\frac{(2d-5)(3d-8)}{16(d-4)}\,\text{⬭} + \frac{(d-2)(3d-8)}{4(2d-7)}\,\text{⬭}\,\bigcirc -$$
$$-\frac{3(d-2)^3}{32(d-4)(d-3)}\left(\bigcirc\right)^4 \tag{6.56}$$

$$\text{⬭} = \frac{(2d-5)(3d-8)}{16(d-3)}\,\text{⬭} + \frac{(d-2)(3d-8)}{8(d-4)(d-3)}\,\text{⬭}\,\bigcirc -$$
$$-\frac{(d-2)(3d-8)}{8(d-3)}\,\text{⬭}\,\bigcirc + \frac{(d-2)^3(3d-4)}{32(d-4)(d-3)^2}\left(\bigcirc\right)^4 \tag{6.57}$$

There are four QED-type colorings of U. All of them reduce.

$$\text{⬭} = \frac{2}{3}\,\text{△} - \frac{(d-2)(3d-8)}{8(d-3)^2}\,\text{⬭}\,\bigcirc - \frac{(d-2)^3}{8(d-3)^3}\left(\bigcirc\right)^4 \tag{6.58}$$

$$\text{⬭} = -\frac{d-3}{d-5}\,\text{△} - \frac{3(d-2)(3d-8)}{8(d-5)(d-4)}\,\text{⬭}\,\bigcirc - \frac{3(d-2)^3}{4(d-5)(d-4)(d-3)}\left(\bigcirc\right)^4 \tag{6.59}$$

$$\text{⬭} = -\frac{d-3}{2(d-4)}\,\text{△} - \frac{(d-2)(3d-8)}{8(d-4)(2d-7)}\,\text{⬭}\,\bigcirc \tag{6.60}$$

$$\text{⬭} = -\frac{d-3}{3d-11}\,\text{△} \tag{6.61}$$

4-loop QED-type cases, 8 lines: there are two topologies, VV and W.

There are seven QED-type colorings of VV. All of them reduce.

$$\text{⬭} = -\frac{(2d-7)(2d-5)(3d-10)(3d-8)}{6(d-4)^2(3d-13)(3d-11)}\,\text{⬭} - \frac{(d-3)^2(2d-7)}{(d-4)(3d-13)(3d-11)}\,\text{⬭} \tag{6.62}$$

$$\text{⬭} = \frac{(2d-7)(2d-5)(3d-10)(3d-8)}{18(d-4)^2(d-3)(3d-11)}\,\text{⬭} - \frac{(d-3)(2d-7)}{3(d-4)(3d-11)}\,\text{⬭} -$$
$$-\frac{(d-2)(3d-10)(3d-8)}{48(d-4)(d-3)(2d-7)}\,\text{⬭}\,\bigcirc \tag{6.63}$$

$$\text{⬭} = -\frac{(2d-7)(2d-5)(3d-10)(3d-8)}{6(d-4)^2(d-3)(3d-11)}\,\text{⬭} + \frac{(d-3)(2d-7)}{4(d-4)^2}\,\text{⬭} +$$
$$+\frac{(d-2)(3d-8)(5d^2-35d+61)}{16(d-4)^2(d-3)(2d-7)}\,\text{⬭}\,\bigcirc \tag{6.64}$$

$$\text{⬭} = -\frac{(2d-7)(2d-5)(3d-10)(3d-8)}{6(d-4)^2(d-3)(3d-11)}\,\text{⬭} - \frac{4(d-3)^2(2d-7)}{3(d-4)(3d-11)(3d-10)}\,\text{△} +$$
$$+\frac{(d-2)(3d-8)(95d^3-989d^2+3428d-3956)}{32(d-4)(d-3)(2d-7)(3d-11)(3d-10)}\,\text{⬭}\,\bigcirc +$$
$$+\frac{(d-2)^3}{16(d-4)(d-3)^2}\left(\bigcirc\right)^4 \tag{6.65}$$

$$\text{(W)} = -\frac{(2d-5)(3d-11)(3d-8)}{32(d-4)(2d-9)}\,\text{(diagram)} - \frac{(d-3)^2}{4(d-4)(2d-9)}\,\text{(diagram)} -$$

$$-\frac{(3d-10)}{4(2d-9)}\,\text{(diagram)} + \frac{(d-2)(3d-8)(12d^2-101d+204)}{32(d-4)(2d-9)(2d-7)}\,\text{(diagram)} -$$

$$-\frac{(d-2)(3d-8)}{16(d-4)(2d-9)}\,\text{(diagram)} - \frac{3(d-2)^3(3d-7)}{64(d-4)(d-3)(2d-9)}\left(\text{(diagram)}\right)^4 \qquad (6.66)$$

$$\text{(diagram)} = \frac{(2d-5)(3d-8)}{12(d-3)(2d-7)}\,\text{(diagram)} + \frac{(2d-5)(3d-8)}{64(d-3)(2d-7)}\,\text{(diagram)} - \frac{2(d-3)^2}{3(2d-7)(3d-10)}\,\text{(diagram)} +$$

$$+\frac{3d-10}{2(2d-7)}\,\text{(diagram)} - \frac{(d-2)^3(73d^2-512d+896)}{128(d-4)^2(d-3)^2(2d-7)}\left(\text{(diagram)}\right)^4 -$$

$$-\frac{(d-2)(3d-8)(19d^2-128d+216)}{(16(d-4)(d-3)(2d-7)(3d-10)}\,\text{(diagram)} - \qquad (6.67)$$

$$-\frac{(d-2)(3d-10)(3d-8)}{32(d-4)^2(d-3)}\,\text{(diagram)} - \frac{(d-2)^3(73d^2-512d+896)}{128(d-4)^2(d-3)^2(2d-7)}\left(\text{(diagram)}\right)^4$$

$$\text{(diagram)} = \frac{(2d-7)(2d-5)(3d-10)(3d-8)}{64(d-4)^2(d-3)}\,\text{(diagram)} + \frac{(d-3)(2d-7)}{3(d-5)(d-4)}\,\text{(diagram)} -$$

$$-\frac{(d-2)(3d-10)(3d-8)}{8(d-4)(2d-7)}\,\text{(diagram)} +$$

$$+\frac{(d-2)(3d-8)(11d^2-77d+134)}{32(d-5)(d-4)^2(d-3)}\,\text{(diagram)} +$$

$$+\frac{(d-2)^3(18d^3-129d^2+245d-58)}{128(d-5)(d-4)^2(d-3)^2}\left(\text{(diagram)}\right)^4 \qquad (6.68)$$

There are five QED-type colorings of W. Four of them reduce. There is one master integral, whose leading term in 4d can be read from ref. [30] due to the fact that it does not contain any infrared divergences.

$$\text{(diagram)} = -\frac{(2d-5)(3d-8)(27d^3-283d^2+990d-1156)}{12(d-4)^3(2d-7)(3d-11)}\,\text{(diagram)} -$$

$$-\frac{(d-3)(3d-10)}{2(d-4)(2d-7)}\,\text{(diagram)} - \frac{2(d-3)^4(5d-18)}{3(d-4)^2(2d-7)(3d-11)(3d-10)}\,\text{(diagram)} -$$

$$-\frac{(2d-5)(3d-8)}{64(d-4)(2d-7)}\,\text{(diagram)} + \frac{(d-2)(3d-8)(5d-18)}{16(d-4)(3d-11)(3d-10)}\,\text{(diagram)} -$$

$$-\frac{7(d-2)^3}{128(d-4)(d-3)(2d-7)}\left(\text{(diagram)}\right)^4 \qquad (6.69)$$

$$\text{(diagram)} = \frac{2(2d-7)(2d-5)(3d-10)(3d-8)}{9(d-4)^3(3d-11)}\,\text{(diagram)} +$$

$$+\frac{8(d-3)^3(2d-7)}{9(d-4)^2(3d-11)(3d-10)}\,\text{(diagram)} + \frac{2(d-3)^3(2d-7)}{3(d-4)^2(3d-11)}\,\text{(diagram)} -$$

$$-\frac{(d-2)(3d-8)(7d^2-48d+82)}{24(d-4)(2d-7)(3d-11)(3d-10)}\,\text{(diagram)} \qquad (6.70)$$

$$\text{(diagram)} = \frac{(2d-5)(3d-8)}{6(d-4)(2d-7)}\,\text{(diagram)} - \frac{(2d-5)(3d-8)}{32(d-3)(2d-7)}\,\text{(diagram)} + \frac{d-3}{2(d-4)}\,\text{(diagram)} -$$

$$-\frac{4(d-3)^3}{3(d-4)(2d-7)(3d-10)}\,\triangle + \frac{(d-3)(3d-10)}{(d-4)(2d-7)}\,\ominus -$$

$$-\frac{3d-10}{2(d-4)}\,\oplus - \frac{(d-2)(3d-8)}{8(2d-7)(3d-10)}\,\infty\!\bigcirc + \tag{6.71}$$

$$+\frac{(d-2)(3d-8)}{16(d-4)(d-3)}\,\infty\!\bigcirc + \frac{(d-2)^3(9d-28)}{64(d-4)(d-3)^2(2d-7)}\left(\bigcirc\right)^4$$

$$\oplus \;=\; \frac{(2d-5)(3d-8)}{32(d-4)(d-3)}\,\otimes + \frac{2(d-3)^2(2d-7)}{3(d-4)^2(3d-11)}\,\triangle - \frac{d-3}{2(d-4)}\,\triangle +$$

$$+\frac{3d-10}{2(d-4)}\,\oplus + \frac{(d-2)(3d-8)(d^2-4d+2)}{8(d-4)^2(d-3)(3d-11)}\,\infty\!\bigcirc +$$

$$+\frac{(d-2)^3(29d^2-177d+268)}{64(d-4)^2(d-3)^2(3d-11)}\left(\bigcirc\right)^4 \tag{6.72}$$

$$\frac{\ominus}{J^4} \;\overset{d=4-2\epsilon}{=}\; 5\zeta_5\epsilon^3 + \mathcal{O}\left(\epsilon^4\right) \tag{6.73}$$

4-loop QED-type cases, 9 lines: there are two topologies, H and X.

There are five QED-type colorings of H. All of them reduce.

$$\boxplus \;=\; -\frac{3(2d-5)(3d-11)(3d-8)(54-29d+4d^2)}{256(d-5)(d-4)^2(d-3)(2d-9)}\,\otimes -$$

$$-\frac{4(d-3)^2(2d-7)}{3(d-5)(3d-13)(3d-11)}\,\triangle +$$

$$+\frac{3(d-3)(d^2-11d+27)}{8(d-5)(d-4)(2d-9)}\,\ominus - \frac{9(d-4)(3d-10)}{8(d-5)(2d-9)}\,\oplus -$$

$$-\frac{(d-2)(3d-8)(13d^3-77d^2+9d+351)}{32(d-5)(d-3)(2d-9)(3d-13)(3d-11)}\,\infty\!\bigcirc -$$

$$-\frac{3(d-2)(3d-8)(13d^2-92d+162)}{64(d-5)(d-4)(2d-9)(2d-7)}\,\infty\!\bigcirc -$$

$$-\frac{(d-2)^3(2452d^5-43031d^4+329345d^3-1198763d^2+2170827d-1564110)}{512(d-5)(d-4)^2(d-3)^2(2d-9)(3d-13)(3d-11)}\times$$

$$\times\left(\bigcirc\right)^4 \tag{6.74}$$

$$\boxplus \;=\; -\frac{3(2d-7)(2d-5)(3d-10)(3d-8)}{2(d-4)(3d-14)(3d-13)(3d-11)}\,\otimes -$$

$$-\frac{6(d-3)^2(2d-7)}{(3d-14)(3d-13)(3d-11)}\,\ominus -$$

$$-\frac{32(d-3)^3(2d-7)}{9(3d-14)(3d-13)(3d-11)(3d-10)}\,\triangle +$$

$$+\frac{(d-2)(3d-8)(139d^3-1495d^2+5344d-6348)}{96(2d-7)(3d-14)(3d-13)(3d-11)(3d-10)}\,\infty\!\bigcirc \tag{6.75}$$

$$\boxplus \;=\; \frac{7(2d-7)(2d-5)(3d-10)(3d-8)}{9(d-4)^2(3d-13)(3d-11)}\,\otimes + \frac{4(d-3)^2(2d-7)}{3(d-4)(3d-13)(3d-11)}\,\ominus +$$

$$+ \frac{32(d-3)^3(2d-7)}{9(d-4)(3d-13)(3d-11)(3d-10)} \,\triangle\, - \frac{d-4}{2(3d-13)} \,\oplus\, -$$

$$- \frac{(d-2)(3d-8)(409d^3 - 4285d^2 + 14944d - 17348)}{96(d-4)(2d-7)(3d-13)(3d-11)(3d-10)} \,\bigcirc\!\bigcirc\, -$$

$$- \frac{(d-2)^3}{16(d-4)(d-3)(3d-13)} \left(\bigcirc\right)^4 \tag{6.76}$$

$$\boxminus = - \frac{(2d-5)(3d-8)(3d^3 - 19d^2 + 19d + 38)}{12(d-5)(d-4)^2(2d-7)(3d-11)} \,\bigcirc\, +$$

$$+ \frac{(2d-5)(3d-11)(3d-8)(2d^3 - 14d^2 + 23d + 6)}{128(d-5)(d-4)^3(d-3)(2d-7)} \,\bigcirc\, -$$

$$- \frac{2(d-3)^2(2d-7)}{3(d-5)(d-4)(3d-11)} \,\triangle\, -$$

$$- \frac{2(d-3)^3(17d^2 - 125d + 230)}{3(d-5)(d-4)(2d-7)(3d-11)(3d-10)} \,\triangle\, +$$

$$+ \frac{(d-3)(5d^2 - 37d + 69)}{4(d-5)(d-4)^2} \,\bigcirc\, + \frac{3(d-3)(3d-10)}{2(d-5)(2d-7)} \,\bigcirc\, - \tag{6.77}$$

$$- \frac{3(3d-10)}{4(d-5)} \,\bigcirc\, - \frac{(d-2)(3d-8)(10d^3 - 87d^2 + 235d - 186)}{32(d-5)(d-4)^2(d-3)(3d-11)} \,\bigcirc\!\bigcirc\, -$$

$$- \frac{(d-2)(3d-8)(38d^4 - 568d^3 + 3174d^2 - 7863d + 7290)}{16(d-5)(d-4)^2(2d-7)(3d-11)(3d-10)} \,\bigcirc\!\bigcirc\, -$$

$$- \frac{(d-2)^3(418d^5 - 7346d^4 + 51389d^3 - 178846d^2 + 309603d - 213234)}{256(d-5)(d-4)^3(d-3)^2(2d-7)(3d-11)} \left(\bigcirc\right)^4$$

$$\boxminus = - \frac{(2d-5)(3d-8)(69d^3 - 725d^2 - 2543d - 2978)}{12(d-4)^2(2d-9)(2d-7)(3d-11)} \,\bigcirc\, -$$

$$- \frac{3(2d-5)(3d-8)}{128(d-3)(2d-9)(2d-7)} \,\bigcirc\, -$$

$$- \frac{2(d-3)^3(d-2)(13d-47)}{9(d-4)(2d-9)(2d-7)(3d-11)(3d-10)} \,\triangle\, -$$

$$- \frac{(d-3)(d^2 - 11d + 27)}{8(d-4)^2(2d-9)} \,\bigcirc\, - \frac{3(d-3)(3d-10)}{2(2d-9)(2d-7)} \,\bigcirc\, +$$

$$+ \frac{3(3d-10)}{8(2d-9)} \,\bigcirc\, + \frac{(d-2)(3d-8)(5d-18)}{64(d-4)^2(d-3)(2d-9)} \,\bigcirc\!\bigcirc\, +$$

$$+ \frac{(d-2)(3d-8)(1139d^4 - 16453d^3 + 89068d^2 - 214178 + 193044)}{192(d-4)^2(2d-9)(2d-7)(3d-11)(3d-10)} \,\bigcirc\!\bigcirc\, +$$

$$+ \frac{(d-2)^3(48d^3 - 445d^2 + 1352d - 1344)}{256(d-4)^2(d-3)^2(2d-9)(2d-7)} \left(\bigcirc\right)^4 \tag{6.78}$$

There are two QED-type colorings of X. One reduces. The other one is a master integral. Its leading coefficient (denoted by X_0 below) is not yet known analytically.

$$\boxtimes = \frac{(2d-5)(3d-8)(2109d^4 - 31288d^3 + 173302d^2 - 425005d + 389562)}{36(d-4)(2d-9)^2(2d-7)(3d-13)(3d-11)} \,\bigcirc\, +$$

$$+ \frac{(2d-5)(3d-8)(24d^3 - 268d^2 + 1003d - 1258)}{256(d-4)^2(2d-9)^2(2d-7)} \,\bigcirc\, +$$

$$
+\frac{14(d-3)^2(2d-7)}{3(2d-9)(3d-13)(3d-11)} \ \text{(diagram)} \ +
$$

$$
+\frac{2(d-3)^3(295d^3-3332d^2+12431d-15334)}{9(2d-9)^2(2d-7)(3d-13)(3d-11)(3d-10)} \ \text{(diagram)} \ +
$$

$$
+\frac{3(d-4)(d-3)(3d-10)}{2(2d-9)^2(2d-7)} \ \text{(diagram)} \ +\frac{(d-4)^2}{2(2d-9)(3d-13)} \ \text{(diagram)} \ -
$$

$$
-\frac{(d-2)(3d-8)(599d^4-9067d^3+51340d^2-12886d+121044)}{48(2d-9)^2(2d-7)(3d-13)(3d-11)(3d-10)} \ \text{(diagram)} \ +
$$

$$
+\frac{(d-2)^3(392d^4-6204d^3+36843d^2-97323d+96502)}{512(d-4)^2(d-3)(2d-9)^2(2d-7)(3d-13)} \left(\text{(diagram)} \right)^4 \tag{6.79}
$$

$$
\frac{\text{(diagram)}}{J^4} \overset{d=4-2\epsilon}{=} X_0\epsilon^4 + \mathcal{O}\left(\epsilon^5\right) \tag{6.80}
$$

All the above formulas agree with our numerical results of section 4.

7. Conclusions

We have employed the general method of numerically solving single-scale integrals in terms of their ϵ-expansion around $d = 4 - 2\epsilon$ via difference equations, to high precision and to high ϵ-orders. We have covered the set of all vacuum master integrals up to three loops, as well as 'QED-type' vacuum master integrals at 4-loop order. These integrals play a role in state-of-the-art perturbative calculations for precision tests of the standard model.

The main vehicle of solving the difference equations treated in this work was a formal representation in terms of factorial series, which could then be evaluated numerically in a truncated form.

In cases where the factorial series representation does not converge, a more general (and hence more complicated) method can be used, which transforms the problem into differential equations. We have encountered only one such case, and have shown in detail how it can be represented in terms of multiple integrals, which we then solved numerically.

Furthermore, we have made an attempt to collect all presently known analytic results for the class of vacuum master integrals that we have treated here, up to the 4-loop level. This is meant as a concise reference for practitioners in the field.

Acknowledgments

A. Numerical results for analytically known master integrals

As a complement to section 4, we here list the first few terms of the Laurent expansions in $\epsilon = (4 - d)/2$ of those single-mass-scale vacuum master integrals up to four loops that are known analytically (see the explicit d-dimensional expressions of section 6).

Notation and integral measure are as in section 4, which in particular determines the 1-loop tadpole to be $J = \frac{1}{\Gamma(2+\epsilon)} \int \frac{\mathrm{d}^{4-2\epsilon}p}{\pi^{2-\epsilon}} \frac{1}{p^2+1} = \frac{-1}{\epsilon(1-\epsilon^2)} = -\sum_{n=0}^{\infty} \epsilon^{2n-1}$.

$$
\bigcirc = -1.0000000000000000000000000000000000000000000000000 \, \epsilon^{-1} - \\
- 1.0000000000000000000000000000000000000000000000000 \, \epsilon - \\
- 1.0000000000000000000000000000000000000000000000000 \, \epsilon^3 + \\
+ \mathcal{O}\left(\epsilon^5\right) \tag{A.1}
$$

$$
\ominus = -0.5000000000000000000000000000000000000000000000000 \, \epsilon^{-2} - \\
- 0.5000000000000000000000000000000000000000000000000 \, \epsilon^{-1} - \\
- 3.6449340668482264364724151666460251892189499012068 - \\
- 3.4428771636886321510726770051345751984539636088663 \, \epsilon - \\
- 17.748133915933433223119391395079063285971925961 21 \, \epsilon^2 - \\
- 16.366439374126401323669287645924253086404587829687 \, \epsilon^3 + \\
+ \mathcal{O}\left(\epsilon^4\right) \tag{A.2}
$$

$$
\bigcirc\!\!\!\!\!\dashv = -0.0833333333333333333333333333333333333333333333333 \, \epsilon^{-2} - \\
- 0.3750000000000000000000000000000000000000000000000 \, \epsilon^{-1} - \\
- 2.4683003667574465515695409166563459279428082839367 - \\
- 8.5848042311088475775631523236940150167718153674315 \, \epsilon - \\
- 38.120827450450135424466436253406610052456582985006 \, \epsilon^2 + \\
+ \mathcal{O}\left(\epsilon^3\right) \tag{A.3}
$$

$$
\bigcirc\!\!\!\!\dashv = +0.3333333333333333333333333333333333333333333333333 \, \epsilon^{-3} + \\
+ 0.1666666666666666666666666666666666666666666666667 \, \epsilon^{-2} + \\
+ 0.5833333333333333333333333333333333333333333333333 \, \epsilon^{-1} + \\
+ 0.41381840842558476106596843069719997537329677957466 - \\
- 24.905969600320865917659060143145414845610363033237 \, \epsilon - \\
- 12.059724940640299353325034075589267393005352211165 \, \epsilon^2 + \\
+ \mathcal{O}\left(\epsilon^3\right) \tag{A.4}
$$

$$
\widehat{V} = -0.3333333333333333333333333333333333333333333333333 \, \epsilon^{-3} - \\
- 0.6666666666666666666666666666666666666666666666667 \, \epsilon^{-2} - \\
- 5.9565348003631195396114969999587170451045664690803 \, \epsilon^{-1} - \\
- 10.976993729846780032023343117902167435855817881707 - \\
- 67.587197404302297868575437012376235190940093056288 \, \epsilon -
$$

$$- 120.04368176952781664333978568556636327245719008030 \; \epsilon^2 +$$
$$+ \mathcal{O}\left(\epsilon^3\right) \tag{A.5}$$

$$\begin{aligned} = \; & + 0.083333333333333333333333333333333333333333333 \; \epsilon^{-3} + \\ & + 0.236111111111111111111111111111111111111111 \; \epsilon^{-2} + \\ & + 0.418981481481481481481481481481481481481481 \; \epsilon^{-1} + \\ & + 0.587043717067560069707943739339175284153 - \\ & - 38.15649063807203021274518890590965524153 \; \epsilon + \mathcal{O}\left(\epsilon^2\right) \end{aligned} \tag{A.6}$$

$$\begin{aligned} = \; & + 0.166666666666666666666666666666666666666667 \; \epsilon^{-4} + \\ & + 0.166666666666666666666666666666666666666667 \; \epsilon^{-3} - \\ & - 0.166666666666666666666666666666666666666667 \; \epsilon^{-2} + \\ & + 0.113027053344097140865008356239183274849 \; \epsilon^{-1} - \\ & - 78.06045784302350379977045250776444270422 - \\ & - 77.68037792722049725359022296531379645497 \; \epsilon + \mathcal{O}\left(\epsilon^2\right) \end{aligned} \tag{A.7}$$

In fact, the results shown here have been obtained via numerically evaluating truncated factorial series along the lines of sections 2 and 3, but they of course coincide perfectly with the analytical results of section 6 (note the different normalization there).

References

[1] K. Kajantie, M. Laine and Y. Schröder, *A simple way to generate high order vacuum graphs*, *Phys. Rev.* **D 65** (2002) 045008 [`hep-ph/0109100`].

[2] K.G. Chetyrkin and F.V. Tkachov, *Integration by parts: the algorithm to calculate beta functions in 4 loops*, *Nucl. Phys.* **B 192** (1981) 159; F.V. Tkachov, *A theorem on analytical calculability of four loop renormalization group functions*, *Phys. Lett.* **B 100** (1981) 65.

[3] S. Laporta, *High-precision calculation of multi-loop Feynman integrals by difference equations*, *Int. J. Mod. Phys.* **A 15** (2000) 5087 [`hep-ph/0102033`].

[4] Y. Schröder, *Automatic reduction of four-loop bubbles*, *Nucl. Phys.* **116** *(Proc. Suppl.)* (2003) 402 [`hep-ph/0211288`].

[5] V.A. Smirnov, *Applied asymptotic expansions in momenta and masses*, Springer, Berlin 2002; M. Misiak and M. Münz, *Two loop mixing of dimension five flavor changing operators*, *Phys. Lett.* **B 344** (1995) 308 [`hep-ph/9409454`].

[6] Y. Schröder, *Tackling the infrared problem of thermal QCD*, *Nucl. Phys.* **129** *(Proc. Suppl.)* (2004) 572 [`hep-lat/0309112`].

[7] S. Laporta, *High-precision epsilon expansions of massive four-loop vacuum bubbles*, *Phys. Lett.* **B 549** (2002) 115 [`hep-ph/0210336`].

[8] T. van Ritbergen, J.A.M. Vermaseren and S.A. Larin, *The four-loop beta function in quantum chromodynamics*, *Phys. Lett.* **B 400** (1997) 379 [`hep-ph/9701390`]; K.G. Chetyrkin, *Four-loop renormalization of QCD: full set of renormalization constants and anomalous dimensions*, *Nucl. Phys.* **B 710** (2005) 499 [`hep-ph/0405193`];

M. Czakon, *The four-loop QCD beta-function and anomalous dimensions*, *Nucl. Phys.* **B 710** (2005) 485 [hep-ph/0411261].

[9] K. Kajantie, M. Laine, K. Rummukainen and Y. Schröder, *The pressure of hot QCD up to* $g^6 \ln(1/g)$, *Phys. Rev.* **D 67** (2003) 105008 [hep-ph/0211321];
K. Kajantie, M. Laine, K. Rummukainen and Y. Schröder, *Four-loop vacuum energy density of the* $\mathrm{SU}(N_c)$ + *adjoint Higgs theory*, *JHEP* **04** (2003) 036 [hep-ph/0304048].

[10] Y. Schröder and A. Vuorinen, *High-precision evaluation of four-loop vacuum bubbles in three dimensions*, hep-ph/0311323.

[11] K.G. Chetyrkin, J.H. Kühn, P. Mastrolia and C. Sturm, *Heavy-quark vacuum polarization: first two moments of the* $O(\alpha_s^3 n_f^2)$ *contribution*, *Eur. Phys. J.* **C 40** (2005) 361 [hep-ph/0412055].

[12] Computer-readable files can be obtained from the URL http://www.physik.uni-bielefeld.de/theory/e6/publiframe.html.

[13] S. Laporta, *High-precision epsilon-expansions of three-loop master integrals contributing to the electron* $g - 2$ *in QED*, *Phys. Lett.* **B 523** (2001) 95 [hep-ph/0111123].

[14] J.A.M. Vermaseren, *New features of FORM*, math-ph/0010025.

[15] L.V. Avdeev, *Recurrence relations for three-loop prototypes of bubble diagrams with a mass*, *Comput. Phys. Commun.* **98** (1996) 15 [hep-ph/9512442].

[16] M. Steinhauser, *MATAD: a program package for the computation of massive tadpoles*, *Comput. Phys. Commun.* **134** (2001) 335 [hep-ph/0009029].

[17] H.R.P. Ferguson, D.H. Bailey and S. Arno, *Analysis of PSLQ, an integer relation finding algorithm*, *Math. Comput.* **68** (1999) 351.

[18] S. Moch, J.A.M. Vermaseren and A. Vogt, *The QCD splitting functions at three loops: methods and results*, *Nucl. Phys.* **135** *(Proc. Suppl.)* (2004) 137 [hep-ph/0408075].

[19] A.I. Davydychev and J.B. Tausk, *Two loop selfenergy diagrams with different masses and the momentum expansion*, *Nucl. Phys.* **B 397** (1993) 123.

[20] A.I. Davydychev, *Explicit results for all orders of the epsilon-expansion of certain massive and massless diagrams*, *Phys. Rev.* **D 61** (2000) 087701 [hep-ph/9910224].

[21] A.I. Davydychev and M.Y. Kalmykov, *New results for the epsilon-expansion of certain one-, two- and three-loop Feynman diagrams*, *Nucl. Phys.* **B 605** (2001) 266 [hep-th/0012189].

[22] M.Y. Kalmykov and O. Veretin, *Single-scale diagrams and multiple binomial sums*, *Phys. Lett.* **B 483** (2000) 315 [hep-th/0004010].

[23] A.I. Davydychev and M.Y. Kalmykov, *Massive Feynman diagrams and inverse binomial sums*, *Nucl. Phys.* **B 699** (2004) 3 [hep-th/0303162].

[24] D.J. Broadhurst, *Three loop on-shell charge renormalization without integration:* λ-*MS (QED) to four loops*, *Z. Physik* **C 54** (1992) 599.

[25] D.J. Broadhurst, *On the enumeration of irreducible k-fold Euler sums and their roles in knot theory and field theory*, hep-th/9604128.

[26] D.J. Broadhurst, *Massive 3-loop Feynman diagrams reducible to SC* primitives of algebras of the sixth root of unity*, *Eur. Phys. J.* **C 8** (1999) 311 [hep-th/9803091].

[27] M.Y. Kalmykov, *About higher order epsilon-expansion of some massive two- and three-loop master-integrals*, *Nucl. Phys.* **B 718** (2005) 276 [`hep-ph/0503070`].

[28] P. Mastrolia, *Differential equations for Feynman graph integrals*, Ph.D. thesis, Bologna, Italy May 2004 (unpublished).

[29] Y. Schröder and M. Steinhauser, *Four-loop singlet contribution to the ρ parameter*, `hep-ph/0504055`.

[30] D.I. Kazakov, O.V. Tarasov and A.A. Vladimirov, *Calculation of critical exponents by quantum field theory methods*, *Sov. Phys. JETP* **50** (1979) 521.

[31] *Condor, high throughput computing*, `http://www.cs.wisc.edu/condor`.

[YS13]

Four-loop singlet contribution to the electroweak rho parameter

ELSEVIER

Four-loop singlet contribution to the electroweak ρ parameter

Y. Schröder [a], M. Steinhauser [b]

[a] *Fakultät für Physik, Universität Bielefeld, 33501 Bielefeld, Germany*
[b] *Institut für Theoretische Teilchenphysik, Universität Karlsruhe, 76128 Karlsruhe, Germany*

Abstract

We compute the four-loop QCD contribution to the electroweak ρ parameter induced by the singlet diagrams of the Z-boson self-energy. The numerical impact on the weak mixing angle and the W-boson mass is small.
© 2005 Elsevier B.V. All rights reserved.

PACS: 12.38.-t; 14.65.Ha; 13.66.Jn

1. Introduction

The electroweak ρ parameter as introduced by Veltman [1] measures the relative strength of the charged and neutral current. Considering QCD corrections it can be written as

$$\rho = 1 + \delta\rho, \tag{1}$$

with

$$\delta\rho = \frac{\Pi_{ZZ}(0)}{M_Z^2} - \frac{\Pi_{WW}(0)}{M_W^2}. \tag{2}$$

$\Pi_{ZZ}(0)$ and $\Pi_{WW}(0)$ are the transverse parts of the W- and Z-boson self-energies evaluated for vanishing external momentum. The parameter $\delta\rho$ enters a variety of quantities which are determined from experiment with an enormous precision. In particular, it enters the relation between the W-boson mass, M_W, the fine structure constant, α,
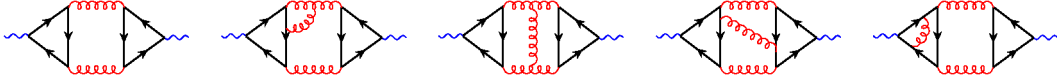
Fig. 1. Sample three- and four-loop singlet diagrams contributing to the ρ parameter. In the fermion loops either top- or bottom-quarks are present.

the Fermi constant, G_F, and the Z-boson mass, M_Z, which is given by [2]

$$M_W^2 = \frac{M_Z^2}{2}\left(1 + \sqrt{1 - \frac{4\pi\alpha}{\sqrt{2}\,M_Z^2 G_F(1-\Delta r)}}\right). \tag{3}$$

The quantity Δr is conveniently parameterized in the form

$$\Delta r = \Delta\alpha - \frac{c_W^2}{s_W^2}\delta\rho + \Delta r^{\text{rem}}, \tag{4}$$

with $c_W = M_W/M_Z$ and $s_W^2 = 1 - c_W^2$. $\Delta\alpha$ contains contributions from light fermions giving rise to a correction of about 6%. The leading corrections proportional to $G_F M_t^2$ are incorporated in $\delta\rho$ and amount at one-loop order to roughly -3% whereas the remaining part is small.

Eqs. (3) and (4) can be used to predict M_W, where the formula

$$\delta M_W = \frac{M_W}{2}\frac{c_W^2}{c_W^2 - s_W^2}\delta\rho \tag{5}$$

immediately accounts for the dominant shift in M_W due to the corrections to the ρ parameter. We can also look at the change of the effective leptonic weak mixing angle, $\sin^2\theta_{\text{eff}}^{\text{lept}}$, defined through the coupling of the Z-boson to leptons. The leading universal corrections originating from $\delta\rho$ can in analogy to Eq. (5) be written as

$$\delta\sin^2\theta_{\text{eff}}^{\text{lept}} = -\frac{c_W^2 s_W^2}{c_W^2 - s_W^2}\,\delta\rho. \tag{6}$$

Currently the uncertainties for M_W and $\sin^2\theta_{\text{eff}}^{\text{lept}}$ are given by $\delta M_W = 34$ MeV and $\delta\sin^2\theta_{\text{eff}}^{\text{lept}} = 1.7 \times 10^{-4}$ [3], respectively. However, a future linear collider running at the Z-boson pole, the so-called Giga-Z option, and around the W-pair threshold might reduce the uncertainties to $\delta M_W = 6$ MeV and $\delta\sin^2\theta_{\text{eff}}^{\text{lept}} = 1.3 \times 10^{-5}$ [4].

The one-loop corrections to ρ have been computed in 1977 [1] and also the two-loop QCD corrections are known since almost 20 years [5–7]. Roughly 10 years ago the order $G_F M_t^2 \alpha_s^2$ QCD corrections [8,9] constituted one of the first applications of the three-loop massive vacuum integrals. At three-loop order for the first time a new kind of Feynman graphs has to be considered, the so-called singlet diagrams as shown in Fig. 1 which only contribute to the Z-boson self-energy. They are characterized by the fact that in contrast to the non-singlet contribution the external Z-bosons couple to different fermion lines. We want to note that the singlet contribution forms a finite and gauge-independent subset. At three-loop order it completely dominates the numerical corrections if the $\overline{\text{MS}}$ definition is adopted for the top-quark mass. In the case of the pole mass definition the singlet part still amounts to about 30% of the total three-loop contribution. We want to mention that also two-loop [10,11] and three-loop mixed electroweak/QCD [12] and even three-loop pure electroweak corrections [12] have been evaluated. Recently also corrections in the large Higgs boson mass limit have been considered [13,14]. For non-universal corrections to M_W and $\sin^2\theta_{\text{eff}}^{\text{lept}}$ we refer to [15,16].

In this Letter we consider the four-loop contribution to the ρ parameter originating from the singlet diagrams. In Fig. 1 some sample diagrams are shown. This constitutes one of the first applications of the four-loop vacuum master integrals evaluated recently in Ref. [17].

2. Technicalities

Since the boson self-energies have to be evaluated for zero external momentum and only QCD corrections are considered, only the axial-vector part of the Z-boson correlator gives a non-zero contribution. Whereas for the non-singlet contribution the naive anti-commuting definition of γ_5 can be adopted, special care has to be taken in the singlet case. Actually, the definition of 't Hooft and Veltman [18] has to be adopted and additional counterterms have to be introduced in order to ensure the validity of the Ward identities. In the practical calculation we follow Ref. [19] and perform the following replacement in the axial-vector current

$$\gamma^\mu \gamma^5 = \frac{1}{3!} \varepsilon^{\mu\nu\rho\sigma} \gamma_\nu \gamma_\rho \gamma_\sigma. \tag{7}$$

We pull out the ε-tensor from the actual integral and consider instead the completely antisymmetrized product of the three γ-matrices which can be written as

$$\gamma^{[\nu} \gamma^\rho \gamma^{\sigma]} = \frac{1}{2} \left(\gamma^\nu \gamma^\rho \gamma^\sigma - \gamma^\sigma \gamma^\rho \gamma^\nu \right). \tag{8}$$

As a consequence we have to deal with an object with six indices. Thus, for zero external momentum we obtain

$$\Pi_{ZZ} = \frac{g_{\mu\mu'}}{4} \Pi_{ZZ}^{\mu\mu'} = \frac{g_{\mu\mu'} \varepsilon^{\mu\nu\rho\sigma} \varepsilon^{\mu'\nu'\rho'\sigma'}}{144} \Pi_{[\nu\rho\sigma][\nu'\rho'\sigma']} = -\frac{1}{24} \Pi_{[\nu\rho\sigma]}^{[\nu\rho\sigma]}. \tag{9}$$

In the practical calculation we consider the object $\Pi_{[\nu\rho\sigma]}^{[\nu\rho\sigma]}$ for which we also perform the renormalization as described in the following. Thus, in Eq. (9) the limit $D \to 4$ has been considered where $D = 4 - 2\epsilon$ is the space–time dimension.

The additional finite counterterm is only needed to one-loop order, since the singlet diagrams appear the first time at three-loop level. For each axial-vector vertex a factor [19,20]

$$Z_5^s = 1 - C_F \frac{\alpha_s}{\pi} + \mathcal{O}(\alpha_s^2), \tag{10}$$

with $C_F = (N_c^2 - 1)/(2N_c)$ has to be considered. Furthermore, we have to consider the one-loop counterterms for the strong coupling constant and the top-quark mass defined by

$$\alpha_s^0 = Z_{\alpha_s} \alpha_s, \qquad m_t^0 = Z_m m_t, \tag{11}$$

where $m_t \equiv m_t(\mu)$ is renormalized in the $\overline{\text{MS}}$ scheme. The renormalization constants are given by

$$Z_{\alpha_s} = 1 + \frac{1}{\epsilon} \left(-\frac{11}{12} C_A + \frac{1}{3} T n_f \right) \frac{\alpha_s}{\pi} + \mathcal{O}(\alpha_s^2), \qquad Z_m = 1 - \frac{3}{4\epsilon} C_F \frac{\alpha_s}{\pi} + \mathcal{O}(\alpha_s^2), \tag{12}$$

with $C_A = N_c$ and $T = 1/2$. $n_f = 6$ is the number of active flavours. The transition to the pole mass is achieved via

$$m_t(\mu) = \left[1 + C_F \left(-1 - \frac{3}{4} \ln \frac{\mu^2}{M_t^2} \right) \frac{\alpha_s}{\pi} + \mathcal{O}(\alpha_s^2) \right] M_t. \tag{13}$$

We generate the Feynman diagrams with QGRAF [21] and adopt with the help of the packages q2e and exp [22,23] the topologies and notation to the program performing the reduction of the four-loop vacuum diagrams [24]. As an output we obtain the corrections to the ρ parameter as a linear combination of several master integrals. All of them have been computed in Ref. [17].

It is interesting to note that some of the master integrals are multiplied by spurious poles of order $1/\epsilon^2$. As a consequence, for these the $\mathcal{O}(\epsilon)$ and even the $\mathcal{O}(\epsilon^2)$ contribution is needed. In the case of the master integral BB4 (which is the four-loop sunset vacuum bubble with one massless and four massive lines, see Eqs. (4.8) and (6.36) of

Ref. [17]) it happens that the coefficient of order ϵ, which originally has only been evaluated in numerical form [17], enters the pole part of $\delta\rho$. Thus an analytical expression can be deduced (in Eq. (14) below denoted by BB4$^{(1)}$) which perfectly agrees with the known numerical result. Furthermore, we have obtained an analytical expression for the coefficient of order ϵ^2, by combining the numerically known value with the basis of transcendentals known from an independent investigation [25]. These two coefficients read

$$
\text{BB4} = J^4 \sum_{n \geq 0} \epsilon^n \text{BB4}^{(n-4)},
$$

$$
\text{BB4}^{(1)} = -\frac{1976975}{7776} + \frac{1792}{9}\zeta(3) = -14.8977265330295888692142748700082319534267\ldots,
$$

$$
\text{BB4}^{(2)} = -\frac{72443143}{46656} + \frac{47488}{27}\zeta(3) - \frac{8704}{3}\zeta(4) + \frac{1024}{9}\ln^4 2 - \frac{2048}{3}\zeta(2)\ln^2 2 + \frac{8192}{3}a_4
$$
$$
= -1678.8869291077729634030303102679175091 51\ldots, \tag{14}
$$

where J is the one-loop tadpole, $\zeta(n)$ is Riemann's zeta function and

$$
a_4 = \text{Li}_4(1/2) \approx 0.51747906167389938633. \tag{15}
$$

Let us mention that we performed the calculation using an arbitrary gauge parameter of the QCD gluon propagator, ξ. As expected the final result is independent of ξ even before inserting the values for the master integrals. This constitutes a nice check of our result.

3. Results and discussion

Let us in the following present our analytical result and discuss its numerical implications. For completeness we also repeat the QCD corrections up to three-loop order. For the $\overline{\text{MS}}$ definition of the top-quark mass we obtain

$$
\delta\rho^{\overline{\text{MS}}} = 3x_t \left\{ 1 + \frac{\alpha_s}{4\pi}\left[8 - \frac{16}{3}\zeta(2) + 8\ln\frac{\mu^2}{m_t^2} \right] \right.
$$
$$
+ \left(\frac{\alpha_s}{4\pi}\right)^2 \left[\frac{26459}{81} - \frac{25064}{81}\zeta(2) - \frac{3560}{27}\zeta(3) + \frac{1144}{9}\zeta(4) - \frac{16}{9}B_4 - \frac{8}{9}D_3 + 882S_2 \right.
$$
$$
+ n_f\left(-\frac{50}{3} + \frac{112}{9}\zeta(2) - \frac{64}{9}\zeta(3) \right) - 56\zeta(3)
$$
$$
+ \left(\frac{668}{3} - \frac{304}{3}\zeta(2) + n_f\left(-\frac{88}{9} + \frac{32}{9}\zeta(2) \right) \right)\ln\frac{\mu^2}{m_t^2} + \left(76 - \frac{8}{3}n_f \right)\ln^2\frac{\mu^2}{m_t^2} \right]
$$
$$
+ \left(\frac{\alpha_s}{4\pi}\right)^3 \left[\frac{256}{9} - 4528\zeta(3) + \frac{20816}{3}\zeta(4) - \frac{2624}{9}\ln^4 2 + \frac{5248}{3}\zeta(2)\ln^2 2 \right.
$$
$$
\left. \left. - \frac{20992}{3}a_4 - 1232\zeta(3)\ln\frac{\mu^2}{m_t^2} \right] + \cdots \right\}, \tag{16}
$$

where the "$-56\zeta(3)$" in the third line stems from the three-loop singlet diagram. In order α_s^3 only the singlet contribution is presented. Furthermore, we have

$$
x_t = \frac{G_F m_t^2}{8\pi^2\sqrt{2}},
$$
$$
S_2 = \frac{4}{9\sqrt{3}}\text{Im}\left(\text{Li}_2\left(e^{i\pi/3}\right)\right) \approx 0.26043413763216209896,
$$

$$B_4 = 16a_4 + \frac{2}{3}\ln^4 2 - 4\zeta(2)\ln^2 2 - \frac{13}{2}\zeta(4) \approx -1.7628000870737708641,$$

$$D_3 = 6\zeta(3) - \frac{15}{4}\zeta(4) - 6\big[\text{Im}\big(\text{Li}_2\big(e^{i\pi/3}\big)\big)\big]^2 \approx -3.0270094939876520198.$$

In Appendix A, we present the three- and four-loop result for the singlet contribution corresponding to Eq. (16) retaining, however, the colour factors C_F, C_A and T. With the help of Eq. (13) one obtains the singlet result in the on-shell scheme. Together with the non-singlet terms one gets

$$
\begin{aligned}
\delta\rho^{\text{OS}} = 3X_t\bigg\{ &1 + \frac{\alpha_s}{4\pi}\bigg[-\frac{8}{3} - \frac{16}{3}\zeta(2)\bigg] \\
&+ \bigg(\frac{\alpha_s}{4\pi}\bigg)^2\bigg[\frac{314}{81} - \frac{26504}{81}\zeta(2) - \frac{3416}{27}\zeta(3) - \frac{64}{3}\zeta(2)\ln 2 + \frac{1144}{9}\zeta(4) - \frac{16}{9}B_4 - \frac{8}{9}D_3 + 882S_2 \\
&+ n_f\bigg(-\frac{8}{9} - \frac{208}{9}\zeta(2) - \frac{64}{9}\zeta(3)\bigg) - 56\zeta(3) + \bigg(-\frac{88}{3} - \frac{176}{3}\zeta(2) + n_f\bigg(\frac{16}{9} + \frac{32}{9}\zeta(2)\bigg)\bigg)\ln\frac{\mu^2}{M_t^2}\bigg] \\
&+ \bigg(\frac{\alpha_s}{4\pi}\bigg)^3\bigg[\frac{256}{9} - \frac{11792}{3}\zeta(3) + \frac{20816}{3}\zeta(4) - \frac{2624}{9}\ln^4 2 + \frac{5248}{3}\zeta(2)\ln^2 2 \\
&- \frac{20992}{3}a_4 - 784\zeta(3)\ln\frac{\mu^2}{M_t^2}\bigg] + \cdots\bigg\},
\end{aligned}
\tag{17}
$$

with $X_t = G_F M_t^2/(8\pi^2\sqrt{2})$.

Inserting the numerical values for the constants in Eqs. (16) and (17) and adopting $\mu = m_t$ and $\mu = M_t$, respectively, the numerical corrections read

$$\delta\rho^{\overline{\text{MS}}} = 3x_t\bigg[1 - 0.19325\frac{\alpha_s}{\pi} + (-4.2072 + 0.23764)\bigg(\frac{\alpha_s}{\pi}\bigg)^2 - 3.2866\bigg(\frac{\alpha_s}{\pi}\bigg)^3\bigg],$$

$$\delta\rho^{\text{OS}} = 3X_t\bigg[1 - 2.8599\frac{\alpha_s}{\pi} + (-4.2072 - 10.387)\bigg(\frac{\alpha_s}{\pi}\bigg)^2 + 7.9326\bigg(\frac{\alpha_s}{\pi}\bigg)^3\bigg],
\tag{18}
$$

where the three-loop contribution is split into the singlet (first number in round brackets) and the non-singlet piece. If we furthermore adopt $\alpha_s(m_t) = 0.108$ and $\alpha_s(M_t) = 0.107$, the expression for $\delta\rho$ looks like

$$\delta\rho^{\overline{\text{MS}}} = 3x_t(1 - 0.00664 - 0.00469 - 0.00013),$$

$$\delta\rho^{\text{OS}} = 3X_t(1 - 0.09741 - 0.01693 + 0.00031),
\tag{19}
$$

where the nth term inside the round brackets corresponds to the contribution of order $G_F M_t^2 \alpha_s^{(n-1)}$. One observes that the new four-loop singlet contribution is numerically small and amounts to about 3% of the three-loop result in the $\overline{\text{MS}}$ scheme and to less than 2% for on-shell top-quark masses. Note that the correction is positive in the on-shell and negative in the $\overline{\text{MS}}$ scheme. In the on-shell scheme the shift in M_W and $\sin^2\theta_{\text{eff}}^{\text{lept}}$ according to Eqs. (5) and (6) amounts to 0.175 MeV and 10^{-6}, respectively, which is significantly below the recent estimates of higher order contributions and variations of input parameters [15,16].

It is interesting to mention that at three-loop order the singlet contribution completely dominates for $\overline{\text{MS}}$ top-quark masses and amounts to about 30% in the on-shell scheme. Thus, in case the same pattern also holds at four-loop order, the complete QCD corrections would be well under control. However, the numerical values in Eq. (18) suggest that for some reason the four-loop singlet contribution seems to be accidentally small.

Let us also comment on the dependence of the singlet contribution on the renormalization scale μ which can be done separately from the non-singlet part. The latter is discussed in Ref. [9] (cf. Fig. 1 of Ref. [9]). As far as the singlet contribution is concerned one obtains for the quantity $(\delta\rho^{\text{OS}}/(3X_t) - 1)_{\text{singlet}}$ the values

$\{-0.00457, -0.00437, -0.00455\}$ corresponding to $\mu = \{M_t, M_t/2, 2M_t\}$. The μ-dependence, being formally of higher order, is less then 5% of the sum of the three- and four-loop singlet part which can be used as an estimate of the $\mathcal{O}(\alpha_s^4)$ term.

In the remaining part of this section we briefly compare the numerical effect of the new terms with known corrections to $\delta\rho$. In the on-shell scheme the three-loop QCD corrections of order $\alpha_s^2 X_t$ lead to a shift of about -10 MeV in the W-boson mass and to $+5 \times 10^{-5}$ in the effective weak mixing angle. For Higgs-boson masses between 200 GeV and 300 GeV the three-loop corrections of order $\alpha_s X_t^2$ [12] have the opposite sign and with roughly half the magnitude they are still relevant for the precision to be reached at the Giga-Z option of a future $e^+ e^-$ linear collider. However, the pure electroweak corrections of order X_t^3 are very small and give rise to corrections well below 1 MeV for the shift in the W-boson mass. The same is true for the four-loop QCD singlet contributions considered in this Letter.

In conclusion, we computed the four-loop singlet contribution to the ρ parameter which constitutes one of the first applications of the four-loop massive vacuum integrals to a physical quantity. The numerical size of the corrections turn out to be surprisingly small and lead to a shift in the W-boson mass below 1 MeV and to the effective weak mixing angle below 10^{-5}—beyond the accuracy foreseen in a future linear collider. This illustrates the good convergence properties of the perturbation theory and confirms the stable predictions based on the three-loop corrections. However, for a definite conclusion also the non-singlet contribution has to be evaluated.

Appendix A. Singlet contribution to the ρ parameter

In this appendix we present the three- and four-loop singlet result expressed in terms of $C_A = N_c$, $C_F = (N_c^2 - 1)/(2N_c)$ and $T = 1/2$. Furthermore, we keep the label n_l which counts the number of massless quarks. The three-loop term can also be found in Ref. [26].

$$
\begin{aligned}
\delta\rho_{\text{sing}}^{\overline{\text{MS}}} = 3x_t \left(\frac{\alpha_s}{4\pi}\right)^2 C_F T \Bigg\{ & -84\zeta(3) \\
& + \frac{\alpha_s}{4\pi} \Bigg[C_F \left(-336\zeta(3) + 2400\zeta(4) - 128\ln^4 2 + 768\zeta(2)\ln^2 2 - 3072 a_4 - 504\zeta(3)\ln\frac{\mu^2}{m_t^2} \right) \\
& + C_A \left(-\frac{7064}{3}\zeta(3) + 3056\zeta(4) - \frac{320}{3}\ln^4 2 + 640\zeta(2)\ln^2 2 - 2560 a_4 - 616\zeta(3)\ln\frac{\mu^2}{m_t^2} \right) \\
& + n_l T \left(\frac{1120}{3}\zeta(3) - 784\zeta(4) + \frac{64}{3}\ln^4 2 - 128\zeta(2)\ln^2 2 + 512 a_4 + 224\zeta(3)\ln\frac{\mu^2}{m_t^2} \right) \\
& + T \left(\frac{256}{3} - \frac{1280}{3}\zeta(3) + 224\zeta(3)\ln\frac{\mu^2}{m_t^2} \right) \Bigg] + \mathcal{O}(\alpha_s^2) \Bigg\}.
\end{aligned}
\tag{A.1}
$$

References

[1] M.J.G. Veltman, Nucl. Phys. B 123 (1977) 89.
[2] A. Sirlin, Phys. Rev. D 22 (1980) 971.

 [3] See, e.g., http://lepewwg.web.cern.ch/LEPEWWG/Welcome.html.
 [4] J.A. Aguilar-Saavedra, et al., ECFA/DESY LC Physics Working Group, hep-ph/0106315.
 [5] A. Djouadi, C. Verzegnassi, Phys. Lett. B 195 (1987) 265.
 [6] A. Djouadi, Nuovo Cimento A 100 (1988) 357.
 [7] B.A. Kniehl, J.H. Kühn, R.G. Stuart, Phys. Lett. B 214 (1988) 621.
 [8] L. Avdeev, J. Fleischer, S. Mikhailov, O. Tarasov, Phys. Lett. B 336 (1994) 560, hep-ph/9406363;
     L. Avdeev, J. Fleischer, S. Mikhailov, O. Tarasov, Phys. Lett. B 349 (1995) 597, Erratum.
 [9] K.G. Chetyrkin, J.H. Kühn, M. Steinhauser, Phys. Lett. B 351 (1995) 331, hep-ph/9502291.
[10] J.J. van der Bij, F. Hoogeveen, Nucl. Phys. B 283 (1987) 477.
[11] R. Barbieri, M. Beccaria, P. Ciafaloni, G. Curci, A. Vicere, Phys. Lett. B 288 (1992) 95, hep-ph/9205238;
     R. Barbieri, M. Beccaria, P. Ciafaloni, G. Curci, A. Vicere, Phys. Lett. B 312 (1993) 511, Erratum;
     J. Fleischer, O.V. Tarasov, F. Jegerlehner, Phys. Lett. B 319 (1993) 249.
[12] M. Faisst, J.H. Kühn, T. Seidensticker, O. Veretin, Nucl. Phys. B 665 (2003) 649, hep-ph/0302275.
[13] R. Boughezal, J.B. Tausk, J.J. van der Bij, Nucl. Phys. B 713 (2005) 278, hep-ph/0410216.
[14] R. Boughezal, J.B. Tausk, J.J. van der Bij, hep-ph/0504092.
[15] M. Awramik, M. Czakon, A. Freitas, G. Weiglein, Phys. Rev. D 69 (2004) 053006, hep-ph/0311148.
[16] M. Awramik, M. Czakon, A. Freitas, G. Weiglein, Phys. Rev. Lett. 93 (2004) 201805, hep-ph/0407317.
[17] Y. Schröder, A. Vuorinen, JHEP 0506 (2005) 051, hep-ph/0503209.
[18] G. 't Hooft, M.J.G. Veltman, Nucl. Phys. B 44 (1972) 189.
[19] S.A. Larin, Phys. Lett. B 303 (1993) 113, hep-ph/9302240.
[20] T.L. Trueman, Phys. Lett. B 88 (1979) 331.
[21] P. Nogueira, J. Comput. Phys. 105 (1993) 279.
[22] T. Seidensticker, hep-ph/9905298.
[23] R. Harlander, T. Seidensticker, M. Steinhauser, Phys. Lett. B 426 (1998) 125, hep-ph/9712228.
[24] Y. Schröder, Nucl. Phys. B (Proc. Suppl.) 116 (2003) 402, hep-ph/0211288.
[25] P. Mastrolia, PhD thesis, May 2004, Bologna University, Italy, unpublished.
[26] A. Anselm, N. Dombey, E. Leader, Phys. Lett. B 312 (1993) 232.

[YS14]

Four-loop plaquette in 3d with a mass regulator

Four-loop plaquette in 3d with a mass regulator

Christian Torrero[*]
University of Parma and INFN
E-mail: torrero@fis.unipr.it

Francesco Di Renzo
University of Parma and INFN
E-mail: direnzo@fis.unipr.it

Vincenzo Miccio
University of Milano Bicocca and INFN
E-mail: vincenzo.miccio@mib.infn.it

Mikko Laine
University of Bielefeld
E-mail: laine@physik.uni-bielefeld.de

York Schröder
University of Bielefeld
E-mail: yorks@physik.uni-bielefeld.de

The QCD free energy can be studied by dimensional reduction to a three-dimensional (3d) effective theory, whereby non-perturbative lattice simulations become less demanding. To connect to the original QCD a perturbative matching computation is required, which is conventionally carried out in dimensional regularization. Therefore the 3d lattice results need to be converted to this regularization scheme as well. The conversion must be carried up to 4-loop order, where the free energy displays an infrared (IR) singularity. We therefore need a regulator which can be implemented both on the lattice and in the continuum computation. We introduce a mass regulator to perform Numerical Stochastic Perturbation Theory computations. Covariant gauge is fixed in the Faddeev-Popov scheme without introducing any ghost fields.

---

[*]Speaker.

1. Introduction

As is well known, finite-temperature QCD seems to show two different phases: it is confining at low temperatures (the realm of mesons and baryons) while asymptotic freedom and a quark-gluon plasma are expected to appear in the high-temperature regime. A good observable to witness the change is the QCD free energy density, given essentially by the familiar Stefan-Boltzmann law of blackbody radiation, multiplied by the number of light effective degrees of freedom.

To study the free energy density requires different methods in different regimes. At low temperatures the problem has to be treated with numerical lattice simulations, while at high temperatures perturbation theory should allow at least for some progress, given that the coupling constant g is small. Nevertheless, even for small g, certain coefficients in the weak-coupling expansion do remain non-perturbative [1], and can only be determined with numerical techniques.

In the high-temperature regime, the theory contains three different momentum scales [2], namely T (hard modes), gT (soft modes) and g^2T (ultrasoft modes). The contribution of each of these modes is best isolated in an effective theory setup. This is accomplished via *dimensional reduction* [2, 3, 4] by integrating out the hard and soft modes to obtain a 3d pure Yang-Mills SU(3) theory ("MQCD"). MQCD can then be analysed on the lattice and the results can be added to the various perturbative contributions to obtain the complete answer.

To add the MQCD lattice results to the perturbative ones, we need to change regularization scheme from lattice to dimensional regularization. To this aim, a matching between lattice and continuum computations is needed and this is achieved by means of Lattice Perturbation Theory applied to MQCD. The strategy we adopt for this purpose here is the one of *Numerical Stochastic Perturbation Theory* (NSPT) developed in recent years by the Parma group.

2. The NSPT method

NSPT relies on *Stochastic Quantization* [5] which is characterized by the introduction of an extra coordinate, a stochastic time t, together with an evolution equation called the Langevin equation,

$$\frac{\partial \phi(x,t)}{\partial t} = -\frac{\partial S[\phi]}{\partial \phi} + \eta(x,t) \,, \tag{2.1}$$

where $\eta(x,t)$ is a Gaussian noise which effectively generates the quantum fluctuations of the theory.

The average over this noise is such that, together with the appropriate limit in t, the desired Feynman-Gibbs functional integration is reproduced:

$$\left\langle O[\phi_\eta(x,t)]\right\rangle_\eta \overset{t\to\infty}{\longrightarrow} \frac{1}{Z}\int [D\phi]O[\phi(x)]e^{-S[\phi(x)]} \,. \tag{2.2}$$

For SU(3) Yang-Mills theory, the Langevin equation becomes

$$\partial_t U_\eta = -i\Big(\nabla S[U_\eta] + \eta\Big)U_\eta \,, \tag{2.3}$$

guaranteeing the proper evolution of variables within the group.

In this framework, perturbation theory comes into play by means of the expansion [6]

$$U_\eta(x,t) \longrightarrow \sum_k g_0^k U_\eta^{(k)}(x,t) \,, \tag{2.4}$$

where g_0 is the bare gauge coupling. This results in a system of coupled equations that can be numerically solved via a discretization of the stochastic time $t = n\tau$, where τ is a time step. In practice, we let the system evolve according to the Langevin equation for different values of τ, average over each thermalized signal (this is the meaning of the above-mentioned limit $t \rightarrow \infty$), and then extrapolate in order to get the $\tau = 0$ value of the desired observable. This procedure is then repeated for different values of the various parameters appearing in the action.

3. Mass as an IR regulator

As stated above, the quantity we are interested in is the contribution to the QCD free energy density f coming from the 3d pure SU(3) theory. On the lattice, this observable is related to the trace of the plaquette $\langle 1 - \Pi_P \rangle$, where $\Pi_P \equiv N_c^{-1} \operatorname{Re} \operatorname{Tr} P$ and P is the elementary plaquette, via

$$\langle 1 - \Pi_p \rangle = \frac{2a^d}{d(d-1)} \frac{\partial}{\partial \beta_0} \left(\frac{f}{T} \right) , \tag{3.1}$$

with bare lattice coupling $\beta_0 = 2N_c/(a^{4-d}g_0^2)$. The outcome can be expanded in powers of β_0 as

$$\langle 1 - \Pi_p \rangle = \frac{c_1}{\beta_0} + \frac{c_2}{\beta_0^2} + \frac{c_3}{\beta_0^3} + \frac{\widetilde{c}_4}{\beta_0^4} + O(\beta_0^{-5}) . \tag{3.2}$$

The determinations of the first three coefficients in the present setting have been discussed in Ref. [7]. The non-perturbative value of the whole quantity has been determined with lattice simulations in Ref. [8]. Terms of $O(\beta_0^{-5})$ disappear in the continuum limit, thanks to the super-renormalizability of the theory. Thus only the fourth order coefficient is missing at the moment.

As shown parametrically in Ref. [1] and explicitly in Refs. [9], the coefficient $\widetilde{c}_4$ is actually IR divergent, and consequently an appropriate regulator must be introduced for its determination. In a non-perturbative setting this is provided by confinement, while in fixed-order computations one could employ a finite volume (as in Ref. [7]) or a mass. Since the use of a mass is more convenient in continuum computations involving dimensional regularization, we need to implement it in lattice perturbation theory as well.

Apart from introducing a mass, we also fix the gauge in order to match the setting of the continuum computations. Consequently, the functional integral is given by

$$Z = \int [D\phi] \operatorname{Det} \left(- \sum_\mu \hat{\partial}_\mu^L \hat{D}_\mu[\phi] + m^2 \right) \exp \left(- S_W - S_{GF} \right) = \int [D\phi] \exp \left(- S_W - S_{GF} - S_{FP} \right) , \tag{3.3}$$

where we assume the use of lattice units (i.e. $a = 1$), and

$$S_W = \beta_0 \sum_P (1 - \Pi_P) + \frac{\beta_0 m^2}{4N_c} \sum_{x,\mu,A} \phi_\mu^A(x)\phi_\mu^A(x) , \tag{3.4}$$

$$S_{GF} = \frac{\beta_0}{4N_c\alpha} \sum_{x,A} \Big[\sum_\mu \hat{\partial}_\mu^L \phi_\mu^A(x) \Big]^2 , \tag{3.5}$$

$$S_{FP} = - \operatorname{Tr} \Big[\ln \Big(- \sum_\mu \hat{\partial}_\mu^L \hat{D}_\mu[\phi] + m^2 \Big) \Big] , \tag{3.6}$$

where we have followed the conventions of Ref. [10], writing in particular $U_\mu = \exp(i\phi_\mu)$, $\phi_\mu = \phi_\mu^A T^A$, with the normalization $\text{Tr}[T^A T^B] = \delta^{AB}/2$. Moreover m is the common gluon and ghost mass, α is the gauge parameter, and $\hat{D}_\mu$ is the discrete Faddeev-Popov operator, given by [10]

$$\hat{D}_\mu[\phi] = \left[1 + \frac{i}{2}\Phi_\mu - \frac{1}{12}\Phi_\mu^2 - \frac{1}{720}\Phi_\mu^4 - \frac{1}{30240}\Phi_\mu^6 + O(\Phi_\mu^8) \right] \hat{\partial}_\mu^R + i\Phi_\mu , \qquad (3.7)$$

with $\Phi_\mu = \phi_\mu^A F^A$, where $[F^A]_{BC} \equiv -if^{ABC}$ are the generators of the adjoint representation.

To treat the Faddeev-Popov determinant as a part of the action means that, because of the Langevin equation, one has to face the quantity $\nabla S_{FP} = -\nabla \text{Tr}[\ln B] = -\text{Tr}[\nabla B B^{-1}]$ with $B[\phi] = -\sum_\mu \hat{\partial}_\mu^L \hat{D}_\mu[\phi] + m^2$. We perform the inversion as in Ref. [11], while the trace is computed by means of sources in the usual way.

The global strategy is then to perform simulations with lattices of different sizes at fixed mass in order to extrapolate to infinite volume and, afterwards, to repeat this procedure for other values of the mass. At this point, after subtracting the expected logarithmic divergence, one extrapolates to zero mass, obtaining the needed fourth order coefficient. It is crucial to take the infinite-volume limit before the zero-mass one because, by performing the limits in the opposite order, the final IR regulator would be the volume and not the mass as we want.

4. First (benchmark) results

So far, the statistics we took are not sufficient to carry out the infinite-volume and zero-mass limits for the fourth order coefficient $\tilde{c}_4$, but it is already possible to crosscheck the reliability of the general method. As a first test, we compare the 1-loop numerical results for the trace of the plaquette for the various masses with the known analytic values. As shown in Fig. 1 for a lattice extent $L = 5$, the agreement between the numerical values and the analytic curve is very good.

A second check could consist of extrapolating at fixed lattice extent to zero mass, to see if one recovers the already known coefficients [7]. Figs. 2 – 5 show these extrapolations for a lattice extent $L = 7$: the fitting curve is a polynomial in m^2 (the most naive choice) and it seems to approach the expected result (the point at $m = 0$) very well for all the loop orders. The numerical values are given in Table 1. Both of the mentioned checks are well satisfied also for the other lattice extents that we have employed so far.

Loop	Result from a fit to $m = 0$	Direct measurement at $m = 0$
1	-2.6594(17)	-2.6580(8)
2	-1.9166(63)	-1.9095(30)
3	-6.304(37)	-6.307(21)
4	-28.43(27)	-28.68(15)

Table 1: Comparison of the zero-mass extrapolations with the known results [7] (lattice extent $= 7$).

As for the 4-loop order, Fig. 6 shows the behavior with respect to the lattice size at fixed mass: the result seems to stabilise towards the infinite-volume value in the way one would expect. Once a few more lattice sizes are available and similar extrapolations can be carried out for all masses, we will finally be in a position to carry out the mass extrapolation that is our ultimate goal.
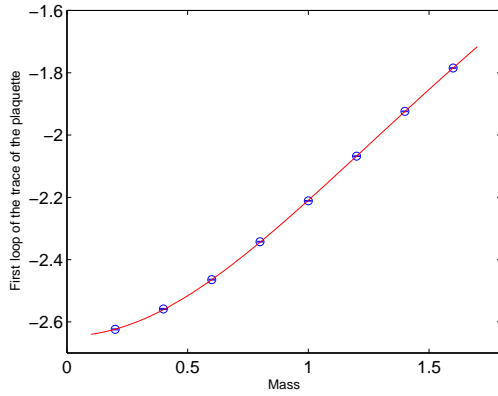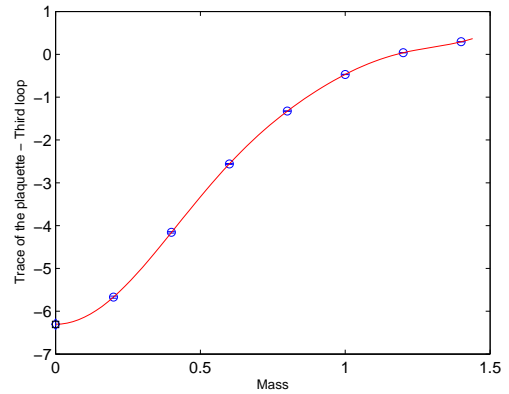
Figure 1: The 1-loop trace of the plaquette vs. mass (for $L = 5$): the numerical results (blue dots) agree with the analytical red curve.
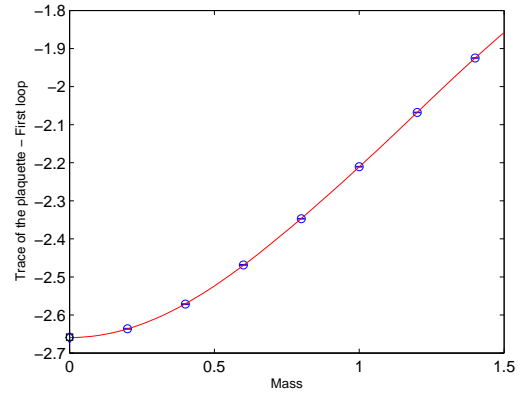
Figure 2: The 1-loop trace of the plaquette vs. mass (for $L = 7$): the fitted curve in red approaches the expected value at $m = 0$.
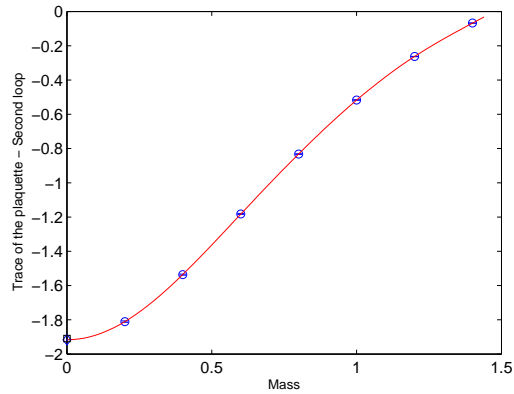
Figure 3: The 2-loop trace of the plaquette (for $L = 7$), together with a polynomial fit in m^2.

Figure 4: The 3-loop trace of the plaquette (for $L = 7$), together with a polynomial fit in m^2.

5. Conclusions and prospects

It is worth stressing once again that our approach has successfully passed the reliability checks we adopted: known zero-mass limits are reproduced through an extrapolation, and the volume dependence at a fixed mass appears to disappear once the dimensionless combination mL, where m is the mass and L the lattice extent, is large enough.

In order to obtain the asymptotic large-volume value at a fixed mass, it is still necessary to collect more statistics on bigger lattices (for example, $L = 12$ and 14) at least for the two or three smallest masses. Then, the fitting function should be a combination of a negative exponential and polynomials in mL, as explained for instance in Ref. [12].

After subtracting the logarithmic divergence from the fitted infinite-volume values, the subsequent extrapolation to zero mass does not appear to be troublesome, given that tests with lower loop orders have produced good results so far.
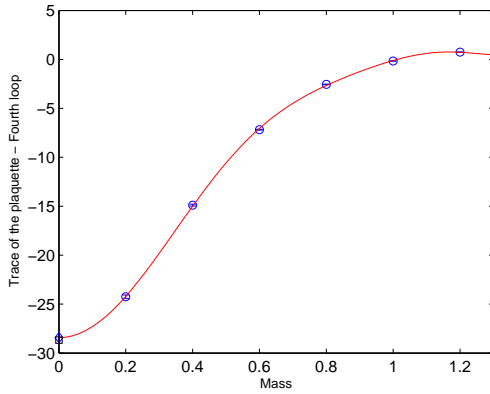
Figure 5: The 4-loop trace of the plaquette (for $L = 7$), together with a polynomial fit in m^2.
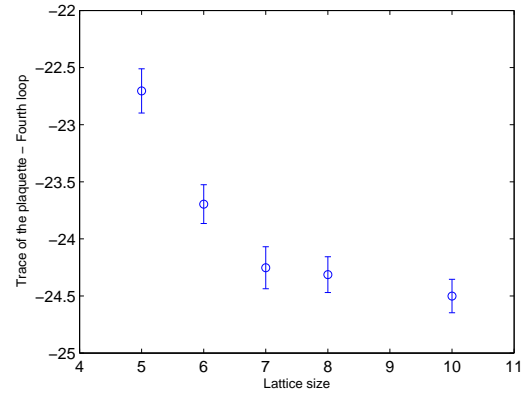
Figure 6: The 4-loop trace of the plaquette vs. lattice size, for a fixed mass $m = 0.2$.

References

[1] A.D. Linde, *Infrared problem in thermodynamics of the Yang-Mills gas,* Phys. Lett. B 96 (1980) 289.

[2] P. Ginsparg, *First and second order phase transitions in gauge theories at finite temperature,* Nucl. Phys. B 170 (1980) 388; T. Appelquist and R.D. Pisarski, *High-temperature Yang-Mills theories and three-dimensional Quantum Chromodynamics,* Phys. Rev. D 23 (1981) 2305.

[3] K. Kajantie, M. Laine, K. Rummukainen and M. Shaposhnikov, *Generic rules for high temperature dimensional reduction and their application to the Standard Model,* Nucl. Phys. B 458 (1996) 90 [hep-ph/9508379].

[4] E. Braaten and A. Nieto, *Free energy of QCD at high temperature,* Phys. Rev. D 53 (1996) 3421 [hep-ph/9510408].

[5] G. Parisi and Y. Wu, *Perturbation Theory Without Gauge Fixing,* Sci. Sin. 24 (1981) 483.

[6] F. Di Renzo, E. Onofri, G. Marchesini and P. Marenzoni, *Four loop result in SU(3) lattice gauge theory by a stochastic method: Lattice correction to the condensate,* Nucl. Phys. B 426 (1994) 675 [hep-lat/9405019].

[7] F. Di Renzo, A. Mantovi, V. Miccio and Y. Schröder, *3-d lattice Yang-Mills free energy to four loops,* JHEP 05 (2004) 006 [hep-lat/0404003].

[8] A. Hietanen, K. Kajantie, M. Laine, K. Rummukainen and Y. Schröder, *Plaquette expectation value and gluon condensate in three dimensions,* JHEP 01 (2005) 013 [hep-lat/0412008].

[9] K. Kajantie, M. Laine, K. Rummukainen and Y. Schröder, *The pressure of hot QCD up to $g^6 \ln(1/g)$,* Phys. Rev. D 67 (2003) 105008 [hep-ph/0211321]; Y. Schröder, *Tackling the infrared problem of thermal QCD,* Nucl. Phys. B (Proc. Suppl.) 129 (2004) 572 [hep-lat/0309112].

[10] H.J. Rothe, *Lattice gauge theories: An Introduction,* World Sci. Lect. Notes Phys. 74 (2005) 1.

[11] F. Di Renzo and L. Scorzato, *Fermionic loops in numerical stochastic perturbation theory,* Nucl. Phys. B (Proc. Suppl.) 94 (2001) 567 [hep-lat/0010064].

[12] I. Montvay and G. Münster, *Quantum fields on a lattice* (Cambridge University Press, Cambridge, 1994).

[YS15]

Four-Loop decoupling relations for the strong coupling

Four-loop decoupling relations for the strong coupling

York Schröder

Fakultät für Physik, Universität Bielefeld
33501 Bielefeld, Germany
E-mail: `yorks@physik.uni-bielefeld.de`

Matthias Steinhauser

Institut für Theoretische Teilchenphysik, Universität Karlsruhe
76128 Karlsruhe, Germany
E-mail: `matthias.steinhauser@uka.de`

Abstract: We compute the matching relation for the strong coupling constant within the framework of QCD up to four-loop order. This allows a consistent five-loop running (once the β function is available to this order) taking into account threshold effects. As a side product we obtain the effective coupling of a Higgs boson to gluons with five-loop accuracy.

Contents

1. Introduction

The strong coupling constant, α_s, constitutes a fundamental parameter in the Standard Model and thus its precise numerical value is very important for many physical predictions. An interesting property of α_s is its scale dependence, in particular its strong rise for low and its small value for high energies which make perturbative calculations within the framework of QCD possible. The scale dependence is governed by the β function. However, in order to relate α_s at two different scales it is also necessary to incorporate threshold effects of heavy quarks which is achieved with the help of the so-called matching or decoupling relations. Thus, when specifying α_s it is necessary to indicate next to the scale also the number of active flavours. In this paper we evaluate the decoupling relations to four-loop accuracy. This makes it possible to perform a consistent running of the strong coupling evaluated at a low scale, like, e.g., the mass of the τ lepton, to a high scale like the Z boson mass — once the five-loop β function is available.

Many different techniques have been developed and applied to various classes of Feynman diagrams. The complexity increases both with the number of legs and the number of loops. As far as the application of multi-loop diagrams to physical processes is concerned the current limit are four-loop single-scale Feynman diagrams, where either all internal particles are massless and one external momentum flows through the diagram (see, e.g., ref. [1] for a recent publication), or all external momenta are zero and besides massless lines there are also particles with a common mass M. The latter case has been developed in refs. [2, 3] and first applications can be found in refs. [4, 5]. In this paper we consider a further very important application: the four-loop contribution to the matching or decoupling relation for the strong coupling.

The paper is organized as follows: In the next section we define the decoupling constants and the theoretical framework of our calculation. In section 3 we present analytical

results and discuss the numerical consequences. In section 4 the connection of the decoupling constant to the coupling of a Higgs boson to two gluons is explained and the corresponding coupling strength is evaluated to five-loop order. Finally, we conclude in section 5. In the appendix we present the result for the decoupling constant parameterized in terms of the on-shell heavy quark mass.

2. Theoretical framework

We consider QCD with n_f active quark flavours. Furthermore it is assumed that n_l quarks are massless and n_h quarks are massive, i.e. we have $n_f = n_l + n_h$. In practice one often has $n_h = 1$, however, it is convenient to keep a generic label for the massive quarks.

The decoupling relations relate quantities in the full and effective theory where the latter is defined through the lagrangian $\mathcal{L}'$ given by

$$\mathcal{L}'\left(g_s^0, m_q^0, \xi^0; \psi_q^0, G_\mu^{0,a}, c^{0,a}; \zeta_i^0\right) = \mathcal{L}^{\text{QCD}}\left(g_s^{0\prime}, m_q^{0\prime}, \xi^{0\prime}; \psi_q^{0\prime}, G_\mu^{0\prime,a}, c^{0\prime,a}\right). \quad (2.1)$$

ψ_q, G_μ^a and c^a are the fermion, gluon and ghost fields, respectively, m_q are the quark masses, ξ is the gauge parameter, and $\alpha_s = g_s^2/(4\pi)$ is the strong coupling constant. $\mathcal{L}^{\text{QCD}}$ is the usual QCD Lagrange density and the effective n_l-flavour quantities are marked by a prime. Eq. (2.1) states that the lagrangian in the effective theory has the same form as the original one with rescaled fields, masses and coupling. It is convenient to define the decoupling constants ζ_i in the bare theory through

$$g_s^{0\prime} = \zeta_g^0 g_s^0, \qquad m_q^{0\prime} = \zeta_m^0 m_q^0, \qquad \xi^{0\prime} - 1 = \zeta_3^0(\xi^0 - 1),$$

$$\psi_q^{0\prime} = \sqrt{\zeta_2^0}\,\psi_q^0, \qquad G_\mu^{0\prime,a} = \sqrt{\zeta_3^0}\,G_\mu^{0,a}, \qquad c^{0\prime,a} = \sqrt{\tilde{\zeta}_3^0}\,c^{0,a}. \quad (2.2)$$

In a next step the renormalized quantities are obtained by the usual renormalization procedure introduced by the multiplicative renormalization constants through [6]

$$g_s^0 = \mu^\varepsilon Z_g g_s, \qquad m_q^0 = Z_m m_q, \qquad \xi^0 - 1 = Z_3(\xi - 1),$$

$$\psi_q^0 = \sqrt{Z_2}\,\psi_q, \qquad G_\mu^{0,a} = \sqrt{Z_3}\,G_\mu^a, \qquad c^{0,a} = \sqrt{\tilde{Z}_3}\,c^a. \quad (2.3)$$

Combining eqs. (2.2) and (2.3) leads to renormalized decoupling constants, e.g.

$$\zeta_g = \frac{Z_g}{Z_g'}\zeta_g^0, \qquad \zeta_3 = \frac{Z_3}{Z_3'}\zeta_3^0, \qquad \tilde{\zeta}_3 = \frac{\tilde{Z}_3}{\tilde{Z}_3'}\tilde{\zeta}_3^0. \quad (2.4)$$

Note that since we are interested in the four-loop results for ζ_i the corresponding renormalization constants have to be known with the same accuracy. In ref. [7] the results up to four-loop order have nicely been summarized (see also refs. [8, 9]).

Due to the well-known Ward identities [6] there are several ways to compute the renormalization constant for the strong coupling, Z_g. A convenient relation, which has the advantage that due to the appearance of renormalization constants involving ghosts less diagrams contribute, is given by

$$Z_g = \frac{\tilde{Z}_1}{\tilde{Z}_3\sqrt{Z_3}}, \quad (2.5)$$

where $\tilde{Z}_1$ is the renormalization constant of the ghost-gluon vertex $g_s G\bar{c}c$. The same is true for the corresponding equation for the decoupling constant, such that one can use the relation

$$\zeta_g^0 = \frac{\tilde{\zeta}_1^0}{\tilde{\zeta}_3^0 \sqrt{\zeta_3^0}}, \qquad (2.6)$$

where $\tilde{\zeta}_1^0$ denotes the decoupling constant for the ghost-gluon vertex. Alternatively, one can use the renormalized objects ζ_3, $\tilde{\zeta}_3$ from eq. (2.4) as well as $\tilde{\zeta}_1 = \frac{\tilde{Z}_1}{\tilde{Z}_1'}\tilde{\zeta}_1^0$ and then obtain ζ_g from the renormalized version of eq. (2.6).

In refs. [10, 11] formulae for the bare decoupling constants ζ_i^0 are derived which relate the n-loop decoupling constants to n-loop vacuum integrals. In particular, one has

$$\zeta_3^0 = 1 + \Pi_G^{0h}(0),$$
$$\tilde{\zeta}_3^0 = 1 + \Pi_c^{0h}(0),$$
$$\tilde{\zeta}_1^0 = 1 + \Gamma_{G\bar{c}c}^{0h}(0,0), \qquad (2.7)$$

where $\Pi_G(p^2)$ and $\Pi_c(p^2)$ are the gluon and ghost vacuum polarizations, respectively, and the superscript h denotes the so-called hard part which survives after setting the external momentum to zero. Specifically, $\Pi_G(p^2)$ and $\Pi_c(p^2)$ are related to the gluon and ghost propagators through

$$i \int \mathrm{d}x\, e^{ip\cdot x} \left\langle TG^{0,a\mu}(x)G^{0,b\nu}(0) \right\rangle = \delta^{ab} \left\{ \frac{g^{\mu\nu}}{p^2 \left[1 + \Pi_G^0(p^2)\right]} + \text{terms proportional to } p^\mu p^\nu \right\},$$
$$i \int \mathrm{d}x\, e^{ip\cdot x} \left\langle Tc^{0,a}(x)\bar{c}^{0,b}(0) \right\rangle = -\frac{\delta^{ab}}{p^2 \left[1 + \Pi_c^0(p^2)\right]}, \qquad (2.8)$$

respectively, while $\Gamma_{G\bar{c}c}^0(p,k)$ is defined through the one-particle-irreducible (1PI) part of the amputated $G\bar{c}c$ Green function as

$$i^2 \int \mathrm{d}x\mathrm{d}y\, e^{i(p\cdot x + k\cdot y)} \left\langle Tc^{0,a}(x)\bar{c}^{0,b}(0)G^{0,c\mu}(y) \right\rangle^{\text{1PI}}$$
$$= p^\mu g_s^0 \left\{ -if^{abc}\left[1 + \Gamma_{G\bar{c}c}^0(p,k)\right] + \text{other colour structures} \right\}, \quad (2.9)$$

where p and k are the outgoing four-momenta of c and G, respectively, and f^{abc} are the structure constants of the QCD gauge group. Sample four-loop diagrams for each line of eq. (2.7) are shown in figure 1(a)–(c).

From eqs. (2.6), (2.4) and (2.7) it becomes clear that for the calculation of ζ_g four-loop vacuum diagrams are needed. Currently the only practical method to express an arbitrary four-loop vacuum integral in terms of a small set of master integrals is based on the algorithm developed in ref. [12]. The application to four-loop bubbles has been discussed in ref. [2]. First physical results deal with moments of the photon polarization function [4] and the singlet contribution to the electroweak ρ parameter [5]. The essence of the Laporta algorithm [12] is the generation of large tables containing relations between
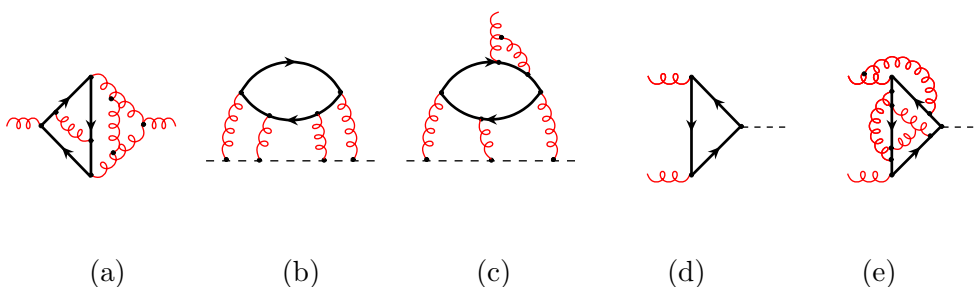
Figure 1: Sample diagrams for the gluon (a) and ghost (b) propagator and the ghost-gluon vertex (c). In (d) the lowest-order diagram is shown mediating the Higgs-gluon coupling in the Standard Model and (e) shows an example for a five-loop diagram contributing to the result in eq. (4.4).

arbitrary integrals and the so-called master integrals. For the calculation at hand the tables have a size of about 8 GB and contain 6 million equations.

The master integrals needed for the evaluation of ζ_g have been computed in ref. [13], where, however, some of the higher order coefficients in ϵ could only be determined numerically.

3. Running and decoupling for α_s

Whereas at three-loop level of the order of 1000 diagrams have to be considered, at four loops there are almost 20000 diagrams which contribute to the gluon and ghost propagators and the ghost-gluon vertex. They are generated with the program QGRAF [14]. With the help of the packages q2e and exp [15, 16] the topologies and notation are adopted to the program performing the reduction of the four-loop vacuum diagrams [2]. As an output we obtain the bare four-loop results as a linear combination of several master integrals. All of them have been computed in ref. [13].

Since at four-loop order the renormalization is quite non-trivial, let us in the following briefly describe the procedure necessary to arrive at a finite result. It is convenient to build in a first step the sum of the bare contributions to ζ_3^0, $\tilde{\zeta}_3^0$ and $\tilde{\zeta}_1^0$ and combine them immediately to ζ_g^0 according to eq. (2.6). Already at this point the gauge parameter, ξ, which for the individual pieces starts to appear at three-loop order, drops out and hence spares us from renormalizing ξ. Let us mention that due to the complexity of the intermediate expressions, the four-loop diagrams have been evaluated for Feynman gauge, whereas the lower-order diagrams were computed for general ξ.

In a next step it is convenient to renormalize the parameters $\alpha_s = g_s^2/(4\pi)$ and m_h applying the usual multiplicative renormalization (cf. eq. (2.3)). The corresponding counterterms have to be known up to the three-loop order. At this point one has to apply eq. (2.4) which requires the ratio Z_g/Z_g' up to four-loop order. In order to evaluate this ratio one has to remember that Z_g' is defined in the effective theory and thus depends on α_s' and n_l whereas Z_g depends on α_s and $(n_l + n_h)$. Thus it is necessary to use ζ_g up to three-loop level in order to transform α_s' to α_s where due to the presence of the divergences in Z_g' also higher-order terms in ϵ of ζ_g have to be taken into account.

Finally one arrives at the following finite result for $(\zeta_g)^2$ which for $N_c = 3$ and $n_h = 1$ is given by

$$
\begin{aligned}
\zeta_g^2 = {} & 1 + \frac{\alpha_s^{(n_l+1)}(\mu)}{\pi}\left(-\frac{1}{6}\ln\frac{\mu^2}{m_h^2}\right) + \left(\frac{\alpha_s^{(n_l+1)}(\mu)}{\pi}\right)^2\left(\frac{11}{72} - \frac{11}{24}\ln\frac{\mu^2}{m_h^2} + \frac{1}{36}\ln^2\frac{\mu^2}{m_h^2}\right) \\
& + \left(\frac{\alpha_s^{(n_l+1)}(\mu)}{\pi}\right)^3\left[\frac{564731}{124416} - \frac{82043}{27648}\zeta(3) - \frac{955}{576}\ln\frac{\mu^2}{m_h^2} + \frac{53}{576}\ln^2\frac{\mu^2}{m_h^2} - \frac{1}{216}\ln^3\frac{\mu^2}{m_h^2}\right. \\
& \left. + n_l\left(-\frac{2633}{31104} + \frac{67}{576}\ln\frac{\mu^2}{m_h^2} - \frac{1}{36}\ln^2\frac{\mu^2}{m_h^2}\right)\right] + \left(\frac{\alpha_s^{(n_l+1)}(\mu)}{\pi}\right)^4\left[\frac{291716893}{6123600}\right. \\
& + \frac{3031309}{1306368}\ln^4 2 - \frac{121}{4320}\ln^5 2 - \frac{3031309}{217728}\zeta(2)\ln^2 2 + \frac{121}{432}\zeta(2)\ln^3 2 - \frac{2362581983}{87091200}\zeta(3) \\
& - \frac{76940219}{2177280}\zeta(4) + \frac{2057}{576}\zeta(4)\ln 2 + \frac{1389}{256}\zeta(5) + \frac{3031309}{54432}a_4 + \frac{121}{36}a_5 - \frac{151369}{2177280}X_0 \\
& + \left(\frac{7391699}{746496} - \frac{2529743}{165888}\zeta(3)\right)\ln\frac{\mu^2}{m_h^2} + \frac{2177}{3456}\ln^2\frac{\mu^2}{m_h^2} - \frac{1883}{10368}\ln^3\frac{\mu^2}{m_h^2} + \frac{1}{1296}\ln^4\frac{\mu^2}{m_h^2} \\
& + n_l\left(-\frac{4770941}{2239488} + \frac{685}{124416}\ln^4 2 - \frac{685}{20736}\zeta(2)\ln^2 2 + \frac{3645913}{995328}\zeta(3)\right. \\
& - \frac{541549}{165888}\zeta(4) + \frac{115}{576}\zeta(5) + \frac{685}{5184}a_4 + \left(-\frac{110341}{373248} + \frac{110779}{82944}\zeta(3)\right)\ln\frac{\mu^2}{m_h^2} \\
& \left. - \frac{1483}{10368}\ln^2\frac{\mu^2}{m_h^2} - \frac{127}{5184}\ln^3\frac{\mu^2}{m_h^2}\right) + n_l^2\left(-\frac{271883}{4478976} + \frac{167}{5184}\zeta(3) + \frac{6865}{186624}\ln\frac{\mu^2}{m_h^2}\right. \\
& \left.\left. - \frac{77}{20736}\ln^2\frac{\mu^2}{m_h^2} + \frac{1}{324}\ln^3\frac{\mu^2}{m_h^2}\right)\right] + \mathcal{O}\left(\left(\frac{\alpha_s^{(n_l+1)}(\mu)}{\pi}\right)^5\right),
\end{aligned}
\tag{3.1}
$$

where the heavy quark mass m_h is renormalized in the $\overline{\text{MS}}$ scheme at the scale μ. The corresponding expression for the on-shell mass is given in appendix A. In eq. (3.1), $\zeta(n)$ is Riemann's zeta function and $a_n = \text{Li}_n(1/2) = \sum_{k=1}^{\infty} 1/(2^k k^n)$. The constant X_0, which is the leading coefficient of a certain finite four-loop master integral, is only known numerically with the value [13]

$$
X_0 = +1.808879546208334741426364595086952090.
\tag{3.2}
$$

Interestingly, in principle the number of numerical coefficients occurring in eq. (3.1) should be three. One relation among them can be established through the separate renormalization of the ghost propagator while a further constant has become available recently in analytical form [17]. Thus one remains with one coefficient which is only known numerically.

Inserting numerical values into eq. (3.1) one obtains

$$
\begin{aligned}
\zeta_g^2 \approx {} & 1 + 0.1528\left(\frac{\alpha_s^{(n_l+1)}(m_h)}{\pi}\right)^2 + (0.9721 - 0.0847\,n_l)\left(\frac{\alpha_s^{(n_l+1)}(m_h)}{\pi}\right)^3 \\
& + \left(5.1703 - 1.0099\,n_l - 0.0220\,n_l^2\right)\left(\frac{\alpha_s^{(n_l+1)}(m_h)}{\pi}\right)^4.
\end{aligned}
\tag{3.3}
$$

– 5 –

It is interesting to note that the n_l-independent four-loop coefficient is relatively big as compared to the corresponding constants at lower loop-order. However, for the interesting values $n_l = (3, 4, 5)$ one observes a big cancellation leading to a well-defined perturbative series with coefficients $(-0.4288, +0.7790, +1.9428)$ in front of $(\alpha_s/\pi)^4$. Note, that the two-loop result for ζ_g has been computed in refs. [18, 19] and the three-loop terms have been evaluated for the first time in ref. [20].

We are now in a position to study the numerical impact of our result. As an example we consider the evaluation of $\alpha_s^{(5)}(M_Z)$ from $\alpha_s^{(4)}(M_\tau)$, i.e. we apply our formalism to the crossing of the bottom quark threshold with $n_l = 4$. In general one assumes that the value of the scale μ_b, where the matching has to be performed, is of order m_b. However, it is not determined by theory. Thus this uncertainty contributes significantly to the error of physical predictions. On general grounds one expects that while including higher order perturbative corrections the relation between $\alpha_s^{(4)}(M_\tau)$ and $\alpha_s^{(5)}(M_Z)$ becomes insensitive to the choice of the matching scale. This has been demonstrated in refs. [21, 10] for the three- and four-loop evolution, respectively. In the following we want to extend the analysis to five loops.

The procedure is as follows. In a first step we calculate $\alpha_s^{(4)}(\mu_b)$ by exactly integrating the equation

$$\frac{\mu^2 d}{d\mu^2} \frac{\alpha_s^{(n_f)}}{\pi} = \beta^{(n_f)}\left(\alpha_s^{(n_f)}\right) = -\sum_{i \geq 0} \beta_i^{(n_f)} \left(\frac{\alpha_s^{(n_f)}}{\pi}\right)^{i+2}, \qquad (3.4)$$

with the initial condition $\alpha_s^{(4)}(M_\tau) = 0.36$. Afterwards $\alpha_s^{(5)}(\mu_b)$ is obtained from the renormalized version of the first equation in (2.2) where we use ζ_g parameterized in terms of the on-shell mass (cf. eq. (A.1)) $M_b = 4.7$ GeV. Finally, we compute $\alpha_s^{(5)}(M_Z)$ using again eq. (3.4). For consistency, i-loop evolution must be accompanied by $(i-1)$-loop matching, i.e. if we omit terms of $\mathcal{O}(\alpha_s^{i+2})$ on the right-hand side of eq. (3.4), we need to discard those of $\mathcal{O}(\alpha_s^{i+1})$ in eq. (A.1) at the same time. Since the five-loop coefficient in eq. (3.4) is not yet known we set $\beta_4^{(n_f)}$ to zero in our numerical analysis.

In figure 2 the result for $\alpha_s^{(5)}(M_Z)$ as a functions μ_b is displayed for the one- to five-loop analysis. For illustration, μ_b is varied rather extremely, by almost two orders of magnitude. While the leading-order result exhibits a strong logarithmic behaviour, the analysis is gradually getting more stable as we go to higher orders. The five-loop curve is almost flat for $\mu_b \geq 1$ GeV and demonstrates an even more stable behaviour than the four-loop analysis of ref. [10]. It should be noted that around $\mu_b \approx 1$ GeV both the three-, four- and five-loop curves show a strong variation which can be interpreted as a sign for the breakdown of perturbation theory. Besides the μ_b dependence of $\alpha_s^{(5)}(M_Z)$, also its absolute normalization is significantly affected by the higher orders. At the central matching scale $\mu_b = M_b$, we encounter a rapid convergence behaviour.

4. Effective coupling between a Higgs boson and gluons

In this section we want to discuss the relation between ζ_g and the coupling of a scalar Higgs boson to gluons. Due to the fact that gluons are massless, there is no coupling at
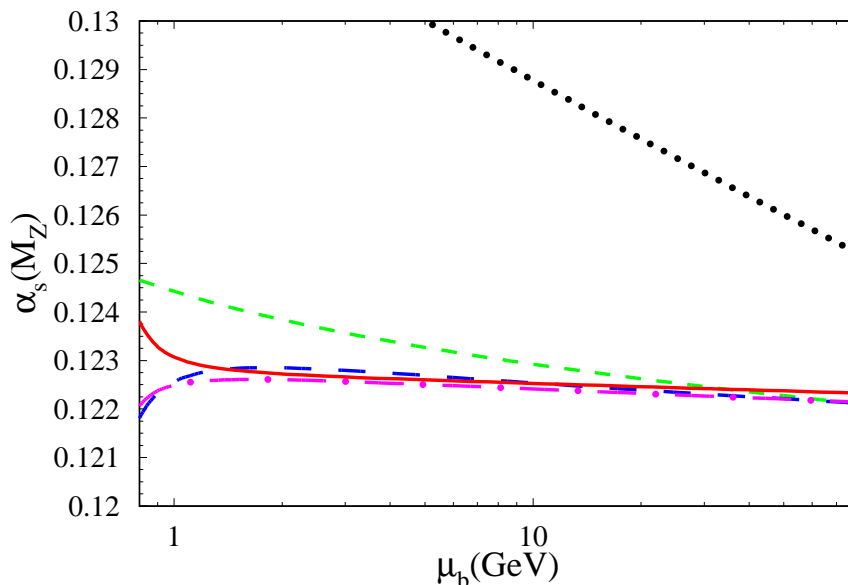
Figure 2: μ_b dependence of $\alpha_s^{(5)}(M_Z)$ calculated from $\alpha_s^{(4)}(M_\tau) = 0.36$ and $M_b = 4.7\,\mathrm{GeV}$. The procedure is described in the text. The dotted, short-dashed, long-dashed and dash-dotted line corresponds to one- to four-loop running. The solid curve includes the effect of the new four-loop matching term.

tree-level. At one-loop order the HGG coupling is mediated via a top-quark loop depicted in figure 1(d).

For an intermediate-mass Higgs boson which formally obeys the relation $M_H \ll m_t$ it is possible to construct an effective lagrangian of the form

$$\mathcal{L}_{\mathrm{eff}} = -\frac{H^0}{v^0} C_1 \mathcal{O}_1 \,, \tag{4.1}$$

with the effective operator

$$\mathcal{O}_1 = \left(G_{\mu\nu}^a \right)^2 \,, \tag{4.2}$$

where $G_{\mu\nu}^a$ is the colour field strength. The coefficient function C_1 incorporates the contribution from the top-quark loops. At one-loop order it is easy to see that the contribution from the triangle diagrams can be obtained through the derivative of the one-loop diagram for Π_G^0 with respect to the top-quark mass. However, at higher-loop orders this simple picture does not hold anymore and the relation between the HGG diagrams and derivatives of the two-point functions containing a top-quark loop gets more involved. In ref. [10] an all-order low-energy theorem has been derived which establishes such a relation and which has a surprisingly simple form (for definiteness we specify to the top-quark in this section):

$$C_1 = -\frac{1}{2} \frac{m_t^2 \partial}{\partial m_t^2} \ln \zeta_g^2 \,. \tag{4.3}$$

An appealing feature of eq. (4.3) is that at a given order in α_s only the logarithmic contributions of ζ_g are needed for the calculation of C_1 at the same order. Thus, from our calculation we can reconstruct the five-loop logarithms of ζ_g from lower-order terms and the β and γ_m functions governing the running of α_s and the top-quark mass, respectively. This leads to the following result, at $N_c = 3$ and $n_h = 1$,

$$
\begin{aligned}
C_1 = -\frac{1}{12}\frac{\alpha_s^{(n_l+1)}(\mu)}{\pi}\Bigg\{ & 1 + \frac{\alpha_s^{(n_l+1)}(\mu)}{\pi}\left(\frac{11}{4} - \frac{1}{6}\ln\frac{\mu^2}{m_t^2}\right) \\
& + \left(\frac{\alpha_s^{(n_l+1)}(\mu)}{\pi}\right)^2\left[\frac{2821}{288} - \frac{3}{16}\ln\frac{\mu^2}{m_t^2} + \frac{1}{36}\ln^2\frac{\mu^2}{m_t^2} + n_l\left(-\frac{67}{96} + \frac{1}{3}\ln\frac{\mu^2}{m_t^2}\right)\right] \\
& + \left(\frac{\alpha_s^{(n_l+1)}(\mu)}{\pi}\right)^3\Bigg[-\frac{4004351}{62208} + \frac{1305893}{13824}\zeta(3) - \frac{859}{288}\ln\frac{\mu^2}{m_t^2} + \frac{431}{144}\ln^2\frac{\mu^2}{m_t^2} - \frac{1}{216}\ln^3\frac{\mu^2}{m_t^2} \\
& + n_l\left(\frac{115607}{62208} - \frac{110779}{13824}\zeta(3) + \frac{641}{432}\ln\frac{\mu^2}{m_t^2} + \frac{151}{288}\ln^2\frac{\mu^2}{m_t^2}\right) \\
& + n_l^2\left(-\frac{6865}{31104} + \frac{77}{1728}\ln\frac{\mu^2}{m_t^2} - \frac{1}{18}\ln^2\frac{\mu^2}{m_t^2}\right)\Bigg] \\
& + \left(\frac{\alpha_s^{(n_l+1)}(\mu)}{\pi}\right)^4\Bigg[-\frac{69820734619}{27993600} - \frac{39407017}{373248}\ln^4 2 + \frac{11011}{8640}\ln^5 2 + \frac{39407017}{62208}\zeta(2)\ln^2 2 \\
& - \frac{11011}{864}\zeta(2)\ln^3 2 + \frac{27642438179}{24883200}\zeta(3) + \frac{996205247}{622080}\zeta(4) - \frac{187187}{1152}\zeta(4)\ln 2 - \frac{894391}{4608}\zeta(5) \\
& - \frac{39407017}{15552}a_4 - \frac{11011}{72}a_5 + \frac{1967797}{622080}X_0 \\
& - \left(\frac{1276661933}{1492992} - \frac{226222121}{331776}\zeta(3)\right)\ln\frac{\mu^2}{m_t^2} + \frac{33517}{1728}\ln^2\frac{\mu^2}{m_t^2} + \frac{140357}{20736}\ln^3\frac{\mu^2}{m_t^2} + \frac{1}{1296}\ln^4\frac{\mu^2}{m_t^2} \\
& + n_l\Bigg(\frac{58259821853}{195955200} + \frac{3896297}{580608}\ln^4 2 - \frac{121}{1440}\ln^5 2 - \frac{3896297}{96768}\zeta(2)\ln^2 2 + \frac{121}{144}\zeta(2)\ln^3 2 \\
& - \frac{74306021071}{348364800}\zeta(3) + \frac{141211087}{3870720}\zeta(4) + \frac{2057}{192}\zeta(4)\ln 2 - \frac{20227}{2304}\zeta(5) + \frac{3896297}{24192}a_4 + \frac{121}{12}a_5 \\
& - \frac{151369}{725760}X_0 + \left(\frac{23250409}{186624} - \frac{8736121}{82944}\zeta(3)\right)\ln\frac{\mu^2}{m_t^2} + \frac{569}{2304}\ln^2\frac{\mu^2}{m_t^2} + \frac{2551}{2592}\ln^3\frac{\mu^2}{m_t^2}\Bigg) \\
& + n_l^2\Bigg(-\frac{33014371}{8957952} + \frac{685}{41472}\ln^4 2 - \frac{685}{6912}\zeta(2)\ln^2 2 + \frac{970259}{110592}\zeta(3) - \frac{518509}{55296}\zeta(4) \\
& + \frac{115}{192}\zeta(5) + \frac{685}{1728}a_4 - \left(\frac{1107181}{186624} - \frac{28297}{9216}\zeta(3)\right)\ln\frac{\mu^2}{m_t^2} - \frac{1729}{13824}\ln^2\frac{\mu^2}{m_t^2} - \frac{1205}{5184}\ln^3\frac{\mu^2}{m_t^2}\Bigg) \\
& + n_l^3\left(-\frac{255947}{1492992} + \frac{5}{64}\zeta(3) + \frac{481}{5184}\ln\frac{\mu^2}{m_t^2} - \frac{77}{6912}\ln^2\frac{\mu^2}{m_t^2} + \frac{1}{108}\ln^3\frac{\mu^2}{m_t^2}\right) \\
& + 6\left(\beta_4^{(n_l)} - \beta_4^{(n_l+1)}\right)\Bigg] + \mathcal{O}\left(\left(\frac{\alpha_s^{(n_l+1)}(\mu)}{\pi}\right)^5\right)\Bigg\},
\end{aligned}
$$
(4.4)

with m_t being the $\overline{\text{MS}}$ top-quark mass renormalized at the scale μ. Note the appearance of the flavour-dependent part of β_4 in the five-loop contribution, whereas the corresponding coefficient from the anomalous mass dimension does not appear. We want to stress that the term of order α_s^5 covers the contributions from five-loop diagrams like the one in figure 1(e).

Evaluating eq. (4.4) numerically leads to

$$
\begin{aligned}
C_1 \approx -\frac{1}{12}\frac{\alpha_s^{(n_l+1)}(m_t)}{\pi}\Bigg[& 1 + 2.7500\,\frac{\alpha_s^{(n_l+1)}(m_t)}{\pi} + (9.7951 - 0.6979\,n_l)\left(\frac{\alpha_s^{(n_l+1)}(m_t)}{\pi}\right)^2 \\
& + \left(49.1827 - 7.7743\,n_l - 0.2207\,n_l^2\right)\left(\frac{\alpha_s^{(n_l+1)}(m_t)}{\pi}\right)^3 \\
& + \left(-662.5065 + 137.6005\,n_l - 2.5367\,n_l^2 - 0.0775\,n_l^3 + 6\left(\beta_4^{(n_l)} - \beta_4^{(n_l+1)}\right)\right) \\
& \times \left(\frac{\alpha_s^{(n_l+1)}(m_t)}{\pi}\right)^4 \Bigg].
\end{aligned}
\tag{4.5}
$$

Again one observes large cancellations between the n_l^0 and n_l^1 term in the five-loop contribution to C_1.

Note that the result of eq. (4.4) constitutes a building block for the N^{4}LO calculation to the Higgs boson production and decay in the two-gluon channel, for which the complete answer currently is certainly out of range. Still, the five-loop result for C_1 constitutes a high-order result in perturbative QCD which is of theoretical interest by itself.

5. Conclusions

In this paper the decoupling constant of the strong coupling is presented to four-loop order. This constitutes a fundamental quantity of QCD and is one of the very few known to such a high order. The decoupling constant is necessary for performing a consistent running of α_s with five-loop accuracy including important effects from the crossing of quark thresholds. The calculation has been performed analytically, and the main result can be found in eq. (3.1). With the help of a low-energy theorem it is possible to derive the five-loop result for the effective coupling of the Higgs boson to gluons, which constitutes a building block in the corresponding production and decay processes.

We want to mention that the result for ζ_g^2 in eq. (3.1) has been obtained independently in ref. [22]. Except for QGRAF, which is used for the generation of the diagrams, there is no common code. Even the master integrals have meanwhile been computed independently [23] and for the renormalization a different procedure has been chosen.

A. Results for ζ_g^{OS}

Replacing in eq. (3.1) the $\overline{\mathrm{MS}}$ mass m_h by the pole mass M_h using the three-loop approximation $[24-26]$ one gets

$$\left(\zeta_g^{\mathrm{OS}}\right)^2 = 1 + \frac{\alpha_s^{(n_l+1)}(\mu)}{\pi}\left(-\frac{1}{6}\ln\frac{\mu^2}{M_h^2}\right) + \left(\frac{\alpha_s^{(n_l+1)}(\mu)}{\pi}\right)^2\left(-\frac{7}{24} - \frac{19}{24}\ln\frac{\mu^2}{M_h^2} + \frac{1}{36}\ln^2\frac{\mu^2}{M_h^2}\right)$$

$$+ \left(\frac{\alpha_s^{(n_l+1)}(\mu)}{\pi}\right)^3\left[-\frac{58933}{124416} - \frac{2}{3}\zeta(2) - \frac{2}{9}\zeta(2)\ln 2 - \frac{80507}{27648}\zeta(3) - \frac{8521}{1728}\ln\frac{\mu^2}{M_h^2}\right.$$

$$\left.-\frac{131}{576}\ln^2\frac{\mu^2}{M_h^2} - \frac{1}{216}\ln^3\frac{\mu^2}{M_h^2} + n_l\left(\frac{2479}{31104} + \frac{1}{9}\zeta(2) + \frac{409}{1728}\ln\frac{\mu^2}{M_h^2}\right)\right]$$

$$+ \left(\frac{\alpha_s^{(n_l+1)}(\mu)}{\pi}\right)^4\left[-\frac{141841753}{24494400} + \frac{3179149}{1306368}\ln^4 2 - \frac{121}{4320}\ln^5 2 - \frac{697121}{19440}\zeta(2)\right.$$

$$+ \frac{1027}{162}\zeta(2)\ln 2 - \frac{2913037}{217728}\zeta(2)\ln^2 2 + \frac{121}{432}\zeta(2)\ln^3 2 - \frac{2408412383}{87091200}\zeta(3)$$

$$+ \frac{1439}{216}\zeta(3)\zeta(2) - \frac{71102219}{2177280}\zeta(4) + \frac{2057}{576}\zeta(4)\ln 2 + \frac{49309}{20736}\zeta(5)$$

$$+ \frac{3179149}{54432}a_4 + \frac{121}{36}a_5 - \frac{151369}{2177280}X_0$$

$$- \left(\frac{19696909}{746496} + \frac{29}{9}\zeta(2) + \frac{29}{27}\zeta(2)\ln 2 + \frac{2439119}{165888}\zeta(3)\right)\ln\frac{\mu^2}{M_h^2} - \frac{7693}{1152}\ln^2\frac{\mu^2}{M_h^2}$$

$$- \frac{8371}{10368}\ln^3\frac{\mu^2}{M_h^2} + \frac{1}{1296}\ln^4\frac{\mu^2}{M_h^2} + n_l\left(\frac{1773073}{746496} + \frac{173}{124416}\ln^4 2 + \frac{557}{162}\zeta(2)\right.$$

$$+ \frac{22}{81}\zeta(2)\ln 2 - \frac{1709}{20736}\zeta(2)\ln^2 2 + \frac{4756441}{995328}\zeta(3) - \frac{697709}{165888}\zeta(4) + \frac{115}{576}\zeta(5) + \frac{173}{5184}a_4$$

$$+ \left(\frac{1110443}{373248} + \frac{41}{54}\zeta(2) + \frac{2}{27}\zeta(2)\ln 2 + \frac{132283}{82944}\zeta(3)\right)\ln\frac{\mu^2}{M_h^2} + \frac{6661}{10368}\ln^2\frac{\mu^2}{M_h^2}$$

$$+ \frac{107}{1728}\ln^3\frac{\mu^2}{M_h^2}\right) + n_l^2\left(-\frac{140825}{1492992} - \frac{13}{162}\zeta(2) - \frac{19}{1728}\zeta(3)\right.$$

$$\left.\left.- \left(\frac{1679}{186624} + \frac{1}{27}\zeta(2)\right)\ln\frac{\mu^2}{M_h^2} - \frac{493}{20736}\ln^2\frac{\mu^2}{M_h^2}\right)\right]$$

$$\approx 1 - 0.2917\left(\frac{\alpha_s^{(n_l+1)}(M_h)}{\pi}\right)^2 + (-5.3239 + 0.2625\, n_l)\left(\frac{\alpha_s^{(n_l+1)}(M_h)}{\pi}\right)^3$$

$$+ \left(-85.8750 + 9.6923\, n_l - 0.2395\, n_l^2\right)\left(\frac{\alpha_s^{(n_l+1)}(M_h)}{\pi}\right)^4. \tag{A.1}$$

References

[1] P.A. Baikov, K.G. Chetyrkin and J.H. Kühn, *Strange quark mass from τ lepton decays with $\mathcal{O}(\alpha_S^3)$ accuracy*, *Phys. Rev. Lett.* **95** (2005) 012003 [hep-ph/0412350].

[2] Y. Schröder, *Automatic reduction of four-loop bubbles*, *Nucl. Phys.* **116** *(Proc. Suppl.)* (2003) 402 [hep-ph/0211288].

[3] C. Sturm, PhD thesis (June 2005), Karlsruhe Univ., Germany (unpublished).

[4] K.G. Chetyrkin, J.H. Kühn, P. Mastrolia and C. Sturm, *Heavy-quark vacuum polarization: first two moments of the $\mathcal{O}(\alpha_s^3 n_f^2)$ contribution*, *Eur. Phys. J.* **C 40** (2005) 361 [hep-ph/0412055].

[5] Y. Schröder and M. Steinhauser, *Four-loop singlet contribution to the ρ parameter*, *Phys. Lett.* **B 622** (2005) 124 [`hep-ph/0504055`].

[6] T. Muta, *Foundations of quantum chromodynamics*, World Scientific, Singapore, 1987.

[7] K.G. Chetyrkin, *Four-loop renormalization of QCD: full set of renormalization constants and anomalous dimensions*, *Nucl. Phys.* **B 710** (2005) 499 [`hep-ph/0405193`].

[8] T. van Ritbergen, J.A.M. Vermaseren and S.A. Larin, *The four-loop beta function in quantum chromodynamics*, *Phys. Lett.* **B 400** (1997) 379 [`hep-ph/9701390`].

[9] M. Czakon, *The four-loop QCD β-function and anomalous dimensions*, *Nucl. Phys.* **B 710** (2005) 485 [`hep-ph/0411261`].

[10] K.G. Chetyrkin, B.A. Kniehl and M. Steinhauser, *Decoupling relations to $\mathcal{O}(\alpha_s^3)$ and their connection to low-energy theorems*, *Nucl. Phys.* **B 510** (1998) 61 [`hep-ph/9708255`].

[11] M. Steinhauser, *Results and techniques of multi-loop calculations*, *Phys. Rept.* **364** (2002) 247 [`hep-ph/0201075`].

[12] S. Laporta, *High-precision calculation of multi-loop Feynman integrals by difference equations*, *Int. J. Mod. Phys.* **A 15** (2000) 5087 [`hep-ph/0102033`].

[13] Y. Schröder and A. Vuorinen, *High-precision epsilon expansions of single-mass-scale four-loop vacuum bubbles*, *JHEP* **06** (2005) 051 [`hep-ph/0503209`].

[14] P. Nogueira, *Automatic Feynman graph generation*, *J. Comput. Phys.* **105** (1993) 279.

[15] T. Seidensticker, *Automatic application of successive asymptotic expansions of Feynman diagrams*, `hep-ph/9905298`.

[16] R. Harlander, T. Seidensticker and M. Steinhauser, *Complete corrections of $O(\alpha\alpha_s)$ to the decay of the Z boson into bottom quarks*, *Phys. Lett.* **B 426** (1998) 125 [`hep-ph/9712228`].

[17] Y. Schröder, in preparation.

[18] W. Bernreuther and W. Wetzel, *Decoupling of heavy quarks in the minimal subtraction scheme*, *Nucl. Phys.* **B 197** (1982) 228, erratum *ibid.* **B513** (1998) 758.

[19] S.A. Larin, T. van Ritbergen and J.A.M. Vermaseren, *The large quark mass expansion of $\Gamma(Z^0 \to hadrons)$ and $\Gamma(\tau^- \to \nu_\tau + hadrons)$ in the order α_s^3*, *Nucl. Phys.* **B 438** (1995) 278 [`hep-ph/9411260`].

[20] K.G. Chetyrkin, B.A. Kniehl and M. Steinhauser, *Strong coupling constant with flavour thresholds at four loops in the $\bar{M}S$ scheme*, *Phys. Rev. Lett.* **79** (1997) 2184 [`hep-ph/9706430`].

[21] G. Rodrigo, A. Pich and A. Santamaria, *$\alpha_s(m_Z)$ from τ decays with matching conditions at three loops*, *Phys. Lett.* **B 424** (1998) 367 [`hep-ph/9707474`].

[22] K.G. Chetyrkin, J.H. Kühn and C. Sturm, *QCD decoupling at four loops*, `hep-ph/0512060`.

[23] K.G. Chetyrkin, M. Faisst, C. Sturm and M. Tentukov, in preparation.

[24] K.G. Chetyrkin and M. Steinhauser, *Short distance mass of a heavy quark at order α_s^3*, *Phys. Rev. Lett.* **83** (1999) 4001 [`hep-ph/9907509`].

[25] K.G. Chetyrkin and M. Steinhauser, *The relation between the $\bar{M}S$ and the on-shell quark mass at order α_s^3*, *Nucl. Phys.* **B 573** (2000) 617 [`hep-ph/9911434`].

[26] K. Melnikov and T. v. Ritbergen, *The three-loop relation between the $\bar{M}S$ and the pole quark masses*, *Phys. Lett.* **B 482** (2000) 99 [`hep-ph/9912391`].

[YS16]

Quark mass thresholds in QCD thermodynamics

Quark mass thresholds in QCD thermodynamics

Mikko Laine* and York Schröder†

Faculty of Physics, University of Bielefeld, D-33501 Bielefeld, Germany

We discuss radiative corrections to how quark mass thresholds are crossed, as a function of the temperature, in basic thermodynamic observables such as the pressure, the energy and entropy densities, and the heat capacity of high temperature QCD. The indication from leading order that the charm quark plays a visible role at surprisingly low temperatures, is confirmed. We also sketch a way to obtain phenomenological estimates relevant for generic expansion rate computations at temperatures between the QCD and electroweak scales, pointing out where improvements over the current knowledge are particularly welcome.

PACS numbers: 11.10.Wx, 11.15.Bt, 12.38.Bx, 98.80.Cq

I. INTRODUCTION

Besides being of fundamental theoretical interest to finite temperature field theory, the thermodynamic pressure of the Standard Model, as a function of the temperature T and of various chemical potentials μ_i, has several potential phenomenological applications. Most notably it dictates, through the Einstein equations, the expansion rate of the radiation dominated Early Universe. The expansion rate in turn determines when various dark matter candidates decouple, thus fixing their relic densities: fine details of the pressure could become observable for instance if dark matter is made of electroweak scale WIMPs [1, 2] or of keV-scale sterile neutrinos [3, 4]. Furthermore, the pressure is in principle visible in the present-day spectrum of the gravitational wave background that was generated during the inflationary epoch [5]. More generally, the pressure incorporates the fact that the Standard Model possesses a trace anomaly, i.e. $T^\mu{}_\mu \neq 0$, which in turn can influence many kinds of gravity-related cosmological scenarios (for recent examples, see Refs. [6]).

Apart from cosmology, the pressure is potentially also relevant for the hydrodynamic expansion that the dense matter generated in current and upcoming heavy ion collision experiments may undergo. In this case there is some room for caution, however, since the issue of whether local thermodynamic equilibrium is reached remains controversial [7].

Given that the biggest theoretical challenges are related to strongly interacting particles, considerable efforts have been devoted to the determination of the QCD part of the pressure over a course of years. Denoting by g the renormalised strong coupling constant, perturbative corrections to the non-interacting Stefan-Boltzmann law have been determined at relative orders $\mathcal{O}(g^2)$ [8], $\mathcal{O}(g^3)$ [9], $\mathcal{O}(g^4 \ln(1/g))$ [10], $\mathcal{O}(g^4)$ [11], $\mathcal{O}(g^5)$ [12], and $\mathcal{O}(g^6 \ln(1/g))$ [13], as a function of the number of colours, N_c, and the number of massless quark flavours, N_f. The first presently unknown order, $\mathcal{O}(g^6)$, contains non-perturbative coefficients [14, 15], but those can also be attacked [16, 17]. All orders of g are available in the formal limit of large N_f [18]. These results have been extended to the case of finite quark chemical potentials [19, 20, 21], and a similar computation has recently also been finalised for the weakly interacting part of the Standard Model, at temperatures higher than the electroweak scale [22]. Moreover, the fact that several orders are available allows to experiment with various kinds of resummations [23, 24].

Surprisingly, however, relatively little seems to be known about the dependence of the QCD pressure on the quark masses m_i, $i = 1, ..., N_f$. While the non-interacting Stefan-Boltzmann law is readily extended to this situation, it in fact appears that even the first non-trivial term, $\mathcal{O}(g^2)$, has not been exhaustively investigated in the literature (see, however, Ref. [25]). In principle this term has of course been available since almost 30 years [9], but in explicit form only in a renormalization scheme for quark masses which differs from the current standard, the $\overline{\text{MS}}$ scheme. Furthermore, no general numerical evaluation of the basic integrals appearing has been presented, as far as we know. For $T = 0$ but $\mu_i \neq 0$, the full $\mathcal{O}(g^2)$ analysis has also only been carried out recently [26].

Several probable reasons for the apparent lack of interest can surely be envisaged. First of all, the dependence on N_f is known to a high order in the massless case, and interpolating between integer values of N_f should give much of the information that we may need for the massive case. Second, including quark masses turns out to be technically cumbersome [9]. Third, there are several indications, for instance from considerations of the baryon chemical potential [19, 20] and of mesonic correlation lengths [27], that the convergence is much better in the quark sector than in

---

*Electronic address: laine@physik.uni-bielefeld.de
†Electronic address: yorks@physik.uni-bielefeld.de

the gluonic sector, so that the lowest non-trivial order may already provide sufficient accuracy. Nevertheless, we feel that the last assumption deserves to be checked, at least at the next-to-leading order (NLO) $\mathcal{O}(g^2)$, and this is the purpose of the present paper.

In short, our general philosophy will then be to account for the gluonic contributions to the highest order available, $\mathcal{O}(g^6 \ln(1/g))$, and consider the change that quarks with finite physical masses inflict on this result at NLO, $\mathcal{O}(g^2)$. We do find that the quark mass effects at NLO are not too different from those at the leading order, $\mathcal{O}(g^0)$, such that the philosophy of terminating at $\mathcal{O}(g^2)$ is at least self-consistent. Nevertheless, we also outline the procedure for determining the quark mass dependence up to the order $\mathcal{O}(g^6)$.

Apart from the theoretical goals mentioned, we also wish to sketch certain phenomenological results in this paper. Consider the temperature evolution of an expanding system in the case of cosmology, for instance. Einstein equations then lead to (see, e.g., Ref. [28])

$$\frac{1}{T}\frac{\mathrm{d}T}{\mathrm{d}t} = -\sqrt{\frac{24\pi e(T)}{m_{\mathrm{Pl}}^2}}\frac{s(T)}{c(T)} \,, \tag{1}$$

where t is the time; we assumed the Universe to be flat ($k = 0$); and we ignored the cosmological constant. All the quantities appearing here follow from the pressure: $s(T) = p'(T)$ is the entropy density, $e(T) = Ts(T) - p(T)$ is the energy density, and $c(T) = e'(T) = Tp''(T)$ is the heat capacity. We wish to present our favoured "fits" for all these functions for temperatures between the QCD and electroweak scales, indicating where further work is required.

The plan of this paper is the following. We start by elaborating on the basic formalism in Sec. II, discuss quark mass thresholds in Sec. III, present a phenomenological evaluation of the various thermodynamic functions relevant for physical QCD in Sec. IV, include weakly interacting particles in Sec. V, and conclude in Sec. VI.

II. BASIC FORMALISM

In order to determine the basic thermodynamic quantities of the Standard Model, all of which can be derived from minus the grand canonical free energy density, or the pressure $p(T, \boldsymbol{\mu})$, where $\boldsymbol{\mu}$ collects together the various chemical potentials associated with conserved global charges [54], we make use of the framework of dimensionally reduced effective field theories [29, 30, 31]. This framework allows to organise the computation in a transparent way, and implements various resummations of higher order effects. We start by briefly reviewing certain aspects of the general framework for QCD; further details can be found in Ref. [13].

Dimensional reduction proceeds by first integrating out the "hard modes", with momenta or Matsubara frequencies of order $2\pi T$. This produces an effective theory [29], called EQCD [31], which is a three-dimensional $\mathrm{SU}(N_c)$ gauge theory with a scalar field in the adjoint representation. The effective theory has a certain number of couplings, parametrised by functions denoted by $\alpha_{\mathrm{E}1}...\alpha_{\mathrm{E}7}$ [contributing up to $\mathcal{O}(g^6 \ln(1/g))$] and $\beta_{\mathrm{E}1}...\beta_{\mathrm{E}5}$ [contributing at $\mathcal{O}(g^6)$] in Ref. [13]; in the following we explicitly specify the definitions for only a subset of them. These parameters contain all the information concerning the hard modes. Assuming the use of dimensional regularization, we denote by $\alpha_{\mathrm{E}i}^{\overline{\mathrm{MS}}}$, $\beta_{\mathrm{E}i}^{\overline{\mathrm{MS}}}$ parameters from which the $1/\epsilon$-divergences have been removed by the $\overline{\mathrm{MS}}$-prescription.

To proceed, we need to specify explicitly the effective mass parameter m_3^2 and the effective gauge coupling g_3^2 of EQCD at NLO:

$$\hat{m}_3^2 \equiv \frac{m_3^2}{T^2} \equiv g^2 \alpha_{\mathrm{E}4}^{\overline{\mathrm{MS}}} + \frac{g^4}{(4\pi)^2}\alpha_{\mathrm{E}6}^{\overline{\mathrm{MS}}} \,, \tag{2}$$

$$\hat{g}_3^2 \equiv \frac{g_3^2}{T} \equiv g^2 + \frac{g^4}{(4\pi)^2}\alpha_{\mathrm{E}7}^{\overline{\mathrm{MS}}} \,. \tag{3}$$

Both parameters are renormalization group invariant up to the order computed, i.e., the dependence on the scale parameter $\bar{\mu}$ is of order $\mathcal{O}(g^6)$.

With this notation, the physical pressure of hot QCD can be written in the form

$$p_{\mathrm{QCD}} \equiv p_{\mathrm{hard}} + p_{\mathrm{soft}} \,, \tag{4}$$

where p_{hard} represents the contribution of the hard modes (by definition containing both all direct hard contributions to the pressure, and all finite terms emerging from products like $\epsilon \cdot 1/\epsilon$), while p_{soft} represents the contribution of the soft modes. Up to the accuracy $\mathcal{O}(g^6)$, p_{hard} can conveniently be expressed as

$$\frac{p_{\mathrm{hard}}}{T^4} = \alpha_{\mathrm{E}1}^{\overline{\mathrm{MS}}} + \hat{g}_3^2 \alpha_{\mathrm{E}2}^{\overline{\mathrm{MS}}} + \frac{\hat{g}_3^4}{(4\pi)^2}\left(\alpha_{\mathrm{E}3}^{\overline{\mathrm{MS}}} - \alpha_{\mathrm{E}2}^{\overline{\mathrm{MS}}}\alpha_{\mathrm{E}7}^{\overline{\mathrm{MS}}} - \frac{1}{4}d_A C_A \alpha_{\mathrm{E}5}^{\overline{\mathrm{MS}}}\right) +$$

$$+ \frac{\hat{g}_3^6}{(4\pi)^4}\left\{\left[d_A C_A(\alpha_{\mathrm{E6}}^{\overline{\mathrm{MS}}} - \alpha_{\mathrm{E4}}^{\overline{\mathrm{MS}}}\alpha_{\mathrm{E7}}^{\overline{\mathrm{MS}}}) - d_A C_A^3\left(\frac{43}{3} - \frac{27}{32}\pi^2\right)\right]\ln\frac{\bar{\mu}}{4\pi T} + \Delta_{\mathrm{hard}}\right\}, \tag{5}$$

where $d_A \equiv N_{\mathrm{c}}^2 - 1$, $C_A \equiv N_{\mathrm{c}}$, and we have separated a term on the last line which cancels the $\bar{\mu}$-dependence of p_{soft} at $\mathcal{O}(g^6)$. The function Δ_{hard},

$$\Delta_{\mathrm{hard}} \equiv \left[d_A C_A(\alpha_{\mathrm{E6}}^{\overline{\mathrm{MS}}} - \alpha_{\mathrm{E4}}^{\overline{\mathrm{MS}}}\alpha_{\mathrm{E7}}^{\overline{\mathrm{MS}}}) - d_A C_A^3\left(\frac{43}{3} - \frac{27}{32}\pi^2\right)\right]\ln\frac{4\pi T}{\bar{\mu}} +$$

$$+ \beta_{\mathrm{E1}}^{\overline{\mathrm{MS}}} + 2\alpha_{\mathrm{E2}}^{\overline{\mathrm{MS}}}(\alpha_{\mathrm{E7}}^{\overline{\mathrm{MS}}})^2 - 2\alpha_{\mathrm{E3}}^{\overline{\mathrm{MS}}}\alpha_{\mathrm{E7}}^{\overline{\mathrm{MS}}} - \frac{1}{4}d_A C_A\left(\beta_{\mathrm{E2}}^{\overline{\mathrm{MS}}} - \alpha_{\mathrm{E5}}^{\overline{\mathrm{MS}}}\alpha_{\mathrm{E7}}^{\overline{\mathrm{MS}}} + \alpha_{\mathrm{E4}}^{\overline{\mathrm{MS}}}\beta_{\mathrm{E3}}^{\overline{\mathrm{MS}}}\right), \tag{6}$$

depends on $N_{\mathrm{c}}, N_{\mathrm{f}}, m_i, \mu_i$, and $\bar{\mu}/T$. The contributions of the soft modes are [13]

$$\frac{p_{\mathrm{soft}}}{T^4} = \frac{\hat{m}_3^3}{12\pi}d_A - \frac{\hat{g}_3^2\hat{m}_3^2}{(4\pi)^2}d_A C_A\left(\ln\frac{\bar{\mu}}{2m_3} + \frac{3}{4}\right) - \frac{\hat{g}_3^4\hat{m}_3}{(4\pi)^3}d_A C_A^2\left(\frac{89}{24} + \frac{\pi^2}{6} - \frac{11}{6}\ln 2\right) +$$

$$+ \frac{\hat{g}_3^6}{(4\pi)^4}d_A C_A^3\left[\left(\frac{43}{4} - \frac{491}{768}\pi^2\right)\ln\frac{\bar{\mu}}{2m_3} + \left(\frac{43}{12} - \frac{157}{768}\pi^2\right)\ln\frac{\bar{\mu}}{2C_A g_3^2} + \Delta_{\mathrm{soft}}\right]. \tag{7}$$

The function Δ_{soft} reads

$$\Delta_{\mathrm{soft}} = \beta_{\mathrm{M}} + \beta_{\mathrm{G}} - \alpha_{\mathrm{E4}}^{\overline{\mathrm{MS}}}\left[\frac{d_A + 2}{4C_A^3}\beta_{\mathrm{E4}}^{\overline{\mathrm{MS}}} + \frac{2d_A - 1}{4C_A^4}\beta_{\mathrm{E5}}^{\overline{\mathrm{MS}}}\right], \tag{8}$$

where β_{M} can be found in Ref. [32], and a numerical estimate of β_{G} in Ref. [17].

Let us stress that the formulae presented apply independently of whether quark masses are included or not: all quark mass effects can be incorporated in the perturbative functions $\alpha_{\mathrm{E1}}^{\overline{\mathrm{MS}}}...\alpha_{\mathrm{E7}}^{\overline{\mathrm{MS}}}$, $\beta_{\mathrm{E1}}^{\overline{\mathrm{MS}}}...\beta_{\mathrm{E5}}^{\overline{\mathrm{MS}}}$. In particular, the non-perturbative numerical value β_{G} and the contribution from the Debye scale β_{M} in Eq. (8) are "universal".

In the following, we refer to the various orders of the weak-coupling expansion according to the power of $\hat{g}_3, \hat{m}_3$ that appear, with the rule $\mathcal{O}(\hat{m}_3) = \mathcal{O}(\hat{g}_3) = \mathcal{O}(g)$. In other words, "$\mathcal{O}(g^n)$" denotes $\mathcal{O}(\hat{g}_3^{n-k}\hat{m}_3^k)$ in the expression constituted by Eqs. (4), (5), (7). If $\hat{g}_3^2, \hat{m}_3^2$ were to be re-expanded in terms of g^2, the result of Ref. [13] would be reproduced up to $\mathcal{O}(g^6)$. In practice, however, it is advisable to keep the result in an unexpanded form, because this makes it more manageable, and because the unexpanded form introduces resummations of higher order contributions.

III. QUARK MASS THRESHOLDS IN THE PRESSURE

In the absence of an explicit $\mathcal{O}(g^6\ln(1/g))$-computation with $m_i \neq 0$, one can envisage various recipes for estimating the change that quark masses cause on the $N_{\mathrm{f}} = 0$ result. For instance, one could multiply the $N_{\mathrm{f}} = 0$ result with the change indicated by the Stefan-Boltzmann law, i.e. by $\alpha_{\mathrm{E1}}^{\overline{\mathrm{MS}}}(N_{\mathrm{f}})/\alpha_{\mathrm{E1}}^{\overline{\mathrm{MS}}}(0)$ [2]. An alternative would be to define an effective non-integer N_{f} by evaluating the massive $\alpha_{\mathrm{E1}}^{\overline{\mathrm{MS}}}$ (Eq. (11) below), fitting it to the massless formula (Eq. (A.1) in Ref. [13]), and using the resulting N_{f} in the massless result of $\mathcal{O}(g^6\ln(1/g))$ [33]. What we propose here is an improvement of the first of these alternatives: we determine the functions $\alpha_{\mathrm{E1}}^{\overline{\mathrm{MS}}}, \alpha_{\mathrm{E2}}^{\overline{\mathrm{MS}}}, \alpha_{\mathrm{E7}}^{\overline{\mathrm{MS}}}$ in the general massive case, which allows us to evaluate the order $\mathcal{O}(g^2)$ result for the pressure, viz.

$$\frac{p_{\mathrm{QCD}}}{T^4} \approx \alpha_{\mathrm{E1}}^{\overline{\mathrm{MS}}} + \hat{g}_3^2\alpha_{\mathrm{E2}}^{\overline{\mathrm{MS}}}. \tag{9}$$

Afterwards, we may modify the $N_{\mathrm{f}} = 0$ result with a "correction factor",

$$\frac{[\alpha_{\mathrm{E1}}^{\overline{\mathrm{MS}}} + \hat{g}_3^2\alpha_{\mathrm{E2}}^{\overline{\mathrm{MS}}}](N_{\mathrm{f}})}{[\alpha_{\mathrm{E1}}^{\overline{\mathrm{MS}}} + \hat{g}_3^2\alpha_{\mathrm{E2}}^{\overline{\mathrm{MS}}}](0)}. \tag{10}$$

Comparing the outcome of this $\mathcal{O}(g^2)$ recipe with the corresponding $\mathcal{O}(g^0)$ recipe allows to probe the convergence. Note that it is important to also determine $\alpha_{\mathrm{E7}}^{\overline{\mathrm{MS}}}$, since only this way can the renormalisation scale that appears in $\hat{g}_3^2$ be reasonably fixed (cf. Eq. (3)).

We thus proceed to compute $\alpha_{\mathrm{E1}}^{\overline{\mathrm{MS}}}, \alpha_{\mathrm{E2}}^{\overline{\mathrm{MS}}}, \alpha_{\mathrm{E7}}^{\overline{\mathrm{MS}}}$. We do this in full generality, keeping $N_{\mathrm{f}}, N_{\mathrm{c}}$, the quark masses m_i, and the chemical potentials μ_i as free parameters. The quark masses and the strong gauge coupling are renormalised
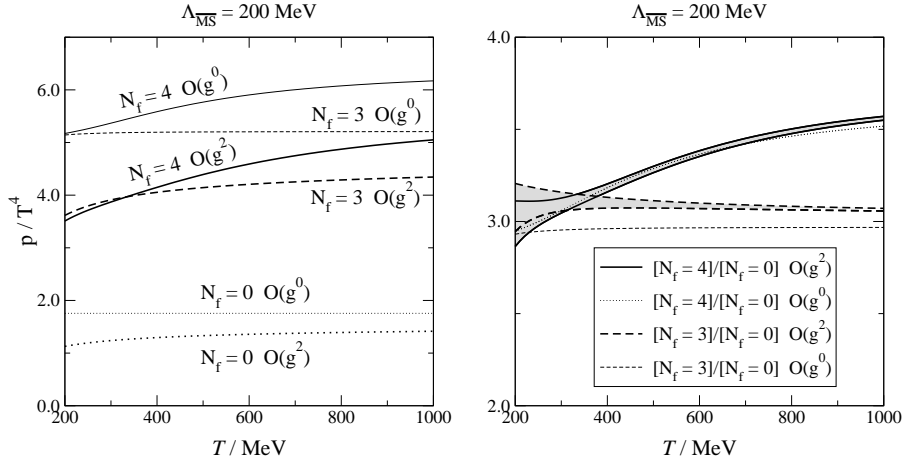
FIG. 1: Left: the pressure for $N_{\mathrm{f}} = 0, 3, 4$, at $\mathcal{O}(g^0)$ and $\mathcal{O}(g^2)$. Right: the "correction factors" accounting for the effects of quarks, at $\mathcal{O}(g^0)$ and $\mathcal{O}(g^2)$ (cf. Eq. (10)). They grey bands indicate the effect of $\overline{\mathrm{MS}}$ scheme scale variations by a factor $0.5 \dots 2.0$ around the "optimal" value. It is observed that while the $\mathcal{O}(g^2)$ corrections are of order 20...30% in the pressure, they are of order 10% in the correction factors for $N_{\mathrm{f}} = 3$, and even less for the physical case $N_{\mathrm{f}} = 4$.

in the $\overline{\mathrm{MS}}$ scheme. Some details concerning the computation are collected in Appendix A. As final results, we obtain

$$\alpha_{\mathrm{E1}}^{\overline{\mathrm{MS}}} = d_A \frac{\pi^2}{45} + 4C_A \sum_{i=1}^{N_{\mathrm{f}}} F_1\left(\frac{m_i^2}{T^2}, \frac{\mu_i}{T}\right) , \tag{11}$$

$$\alpha_{\mathrm{E2}}^{\overline{\mathrm{MS}}} = -\frac{d_A C_A}{144} - d_A \sum_{i=1}^{N_{\mathrm{f}}} \left\{ \frac{1}{6} F_2\left(\frac{m_i^2}{T^2}, \frac{\mu_i}{T}\right)\left[1 + 6F_2\left(\frac{m_i^2}{T^2}, \frac{\mu_i}{T}\right)\right] + \right.$$

$$\left. + \frac{m_i^2}{4\pi^2 T^2}\left(3\ln\frac{\bar{\mu}}{m_i} + 2\right)F_2\left(\frac{m_i^2}{T^2}, \frac{\mu_i}{T}\right) - \frac{2m_i^2}{T^2}F_4\left(\frac{m_i^2}{T^2}, \frac{\mu_i}{T}\right)\right\} , \tag{12}$$

$$\alpha_{\mathrm{E7}}^{\overline{\mathrm{MS}}} = \frac{22C_A}{3}\left[\ln\left(\frac{\bar{\mu}e^{\gamma_E}}{4\pi T}\right) + \frac{1}{22}\right] - \frac{2}{3}\sum_{i=1}^{N_{\mathrm{f}}}\left[2\ln\frac{\bar{\mu}}{m_i} + F_3\left(\frac{m_i^2}{T^2}, \frac{\mu_i}{T}\right)\right] , \tag{13}$$

where the functions $F_1, ..., F_4$ and some of their properties are detailed in Appendix B.

To estimate the numerical importance of the $\mathcal{O}(g^2)$ corrections, we need to assign a value to all the parameters that appear. Following a simple-minded logic, we use 1-loop running,

$$g^2(\bar{\mu}) = \frac{24\pi^2}{(11C_A - 4T_F)\ln(\bar{\mu}/\Lambda_{\overline{\mathrm{MS}}})} , \quad m_i(\bar{\mu}) = m_i(\bar{\mu}_{\mathrm{ref}})\left[\frac{\ln(\bar{\mu}_{\mathrm{ref}}/\Lambda_{\overline{\mathrm{MS}}})}{\ln(\bar{\mu}/\Lambda_{\overline{\mathrm{MS}}})}\right]^{\frac{9C_F}{11C_A - 4T_F}} , \tag{14}$$

where $T_F = N_{\mathrm{f}}/2$, $C_F = (N_c^2 - 1)/2N_c$, $\bar{\mu}_{\mathrm{ref}} \equiv 2$ GeV. The quark masses at $\bar{\mu} = \bar{\mu}_{\mathrm{ref}}$ are taken from Ref. [34]. To choose $\bar{\mu}$, we apply the principle of minimal sensitivity criterion for the parameter $\hat{g}_3^2$, as suggested in Ref. [35]. Furthermore, for illustration, we set $\Lambda_{\overline{\mathrm{MS}}} \equiv 200$ MeV.

The outcome of this procedure is shown in Fig. 1, for $\mu_i = 0$. It is observed that while the $\mathcal{O}(g^2)$ corrections are of order 20...30% in the pressure (left panel), the "correction factors", i.e. the ratios in Eq. (10), only contain $\mathcal{O}(g^2)$ corrections of order 10% for $N_{\mathrm{f}} = 3$, and even less for the physical case $N_{\mathrm{f}} = 4$ (right panel). This implies that the quark mass dependence of the pressure probably converges faster than the weak-coupling expansion as a whole.

Finally, we note from Fig. 1(right) that the charm quark contribution starts to be visible already at fairly low temperatures. At leading order, the quark mass dependence is determined by the function F_1 (cf. Eq. (11)), which at low temperatures has the familiar classical form

$$F_1\left(\frac{m^2}{T^2}, 0\right) \approx \left(\frac{m}{2\pi T}\right)^{\frac{3}{2}} \exp\left(-\frac{m}{T}\right) . \tag{15}$$

It is observed that F_1 obtains 5% of its asymptotic value $7\pi^2/720$ at temperatures as low as $T \approx m/5$. (For the precise numerical values of F_1, see Fig. 5.) As Fig. 1(right) shows, the onset of a visible charm mass dependence is postponed to about $T \sim 350$ MeV at $\mathcal{O}(g^2)$, but the basic pattern remains unchanged.
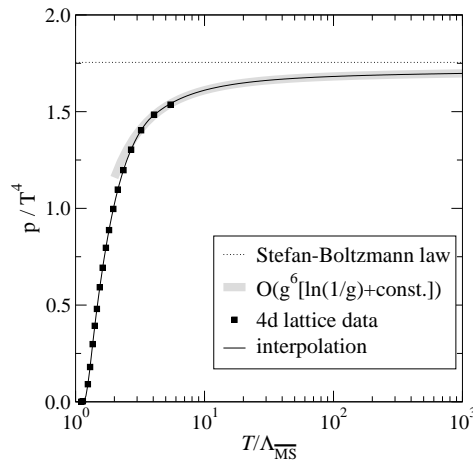
FIG. 2: A phenomenological interpolating curve (solid line) for the QCD pressure at $N_{\rm f} = 0$. In the perturbative curve (grey band) the unknown $\mathcal{O}(g^6)$ constant has been adjusted so that lattice data (closed squares [38]) is matched, once $T > 3.6\Lambda_{\overline{\rm MS}}$.

IV. PHENOMENOLOGICAL RESULTS FOR QCD

We now move from fairly well-defined expressions towards phenomenology. The goal is to present, where possible, an educated numerical guess for the physical QCD pressure. We set all chemical potentials to zero in the following.

The general philosophy we adopt is that, for temperatures above the deconfinement transition, the weak-coupling expansion needs to be evaluated up to the order where the dominant contributions from all the different scales $(2\pi T,\ gT,\ g^2T)$ have made their entrances. There is some support for such a recipe from a number of non-trivial observables [36, 37]. In practice, this means that the QCD pressure would need to be evaluated up to $\mathcal{O}(g^6)$.

Unfortunately, only some of the $\mathcal{O}(g^6)$ terms (parametrised by $\beta_{\rm M}, \beta_{\rm G}, \beta_{\rm Ei}^{\overline{\rm MS}}$ in Sec. II) are known at present. This introduces a certain unknown "constant" into the prediction. We propose to fix the constant by the following recipe.

Let us start by considering the case $N_{\rm f} = 0$, $N_{\rm c} = 3$. Then the expressions in Sec. II depend on only two parameters: on $\bar\mu/T$ (through $\alpha_{\rm E1}^{\overline{\rm MS}}...\alpha_{\rm E7}^{\overline{\rm MS}}$, $\beta_{\rm E1}^{\overline{\rm MS}}...\beta_{\rm E5}^{\overline{\rm MS}}$), and on $\bar\mu/\Lambda_{\overline{\rm MS}}$ (through $g^2(\bar\mu)$). It so happens that the dependence on $\bar\mu$, which formally cancels up to the order of the computation, is numerically non-monotonous (see, e.g., Ref. [23]), so that the specific choice is not terribly important, as long as we are close to the extremum. In practice we choose $\bar\mu/T$ according to the principle of minimal sensitivity criterion for the parameter $\hat g_3^2$, as already mentioned. Thereby the results only depend on $T/\Lambda_{\overline{\rm MS}}$ and on the unknown $\mathcal{O}(g^6)$ terms, contained in $\Delta_{\rm hard}$ and $\Delta_{\rm soft}$, defined in Eqs. (5), (7). It is important to note that once $\bar\mu/T$ has been fixed, the Δ's can be treated as temperature-independent constants. It is furthermore convenient to combine them into a single term [55],

$$\Delta_{\rm hard} + d_A C_A^3 \Delta_{\rm soft} \equiv d_A C_A^3 \Delta \ . \tag{16}$$

In order to now eliminate the dependence on Δ, we "match" the perturbative prediction to 4d lattice simulation results for the case $N_{\rm f} = 0$, where the continuum limit has been reached with reasonable precision [38, 39]. It should be stressed that this step is purely phenomenological: in principle Δ is computable from the theory. On the other hand, there is every reason to expect that results obtained through the dimensionally reduced framework do match 4d lattice results as soon as $T \gtrsim 2T_{\rm c}$, where $T_{\rm c}$ is the temperature of the deconfinement phase transition (see, e.g., Refs. [36], [40]–[42]). Moreover, that a family of functions specified by a single parameter should match a given function for a whole range of argument values, provides for a non-trivial consistency check.

Now, lattice results are usually presented in terms of $T/T_{\rm c}$, rather than $T/\Lambda_{\overline{\rm MS}}$. We thus need a value for $T_{\rm c}/\Lambda_{\overline{\rm MS}}$; we use $T_{\rm c}/\Lambda_{\overline{\rm MS}} \approx 1.20$ which appears to be consistent with all independent determinations (cf. Ref. [37], Sec. 4.2). After this choice, an excellent match can be obtained (we do this by minimising the difference squared of the function values in the range $T > 3T_{\rm c}$), with a value $\Delta \approx -3.287$ (cf. Fig. 2). In the following we will take the cubic spline interpolation shown in Fig. 2 as the "starting point", which will then be "corrected" by the effects of quarks.

To now include quarks, we simply multiply the result just obtained by the correction factor in Eq. (10). We should expect this construction to work the better the higher the temperature, but surely at least $T > 200$ MeV is required.

It needs to be noted, however, that like in Fig. 1, the evaluation of the correction factor necessitates fixing $\Lambda_{\overline{\rm MS}}$ in physical units. This exercise is non-trivial. We again choose a purely phenomenological but rather convenient procedure, which makes use of the pressure produced by the full set of hadronic resonances [34]. Indeed, it has been demonstrated recently that if the resonance masses are tuned to correspond to the quark masses accessible to current
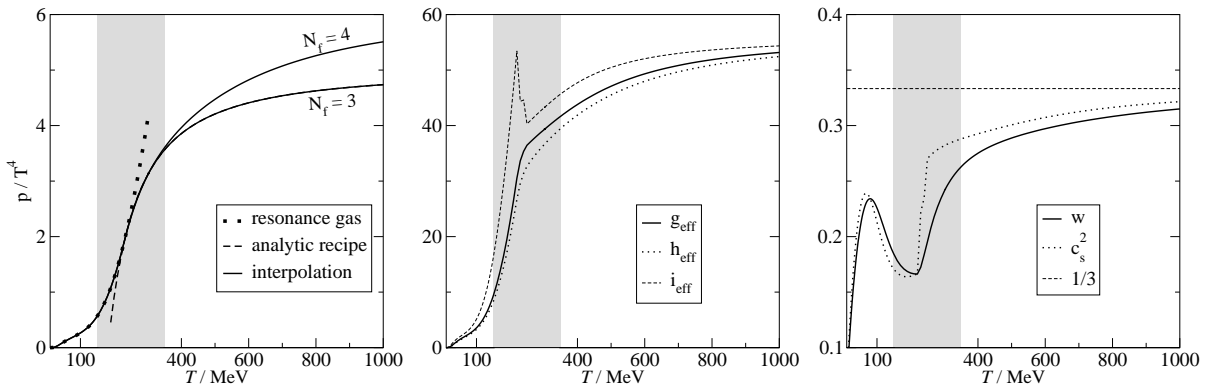
FIG. 3: Left: Phenomenological interpolating curves (solid lines) for the QCD pressure at $N_{\rm f} = 3, 4$. The shaded interval corresponds to the transition region where the results can be reliably determined with lattice simulations only. Middle: $g_{\rm eff}, h_{\rm eff}, i_{\rm eff}$ as defined in Eq. (17), for $N_{\rm f} = 4$. Right: the equation-of-state parameter w and the speed of sound squared c_s^2, for the same system.

lattice simulations, the resulting "resonance gas pressure" works surprisingly well even for temperatures deep into the crossover region [43].

Thus, we tune $\Lambda_{\overline{\rm MS}}$ such that our analytic recipe and the first derivative thereof match the resonance gas result (in which the temperature is automatically measured in physical units) at a certain temperature. Examples are shown in Fig. 3(left). The values of $\Lambda_{\overline{\rm MS}}$ that result depend slightly on $N_{\rm f}$ and on variations of quark masses within their experimental errors, but the typical range is $\Lambda_{\overline{\rm MS}} \approx 175...180$ MeV. We should stress that this matching is of course rather arbitrary, but it does produce qualitatively reasonable results with, for instance, an inflection point on the side $T > T_{\rm c} \sim 175$ MeV, as suggested by lattice results [44]–[47].

Naturally, the resonance gas results cannot really be trusted in quantitative detail for temperatures above, say, 150 MeV. Therefore, for a certain interval (which we choose to be $T = 150...350$ MeV, and shade in all figures), the results remain to be established by lattice simulations. The matter becomes even more urgent, when one considers derivatives of the pressure, to which we now turn.

Apart from the pressure, its first and second derivatives play an important role, as already mentioned in connection with Eq. (1). There are various ways of presenting the information contained in these derivatives: we may for instance parametrise the physical observables $e(T)$, $s(T)$, $c(T)$ through effective numbers of bosonic degrees of freedom,

$$g_{\rm eff}(T) \equiv \frac{e(T)}{\left[\frac{\pi^2 T^4}{30}\right]} , \quad h_{\rm eff}(T) \equiv \frac{s(T)}{\left[\frac{2\pi^2 T^3}{45}\right]} , \quad i_{\rm eff}(T) \equiv \frac{c(T)}{\left[\frac{2\pi^2 T^3}{15}\right]} , \tag{17}$$

in terms of which Eq. (1) becomes

$$\frac{3}{2}\sqrt{\frac{5}{\pi^3}}\frac{m_{\rm Pl}}{T^3}\frac{{\rm d}T}{{\rm d}t} = -\frac{\sqrt{g_{\rm eff}(T)}\,h_{\rm eff}(T)}{i_{\rm eff}(T)} , \tag{18}$$

or we can consider dimensionless ratios like

$$w(T) \equiv \frac{p(T)}{e(T)} = \frac{p(T)}{Tp'(T) - p(T)} , \tag{19}$$

$$c_s^2(T) \equiv \frac{p'(T)}{e'(T)} = \frac{p'(T)}{Tp''(T)} = \frac{s(T)}{c(T)} . \tag{20}$$

Both the "equation-of-state" $w(T)$ and the sound speed squared $c_s^2(T)$ equal 1/3 in the non-interacting limit. The deviation of the parameter $w(T)$ from 1/3 is proportional to the trace anomaly, sometimes also called the interaction measure.

Results for all of these quantities, based on our interpolation, are shown in Fig. 3(middle, right). It can be seen that quantities involving derivatives show a significant amount of structure around the QCD crossover, even if there were no singularities. We remark that to smooth the behaviour we have evaluated $p(T, \boldsymbol{\mu})$ with a relatively sparse temperature grid in the critical region.

Clearly, it is important to correct the results in the "shaded region" by using results from future lattice simulations of the type in Refs. [44]–[47]. In particular, the recent Refs. [46, 47] display direct results for c_s^2 and w, respectively.

Unfortunately, it does not appear that these results would be useful for our present purposes: they for instance fail to reproduce the significant rise in w and c_s^2 that is seen in Fig. 3(right) at temperatures down from the critical one, displaying rather a much deeper dip (down to ~ 0.1) around the critical region, and then rising at most slightly as the temperature is lowered. Therefore, it could be feared that the dip itself is affected by the unphysically heavy quark masses that are used in the simulations.

We finally comment on the peak visible in i_{eff} in Fig. 3(middle). While the details are of course not captured by our phenomenological recipe, the fact that a peak exists in the heat capacity is not unexpected for rapid crossovers; in second order phase transition, the heat capacity even diverges as $T \to T_c$.

V. PHENOMENOLOGICAL RESULTS FOR THE STANDARD MODEL

While in heavy ion collisions at most strongly interacting particles have time to thermalise, the expansion rate is much smaller in cosmology, so that all Standard Model degrees of freedom do reach thermal equilibrium, and remain thermalised until neutrino decoupling at around $T \sim \text{MeV}$. Therefore, their contributions need to be added to the QCD pressure. In practice, we count gluons and the four lightest quarks as the QCD degrees of freedom, while the bottom and top quark are treated as part of the "weakly interacting" sector, so that the result splits into a sum of two terms.

We will assume that it is sufficient to treat the weakly interacting sector at 1-loop level. That is, we construct the free energy density f in the presence of a Higgs expectation value v, temperature T, and chemical potentials μ_i, according to

$$f(v, T, \boldsymbol{\mu}) = -\frac{1}{2} \nu^2(\bar{\mu}) v^2 + \frac{1}{4} \lambda(\bar{\mu}) v^4 + \sum_i \sigma_i \mathcal{J}_i(m_i(v), T, \mu_i) \,, \tag{21}$$

where the sum extends over all physical degrees of freedom, with their proper degeneracies; $\sigma_i = +1$ (-1) for bosons (fermions); and the tree-level masses $m_i(v)$ depend on v in the standard way (it is sufficient at this order to work in unitary gauge). For scalar ($\mathcal{J}_s$), vectors ($\mathcal{J}_v$) and fermions ($\mathcal{J}_f$),

$$\mathcal{J}_s = -\frac{m^4}{64\pi^2} \left(\ln \frac{\bar{\mu}^2}{m^2} + \frac{3}{2} \right) + \frac{T^4}{4\pi^2} \int_0^\infty \mathrm{d}x\, x^{\frac{1}{2}} \ln \left(1 - e^{-\sqrt{x+y}} \right)_{y=\frac{m^2}{T^2}} \,, \tag{22}$$

$$\mathcal{J}_v = -\frac{m^4}{64\pi^2} \left(\ln \frac{\bar{\mu}^2}{m^2} + \frac{5}{6} \right) + \frac{T^4}{4\pi^2} \int_0^\infty \mathrm{d}x\, x^{\frac{1}{2}} \ln \left(1 - e^{-\sqrt{x+y}} \right)_{y=\frac{m^2}{T^2}} \,, \tag{23}$$

$$\mathcal{J}_f = -\frac{m^4}{64\pi^2} \left(\ln \frac{\bar{\mu}^2}{m^2} + \frac{3}{2} \right) + T^4 F_1 \left(\frac{m^2}{T^2}, \frac{\mu}{T} \right) \,. \tag{24}$$

The renormalised pressure is then given by

$$p(T, \boldsymbol{\mu}) = \min_v f(v, 0, \mathbf{0}) - \min_v f(v, T, \boldsymbol{\mu}) \,. \tag{25}$$

The renormalised pressure depends on a number of parameters defined in the $\overline{\text{MS}}$ scheme: the Higgs potential parameters $\nu^2(\bar{\mu})$, $\lambda(\bar{\mu})$ (cf. Eq. (21)); and the weak gauge and the top and bottom Yukawa couplings $g_w^2(\bar{\mu})$, $h_t^2(\bar{\mu})$, $h_b^2(\bar{\mu})$ (through the tree-level masses). The first four of these we express through the Fermi constant and the $W^\pm$, Higgs, and top pole masses, employing the explicit relations listed in Ref. [30], while the last one is fixed through the bottom mass in the $\overline{\text{MS}}$ scheme [34]. Given that the electroweak theory contains a multitude of scales, both zero temperature and thermal, we simply choose a fixed $\bar{\mu} = 100$ GeV for the weakly interacting part of the pressure (we have varied the scale by a factor 0.5 ... 2.0, and seen that the dependence is invisible on our resolution).

Let us remark that Eq. (25) suffers from the problem that it leads to a first order electroweak phase transition at a certain temperature, while there is none if the theory is treated more carefully [48, 49]. In practice this does not lead to any serious complications, however: we again smooth the behaviour by evaluating $p(T, \boldsymbol{\mu})$ with a sparse temperature grid around the critical region. In our figures, we shade the corresponding temperature interval, where our estimates are qualitative at best.

With these reservations, the whole Standard Model pressure, and the parameters defined in Eqs. (17), (19), (20), are shown in Fig. 4.

At temperatures above the electroweak scale, our results are already very close to the ideal gas results. Recently, higher loop corrections in this region have been considered in some detail [22]. The authors find a rather more significant deviation from the ideal gas value, due for instance to the top Yukawa coupling. We have not implemented these corrections, however, since they would require a correspondingly higher order computation in the broken symmetry
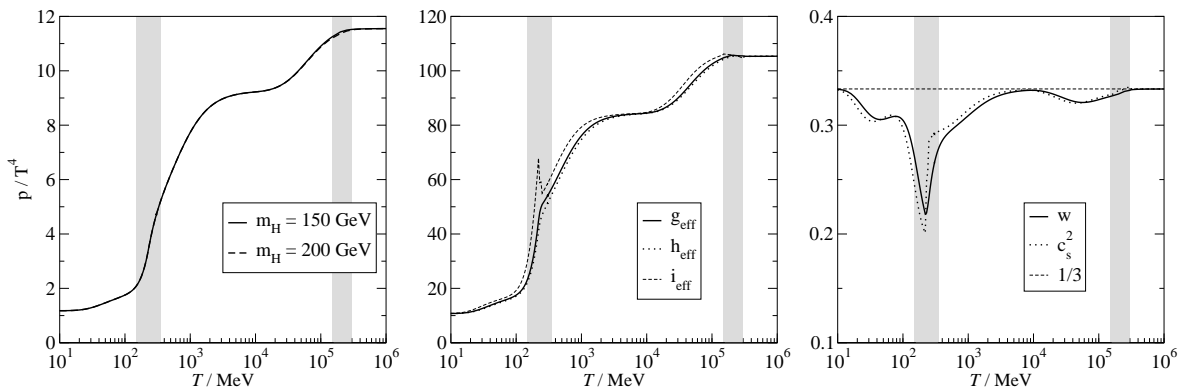
FIG. 4: Left: The Standard Model pressure for $m_H = 150$ GeV, 200 GeV. The shaded intervals correspond to the QCD and electroweak transition regions. Middle: $g_{\text{eff}}, h_{\text{eff}}, i_{\text{eff}}$ as defined in Eq. (17), for $m_H = 150$ GeV. Right: the equation-of-state parameter w and the speed of sound squared c_s^2, for the same system. Various sources of uncertainties are discussed in the text.

phase. Though such a computation exists in principle up to 2-loop level [50], we did not consider the non-trivial challenges posed by its numerical evaluation for general masses to be worth tackling at present, given that in the quantities plotted in Fig. 4(right), the 2-loop contributions (which do not contribute to the trace anomaly on the symmetric phase side) are expected to largely cancel out. Nevertheless, it would be important to finalise this computation, if physics is made with the temperature interval $T = 10...100$ GeV, where the $W^{\pm}, Z^0$ bosons and top quark cross their mass thresholds.

Finally, once a definite Higgs model is available, it will of course be important to carry out lattice simulations for the transition region. Fortunately, for the electroweak theory this can be achieved within the dimensionally reduced effective theory [30], whereby also all fermions with their physical Yukawa couplings can be fully accounted for.

VI. CONCLUSIONS

The functional dependence of the QCD pressure at a high temperature T on most of the parameters of the theory (number of colours N_c, number of active massless flavours N_f, and quark chemical potentials μ_i) is known up to relative order $\mathcal{O}(g^6 \ln(1/g))$, while the dependence on the quark masses m_i has gained much less interest. The purpose of this note has been to study whether it indeed is justified to consider the effects of finite non-zero quark masses at the level of the non-interacting Stefan-Boltzmann law (i.e. $\mathcal{O}(g^0)$), as has been the standard procedure. For this purpose, we have determined the corrections of order $\mathcal{O}(g^2)$ in full generality in the $\overline{\text{MS}}$ scheme, and presented a numerical evaluation of all the integrals that appear in this result.

We find that while the $\mathcal{O}(g^2)$ corrections are in general 20...30% (Fig. 1(left)), they are numerically at most 10% for the quark mass dependence (Fig. 1(right)). This is perhaps in accord with previous observations according to which quarks are fairly perturbative as soon as they are deconfined, even though gluons do display strong interactions up to very high temperatures.

Finally, we have sketched educated "guesses" for the thermodynamic quantities that play a role in various physical contexts, for temperatures between the QCD and electroweak scales. For the case of heavy ion collisions, in particular, it is perhaps relevant to keep in mind that if the charm quark does thermalise, it has a rather significant effect even at relatively low temperatures (Fig. 3(left)). Of course, it is by no means clear whether such a thermalization should take place in practice [51].

In order to improve on our QCD results, the missing perturbative $\mathcal{O}(g^6)$ computations and, naturally, lattice simulations in the transition region, with physical values of the quark masses, remain to be completed.

For the full Standard Model, we have presented similar guesses for the various quantities that are relevant for expansion rate and particle decoupling computations (Figs. 4). Although the deviations from previous phenomenological estimates that have appeared in the literature [1, 2] are in general fairly small, we nevertheless hope that our results help for their part to gauge the systematic uncertainties that still exist in these quantities.

In particular, we have stressed the need for repeating the computations of Ref. [22] in the broken symmetry phase and, of course, the need for effective theory lattice simulations in the transition region, once the electroweak model / Higgs mass is known.

APPENDIX A: OUTLINE OF THE COMPUTATION

In this Appendix we present a few details for the computation leading to Eqs. (11)–(13). We concentrate on the fermionic contributions; the bosonic ones are elementary.

We write the fermionic contributions in terms of the renormalised gauge coupling g^2 and the renormalised quark masses m_i, $i = 1, ..., N_{\rm f}$. The master integrals emerging are

$$I_{\rm b} \equiv \sumint_{P_{\rm b}} \frac{1}{P_{\rm b}^2} \,, \tag{A1}$$

$$J_{\rm f}(m,\mu) \equiv \frac{1}{2} \sumint_{P_{\rm f}} \ln(\tilde{P}_{\rm f}^2 + m^2) \,, \tag{A2}$$

$$I_{\rm f}(m,\mu) \equiv \sumint_{P_{\rm f}} \frac{1}{\tilde{P}_{\rm f}^2 + m^2} \,, \tag{A3}$$

$$H_{\rm f}(m,\mu) \equiv \sumint_{P_{\rm f},Q_{\rm f}} \frac{1}{(\tilde{P}_{\rm f}^2 + m^2)(\tilde{Q}_{\rm f}^2 + m^2)(\tilde{P}_{\rm f} - \tilde{Q}_{\rm f})^2} \,, \tag{A4}$$

where $P_{\rm b}$, $P_{\rm f}$ denote bosonic and fermionic Matsubara four-momenta, respectively, and $\tilde{P}_{\rm f} \equiv P_{\rm f} + (-i\mu, \mathbf{0})$ includes the chemical potential μ. With this notation, the fermionic contributions to the parameters of interest are

$$T^4 \alpha_{\rm E1}^{\rm f} = 4 C_A \sum_{i=1}^{N_{\rm f}} J_{\rm f}(m_i, \mu_i) \,, \tag{A5}$$

$$T^4 \alpha_{\rm E2}^{\rm f} = 2 C_A \hat{\delta}_1 m^2 \sum_{i=1}^{N_{\rm f}} m_i^2 I_{\rm f}(m_i, \mu_i) +$$
$$+ d_A \sum_{i=1}^{N_{\rm f}} \left\{ \frac{d-1}{2} \left[2I_{\rm b} - I_{\rm f}(m_i, \mu_i) \right] I_{\rm f}(m_i, \mu_i) + 2m_i^2 H_{\rm f}(m_i, \mu_i) \right\} \,, \tag{A6}$$

$$\frac{1}{(4\pi)^2} \alpha_{\rm E7}^{\rm f} = \hat{\delta}_1 g^2 + \frac{2}{3} \sum_{i=1}^{N_{\rm f}} \frac{dI_{\rm f}(m_i, \mu_i)}{dm_i^2} \,, \tag{A7}$$

where $\hat{\delta}_1 m^2$, $\hat{\delta}_1 g^2$ are counterterms defined by writing the bare mass parameter and gauge coupling as $m_{Bi}^2 = m_i^2(1 + g^2\hat{\delta}_1 m^2)$, $g_B^2 = g^2(1 + g^2\hat{\delta}_1 g^2)$; it is understood that only the fermionic part of $\hat{\delta}_1 g^2$ is considered; and $d \equiv 3 - 2\epsilon$.

The next step is the evaluation of the Matsubara sums appearing in the master integrals. For the 1-loop structures (Eqs. (A1)–(A3)), it is straightforward to obtain

$$I_{\rm b} = \int \frac{d^d\mathbf{p}}{(2\pi)^d} \frac{1}{2|\mathbf{p}|} \left[1 + 2n_{\rm B}(|\mathbf{p}|) \right] \,, \tag{A8}$$

$$J_{\rm f}(m,\mu) = \int \frac{d^d\mathbf{p}}{(2\pi)^d} \frac{-\mathbf{p}^2}{2dE} \left[1 - n_{\rm F}(E - \mu) - n_{\rm F}(E + \mu) \right]_{E=\sqrt{\mathbf{p}^2+m^2}} \,, \tag{A9}$$

$$I_{\rm f}(m,\mu) = \int \frac{d^d\mathbf{p}}{(2\pi)^d} \frac{1}{2E} \left[1 - n_{\rm F}(E - \mu) - n_{\rm F}(E + \mu) \right]_{E=\sqrt{\mathbf{p}^2+m^2}} \,, \tag{A10}$$

where we have carried out a partial integration after the sum in $J_{\rm f}$, and

$$n_{\rm B}(E) \equiv \frac{1}{e^{\beta E} - 1} \,, \quad n_{\rm F}(E) \equiv \frac{1}{e^{\beta E} + 1} \,. \tag{A11}$$

As is well known, the momentum integral in Eq. (A8) can be carried out explicitly, $I_{\rm b} = \pi^{d/2}T^d\Gamma(1-d/2)\zeta(2-d)/2\pi^2T$, but the ones in Eqs. (A9), (A10) with $m, \mu \neq 0$ cannot in general be integrated in closed form.

For the genuine 2-loop integral H_f in Eq. (A4) the sums are slightly more complicated, so we give here some details. The method we employ follows the standard procedure [9] (see also Refs. [52, 53]). The twofold sum over the Matsubara modes is first written as a threefold sum with a Kronecker delta-function, and the delta-function is then written as $\delta(p_0) = T \int_0^\beta \text{d}x \, \exp(ip_0 x)$. The sums can now be performed:

$$T \sum_{p_\text{b}} \frac{e^{ip_\text{b}x}}{p_\text{b}^2 + E^2} = \frac{1}{2E} n_\text{B}(E)\Big[e^{(\beta-x)E} + e^{xE} \Big] , \tag{A12}$$

$$T \sum_{p_\text{f}} \frac{e^{i\tilde{p}_\text{f}x}}{\tilde{p}_\text{f}^2 + E^2} = \frac{1}{2E} \Big[n_\text{F}(E+\mu)e^{(\beta-x)E+\beta\mu} - n_\text{F}(E-\mu)e^{xE} \Big] , \tag{A13}$$

where p_b, p_f denote the bosonic and fermionic Matsubara frequencies, respectively; and $\tilde{p}_\text{f} = p_\text{f} - i\mu$. The integral over x is then simple. All the exponents appearing can be written in terms of inverses of the distribution functions n_B, n_F, and multiplying with their explicit appearances, we are left with at most quadratic products of the distribution functions, and fractions containing the three "energies".

The fractions containing the energies can be organized in a transparent form, once we introduce the zero-temperature objects

$$H_\text{vac}(m_1^2, m_2^2, m_3^2) = \int \frac{\text{d}^{4-2\epsilon}P}{(2\pi)^{4-2\epsilon}} \int \frac{\text{d}^{4-2\epsilon}Q}{(2\pi)^{4-2\epsilon}} \frac{1}{[P^2 + m_1^2][Q^2 + m_2^2][(P-Q)^2 + m_3^2]} , \tag{A14}$$

$$\Pi(Q^2; m_1^2, m_2^2) = \int \frac{\text{d}^{4-2\epsilon}P}{(2\pi)^{4-2\epsilon}} \frac{1}{[P^2 + m_1^2][(P-Q)^2 + m_2^2]} , \tag{A15}$$

$$\Delta(Q^2; m_3^2) = \frac{1}{Q^2 + m_3^2} . \tag{A16}$$

Indeed, carrying out the integrals over P_0, Q_0 in these functions, one obtains similar energy fractions. Making furthermore use of the $O(4-2\epsilon)$ rotational invariance of the Q-dependence in Eq. (A15), which is present once also the integration over $\mathbf{p}$ is performed, the various fractions can be identified with each other.

In order to write the subsequent result in a compact but generic form, we introduce the notation

$$E_i \equiv \sqrt{\mathbf{p}_i^2 + m_i^2} , \quad P_i \equiv (E_i, \mathbf{p}_i) , \quad P_i \cdot P_j \equiv E_i E_j - \mathbf{p}_i \cdot \mathbf{p}_j , \tag{A17}$$

and denote

$$n_\pm(E_i) \equiv \begin{cases} n_\text{B}(E_i) & \text{for bosons } (\equiv E_3) \\ -n_\text{F}(E_i \pm \mu) & \text{for fermions } (\equiv E_1, E_2) \end{cases} . \tag{A18}$$

Then, allowing for generality for three different masses, like in Eq. (A14),

$$\begin{aligned} H_\text{f} = {}& H_\text{vac}(m_1^2, m_2^2, m_3^2) + \\ & + \sum_{i\neq j\neq k} \sum_{\sigma=\pm 1} \int \frac{\text{d}^d\mathbf{p}_i}{(2\pi)^d} \frac{n_\sigma(E_i)}{2E_i} \Pi(-m_i^2; m_j^2, m_k^2) + \\ & + \sum_{i\neq j\neq k} \sum_{\sigma,\tau=\pm 1} \int \frac{\text{d}^d\mathbf{p}_i}{(2\pi)^d} \int \frac{\text{d}^d\mathbf{p}_j}{(2\pi)^d} \frac{n_\sigma(E_i)n_\tau(E_j)}{4E_i E_j} \Delta[-(\sigma P_i - \tau P_j)^2; m_k^2] , \end{aligned} \tag{A19}$$

where $\sum_{i\neq j\neq k} \equiv \sum_{(i,j,k)=(1,2,3),(2,3,1),(3,1,2)}$. Individual terms in this sum may contain infrared poles (or, after performing some of the integrations in complex plane, imaginary parts), but the expression as a whole is finite and real for $\epsilon \neq 0$.

We return now to the case of physical interest ($m_1^2 = m_2^2 \equiv m^2; m_3^2 \equiv 0$), and ignore all temperature-independent terms. We note, furthermore, that the contribution originating from the last term in Eq. (A19) for $(i,j,k) = (3,1,2)$, contains $\Delta[-(P_3 + P_1)^2; m^2] + \Delta[-(P_3 - P_1)^2; m^2]$ which vanishes, given that $P_1^2 + P_3^2 = m^2$. The same is true for $(i,j,k) = (2,3,1)$. This leaves us with

$$H_\text{f}(m,\mu) = [\text{temperature-independent terms}] +$$

$$+ I_\text{b}\,\Pi(0; m^2, m^2) + 2I_\text{f}(m;\mu)\,\Pi(-m^2; m^2, 0) +$$

$$+ \int \frac{\mathrm{d}^d \mathbf{p}_1}{(2\pi)^d} \int \frac{\mathrm{d}^d \mathbf{p}_2}{(2\pi)^d} \frac{n_-(E_1)n_+(E_2) + n_+(E_1)n_-(E_2)}{8E_1E_2} \frac{1}{\mathbf{p}_1 \cdot \mathbf{p}_2 - m^2 - E_1E_2} +$$

$$+ \int \frac{\mathrm{d}^d \mathbf{p}_1}{(2\pi)^d} \int \frac{\mathrm{d}^d \mathbf{p}_2}{(2\pi)^d} \frac{n_-(E_1)n_-(E_2) + n_+(E_1)n_+(E_2)}{8E_1E_2} \frac{1}{\mathbf{p}_1 \cdot \mathbf{p}_2 - m^2 + E_1E_2} , \tag{A20}$$

where we substituted $\mathbf{p}_1 \to -\mathbf{p}_1$ in the last term. We can still perform the integration over $z \equiv \mathbf{p}_1 \cdot \mathbf{p}_2/|\mathbf{p}_1||\mathbf{p}_2|$, leaving a rapidly convergent integral over $|\mathbf{p}_1|$, $|\mathbf{p}_2|$.

The final step is the expansion in ϵ. The only temperature-dependent ultraviolet divergences are in the factorised terms on the second row in Eq. (A20). Adding together with the contributions from the other master integrals, as specified in Eqs. (A5)–(A7), a straightforward computation reproduces the fermionic parts of Eqs. (11)–(13).

APPENDIX B: FUNCTIONS DETERMINING THE MASS DEPENDENCE

The functions that appear in Eqs. (11)–(13) are defined as

$$F_1(y, \hat{\mu}) \equiv \frac{1}{24\pi^2} \int_0^\infty \mathrm{d}x \left[\frac{x}{x+y} \right]^{\frac{1}{2}} \left[\hat{n}_\mathrm{F}(\sqrt{x+y} - \hat{\mu}) + \hat{n}_\mathrm{F}(\sqrt{x+y} + \hat{\mu}) \right] x , \tag{B1}$$

$$F_2(y, \hat{\mu}) \equiv \frac{1}{8\pi^2} \int_0^\infty \mathrm{d}x \left[\frac{x}{x+y} \right]^{\frac{1}{2}} \left[\hat{n}_\mathrm{F}(\sqrt{x+y} - \hat{\mu}) + \hat{n}_\mathrm{F}(\sqrt{x+y} + \hat{\mu}) \right] , \tag{B2}$$

$$F_3(y, \hat{\mu}) \equiv - \int_0^\infty \mathrm{d}x \left[\frac{x}{x+y} \right]^{\frac{1}{2}} \left[\hat{n}_\mathrm{F}(\sqrt{x+y} - \hat{\mu}) + \hat{n}_\mathrm{F}(\sqrt{x+y} + \hat{\mu}) \right] \frac{1}{x} , \tag{B3}$$

$$F_4(y, \hat{\mu}) \equiv \frac{1}{(4\pi)^4} \int_0^\infty \mathrm{d}x_1 \int_0^\infty \mathrm{d}x_2 \frac{1}{\sqrt{x_1+y}\sqrt{x_2+y}} \times$$
$$\times \Bigg\{ \left[\hat{n}_\mathrm{F}(\sqrt{x_1+y} - \hat{\mu})\hat{n}_\mathrm{F}(\sqrt{x_2+y} + \hat{\mu}) + \hat{n}_\mathrm{F}(\sqrt{x_1+y} + \hat{\mu})\hat{n}_\mathrm{F}(\sqrt{x_2+y} - \hat{\mu}) \right] \times$$
$$\times \ln \left[\frac{\sqrt{x_1+y}\sqrt{x_2+y} + y - \sqrt{x_1 x_2}}{\sqrt{x_1+y}\sqrt{x_2+y} + y + \sqrt{x_1 x_2}} \right] +$$
$$+ \left[\hat{n}_\mathrm{F}(\sqrt{x_1+y} - \hat{\mu})\hat{n}_\mathrm{F}(\sqrt{x_2+y} - \hat{\mu}) + \hat{n}_\mathrm{F}(\sqrt{x_1+y} + \hat{\mu})\hat{n}_\mathrm{F}(\sqrt{x_2+y} + \hat{\mu}) \right] \times$$
$$\times \ln \left[\frac{\sqrt{x_1+y}\sqrt{x_2+y} - y + \sqrt{x_1 x_2}}{\sqrt{x_1+y}\sqrt{x_2+y} - y - \sqrt{x_1 x_2}} \right] \Bigg\} , \tag{B4}$$

where

$$\hat{n}_\mathrm{F}(x) \equiv \frac{1}{e^x + 1} . \tag{B5}$$

These functions are related to the functions J_f, I_f and H_f defined in Eqs. (A2)–(A4): the medium-modified part of J_f reads $T^4 F_1$ for $\epsilon = 0$; the medium-modified part of I_f reads $-T^2 F_2$ for $\epsilon = 0$; the medium-modified part of $\mathrm{d}I_\mathrm{f}/\mathrm{d}m^2$ reads $-F_3/(4\pi)^2$ for $\epsilon = 0$; and the "non-factorizable" part of H_f (the last two terms in Eq. (A20)) reads $T^2 F_4$ for $\epsilon = 0$. The functions F_1, F_2, F_3 are related by

$$F_2(y, \hat{\mu}) = -2\frac{\partial F_1(y, \hat{\mu})}{\partial y} , \quad F_3(y, \hat{\mu}) = (4\pi)^2 \frac{\partial F_2(y, \hat{\mu})}{\partial y} . \tag{B6}$$

The functions introduced possess some solvable limiting values. For $y \to 0$,

$$F_1(0, \hat{\mu}) = \frac{7\pi^2}{720} + \frac{\hat{\mu}^2}{24} + \frac{\hat{\mu}^4}{48\pi^2} , \tag{B7}$$

$$F_2(0, \hat{\mu}) = \frac{1}{24} + \frac{\hat{\mu}^2}{8\pi^2} , \tag{B8}$$

$$F_3(0, \hat{\mu}) \approx \ln \frac{y}{\pi^2} + 2\gamma_E + \mathcal{D}\left(\frac{\hat{\mu}}{\pi}\right) = \ln \frac{y}{16\pi^2} - \left[\psi\left(\frac{1}{2} + i\frac{\hat{\mu}}{2\pi}\right) + \psi\left(\frac{1}{2} - i\frac{\hat{\mu}}{2\pi}\right) \right] , \tag{B9}$$

where "$\approx$" denotes that the logarithmic divergence displayed on the right-hand side needs to be subtracted before setting $y \to 0$, and the function $\mathcal{D}$, which has the property $\mathcal{D}(0) = 0$, corresponds to the notation in Ref. [40].
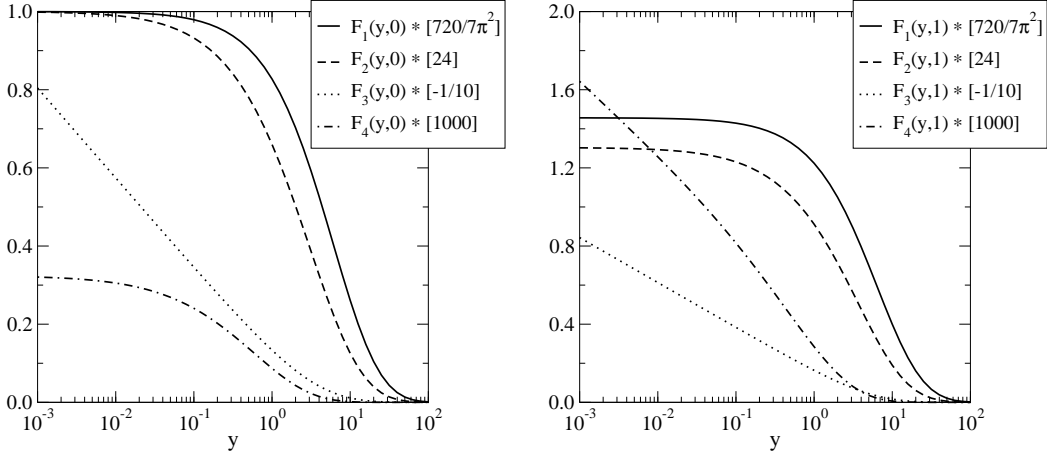
FIG. 5: The functions defined in Eqs. (B1)–(B4), for $\hat{\mu} = 0.0$ (left) and $\hat{\mu} = 1.0$ (right) (all functions are even in $\hat{\mu}$). Note that the ranges of the vertical axes are different in the two plots.

The analytic expression in terms of $\psi(z) = \Gamma'(z)/\Gamma(z)$ comes from Ref. [20]. For $\hat{\mu} \neq 0$, the function F_4 diverges logarithmically at small y, but as it is always multiplied by y, this behaviour has little interest in the present context. Inserting the values in Eqs. (B7)–(B9) into our expressions for $\alpha_{\mathrm{E1}}^{\overline{\mathrm{MS}}}$, $\alpha_{\mathrm{E2}}^{\overline{\mathrm{MS}}}$, $\alpha_{\mathrm{E7}}^{\overline{\mathrm{MS}}}$, Eqs. (3.14), (3.15), (3.20) of Ref. [20] are reproduced.

For $y \to \infty$ and $\hat{\mu}$ fixed, the functions F_1, F_2, F_3 vanish as $\exp(-\sqrt{y})$, the function F_4 as $\exp(-2\sqrt{y})$, modulo a powerlike prefactor. An interesting limit is obtained, however, by setting $y, \hat{\mu}$ simultaneously to infinity but keeping the ratio $z \equiv y/\hat{\mu}^2 = m^2/\mu^2$ fixed. This corresponds to setting the temperature to zero but keeping m, μ finite. Then

$$\lim_{T \to 0} T^4 F_1\left(\frac{m^2}{T^2}, \frac{\mu}{T}\right) = \theta(1-z)\frac{\mu^4}{96\pi^2}(2w^3 - 3zf_2) \,, \tag{B10}$$

$$\lim_{T \to 0} T^2 F_2\left(\frac{m^2}{T^2}, \frac{\mu}{T}\right) = \theta(1-z)\frac{\mu^2}{8\pi^2}f_2 \,, \tag{B11}$$

$$\lim_{T \to 0} F_3\left(\frac{m^2}{T^2}, \frac{\mu}{T}\right) = \theta(1-z)\frac{2}{z}(f_2 - w) \,, \tag{B12}$$

$$\lim_{T \to 0} T^2 F_4\left(\frac{m^2}{T^2}, \frac{\mu}{T}\right) = \theta(1-z)\frac{\mu^2}{64\pi^4 z}(w^4 - f_2^2) \,, \tag{B13}$$

where

$$w \equiv \sqrt{1-z} \,, \quad f_2 \equiv \sqrt{1-z} - z\ln\frac{1+\sqrt{1-z}}{\sqrt{z}} \,. \tag{B14}$$

Inserting into our expressions for $\alpha_{\mathrm{E1}}^{\overline{\mathrm{MS}}}$, $\alpha_{\mathrm{E2}}^{\overline{\mathrm{MS}}}$, Eqs. (1) and (4) of Ref. [26] are reproduced.

Unfortunately the limit $\hat{\mu} \to 0$, of most interest to us in this paper, does not render any of the functions analytically solvable, as far as we know. We show the results of numerical evaluations in Fig. 5.

[1] M. Srednicki, R. Watkins and K.A. Olive, Nucl. Phys. B 310 (1988) 693.

[2] M. Hindmarsh and O. Philipsen, Phys. Rev. D 71 (2005) 087302 [hep-ph/0501232].

[3] S. Dodelson and L.M. Widrow, Phys. Rev. Lett. 72 (1994) 17 [hep-ph/9303287].

[4] K.N. Abazajian and G.M. Fuller, Phys. Rev. D 66 (2002) 023526 [astro-ph/0204293]; T. Asaka, S. Blanchet and M. Shaposhnikov, Phys. Lett. B 631 (2005) 151 [hep-ph/0503065].

[5] D.J. Schwarz, Mod. Phys. Lett. A 13 (1998) 2771 [gr-qc/9709027]; N. Seto and J. Yokoyama, J. Phys. Soc. Jap. 72 (2003) 3082 [gr-qc/0305096]; L.A. Boyle and P.J. Steinhardt, astro-ph/0512014.

[6] H. Davoudiasl, R. Kitano, G.D. Kribs, H. Murayama and P.J. Steinhardt, Phys. Rev. Lett. 93 (2004) 201301 [hep-ph/0403019]; W. Buchmüller, K. Hamaguchi, O. Lebedev and M. Ratz, Nucl. Phys. B 699 (2004) 292 [hep-th/0404168]; P. Brax, C. van de Bruck, A.C. Davis, J. Khoury and A. Weltman, Phys. Rev. D 70 (2004) 123518 [astro-ph/0408415].

[7] U.W. Heinz, AIP Conf. Proc. 739 (2005) 163 [nucl-th/0407067]; P. Huovinen, Nucl. Phys. A 761 (2005) 296 [nucl-th/0505036]; R.S. Bhalerao, J.P. Blaizot, N. Borghini and J.Y. Ollitrault, Phys. Lett. B 627 (2005) 49 [nucl-th/0508009].

[8] E.V. Shuryak, Sov. Phys. JETP 47 (1978) 212; S.A. Chin, Phys. Lett. B 78 (1978) 552.

[9] J.I. Kapusta, Nucl. Phys. B 148 (1979) 461.

[10] T. Toimela, Phys. Lett. B 124 (1983) 407.

[11] P. Arnold and C. Zhai, Phys. Rev. D 50 (1994) 7603 [hep-ph/9408276]; *ibid.* 51 (1995) 1906 [hep-ph/9410360].

[12] C. Zhai and B. Kastening, Phys. Rev. D 52 (1995) 7232 [hep-ph/9507380].

[13] K. Kajantie, M. Laine, K. Rummukainen and Y. Schröder, Phys. Rev. D 67 (2003) 105008 [hep-ph/0211321].

[14] A.D. Linde, Phys. Lett. B 96 (1980) 289.

[15] D.J. Gross, R.D. Pisarski and L.G. Yaffe, Rev. Mod. Phys. 53 (1981) 43.

[16] A. Hietanen, K. Kajantie, M. Laine, K. Rummukainen and Y. Schröder, JHEP 01 (2005) 013 [hep-lat/0412008].

[17] F. Di Renzo, M. Laine, V. Miccio, Y. Schröder and C. Torrero, in preparation.

[18] G.D. Moore, JHEP 10 (2002) 055 [hep-ph/0209190]; A. Ipp, G.D. Moore and A. Rebhan, JHEP 01 (2003) 037 [hep-ph/0301057].

[19] A. Vuorinen, Phys. Rev. D 67 (2003) 074032 [hep-ph/0212283].

[20] A. Vuorinen, Phys. Rev. D 68 (2003) 054017 [hep-ph/0305183].

[21] A. Ipp and A. Rebhan, JHEP 06 (2003) 032 [hep-ph/0305030]; A. Ipp, A. Rebhan and A. Vuorinen, Phys. Rev. D 69 (2004) 077901 [hep-ph/0311200].

[22] A. Gynther and M. Vepsäläinen, JHEP 01 (2006) 060 [hep-ph/0510375]; hep-ph/0512177.

[23] J.P. Blaizot, E. Iancu and A. Rebhan, Phys. Rev. D 68 (2003) 025011 [hep-ph/0303045].

[24] G. Cvetič and R. Kögerler, Phys. Rev. D 70 (2004) 114016 [hep-ph/0406028]; M. Inui, A. Niegawa and H. Ozaki, Prog. Theor. Phys. 115 (2006) 411 [hep-ph/0501277].

[25] X. Wang and J. Li, Commun. Theor. Phys. 33 (2000) 253 [hep-ph/9804246].

[26] E.S. Fraga and P. Romatschke, Phys. Rev. D 71 (2005) 105014 [hep-ph/0412298].

[27] M. Laine and M. Vepsäläinen, JHEP 02 (2004) 004 [hep-ph/0311268].

[28] J. Ignatius, K. Kajantie, H. Kurki-Suonio and M. Laine, Phys. Rev. D 50 (1994) 3738 [hep-ph/9405336].

[29] P. Ginsparg, Nucl. Phys. B 170 (1980) 388; T. Appelquist and R.D. Pisarski, Phys. Rev. D 23 (1981) 2305.

[30] K. Kajantie, M. Laine, K. Rummukainen and M. Shaposhnikov, Nucl. Phys. B 458 (1996) 90 [hep-ph/9508379].

[31] E. Braaten and A. Nieto, Phys. Rev. D 53 (1996) 3421 [hep-ph/9510408].

[32] K. Kajantie, M. Laine, K. Rummukainen and Y. Schröder, JHEP 04 (2003) 036 [hep-ph/0304048].

[33] K. Rummukainen, private communication.

[34] S. Eidelman *et al.* [Particle Data Group], Phys. Lett. B 592 (2004) 1.

[35] K. Kajantie, M. Laine, K. Rummukainen and M. Shaposhnikov, Nucl. Phys. B 503 (1997) 357 [hep-ph/9704416].

[36] M. Laine and O. Philipsen, Phys. Lett. B 459 (1999) 259 [hep-lat/9905004]; A. Hart and O. Philipsen, Nucl. Phys. B 572 (2000) 243 [hep-lat/9908041].

[37] M. Laine and Y. Schröder, JHEP 03 (2005) 067 [hep-ph/0503061].

[38] G. Boyd, J. Engels, F. Karsch, E. Laermann, C. Legeland, M. Lütgemeier and B. Petersson, Nucl. Phys. B 469 (1996) 419 [hep-lat/9602007].

[39] B. Beinlich, F. Karsch, E. Laermann and A. Peikert, Eur. Phys. J. C 6 (1999) 133 [hep-lat/9707023]; M. Okamoto *et al.* [CP-PACS Collaboration], Phys. Rev. D 60 (1999) 094510 [hep-lat/9905005]; Y. Namekawa *et al.* [CP-PACS Collaboration], Phys. Rev. D 64 (2001) 074507 [hep-lat/0105012]; R.V. Gavai, S. Gupta and S. Mukherjee, Phys. Rev. D 71 (2005) 074013 [hep-lat/0412036].

[40] A. Hart, M. Laine and O. Philipsen, Nucl. Phys. B 586 (2000) 443 [hep-ph/0004060].

[41] P. Giovannangeli and C.P. Korthals Altes, Nucl. Phys. B 721 (2005) 1 [hep-ph/0212298]; *ibid.* 721 (2005) 25 [hep-ph/0412322].

[42] P. Bialas, A. Morel, B. Petersson, K. Petrov and T. Reisz, Nucl. Phys. B 581 (2000) 477 [hep-lat/0003004]; *ibid.* 603 (2001) 369 [hep-lat/0012019].

[43] F. Karsch, K. Redlich and A. Tawfik, Eur. Phys. J. C 29 (2003) 549 [hep-ph/0303108].

[44] A. Ali Khan *et al.* [CP-PACS collaboration], Phys. Rev. D 64 (2001) 074510 [hep-lat/0103028].

[45] C. Bernard *et al.*, PoS LAT2005 (2005) 156 [hep-lat/0509053].

[46] Y. Aoki, Z. Fodor, S.D. Katz and K.K. Szabo, JHEP 01 (2006) 089 [hep-lat/0510084].

[47] S. Ejiri, F. Karsch, E. Laermann and C. Schmidt, hep-lat/0512040.

[48] K. Kajantie, M. Laine, K. Rummukainen and M.E. Shaposhnikov, Phys. Rev. Lett. 77 (1996) 2887 [hep-ph/9605288].

[49] K. Kajantie, M. Laine, K. Rummukainen and M.E. Shaposhnikov, Nucl. Phys. B 493 (1997) 413 [hep-lat/9612006].

[50] P. Arnold and O. Espinosa, Phys. Rev. D 47 (1993) 3546 [hep-ph/9212235]; *ibid.* 50 (1994) 6662 (Erratum); Z. Fodor and A. Hebecker, Nucl. Phys. B 432 (1994) 127 [hep-ph/9403219].

[51] G.D. Moore and D. Teaney, Phys. Rev. C 71 (2005) 064904 [hep-ph/0412346]; P. Petreczky and D. Teaney, Phys. Rev. D 73 (2006) 014508 [hep-ph/0507318]; H. van Hees, V. Greco and R. Rapp, hep-ph/0601166.

[52] R.R. Parwani, Phys. Rev. D 45 (1992) 4695 [hep-ph/9204216]; *ibid.* 48 (1993) 5965 (Erratum); A. Jakovác, Phys. Rev. D 53 (1996) 4538 [hep-ph/9502313]; A.I. Bugrii and V.N. Shadura, hep-th/9510232.

[53] M. Laine and M. Losada, Nucl. Phys. B 582 (2000) 277 [hep-ph/0003111].

[54] The notation $p(T, \boldsymbol{\mu})$ always implicitly refers to the ultraviolet finite difference $p(T, \boldsymbol{\mu}) - p(0, \mathbf{0})$.

[55] We note that Δ differs by a certain constant from a similar constant employed in the figures of Ref. [13].

Selbständigkeitserklärung

Ich versichere, die vorgelegte Arbeit selbständig und nur unter Verwendung der angegebenen Hilfsmittel angefertigt zu haben.

Dr. York Schröder